Polymeric Foams

Science and Technology

Kishan C. Khemani, EDITOR
Eastman Chemical Company

Developed from a symposium sponsored
by the Division of Polymer Chemistry, Inc.

American Chemical Society, Washington, DC

Polymeric foams

This book is printed on acid-free, recycled paper.

Advisory Board

ACS Symposium Series

Foreword

THE ACS SYMPOSIUM SERIES was first published in 1974 to provide a mechanism for publishing symposia quickly in book form. The purpose of this series is to publish comprehensive books developed from symposia, which are usually "snapshots in time" of the current research being done on a topic, plus some review material on the topic. For this reason, it is necessary that the papers be published as quickly as possible.

Before a symposium-based book is put under contract, the proposed table of contents is reviewed for appropriateness to the topic and for comprehensiveness of the collection. Some papers are excluded at this point, and others are added to round out the scope of the volume. In addition, a draft of each paper is peer-reviewed prior to final acceptance or rejection. This anonymous review process is supervised by the organizer(s) of the symposium, who become the editor(s) of the book. The authors then revise their papers according to the recommendations of both the reviewers and the editors, prepare camera-ready copy, and submit the final papers to the editors, who check that all necessary revisions have been made.

As a rule, only original research papers and original review papers are included in the volumes. Verbatim reproductions of previously published papers are not accepted.

ACS BOOKS DEPARTMENT

Preface

FOAMED POLYMERS ARE USED BY THE MODERN WORLD in a variety of applications for attributes including weight reduction, insulation, buoyancy, energy dissipation, convenience, and comfort. A vast amount of research and development data on the use of foamed resins has been amassed over the last 50 years. Surprisingly, the area of foams continues to be enriched with new ideas as our understanding of the science and technology of foaming as well as the uses of foamed polymers continue to be challenged by the advent of new polymers, foaming technologies, and applications never imagined before.

This volume was developed from an international symposium presented at the 212th National Meeting of the American Chemical Society, titled "Recent Advances in Polymeric Foam Science and Technology", sponsored by the ACS Division of Polymer Chemistry, in Orlando, Florida, August 25–29, 1996. The chapters of this book are the contributions of symposium participants. The participation and attendance at this symposium, and the interactive scientific discussions that took place after each presentation, attest to the escalating interest and research and development efforts in this field. At the meeting, the need for this volume was apparent. Although it is not possible to cover the topic completely in a book of this nature, an attempt has been made to solicit manuscripts that highlight some of the main areas in this field.

The 15 chapters in this volume represent recent developments in different areas of polymeric foam science and technology. The first chapter is an overview of the field of polymeric foams and their markets. Each of the next 14 chapters is organized so that a comprehensive review of the respective field precedes the discussion of new results. The first five chapters (2–6) discuss new developments in the areas of siloxane, carbon, polyimide, polyester, and polyisocyanurate foams. Chapters 7 and 8 focus on the newly emerging area of microcellular polymeric foams produced via solid-state and extrusion foaming techniques, respectively. The next three chapters (9–11) discuss some recent advances in the area of polyurethane foam. Chapter 12 deals with important issues in the study of the morphology of cellular solids. Chapters 13 and 14 discuss some physical and theoretical aspects of foams and foaming processes. Finally, Chapter 15 discusses modeling studies of inherently foamable (upon exposure to heat) intumescent polymers used as fire retardants.

This volume is intended to be useful to all academic and industrial scientists, engineers, and technicians who work in research and development in the field of polymers and polymeric foams. It is the sincere hope of the contributors of this volume that the work presented here will spawn new ideas, technologies, and applications in this exciting field.

Acknowledgments

KISHAN C. KHEMANI
Research Laboratories
Eastman Chemical Company
200 South Wilcox Drive
Kingsport, TN 37662

February 11, 1997

Chapter 1

Polymeric Foams: An Overview

Kishan C. Khemani

Research Laboratories, Eastman Chemical Company, 200 South Wilcox Drive, Kingsport, TN 37662

It is difficult to go through a whole day without coming in contact with something which does not contain a foamed plastic part somewhere within. The most common examples perhaps are the foamed polyurethane seat cushion of the sofa or chair or the car-seat that you sat on this morning, or the polystyrene foam cup in which you had your morning coffee or tea or some other hot drink! Or the foamed polystyrene take-out boxes or trays which are used extensively at restaurants and cafeterias everywhere.

Since the first introduction of foamed rubber, phenol-formaldehyde and urea-formaldehyde resins in the early twentieth century, the foam industry has come of age, so to speak, in terms of the knowledge gained and the understanding of the fundamentals and principles governing this technology. So much so, that the science and technology of foaming of several specific polymers (for example, polyurethane, polystyrene, phenolics, polyvinyl chloride etc.) have literally become stand-alone research and development areas in themselves.

As a result of the years of research and development work in the field of polymeric foams in general, nowadays it is possible to foam virtually any polymeric material since a lot of the basic principles governing this technology and its processes are applicable to most resins. Of course, the fitness-for-use requirements, the ease or difficulty of production, and most importantly, the cost-of-goods-sold dictate the industry's choice of resins and manufacturing processes for specific applications.

Several types of polymeric materials are foamed to various low densities for applications that derive from attributes such as weight-reduction, insulation, buoyancy, energy dissipation, convenience and comfort. There are two major classes of polymeric foams: thermoplastic and thermoset foams. While thermoplastic foams can be reprocessed and recycled, thermoset foams are intractable since they are generally heavily crosslinked. Within these classes, the polymeric foams are further classified as rigid, semi-rigid, semi-flexible, or flexible, depending upon their compositions, cellular morphology and other physical and thermal characteristics such as Tg, %crystallinity, extent of crosslinking, etc.).

1

Furthermore, a solid polymeric foam can either consist of closed or open cells. Closed cell foams have a cellular structure in which contiguous air bubbles are entrapped within a continuous macromolecular phase. The foam polystyrene coffee cup, for example, consists entirely of closed foam cells. Open cell foams, on the other hand, have a cellular network in which continuous channels are available throughout the solid macromolecular phase for air to flow through at will. The polyurethane seat cushion is a very good example of an open cell foam. Closed cell foams are generally rigid, while open cell foams are generally flexible. All of the aforementioned attributes of foamed polymers is a direct result of the presence of these so called voided architecture.

Most polymeric foams are produced by one of the several known foaming techniques which include, extrusion, compression molding, injection molding, reaction injection molding, solid state method (where pressurized gas is forced into a solid polymer at room temperature followed by depressurization and heating to above its Tg), etc..

The gaseous phase in any polymeric foam material derives from the use of blowing agents in the foam manufacturing process. There are two types of blowing agents used to produce foams: chemical blowing agents and physical blowing agents. As the name implies, the first type are chemical compounds which give-off gases under the foam processing conditions, either due to chemical reactions or due to thermal decomposition. The second type of blowing agents are simply inert gases, such as nitrogen, carbon dioxide etc.; volatile hydrocarbons having boiling points between -40°C to +45°C, such as propane, butane, i-pentane etc.; and low boiling chlorofluorocarbons (CFC's), hydrofluorocarbons (HFC's) and hydrochlorofluoro-carbons (HCFC's).

For some applications, it is a common practice to coextrude or laminate a thin layer of solid unfoamed polymer onto the surface(s) of the foamed material in order to improve certain physical characteristics such as the cut-through resistance, modulus, barrier to various gases, extractables, printability, and finally aesthetics.

Several excellent textbooks and handbooks have been published over the years which give good details of various foam technologies, foaming processes, and foam characterization and properties. Some such recent publications are listed in references *1-4*, and are highly recommended.

The foam industry on the whole has been challenged in recent years by issues ranging from waste disposal, recyclability, flammability, and the depletion of earth's ozone layer by the chlorofluorocarbon blowing agents. This has been further compounded by the issuance of numerous regulations and codes by the government agencies. As a result, the industry has imposed a certain level of self-regulation in several of these areas.

Although the polymeric foam market is growing worldwide, the leading producers and consumers of these products are in North America, Europe and Japan. Some Latin American and other Asian countries (such as Argentina, Mexico, Brazil, India, Taiwan, South Korea etc.) have also been developing foam products and markets in more recent years.

Specific examples of uses of polymeric foams include films, cups, food trays, containers, flooring, decorative items (ribbons, etc.), insulation boards, sound dampening, transportation, bedding, carpet padding, furniture parts, chair cushions,

toys, fibers, automobile parts (seats and back-rests, bumpers, headliners, etc.), sporting goods (helmets, clothing, , etc.), flotation (boat parts, surf boards, life-vests, etc.), footwear parts (soles, inserts, etc.), insulation for appliances, and in packaging of just about all types of non-food items as well.

The statistical data reported hereafter in this overview is derived from a combination of this author's interpretation, extrapolation and interpolation of the data/information reported and published over the past ten years. This author is therefore solely responsible for any inadvertent errors in estimating these values and projections. The numbers are intended merely to give a general feeling of the markets and their trends. In addition to the past issues of various excellent plastics news magazines such as, the Plastics World, Packaging Week, Plastics Business News, Asian Plastics News, European Plastic News, Packaging News, Plastics News, Modern Plastics, Plastics Technology, Materials Engineering, Plastics Engineering, Plastics Packaging, Plastic Trends, etc., the publications listed in references *1-9* are also recommended to the readers interested in broader in-depth analyses of various foamed polymer products, and their applications / markets.

It is estimated that in 1995 close to 6 billion pounds of foamed plastics was produced and consumed in the United States alone, and it is projected that this usage will grow at 3 - 4% annual rate to about 7 billion pounds by the year 2000. Most of this growth will probably come in the automotive, construction, packaging, and consumer products markets. The three major resins used in these markets are polyurethane, polystyrene, and polyvinyl chloride.

Foamed and unfoamed polyurethane is used in a very wide range of commercial applications. The main applications in the foam area are those requiring cushioning and insulation. Flexible polyurethane foam uses include, for example, seat cushions, furniture, carpet underlayment, mattress padding, appliances etc., and those of rigid polyurethane foams include insulation material for construction (as boards) and in appliances (injection molded). About 3 billion pounds of foamed polyurethane was used in these markets in 1995, and it is estimated that this number will grow to over 3.5 billion pounds by 2000. A large part of this growth might be in the newer area of reaction injection molded (RIM) polyurethanes for automotive components. Polyurethane has seen some market erosion in the past 10 years due to the shift from chloroflurocarbon (CFC) blowing agents which were extensively used in the past. However, it is no longer used in most places and presently more than 75% of the volume is blown with water and carbon dioxide. The three current largest producers of polyurethanes are Bayer, Dow, and BASF.

Polystyrene is another very widely used resin for the manufacture of foamed products. However, it is heavily dependent on packaging markets, although demand in construction markets as boardstock used in insulation is poised to take off. In 1995, about 1.7 billion pounds of polystyrene was consumed in these markets. In the packaging markets, general concerns related to waste disposal and recyclability are considered as impediments for this resin, and thus its growth potential is somewhat diminished as compared to polyurethanes. It is expected that the market share for this resin will grow to about 1.8 - 2.0 billion pounds by the year 2000. Foamed polystyrene products are typically manufactured by either molding of the expandable polystyrene (EPS) beads, or the extrusion foaming and thermoforming technology. The major producers of EPS are ARCO, BASF, and Huntsman, and those of extruded polystyrene foams are Amoco, ARCO, and BASF.

Foamed vinyl (polyvinyl chloride) is perhaps the first thermoplastic foam commercialized during World War II and was soon followed by the polyurethane and polystyrene foams. However, it ranks third in terms of volume as compared to the latter two, but still has a strong market share. It topped 300 million pounds in 1995, and is growing at a 2 - 2.5% rate. Some of the major current markets for this product are the construction (flooring, fittings, wire insulation, molding and pipe, conduit, etc.) and the automobile industry (mainly seat covers), with two major suppliers being BF Goodrich and 3M. Both flexible and rigid foamed vinyls are used in these markets.

As mentioned above, a large growth rate is forecast in the reaction injection molded polyurethane foam area. In 1995, about 250 million pounds of this material was consumed. And it is expected to grow at a rate of 7% or better over the next few years mainly due to high demand from the automobile industry where it has found uses in exterior body panels, trims and bumpers.

Foamed polyethylene (low and high density), phenolics, polypropylene, ABS, acrylics, cellulose acetate, urea-formaldehyde (UF), polyimides, polyetherimides, polyphenylene oxide (PPO), polychloroprene (PCP), silicones, epoxy foams, etc. all added up to over half a billion pounds of volume in 1995. Growth for these niche players is expected at anywhere between 4 - 6% per annum for the next few years, with perhaps the most growth being in the phenolics area due to their flame retarding capabilities. The markets served by these resins are quite diverse and include: packaging (HDPE); insulation (cellulose acetate, UF, silicones, polyetherimides); construction (HDPE, LDPE, phenolics, ABS); household products (HDPE, LDPE, acrylics); toys (HDPE, LDPE, ABS, PP); sporting goods (HDPE); floatation (UF), office products (LDPE, PPO); aircraft (phenolics, polyimides, PPO, PCP, silicones); electrical (epoxy, silicones), furniture (HDPE, ABS, PP); appliances (ABS); bottle labels (LDPE, PP); decorative items (LDPE, PP, UF); medical products (PP, UF)); artificial wood (UF, epoxy), etc..

Finally, there has been some progress in the recent years in the development of biodegradable foam materials for several of the same applications as described above. Different approaches developed by various groups include the use of a wide range of resin/material compositions. Some examples include, the compounding of non-degradable polymers such as the polyolefins with degradable materials such as starch, woodflour, jute, hemp, etc., and/or the use of inherently degradable materials such as the partially substituted cellulosics, starch, aliphatic polyesters, aliphatic-aromatic polyesters, polylactic acid, plasticized polyvinyl alcohol, polyesteramide, polycaprolactone, etc.. However, large scale commercial applications in these areas are still years away as much more work is needed. Recently, EarthShell Corporation of Santa Barbara, CA, has been test marketing a potato-starch/cellulose-fiber/calcium-carbonate based foamed food-packaging material (molded into clam-shells, cups, plates and trays, etc.) through McDonald's, which is claimed to degrade readily into its natural ingredients in a compost environment (10).

As mentioned in the beginning, foamed polymers offer unique advantages over non-foamed polymers in terms of specific properties such as weight-reduction, heat-transfer characteristics, buoyancy (for closed cell foams), physical force dissipation via cushioning, and comfort. On the other hand, the technology and

process of foaming a polymer is a challenging one and encompasses the effective utilization of the knowledge base of several different scientific fields including polymer, materials and organic chemistries, physics, chemical and mechanical engineering, process engineering, equipment design and operation, and so on.

This volume deals with some recent developments in several of the different areas of polymeric foam science and technology in fourteen independent chapters. Each chapter is organized such that a comprehensive review of the respective field precedes the discussion of the new results.

The first five chapters (*2* through *6*) discuss some new developments in the areas of Siloxane foams, Carbon foams, Polyimide foams, Polyester foams and Polyisocyanurate foams. The next two chapters (*7* and *8*) focus on the newly emerging areas of microcellular foams produced by solid-state and extrusion foaming techniques respectively. The next three chapters (*9, 10* and *11*) discuss some recent advances in the polyurethane foams area. Finally, chapters *12* through *15* discuss some physical and theoretical aspects of foams and foaming processes.

Specifically, chapter *2* discusses two different approaches to producing injectable elastomeric siloxane foams. The first, a synthetic approach, utilizes a reversed emulsion technique, and the second consists of blending thermally labile particles into the crosslinkable elastomer followed by curing and forced degradation of the labile particles to generate voids.

Interest in carbon foams has been high due to its potential in a wide range of specialized applications. Chapter *3* discusses several of these applications and reports the preparation of carbon foams by the pyrolysis of a series of rigid hypercrosslinked polyaromatic polymers such as the ones obtained from benzene, biphenyl, m-terphenyl, diphenylmethane, and polystyrene monomers and p-dichloroxylene as the crosslinking agent.

In chapter *4*, polymerization of nadimide end-capped oligobenzhydrolimide (BBN) blended with 3% of a linear thermostable polymer to produce rigid thermostable foams is described. During the thermal curing of the BBN, a reverse Diels-Alder reaction takes place with the evolution of cyclopentadiene which acts as an *in-situ* blowing agent. The resulting cellular network has good mechanical properties and other interesting features.

Polyester foams form the content of chapter *5*. Some new approaches for rendering linear polyesters and copolyesters foamable are discussed in this chapter. These include the use of monomeric branching agents, polymeric branching agents, and polymeric concentrates containing monomeric multifunctional branching agents, in order to enhance the rheological properties of the linear resins which is necessary for extrusion processing of foams from these materials. A good discussion of the basic requirements for foaming of a polymeric material in general, is also presented in the background review section of this chapter, and the readers may find Scheme 3 of this chapter particularly useful for this purpose.

Chapter *6* deals with novel polyisocyanurate foams which are modified by the incorporation of thermally stable linkages such as amide, imide or carbodiimide. This yields foams which exhibit improved thermal stability, smoke generation characteristics and have higher inherent flame retarding capacity.

Solid-state microcellular foams typically have cells which are 10 microns in diameter; consequently these materials have a very high cell density as compared to

a more conventional foam of equal density in which the cell diameters range from 50-500 microns. Since their discovery in early 1980's at the Massachusetts Institute of Technology, a lot of development work has been done at other academic and industrial institutions and several different plastics have been foamed *via* this technique to relative densities of 0.1 to 1.0 and containing 10^8 to 10^{11} cells per cm^3. Very simply, the method involves impregnating and saturating a solid plastic material with a suitable gaseous blowing agent under high pressures at below its Tg (glass transition temperature), and followed by releasing the pressure and heating the gas-saturated plastic to a temperature higher than its Tg. Chapter *7* discusses the *pros* and *cons,* and various other issues surrounding this new technology in some detail.

More recently, it has been demonstrated that microcellular foams can also be produced by an extrusion process. Whereas the solid-state process must by its nature be a batch process or a semi-continuous process at best, the extrusion process is a continuous one. It is therefore perhaps more cost effective, and consequently has been the focus of a lot of the recent attention and research and development effort. The technique simply involves the continuous formation of a polymer/gas solution inside an extruder followed by the nucleation of a large number of bubbles using rapid pressure drop and the control of the foaming step *via* pressure control in order to induce a desired volume expansion. Chapter *8* describes some intricacies involved in such a process in the extrusion of microcellular high impact polystyrene foams (HIPS).

Some recent advances in polyurethane foams is covered in Chapters *9, 10* and *11*. In chapter *9*, stabilization of the bubbles during the foaming of flexible polyurethane foams using polymeric silicone surfactants is reported. The structure of the silicone surfactant used has significant effect on the final air flow through the foam. A relationship between the surfactant structure and foam openness is provided which suggests some basic noteworthy trends.

Chapter *10* deals with an *in-situ* study of structure development during the reactive processing of water blown polyurethanes. The kinetics of the reaction-induced phase transformation, its mechanism, and the resultant cellular morphology, all suggest that microphase separation in polyurethane foam occurs *via* spinodal decomposition at a critical conversion of isocyanate functional groups.

Imaging of the three-dimensional cellular network of flexible polyurethane foams is done using a new technique, the laser confocal microscopy, in chapter *11*. This technique acquires sharp 2D images which are then used for 3D reconstruction of the cellular structure. Use of this technique for studying foam compression under different mechanical compressions is also discussed in this chapter.

Chapter *12* discusses the relationships between foam properties and foam cellular morphology and cautions against the inherent limitations and pitfalls of the various methods of quantifying the cellular structure.

Chapters *13* and *14* deal with the fundamental aspects of the key areas of the extrusion foaming processes. Whereas chapter *13* looks at the overall foaming process using the physical blowing agents, chapter *14* focuses on the dynamics of the bubble growth.

Finally chapter *15* discusses the modeling of mechanisms that determine the fire-resistant properties of intumescent polymers, which are designed to swell into

thick robust foams upon exposure to heat and thus protect the underlying materials from fire.

The foam densities reported in this volume are either in g/cm^3 or lb/ft^3 or kg/m^3 units. The interconversion of these units is related by 1 g/cm^3 or g/cc = 62.37 lb/ft^3 or pcf = 1000 kg/m^3 or kcm.

References

1. *Polymer Foams - Processing and Production Technology,* Shutov, F. A., Ed.; Technomic Publishing Co., Lancaster, PA, 1991.

2. *Handbook of Polymeric Foams and Foam Technology,* Klempner, D.; Frisch, K. C., Eds.; Hanser Publishers, Munich, Vienna and New York, 1992.

3. *Handbook of Plastic Foams,* Landrock, A. H., Ed.; Noyes Publications, Park Ridge, NJ, USA, 1995.

4. Throne, J. L. In *Thermoplastic Foams*; Sherwood Publishers, Hinckley, OH, USA, 1996.

5. *U.S. Foamed Plastics Markets & Directory,* Technomic Publishing, Lancaster, PA, USA, 1987.

6. Gibson, L. J.; Ashby, M. F. *Cellular Solids - Structure & Properties*, Pergamon Press, Elmsford, NY, 1988.

7. *SPI Plastics Engineering Handbook* (of the Society of the Plastics Industry, Inc.), Berins, M. L., Ed.; 5th Edition, Van Nostrand Reinhold, New York, N.Y., 1991.

8. *Foamed Plastics*, Study # 485, The Freedonia Group, Inc., Cleveland, OH, USA, 1993.

9. *Polyurethanes IV*, Skeist Inc., Whippanny, NJ, USA, 1994.

10. Schut, J. H. *Plastics World,* **1996**, *54 (12)*, 29.

Chapter 2

Siloxane Elastomer Foams

A. Della Martina[1], J. G. Hilborn[1,3], J. Kiefer[1], J. L. Hedrick[2], S. Srinivasan[2], and R. D. Miller[2]

[1]Polymers Laboratory, Materials Department, Swiss Federal Institute of Technology, CH–1015 Lausanne, Switzerland
[2]IBM Almaden Research Center, 650 Harry Road, San Jose, CA 95120–6099

New approaches to produce injection moldable elastomeric foams with porosities in the micrometer range have been developed. In the first approach, water is dispersed within the siloxane network by first preparing a reverse emulsion in the presence of an appropriate surfactant. Porosity is then generated by evacuation of the water. Supercritical drying was used to avoid surface tension effects and prevent collapse during drying. The measured porosities were in good agreement with the water incorporated into the initial emulsion. The second approach surveyed as a means of generating controlled porosity in elastomers involves blending thermally labile particles into the siloxane resin. Upon network formation, the particles can be selectively degraded to leave voids, the size and shape of which should be identical to that of the initial dispersion morphology. PMMA particles with deliberate low thermal stability were synthesized using a combination of dispersion polymerization and chain transfer. The resulting particles showed a significant decrease in degradation temperature. These two techniques for the preparation of elastomeric foams are described.

Elastomer foams are generally produced using gas blowing techniques. By such techniques, it is very difficult or even impossible to produce narrow pore sizes distributions and to control pore compositions, due to coalescence and ripening phenomena. New applications demand a precise control of both the volume fraction of porosity and pore size. It is also often necessary to injection mold which is not compatible with the gas blowing techniques requiring vented molds to allow for expansion. Based on these considerations it is necessary to find new ways to produce injectable elastomer foams with controlled porosity. The purpose of this paper is to present a new approach to synthesize porous siloxane elastomers with a controlled porosity in the μm-range.

Despite the numerous existing techniques to prepare polymeric foams, few are suitable to prepare porous elastomers with the desired closed porosity. It is not in the scope of this paper to review in detail the existing techniques to porous polymers, but the general strategies of the most important techniques to prepare porous polymers will

[3]Corresponding author

be discussed as possible routes to porous elastomers. One can distinguish three main routes to prepare porous polymers. The first involves the use of dissolved gases as the void forming medium. The second route is based on emulsion derived foams, as the generation of a controlled two phase morphology is realized through the intermediate of tailored surfactants. The porous morphology is subsequently achieved by selective removal of the inner phase, which consists of a low molecular weight liquid or alternatively of a thermally labile polymer. The third category involves the use of a phase separation process to generate a two phase morphology. One of the two phases is successively removed to result in a porous structure. These three routes are illustrated in Figure 1.
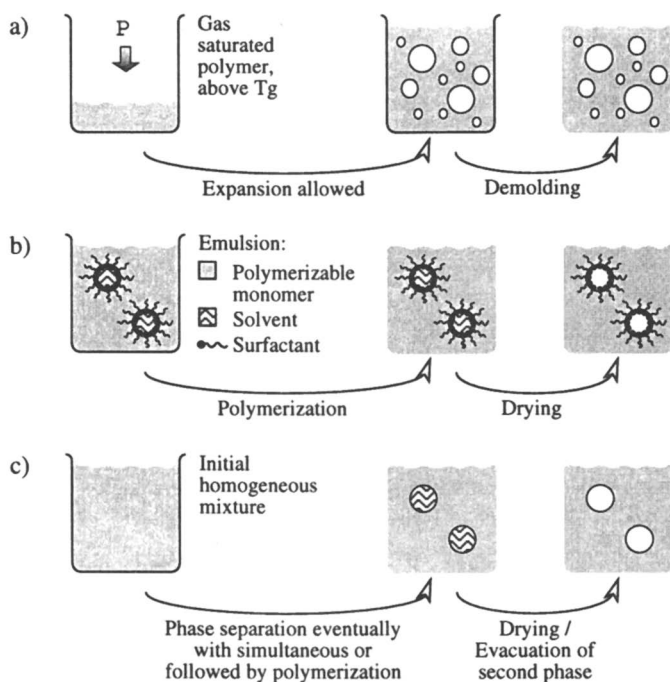
Figure 1:   Schematic illustration of the three major routes to produce foams.

A wide variety of microcellular thermoplastic foams are prepared via gas nucleation (*1, 2*) . This method consists of a two step procedure. In the first step the polymer is saturated with a non reactive gas at fairly elevated pressures. Upon saturation, the polymer is removed from the pressure reactor in order to produce a supersaturated sample. This supersaturated polymer is then heated to a temperature near T_g, thus inducing nucleation and growth of gas bubbles resulting in a porous structure. Carbon dioxide or nitrogen are mostly used as blowing agents. The bubble growth is arrested by quenching the samples in water at room temperature (*3*).

Gases can also develop in situ during the network formation either as a result of the heat development due to the exothermic curing reaction or as a product of a side reaction thus resulting in polymeric foams (*4*). For example flexible polyurethane foams are commercially produced using CO_2 as the blowing agent, that is liberated as a reaction product of the isocyanate monomer with water. Due to the high diffusion rates of gases in polymers, the above techniques provide foams with a large pore size

distribution ranging over several orders of magnitudes. Besides the development of interconnected pores in the mm-range, a microphase separation leads to urea hard segments in the nm-range which are responsible for the mechanical properties such as stiffness and compressibility (5).

The second class of techniques that also provides the formation of polymeric foams is based on emulsion technologies. An emulsion consists mainly of three different parts, the continuous or outer phase, the dispersed or inner phase and the surfactant. The surfactant is an amphilic moiety, that ensures the miscibility between the inner and outer phase. A special type of emulsions are microemulsions, which are thermodynamically stable and have nm size domains. If the outer phase is a polymerizable monomer, a rigid matrix will form upon polymerization. A foam is obtained after removal of the inner phase, that is most often a low molecular weight liquid such as water. We will discuss this technique more in detail later in this chapter.

Fréchet and coworkers have applied the emulsion polymerization technique for the preparation of porous PS beads (6, 7). In this approach the inner phase consists of a mixture containing the reactive styrene and divinylbenzene monomers as well as an unreactive polymeric fraction. After polymerization, the soluble polymeric fraction is washed out, leaving behind macroporous beads with pore sizes of around 100 to 500nm, thus serving as chromatography media.

In contrast to the highly interconnected pores reported previously, closed pores can also be obtained by microemulsion polymerization, if the initial volume fraction of the dispersed phase is lower than 30%. Recently two systems have been reported, where the polymerization of the continuous phase and the subsequent removal of the liquid dispersed phase resulted in the formation of porous thermoplastic materials, such as PS (8) or PMMA (9). However both groups observed independently, that the initial nanosized morphology has been destroyed, as the final pore size was several microns.

The third category of techniques involves the intermediate of a phase separation process. One example is phase inversion membranes, which have been produced commercially for more than 30 years based on a phase inversion process (10). In this strategy a polymer-solvent mixture is immersed in a non-solvent. Precipitation leads to the formation of a polymer rich and solvent rich phase. The morphology of the membranes can be varied from a sponge-like structure to a finger-like structure, depending on the preparation parameters (11, 12).

Amazingly regular porous structures can be obtained from the self-assembly of tailor-made copolymers. Hedrick and coworkers (13-17) have explored a general methodology, enabling for the synthesis of nanoporous polyimides with a well controlled porosity, resulting from the self-assembly of triblock copolymers consisting of a thermally labile and thermally stable block. Thermal degradation of the thermally labile inner phase leads to a well controlled porosity. SAXS measurements revealed closed pores with sizes of around 5 to 20nm, depending on the block length of the thermally labile block. This nanoporous structure lead to materials with significant lower density and dielectric constant, thus offering great potential for applications in microelectronics.

Alternatively porous polymeric materials can be derived based on a phase separation process by carrying out a temperature quench. Therefore, this method has been termed thermally induced phase separation (TIPS) (18, 19). Porous PS foams with densities as low as $0.02-0.2 g/cm^3$ are produced by such a phase separation starting from a PS-cyclohexane system (20, 21). The phase diagram of this particular system is well known and exhibits an upper critical solution temperature. The two components are mixed above the critical solution temperature, where the cyclohexane and polystyrene are miscible. A phase separation is initiated by cooling below the binodal or spinodal line, thus resulting in a two phase morphology. Controlling the morphology requires a detailed knowledge of the phase diagram, as well as the kinetics and thermodynamics of the different phase separation mechanisms. Depending on the

quench rate, the phase separation proceeds either via nucleation and growth or via spinodal decomposition, resulting in different morphologies. Thus the pore size can be varied from less than 1 micron up to around 100 microns. The low volume fraction of the polymeric phase leads to a highly interconnected, porous structure. This technique allows only for the preparation of films with less than 1mm in thickness, that can be used as membranes. This is in principle limited to thermoplastic polymers as it requires a sufficient mobility of the polymeric phase below its Tg.

Recently a new method enabling a controlled porosity in highly crosslinked polymers has been developed (*22-24*). In this strategy the precursor monomers forming the polymeric network are cured in the presence of a low molecular weight liquid, which turns into a non-solvent upon curing, thus initiating a phase separation. This process results in the formation of liquid droplets, spherical in shape due to thermodynamic reasons. The size of the liquid droplets depends on the competing effects between the growth of these domains and the continuous buildup of a highly crosslinked network. The generation of a porous morphology is subsequently achieved by diffusion of the liquid through the crosslinked matrix without any alteration in the size and distribution of the dispersed phase. This technique has been termed chemically induced phase separation (CIPS), as the phase separation process results from a chemical quench (*25*). These macroporous thermosets are characterized by a very narrow size distribution in the μm-range and a significant lower density without any lowering in thermal stability.

It is our aim to understand the underlying mechanism for small pore foams to broaden this group of materials. Furthermore we aim to guide the process to give closed pores and a precise control of the morphology. To this end, we have eliminated the use of gases, directly leading to a porous structure, since large size distributions and high degree of interconnectivity is obtained. Therefore a two phase morphology is envisaged, where the inner phase, which might consist of a liquid or a degradable solid which can be removed easily. For processing, it becomes crucial to select liquids, which fulfills the requirements of pressure in the pores, diffusion through the matrix, solubility in the matrix etc.. Indeed, the only of the above mentioned process suitable would be the emulsion derives foams, however, any attempt to produce elastomer foam by this technique have failed due to the inherent material properties as will be described below.

Results and Discussion

To produce an injectable foam, it is necessary to create an incompressible morphology, but to achieve the final desired compliant deformation, the incompressible dispersed phase has to be removed to leave compressible voids. These considerations allow two choices for the incompressible dispersed phase: liquid droplets or solid spheres. Using the first choice, foams can be produced by preparing an emulsion in which the continuous phase consists of the elastomer precursors, cure the elastomer and finally remove the dispersed phase. The second choice can be exercised by mixing thermally labile microspheres in the elastomer precursors, effect network formation then heat the material to degrade the microspheres in order to leave voids (*26*).

Emulsion Derived Foams. This approach is industrially used to produce foams with highly interconnected pores and very low densities (as low as $0.02 g/cm^3$) with narrow pore sizes distributions resulting from a stable system. The principle is to create an emulsion with an internal phase fraction higher than 74%, which is the volume fraction of close packed monodispersed spheres. In this sort of emulsion, the droplets are distorted to dodecahedrons whose walls are made of the polymerizable monomers. This type of morphology is known as high internal phase emulsion (*27, 28*) or concentrated emulsion (*29, 30*). During the polymerization of the monomer, holes form

in the thin walls resulting in a final open structure from which the originally dispersed phase is easily removed. This technique allows the synthesis of organic (Polyhipe by Unilever) as well as inorganic foams, that offer a wide range of applications (28).

For many new applications, the use of siloxane elastomers demand closed pores and a perfect control of the morphology (26, 31). The use of gases, directly leading to a porous structure, is not appropriate for these purposes because of the large size distributions and the high degree of interconnectivity. Therefore a two phase morphology is envisaged, where the inner phase, which might consist of a liquid, can be easily removed. Our attempt is based on reversed emulsion polymerization as described below.

Foam Production. In emulsions the volume fraction of the dispersed phase is readily determined by the amount of second phase used and, assuming that all the surfactant is accommodated at the interface, the size of the droplets is controlled by the amount of surfactant, usually quantified as a fraction of the second phase. It is therefore possible to control the total volume fraction and the size of the porosity separately.

To have visual control of the morphologies created, we opted for a transparent siloxane elastomer. To perform the initial emulsion, we had to choose an appropriate second phase and an adapted emulsifier. As the second phase, water was considered appropriate because it is completely non miscible with the hydrophobic siloxane, allows for the use of commercially available emulsifiers, and is a small molecule with a high diffusion rate in the siloxane matrix allowing for easy further processing. To chose the emulsifier, the scale based on the hydrophilic and respective lipophilic power of the head and tail of the surfactant, the hydrophilic-lipophilic balance, HLB, is commonly used. A low HLB corresponds to a molecule being more soluble in the oil phase, i.e. in our case more soluble in the siloxane. If the molecule is more soluble in the siloxane, a bigger part of the total chain will be in the siloxane and with the steric hindrance, this will give an interface concave against the siloxane. The emulsifier was a dimethylsiloxane ethylene oxide block copolymer with 25wt% ethylene oxide. As the dimethylsiloxane is quite hydrophobic, the resulting low HLB is optimal to produce a water in siloxane emulsion. This emulsion is shown in Figure 2.

□   Siloxane rubber precursors: base, curing agent & catalyst

▨   Water

∿   Dimethylsiloxane ethylene oxide block copolymer HLB < 9
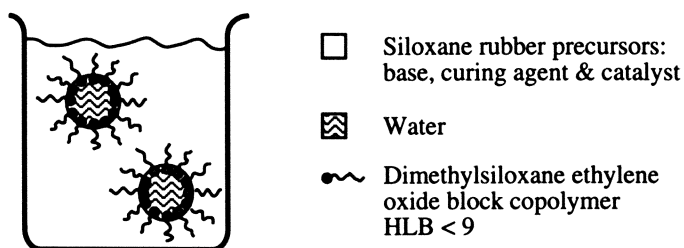
Figure 2:   Initial emulsion used to create the morphology.

The emulsions were prepared using the following procedure. We first mixed the siloxane base, the curing agent, the catalyst, then we added the water and the surfactant and finally the complete mixture was stirred at high speed. The final white and opaque stable emulsion was homogenized using an ultrasonic bath.

The emulsions were then degassed under vacuum to extract the air trapped in the emulsion by the high speed stirring. This operation is very important to avoid the formation in the material, during the curing step, of uncontrolled bubbles produced by the thermal expansion of the air pockets. The emulsions were then molded into closed flasks and cured at 70°C, resulting in a final opaque white rigid material. This

temperature was found to be the right compromise between fast cure and low water evaporation. The network formation is achieved via a platinum catalyzed hydrosilylation reaction between the vinyl end groups and the multiple hydrosilyl functionalities of the curing agent. This reaction is shown in Figure 3.

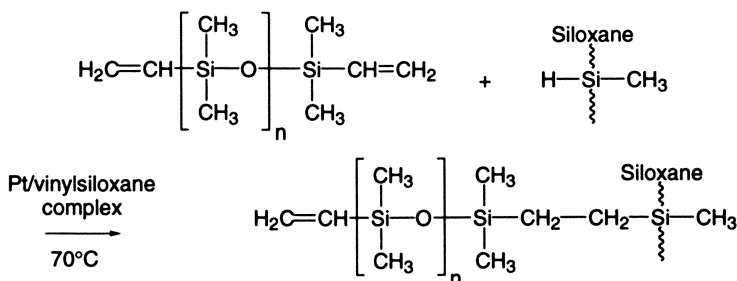

Figure 3: Network formation reaction

The siloxane base already contains enough catalyst to fully cure the siloxane resin, but, since water is known to slightly inhibit this crosslinking reaction, approximately 2wt% (of the siloxane base weight) Pt/vinylsiloxane complex was added to reach full cure of the emulsified samples.

Water had to be removed to produce the final foam. Our initial attempts gave unfortunately disappointing results. Drying in an oven, in air using desiccants or under vacuum successfully removed the water but the morphology was lost and the final density was equivalent to the density of the non-foamed reference siloxane. This collapse of the domains is due to surface tension effects as described below.

To evaporate the water inside the pores with conventional techniques as the above, it is necessary to follow a nucleation and growth process. The free energy of a system made of a liquid with a growing bubble depends on two terms, a term ΔG_i arising from the interface created and a term resulting from the volume of liquid transformed from liquid to gas. The interface term ΔG_i is directly proportional to the amount of interface created and this amount can only be positive. If the system is heated above the evaporation temperature of the liquid, the most stable form for the substance will be the gas and the volume term ΔG_v will be negative, the difference between the free energy of the liquid and of the gaseous phase being proportional to amount of overheating. These considerations are expressed by equations 1 and 2.

$$\Delta G_i = \gamma 4\pi \cdot r^2 \tag{1}$$

$$\Delta G_v = (g_G - g_L)\frac{4}{3}\pi \cdot r^3 \tag{2}$$

Summing these two contributions gives the total free energy variation ΔG_t, expressed by equation 3.

$$\Delta G_t = (g_G - g_L)\frac{4}{3}\pi \cdot r^3 + \gamma 4\pi \cdot r^2 \tag{3}$$

We can see that, when the system is heated above the evaporation temperature, the interface term dominates when the radius tends towards zero, giving a positive ΔG_t at first and the volume term becomes more important for larger radiuses resulting in a negative ΔG_t. This is illustrated by Figure 4.

As a consequence, an activation energy $\Delta G_t(r^*)$ has to be overcome to nucleate a stable bubble. The bubble created by this process will then eventually grow and completely replace the water inside the domain as the water diffuses out of the sample.

It follows from these considerations that the effective surface tension inside the domains in the siloxane has to be close to that of the nucleating water vapor - water interface. Given the low modulus of the siloxane and the high surface tension of the very small bubble with the high interface energy of water, the pressure inside the domains is likely to render the domains mechanically unstable. At low temperatures, i.e. low overheating and thus low free energy difference, the activation energy is not reached. And it is energetically favorable for the water to diffuse out of the sample and for the domains to collapse.
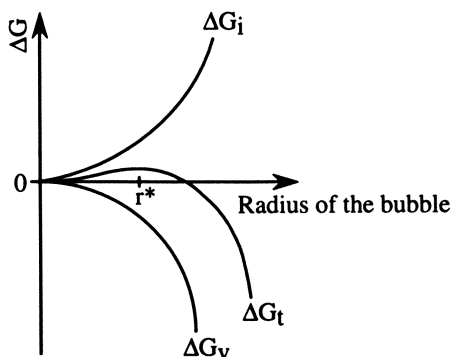

Figure 4:   Typical free energy curves for the nucleation and growth process of a bubble in a liquid. ΔG_i is the free energy arising from the creation of liquid-gas interface. ΔG_v is the free energy resulting from the volume transformed from liquid to gas. $\Delta G_t = \Delta G_i + \Delta G_v$.

A bar-shaped sample cured in a gradient oven illustrates these results. The idea of the gradient oven is to dry the sample in a wide range of temperatures. We noticed that when the samples were dropped on a very hot plate, the samples were dried but completely cracked due to the very high pressure produced by the boiling water inside the pores. On the other hand, the structure of samples dried at low temperatures, collapsed. If some intermediate conditions would give an equilibrium pressure inside the domains, i.e. enough pressure to keep the domains open but not enough to crack the sample, a part of the sample should be white and opaque, without being cracked, indicating a successfully foamed structure.

The oven was set to produce a gradient from 100 to 200°C and the sample containing water domains was let in overnight. Figure 5 shows part of the sample after drying.

The micrograph shows no homogeneously white and opaque part in the sample, and the observable white, pellet-shaped objects inside the transparent material are cracks. This tells us that the nucleation is the limiting process. Where the temperature is high, the nucleation rate is high but the overheating necessary for this nucleation induces a too violent bubble growth leading to the observable numerous small cracks (left end of Figure 5). Where the temperature is not high enough to nucleate the bubbles, the sample is completely transparent (right end of Figure 5). As the nucleation is a random process all the intermediate results in terms of number of cracks (i.e. number of nucleated bubbles that led to cracks) are present (see isolated cracks in the middle of Figure 5), but no homogeneous foam resulted.
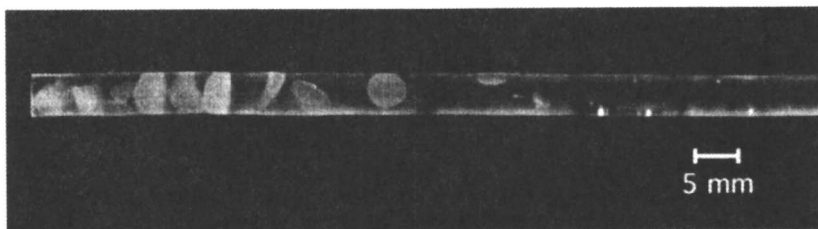
Figure 5:   Micrograph of the sample, containing initially 20wt% water and 10wt% (of water mass) surfactant, cured in the gradient oven. This visible part of the sample was dried between 197°C (end of the sample) and 170°C (right end of the figure).

A method to avoid this collapse of the domains, due to surface tension effects, is to evacuate the water without creating a surface. This is only possible by using a processing route which circumvents the critical point of the dispersed solvent. This technique is currently used to dry ceramic aerogels produced by the sol-gel technique (*32-34*). In that case, the sizes of the structures created are small enough to induce surface tension collapse upon drying even with very rigid materials as silica, alumina or zirconia.

The idea of supercritical drying is to gradually transform the liquid into the gas without crossing the evaporation/liquefaction line. If this line is not crossed, the phase transformation will not undergo a nucleation and growth process, no interface will be created and consequently surface tension will not play a role. Starting from the liquid phase, the pressure is first raised above the critical pressure of the solvent. Then the system is heated above the critical temperature at constant pressure. Finally the system is isothermally depressurized and then cooled down and purged with air to exchange the vapor of the solvent inside the sample.

In the case of ceramic aerogels, carbon dioxide is currently used as the solvent for this processing because it has a very low critical point and is miscible with the alcohol based solvents used for the sol-gel. In our case we had to adapt this to a different solvent because the carbon dioxide would swell the siloxane and the desired porous morphology would therefore be lost. As a consequence, we opted for acetone that is a poor solvent for the siloxane, is miscible with water and has a reasonably low critical point (temperature and pressure). The water inside the domains was exchanged for the acetone using a soxhlet extractor before the supercritical processing.

The supercritical drying used here is similar in principle to the one used for the aerogels and is shown in Figure 6.

Starting from the liquid phase (point "i" in Figure 6), following the steps described above (route through points "1" and "2" in Figure 6), we reached the gas phase without phase transformation (point "3" in Figure 6). At this point, the pores contain only gaseous acetone. To accelerate the gas exchange, that has to be achieved by diffusion through the siloxane because the porosity is closed, we decided to perform it at high temperature. As the critical point of the acetone is 235,5 °C and 47 atm, we had to preclude air to prevent autoignition. For these reasons we decided to exchange (at point 3 in Figure 6) the acetone with helium and then let the system cool down to room temperature.

This procedure gave white opaque samples, presumably porous. Surprisingly these samples turned transparent after approximately half an hour in ambient conditions, resulting from a self-collapse of the porosity. This may be easily understandable by considering the osmotic pressure driving the equilibration of the concentrations between the ambient atmosphere and the inside of the pores. The helium, being a noble monoatomic gas diffuses faster than the diatomic molecules of

the air (N_2, O_2, H_2) so that the foam collapses under the external pressure. This was resolved by exchanging the acetone directly with air after a slight cooling to avoid fire hazards (point "E" in Figure 6). As the air purged the pressure chamber, the system was allowed to cool down slowly. The samples were taken out of the chamber when ambient temperature was reached. The resulting opaque foamed samples were stable.
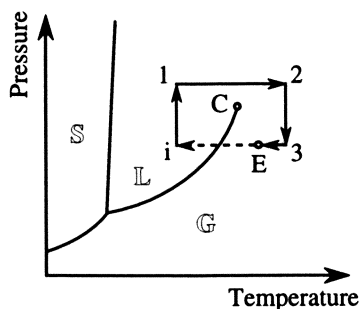

Figure 6:   Schematical representation of the supercritical drying process. S is the solid phase, L is the liquid phase, G is the gas phase and C is the critical point. In the processing route, i is the initial state and E the gas exchange point when air was used.

To evaluate the efficiency of this processing and to be sure that all of the water was evacuated we performed a TGA test that resulted in a weight loss of 0.27% at 300°C (curve a) of Figure 7). This can be compared to the weight loss of the same sample prior drying, illustrated by curve b) of Figure 7 (total weight loss of 9.65%).
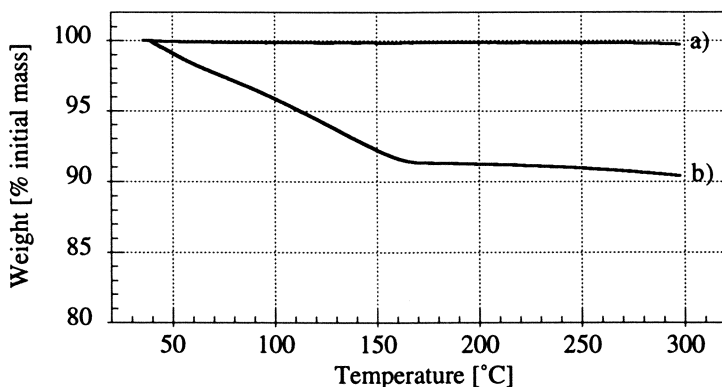
Figure 7:   TGA under N_2 curve of samples containing initially 10wt% water and 5% (of water mass) surfactant. Curves: a) foamed sample, b) sample prior drying.

The initial siloxane used is transparent so that the white appearance of the samples is the result of light scattering caused by the presence of different refractive index domains inside the samples. This aspect has been very useful to determine success or failure of the different techniques. Figure 8 shows a transparent reference sample of the siloxane without any porosity, an oven dried translucent sample with collapsed porosity and finally a successfully foamed opaque white sample obtained with by the supercritical drying described above.

Figure 8:   Siloxane samples. a) Transparent reference. b) Translucent sample, collapsed by conventional drying. c) Opaque sample, foamed by supercritical drying (scales shown are millimeters).

Foam Characterization. To determine the generality of this approach to samples with varying porosities, we prepared samples with varying initial water and surfactant contents. Pictures of cryo-fractured samples are shown by Figure 9.
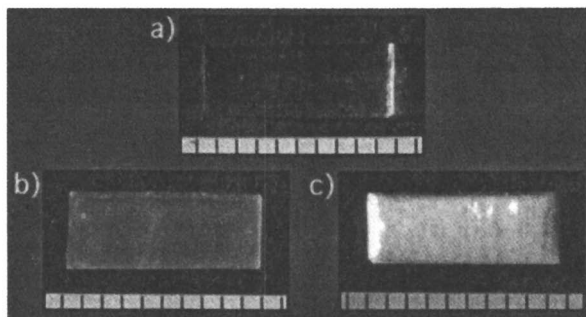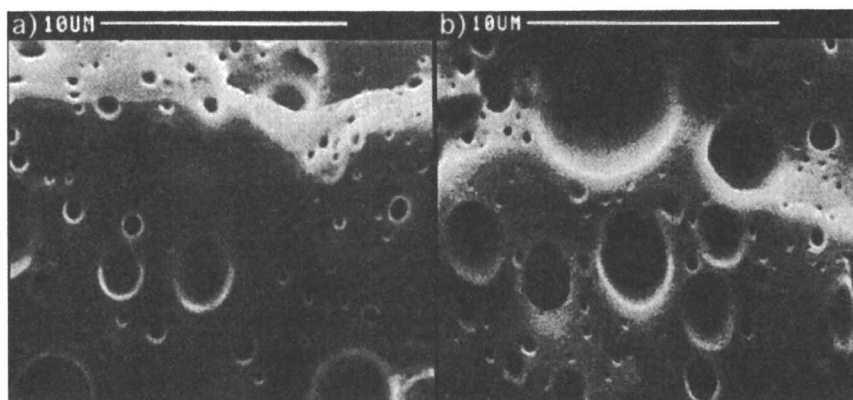

Figure 9:   Scanning electron micrographs of a) sample containing initially 10wt% water and 5% (of water mass) surfactant b) sample containing initially 20wt% water and 5% (of water mass) surfactant.

Equivalent pictures were used for image analysis (software: Optilab Pro 2.6) to establish the pore sizes distributions for all the samples. An example of these pore sizes distributions is given by Figure 10.

It is very important when discussing the pore sizes to talk about the amount of surfactant calculated as a fraction of the dispersed phase. Assuming that all the surfactant is accomodated at the interface, the amount of surfactant to amount of dispersed phase ratio, i.e. the surface to volume ratio, gives an equilibrium size for the domains. The high speed stirring and the subsequent ultrasounds produce droplet sizes smaller that the equilibrium size. However, some random coalescence takes place during the beginning of the curing, while heating the emulsion prior the gelation of the siloxane. The big droplets have a surface to volume ratio smaller than that of the equilibrium size droplets, so the still very small droplets have to accommodate the excess of surfactant and can not grow to the equilibrium size. These considerations explain the dispersion of the sizes shown by Figure 10.
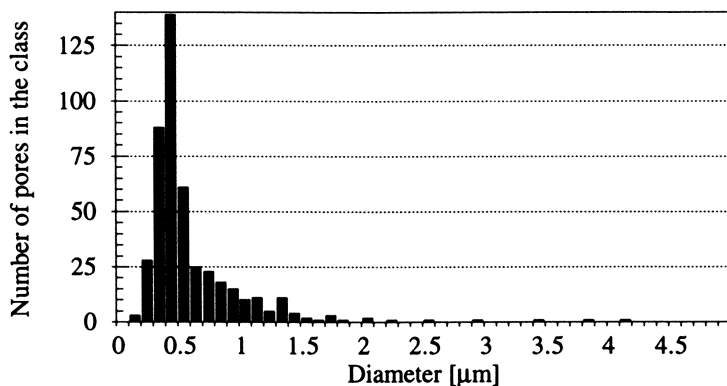
Figure 10:   Pore sizes distribution of the sample containing initially 10wt% water and 5% (of water mass) surfactant. Class diameter range: 0.1μm.

From the pore sizes distributions, mean pore sizes for all the samples were calculated as the number average of the distribution. The resulting mean pore sizes, plotted in Figure 11, clearly shows the decrease of the pore size with an increase of the amount of surfactant.
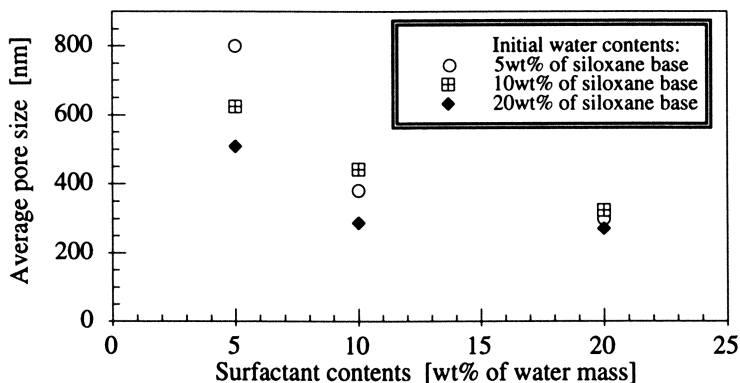
Figure 11:   Average pore sizes of the different samples.

Density measurements have also been performed on the different samples. The results were compared to the density of the non porous reference to calculate the amount porosity of the foamed samples.

Figure 12 gives the porosities of the samples as a function of their initial water contents. The porosity is directly proportional to the initial amount of water. This result, together with Figure 11, indicates that the final porosity is controlled by the characteristics of the initial emulsion. We also notice that the final porosity decreases with increasing surfactant content (calculated as a fraction of the water contents). That 10 to 50% decrease in volume fraction is probably due to the surface tension at the surface of the domains according to equation 4.

$$P = \frac{2\gamma}{r}$$ [4]

Therefore, the smaller pores, created by higher surfactant concentrations, experience a higher pressure and tend to collapse more. For example, assuming a surface tension of $20 \cdot 10^{-3}$ J/m^2, the pressure exerted on a pore of 200 nm in diameter would be of 0.4 MPa. In a case of uniaxial tension, this would result in a strain of 20% for a linear material having the Young's modulus of polysiloxane. Such a stress can easily force the collapse of the pores as the processing and the storage temperatures are above the T_g of the foamed elastomer. However, even if these arguments suggest that the effects of the internal pressure is not negligible, an estimate of these effects on the external dimensions of the foams would require complex and detailed numerical calculations beyond the scope of this chapter.
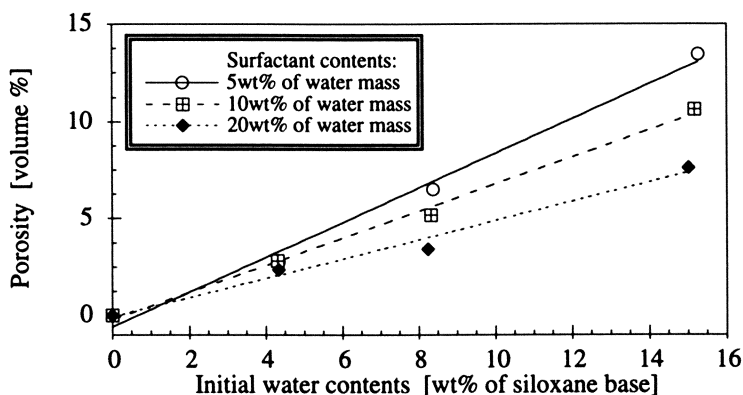

Figure 12: Final porosity versus the initial water contents. The porosity in volume % is based on density measurements compared to a non-foamed reference as: $100 \cdot (1-(\rho_{foam}/\rho_{reference}))$.

When the samples are extensively compressed, the opaque foams turn translucent and their density reaches the density of the non-porous reference, indicating a loss of the porosity. This porosity is not recovered even if the compression-collapsed foams are annealed in an oven at high temperature. This behavior arises from tacky internal pore surfaces due to the presence of water inside the domains during the curing of the siloxane. Water being known to be an inhibitor for the platinum catalyzed hydrosilylation, the siloxane pores surfaces are unlikely to be fully crosslinked. Indeed, a test sample cured under water using the same conditions as the emulsion showed a surface with a high degree of tack. In the case of the foams, the surfaces pressed together adhered strongly via chain interpenetration and the elastic energy stored in the matrix was insufficient to force them to reopen when the samples were unloaded.

Foams via Thermally Labile Particles. Our second approach to generate elastomeric foams was to compound the crosslinkable elastomer with preformed, thermally-labile polymethylmethacrylate (PMMA) particles. The elastomer is subsequently thermally crosslinked. Foam formation is further accomplished by a subsequent heat treatment to thermally decompose the PMMA particles, and leave behind microvoids similar in size and shape to those of the PMMA particles. The key features of this technique are twofold:

1. Balance the degradation rate so as to give enough pressure to nucleate and stabilize the pores but avoid the instantaneous conversion for solid to gas (which would lead to cracks shown earlier).

2. Assure particles degradation at sufficiently low temperature to avoid matrix degradation

Dispersion polymerization is a heterogeneous technique used to polymerize vinylic monomers in an organic diluent in the presence of an amphipathic graft or block copolymer to form insoluble micronsized polymer particles. The graft of block copolymer, commonly called a stabilizer, lends colloidal stability to the insoluble polymer. Dispersion polymerizations are characterized by the solubility of both the monomer and the initiator in the continuous phase and the insolubility of the resulting polymer in the continuous phase. The presence of the stabilizer allows the polymerization to proceed to a higher degree than is possible in the analogous precipitation polymerization. In addition, dispersion polymerization results in spherical particles typically ranging from 100 nm to 10 microns (35-39).

Catalytic chain transfer to monomer has been previously reported as a means of effectively controlling molecular weight in free radical polymerizations. The use of cobalt porphine chain transfer catalysts (Co-CTC) in the free radical polymerization of PMMA, results in oligomers with vinylic end-groups (PMMA-CH=CH$_2$) and significantly fewer head-to-head coupling than PMMA polymerized without Co CTC (40-42). Therefore, this route offers an effective pathway to low molecular weight PMMA which is also more thermally labile than saturated PMMA (PMMA-H). Thus employing Co-CTC, low molecular weight PMMA can be prepared via free radical techniques without the need for high initiator concentrations, elevated polymerization temperatures (>120°C) or sulfur containing chain transfer agents with their associated odor problems (42).

The thermal decomposition of PMMA is strongly dependent on the polymer microstructure and the resulting chain end-functionalities (43-49). For example, it has been reported that vinyl terminated PMMA is considerably more thermally labile than saturated PMMA. More specifically, unsaturated PMMA (PMMA-CH=CH$_2$) degrades between 230 and 300°C, whereas the saturated polymer decomposed between 300 and 400°C (44, 47, 48). Random chain scission and subsequent depolymerization is widely accepted as the mechanism for the degradation of saturated PMMA. Facile scission of the weak C-C bond beta to the vinyl group and efficient radical transfer to the vinyl chain ends has been proposed as the route to PMMA-CH=CH$_2$ degradation. Head-to-head chain likages also thermally destabilize PMMA. The use of dimethylmaleic anhydride as a comonomer in free radical initiated PMMA synthesis results in the introduction of additional head-to-head linkages in addition to those formed via coupling termination.

Earlier studies on the thermal degradation of oligomers containing head-to-head linkages (PMMA-HH) indicated that they were less stable than PMMA-CH=CH$_2$ (40). However, recent results suggest otherwise: That PMMA with head-to-head linkages (PMMA-HH) is actually more stable than PMMA-CH=CH$_2$ but less stable than saturated PMMA (45). Those authors observed a significant molecular weight effect since PMMA with head-to-head defects undergoes more facile degradation than saturated PMMA only when DP < 100. At higher values, the thermal degradation of both were comparable, a result attributed to a large cage recombination effects of radicals in the viscous polymer melt.

The presented work describes the deliberate synthesis of PMMA particles with lower thermal stability. To achieve this result, a combination of dispersion polymerization and chain transfer techniques was employed. The PMMA particles thus generated have been used as additives for the generation of crosslinked siloxane elastomeric foams. For this application, the PMMA serves as a thermally labile organic filler which is first compounded into the crosslinkable elastomeric network. Upon subsequent thermal treatment, the organic filler is thermally decomposed leaving behind pores, with the sizes and shapes of the PMMA filler particles.

Particles Synthesis. In dispersion polymerization, an initially homogeneous solution is transformed into an opaque suspension by homogeneous nucleation of particles from the reaction medium. The molecular weight of the growing polymer chain and its intrinsic insolubility in the solvent medium are two critical parameters that influence the formation of the dispersion. The stabilizer primarily controls the stability of the dispersion. The reaction medium is therefore selected on the basis of its nonsolvent properties for the growing polymer and the solubility of both the stabilizer and the monomer.

For free radical reactions employing cobalt porphine chain transfer catalysts, the concentration of the chain transfer agent is very critical. Very low concentrations result in inefficient molecular weight control whereas high concentrations limit the formation of higher molecular weights. It has been shown (*41*) that after interaction with the growing polymer radical, the regeneration of the cobalt porphine catalyst occurs very rapidly and the concentration of the intermediate species is less than 1% of the initial Co-CTC concentration.

Our efforts have focused on the combination of dispersion polymerization techniques and cobalt chain transfer catalysis, to synthesize spherical PMMA particles which are thermally labile. Such a procedure is not trivial and is complicated by the kinetics of the two processes which are very different. Dispersion polymerization proceeds rapidly whereas chain transfer occurs relatively slowly. To form a dispersion, the polymer chains must be of high enough molecular weight so as to phase separate from the solution. Thus the chain transfer process must allow the formation of a polymer dispersion while introducing a high concentration of vinyl end-groups that result in the desired thermal instability.

Our initial experiments involved the copolymerization of the methyl methacrylate with the 1,200g/mol polydimethylsiloxane (PDMS) macromer as a steric stabilizer. These experiments did demonstrate that the use of Co-CTC did indeed result in a significant decrease in molecular weight. Furthermore, the PMMA samples which were synthesized in the presence of cobalt porphine chain transfer catalyst, were significantly less thermally stable. However, a major problem in these initial experiments was that all four PMMA samples were prepared using the 1,200 PDMS as a steric stabilizer did not form stable dispersions in hexane. The individual particles tended to aggregate and it was not possible to sterically isolate and stabilize the individual particles as a dispersion.

Experiments using 25,000g/mol PDMS macromer were significantly more encouraging. PMMA 13 was synthesized from a mixture of 16g MMA, 2g of 25,000 g/mol PDMS and 0.3g AIBN in 200ml hexane at 70°C. Likewise, PMMA 29 was synthesized by polymerizing a mixture of 16g MMA, 2g of 25,000 g/mol PDMS, 0.3g AIBN and $6.2 \cdot 10^{-6}$mol of cobalt porphine (0.0042g of Co CTC catalyst in 10ml THF) in 200ml hexane. Shown in Figure 13 are the dynamic TGA spectra of two different PMMA samples prepared with the 25,000 PDMS stabilizer with (PMMA 29) and without (PMMA 13) the Co-CTC chain transfer agent.

The use of the chain transfer agent once again results in PMMA (PMMA 29) with a significantly lower thermal stability in comparison to PMMA without any chain transfer agent (PMMA 13). The reported mechanism of cobalt porphine chain transfer catalysis (*42*) suggests the formation of a high concentration of vinylic end-groups. These undergo depolymerization at much lower temperature than saturated PMMA, thus accounting for the trends shown in Figure 13.

It should be noted however that the concentration of cobalt porphine catalyst in the mixture is very critical. When $7.7 \cdot 10^{-6}$mol (0.0052g) of cobalt porphine was employed, the chain transfer was so effective that the low molecular weight PMMA formed remained soluble in hexane and consequently did not form a dispersion even after 12 hours at 70°C. On the other hand, when $4.8 \cdot 10^{-6}$mol (0.0032g) of cobalt porphine was employed, the dispersion formed within 15 minutes, but the thermal

stability of the resulting polymer was comparable to that of PMMA 13, suggesting that the chain transfer was ineffective. Unlike the results obtained using 1,200g/mol PDMS stabilizer, the use of the 25,000g/mol PDMS stabilizer results in stable dispersions of spherical PMMA 29 particles in hexane (see Figure 14).

Thus we have succeeded in synthesizing PMMA particles with evident lower thermal stability by a combination of dispersion polymerization and chain transfer techniques and have demonstrated the need to carefully control the amount of chain transfer agent.
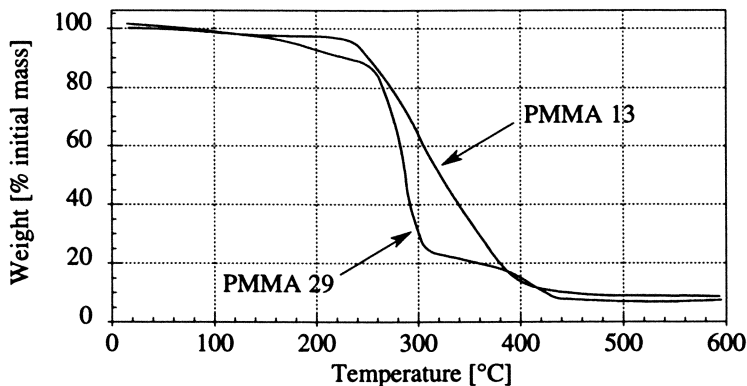
Figure 13:   Dynamic TGA curve under N_2 for PMMA 13 and PMMA 29 (with Co-CTC).
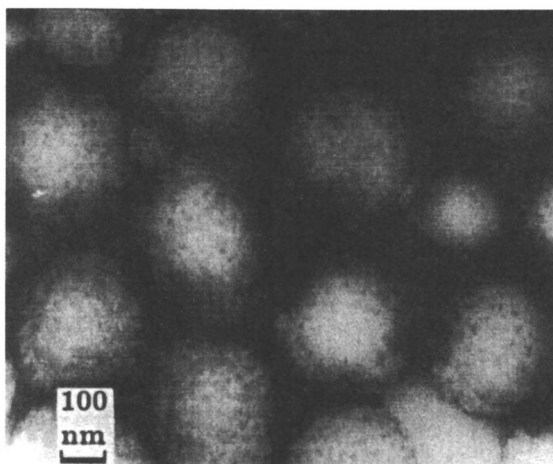
Figure 14:   Scanning electron micrograph of PMMA 29 particles.

Foam Formation. The PMMA particles (10wt%) were suspended in a hexane solution of dimethyldiphenylsiloxane vinyl terminated oligomer with a conventional oligomeric curing agent and a vinylsiloxane Platinum complex catalyst. This resin was chosen as the matrix elastomer since it is significantly more thermally stable than the polydimethylsiloxane resin (50). Films were cast and cured to effect network formation (200°C, 2 hours). The resulting films were opaque and SEM

micrography clearly showed an even dispersion of the particles in the matrix, without the evidence of particle aggregation. The filled network were subjected to a subsequent thermal treatment (300°C, 1.5 hours) to effect the degradation of the PMMA filler. An SEM micrograph of the resulting foam is shown in Figure 15. Isothermal thermogravimetric analysis showed quantitative degradation of the PMMA component by this treatment. The elastomers show an approximative 8% drop in density by this treatment, consistent with the formation of a foam. Shown in Figure 15 is the TEM micrograph of a cold-snap fracture surface after this foaming treatment. Clearly a porous morphology is formed where the pore size, shape and dispersion are identical to that of the initial dispersion and particle size and shape.

The use of a dispersion of thermally labile particles is an effective means to control the porosity in an elastomer. Ease of processing is realized since the labile component is simply blended or compounded as a filler or co-filler in an elastomeric resin. The compounded resin is ideally suited for injection molding processing. Furthermore, control of porosity is simply achieved by varying the PMMA particles size and concentration in the blend.
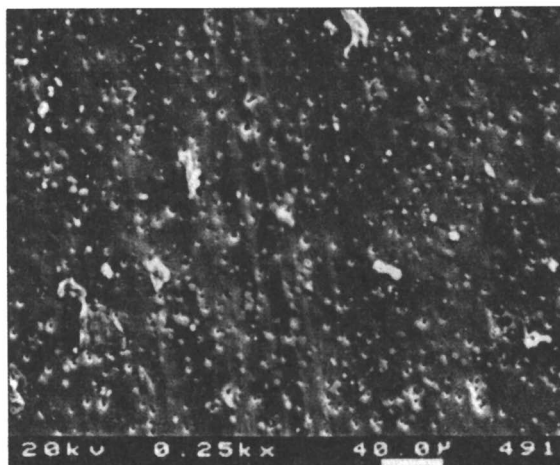

Figure 15:   Scanning electron micrograph of the foam obtained after thermal degradation of the PMMA filler.

Conclusions.

Siloxane elastomeric foams with controlled pore sizes in the micron range were successfully produced. The emulsion derived structures were dried, avoiding surface tension collapse of the domains, using supercritical drying with acetone. The reproducibility of the density results proves that the this technique allows good control of the structure. The produced foams showed a relatively narrow pore size distribution with mean pore sizes easily controllable with the initial emulsion parameters.

Micron-sized, thermally labile PMMA particles were successfully synthesized by a combination of dispersion polymerization in hexane and chain transfer employing cobalt porphine chain transfer catalyst. The dispersion polymerization allowed the synthesis of μm-sized particles while the chain transfer agent led to the formation of vinylic end-functionalities that contributed to thermal instability. These thermally degradable PMMA particles have been further employed as modifiers for crosslikable siloxane rubbers in efforts to generate porous elastomeric networks.

Legend of Symbols.

Variables				Subscripts	
g	Free energy per unit volume	$[J/m^3]$		G	Gas
r	Radius	$[m^2]$		i	Interface
r*	Critical radius	$[m]$		L	Liquid
ΔG	Free energy variation	$[J]$		t	Total
γ	Interface energy	$[J/m^2]$		v	Volume
ρ	Density	$[g/cm^3]$			

Acknowledgments.

References

1   Kumar, V. *Cell. Polym. Int. Conf.* **1993**, pp. 54.
2   Ramesh, N. S.; Rasmussen, D. H.; Campbell, G. A. *Polym. Eng. Sci.* **1994**, *34*, pp. 1698.
3   Kumar, V.; Wing, G.; Pasricha, A.; Tuttle, M. *Polym. Eng. Sci.* **1995**, *35*, pp. 673.
4   Klempner, D.; Frisch, K. C. *Handbook of Polymeric Foams and Foam Technology*; Hanser: München, Germany, 1991.
5   Neff, R.; Adedeji, A.; Macosko, C. W. *Polycondensation '96*, Paris, France, Polycondensation Symposium, **1996**, pp. 17.
6   Fréchet, J. M. *Makromol. Chem., Macromol. Symp.* **1993**, *70/71*, pp. 289.
7   Fréchet, J. M.; Svec, F. *Chem. Mater.* **1995**, *7*, pp. 707.
8   Qutubuddin, S.; Lin, C. S.; Tajuddin, Y. *Polymer* **1994**, *35*, pp. 4606.
9   Gan, L. M. *Langmuir* **1994**, *10*, pp. 4022.
10 Loeb, S.; Sourirajan, S. *Adv. Chem. Series* **1962**, *38*, pp. 117.
11 Fujita, S. M.; Soane, D. S. *Polym. Eng. Sci.* **1988**, *28*, pp. 341.
12 Strathmann, H.; Kock, K. *Desalination* **1977**, *21*, pp. 241.
13 Hedrick, J. L.; Hilborn, J. G.; Palmer, T. D.; Labadie, J. W. *J. Polym. Sci., Part A: Polym. Chem.* **1990**, *28*, pp. 2255.
14 Hedrick, J. L.; Russell, T. P. *MRS Symp. Proc.* **1992**, *274*, pp. 37.
15 Hedrick, J. L.; Charlier, Y.; Russell, T. P. *MRS Symp. Proc.* **1994**, *323*, pp. 277.
16 Hedrick, J. L.; Pietro, R. D.; Charlier, Y.; Jerome, R. *High Perform. Polym.* **1995**, *7*, pp. 133.
17 Hedrick, J. L.; Russell, T. P.; Labadie, J.; Lucas, M.; Swanson, S. *Polymer* **1995**, *36 (14)*, pp. 2685.
18 Torkelson, J. M.; Song, S. W. *Polym. Prepr.* **1993**, *34 (2)*, pp. 496.
19 Torkelson, J. M.; Song, S. W. *Macromolecules* **1994**, *27*, pp. 6389.
20 Aubert, J. H.; Clough, R. L. *Polymer* **1985**, *26*, pp. 2047.
21 Lal, J.; Bansil, R. *Macromolecules* **1991**, *24*, pp. 290.
22 Kiefer, J.; Hilborn, J. G.; Manson, J.-A. E.; Leterrier, Y.; Hedrick, J. L. *Macromolecules* **1996**, *29*, pp. 4158.
23 Kiefer, J.; Porouchani, R.; Mendels, D.; Ferrer, J. B.; Fond, C.; Hedrick, J. L.; Kausch, H. H.; Hilborn, J. G. *Microporous and Macroporous Materials*, San Francisco, CA, MRS Symposium Proceedings, **1996**, *431*, pp. 527.
24 Kiefer, J.; Hilborn, J. G.; Hedrick, J. L. *Polymer* **1996**, *37*, pp. 5715.

25 Pascault, J. P. *Macromol. Symp.* **1995**, *93*, pp. 43.
26 Hedrick, J. L.; Srinivasan, S.; Miller, R. D.; Shih, D. Y.; Liao, Y.-H.; Hilborn, J. G.; Plummer, C. J. G.; Della Martina, A. *Microporous and Macroporous Materials*, San Francisco, CA, MRS Symposium Proceedings, **1996**, *431*, pp. 511.
27 Lissant, K. J.; Mayhan, K. G. *J. Coll. Interf. Sci.* **1973**, *42 (1)*, pp. 201.
28 Even Jr., W. R.; Gregory, D. P. *MRS Bull.* **1994**, *19 (4)*, pp. 29.
29 Princen, H. M.; Aronson, M. P.; Moser, J. C. *J. Coll. Interf. Sci.* **1980**, *75 (1)*, pp. 246.
30 Ruckenstein, E.; Park, J. S. *Polymer* **1992**, *33*, pp. 405.
31 Hilborn, J. G.; Della Martina, A.; Plummer, C. J. G.; Hedrick, J. L.; Miller, R. D. *ACS Polymer Preprints* **1996**, *37 (#2)*, pp. 773.
32 Molhern, G. T.; Scrame, D. S.; Howe, R. T. *Transducers '93 (7th ICSSSA)*, Proceedings of the International Conference on Solid-State Sensors and Actuators, **1993**, pp. 296.
33 Pethybridge, G. D.; Dobson, P. J.; Brook, R. J. *Br. Ceram. Proc.* **1994**, *53*, pp. 73.
34 Van Bommel, M. J.; de Haan, A. B. *Journal of Non-Crystalline Solids* **1995**, *186*, pp. 78.
35 Arshady, R. *Colloid. Polym. Sci.* **1992**, *270*, pp. 717.
36 Barrett, K. E. J. *Dispersion Polymerzation in Organic Media*; John Wiley & Sons: New York, NY, 1975.
37 Ober, C. K.; Lok, K. P.; Hair, M. L. *J. Polym. Sci.: Polym. Lett. Ed.* **1985**, *23*, pp. 103.
38 Ober, C. K. *Macromolecules* **1987**, *20*, pp. 268.
39 Ober, C. K. *Makromol. Chem., Macromol. Symp.* **1990**, *35/36*, pp. 87.
40 Cacioli, P.; Moad, G.; Rizzardo, E.; Serelis, A. K.; Soloman, D. *Polym. Bull. (Berlin)* **1984**, *11*, pp. 325.
41 Enikolopyan, N. S.; Smirnov, B. R.; Ponomarev, G.; Belgorskii, I. *J. Polym. Sci., Polym. Chem.* **1981**, *19*, pp. 879.
42 Janowicz, A. H. US Patent 4, 694, 054.
43 Manring, L. E. *Macromolecules* **1988**, *21*, pp. 528.
44 Manring, L. E. *Macromolecules* **1989**, *22*, pp. 2673.
45 Manring, L. E.; Sogah, D. Y.; Cohen, G. M. *Macromolecules* **1989**, *22*, pp. 4652.
46 Inaba, A.; Kashiwagi, T.; Brown, J. E. *Polym. Degrad. Stab.* **1988**, *21*, pp. 1.
47 Kashiwagi, T.; Inaba, A.; Brown, J. E.; Hatada, K.; Kitayama, T.; Masuda, E. *Macromolecules* **1986**, *19*, pp. 2168.
48 Chiantore, O.; Guaita, M. *Makromol. Chem.* **1989**, *190*, pp. 449.
49 Hedrick, J. L.; Labadie, J.; Russell, T.; Hofer, D.; Walkharker, V. *Polymer* **1993**, *34 (22)*, pp. 4717.
50 Shih, D.-Y.; Lauro, P.; Fogel, K.; Norcott, M.; Walker, G. F.; Hedrick, J.; Shi, L.; Doany, F. et al. *1995 IEEE 45th Electronic Components & Technology Conference*, Las Vegas, NV, Proceedings - ECTC, **1995**, pp. 126.

Chapter 3

Carbon Foams Prepared from Hyper-Cross-Linked Polymer Foams

Warren P. Steckle, Jr.

Polymer and Coatings Group, MST–7, Materials Science and Technology Division, Los Alamos National Laboratory, Los Alamos, NM 87545

Carbon foams prepared from hypercrosslinked polymer foams retain high surface areas as well as tailorable pore size distributions ranging from under 10 Å to 1,000 Å. A series of rigid hypercrosslinked foams has been prepared using simple rigid polyaromatic hydrocarbons such as benzene, biphenyl, m-terphenyl, diphenylmethane, and polystyrene, with p-dichloroxylene as the crosslinking agent. Surface areas for these materials range from 160 m^2/g to 1,200 m^2/g Unlike current methods for preparing carbogenic molecular sieves, the resulting porosity of the foams is determined by the porosity of the starting material, not the pyrolysis conditions, although pyrolysis conditions do alter the yield and other properties as well.

Carbon foams have a wide range of applications ranging from fuel cell electrocatalysts, general catalyst supports, porous adsorbents, foam electrodes for use in batteries and supercapacitors, to reinforcing matrix in composites, as well as separation of gases. Porosity of the materials are equally diverse and results from the processes from which they are derived. Micropores are defined as pores not wider than 20 Å, mesopores have widths between 20 Å and 500 Å, and macropores consist of pores larger than 500 Å by definition in accordance to the International Union of Pure and Applied Chemistry (IUPAC)(*1*). Polymers are known to degrade upon heating to high temperatures, but very few will produce foams upon pyrolysis. Polyvinyl chloride (PVC), polyvinylidine chloride (PVDC), polyfurfuryl alcohol (PFA), polyacrylonitrile (PAN), phenol/resorcinol - formaldehyde, and cellulose are known to undergo molecular eliminations to yield high carbon residues.

The pyrolysis of these polymers is generally broken down into four distinct stages as a function of temperature. The initial pre-carbonization stage, occurring below 300°C, usually involves the loss of heteroatoms from the polymer network. Between 300°C and 600°C the polymer degrades producing small molecules and a carbogenic solid. It is during these stages where the bulk of the chemical transformations occur. As temperature is increased from 600°C to 1,200°C, dehydrogenation occurs. It is through this condensation that polyaromatic cores grow. Once hydrogens are removed, a rearrangement of carbon atom occurs at temperatures higher than 1,200°C. Less crosslinked chars tend to undergo graphitization at these elevated temperatures whereas the structure of highly crosslinked chars tends to be kinetically frozen as an amorphous carbon (*2*).

Carbogenic Molecular Sieves   Carbogenic Molecular Sieves (CMS) are microporous foams predominantly used in the area of separation of nitrogen from air. CMS differ from activated carbons in that separation occurs on the basis of differing rates of adsorption rather than on the extent of adsorption. Unlike zeolites, CMS are globally amorphous and exhibit no long range order. Carbogenic molecular sieves are commonly made from: PFA (*3-6*), PAN (*7-10*), PVDC (*9-12*), PVC (*13-14*), as well as from coal tars (*15-16*). PAN and PVC are known as graphite formers whereas PFA and PVDC are non-graphitizing carbons. Both PFA and PVDC undergo significant crosslinking during the precarbonization stage. As mentioned earlier, the pathway to graphite for these highly crosslinked systems is blocked. However, upon further heating the lightly crosslinked PAN and PVC chars are converted to the more thermodynamically favored graphite. A dramatic example of this phenomenon is seen by heating a PVDC derived carbon to 3,000°C and a PVC derived carbon to only 1,700°C. The average number of layers in the graphitic domains in the former system is only seven or eight verses over thirty-three in the latter, indicating a fully developed three-dimensional graphitic structure(*2*).

Surface areas of these material fall in the range of 300 m^2/g to over 2,000 m^2/g depending on the precursor as well as the temperature profile used to prepare them. Nearly monodisperse porosities have been reported for PVDC and PFA derived CMS with average pore sizes of 5 Å and 5.5 Å respectively (*17*). Pore shapes have been reported as ranging from cylindrical, slit-like, to bottle-necked. Shapes and diameters of these pores have also been modified by the deposition of carbon derived from the pyrolysis of various hydrocarbons onto a carbon substrate (*18-22*). These "gate-keeping" layers are a region near the opening of the pore that further restricts flow through the pore. Through this chemical vapor deposition process the effective pore size can be tailored via openings of the pores alone verses the overall size of the pore.

Replica Carbon Foams This class of foams is prepared by compounding a salt into a polymeric matrix. This polymer/salt composite is then cured at elevated temperatures to produce an amorphous carbon. The salt is then extracted, leaving a carbon foam with pores the dimensions of the filler salt particles. These foams are often subjected to higher temperatures to deactivate the carbon surface and to improve the mechanical properties (*23-24*). A carbon replica foam is also produced when a sulfonated polystyrene/divinylbenzene macroreticular foam is heated in an inert atmosphere. Rohm and Haas markets these materials under the trade name Ambersorb (*25-27*). Sulfonation is one method to increase the yield of carbonaceous product upon pyrolysis. Oxygenation, chlorination, chloromethylation, amination, and halosulfonation are amongst other methods which have been investigated to increase the yield (*25-28*). Macroporosity of these carbonaceous materials is retained along with an increase of both meso- and microporosity. The development of this additional porosity is dependent on both the precursor as well as the pyrolysis temperature which ranges between 300°C and 1,200°C.

Foams Produced from Pitch Similar to foams prepared from coal tar, foams may be prepared from pitch by the blowing of an open-celled foam from a carbon fiber precursor such as mesophase pitch or even PAN (*29-30*). Although these materials are known to form high modulus fibers, foams can be prepared by using blowing agents. Typically, a blowing agent such as 5-phenyltetrazole is blended in with the pitch and is subsequently heated in a pressure vessel beyond its decomposition point. In a similar fashion a homogeneous nucleation process is performed by saturating the pitch with nitrogen in a pressure vessel then releasing the pressure. The thermodynamic instability leads to the formation of uniform pores. Pores prepared by these methods yield foams ranging from 80μm to 100μm in diameter. Use of talc as a nucleating agent results in the formation of larger non-uniform pores (*31-32*). Upon

graphitization of these materials the cell walls crack due to shrinkage, yet there tends to be an overall increase in the mechanical properties of the foams.

Hypercrosslinked Polymeric Foams   Polycondensation of polyaromatic hydrocarbons using rigid aromatic crosslinking agents provides a simple, yet versatile, method for preparing rigid hypercrosslinked foams.   This straightforward polycondensation, known as Friedel-Crafts polycondensation, has been applied to similar aromatic systems in an attempt to obtain linear poly(arylene methylenes). In this early work, researchers were unable to prevent crosslinking and typically recovered insoluble, infusible polymers (*33-35*). It is this crosslinking process that is utilized for preparing a series of rigid hypercrosslinked foams. Surprisingly, highly or hypercrosslinked forms of polystyrene are relatively unknown and are not commonly used for separations. However, there are several reports describing truly phenomenal properties in hypercrosslinked polystyrene which suggest that these materials may be superior to traditional polystyrene resins (*36-37*). Hypercrosslinked polystyrenes have extraordinarily high surface areas, swell in thermodynamically unfavorable solvents, absorb dyes and hydrocarbons, and readily absorb gases.   These phenomena, which are not observed in linear or lightly crosslinked polystyrene resins and beads, are attributed to the high frequency of rigid crosslinks which do not allow the polymeric network to collapse. This leaves a true microporous material with extraordinarily high surface areas and exceptional absorptive capacity.

A simple, three step process from inexpensive raw materials to microporous hypercrosslinked polymers has been reported earlier (*38-39*). Transparent gels are formed suggesting a very small pore size. After supercritical drying, the foams are robust and rigid. Without supercritical extraction , a zerogel would result. Densities of the resulting foams can range from 0.15g/cc to 0.75g/cc. Nitrogen adsorption studies have shown that by judiciously selecting monomers and crosslinking agents along with the level of crosslinking and the cure time of the resulting gel, the pore size, pore size distribution, and the total surface area of the foam can be tailored. Surface areas range from 160 m^2/g to 1,200 m^2/g with pore sizes ranging from 6Å to 2,000Å. These hypercrosslinked polymeric foams provide a material rigid and robust enough to undergo pyrolysis with retention of shape and pore structure. Carbonization of these material will be described herein.

Preparation of Carbon Foams from Hypercrosslinked Foams. All of the polyaromatic hydrocarbons (PAH), crosslinking agents (XL), catalyst, and all solvents were purchased from Aldrich, except for the three polystyrene precursors which were purchased from Polysciences. Carbon dioxide and ultra-high purity nitrogen and helium were purchased from Air Products. All of the reactants, solvents and catalyst were used as supplied.

Hypercrosslinked samples were typically prepared by first dissolving the PAH and XL in dichloroethane. The concentrations of PAH and XL varied from 0.10g/cc to 0.20g/cc in the precursor solution. Tin tetrachloride, used as the Friedel-Crafts catalyst, was added at this point. This solution was allowed to react for 18 hours at 60°C. Once the gel had cured, any catalyst and unreacted monomers were extracted from the gel using acetone. In order to retain porosity, the solvent was removed from the gel via supercritical extraction with carbon dioxide.

Pyrolysis of these polymeric foams was done in a Lindberg single zone quartz tube furnace equipped with a temperature profile controller. Heating rates ranged from 1°C/min. to 10°C/min. to temperatures as high as 1,000°C. Soak times of 8 hours were generally used to allow for uniformity throughout the sample. Samples were cooled down to room temperature before removal from the furnace. Ports on the

furnace readily allowed for different pyrolysis atmospheres. Samples were suspended in the furnace on a platinum hangdown to a point where the thermocouple was located.

The following sample designation was used: carbXXYYY/ZZZ. Where carb denotes that the sample was pyrolyzed, XX denotes the precursor foam, YYY is the initial pyrolysis temperature, and ZZZ is the second pyrolysis temperature where two step pyrolysis was employed. Although many different hypercrosslinked samples have been previously prepared, the following(XX) were chosen for this study: benz - benzene, BP - biphenyl, TP - m-terphenyl, and PS - polystyrene. A crosslinking ratio of 1:2 (PAH:XL) was chosen.

Instrumentation and Analysis. Surface area analysis was done using a Micromeritics ASAP 2010 Surface Area Analyzer. Nitrogen adsorption measurements were performed at 77°K. Surface areas were calculated according to theory as developed by Brunauer, Emmett, and Teller (BET) (*40*). Micropore volume and surface area distributions were calculated according to Horvath - Kawazoe (H-K) theory (*41*). The Barrett, Joyner, and Halenda (BJH) (*42*) method was used in determining the pore volume and surface area distributions for the mesopores. More recently, Density Functional Theory (DFT) (*43*) has become a powerful tool in the area of pore size analysis. This provides a profile of both surface area and pore volume from 2 Å up to 4,000 Å in a single analysis, unlike any of the aforementioned popular techniques.

Nuclear magnetic resonance (NMR) spectra were obtained on a Bruker ASX-300 solid state NMR spectrometer. Data was collected using either high power decoupling (HPDEC) or cross polarization magic angle spinning (CP-MAS) experiments. The experiments were generally carried out with a 1 ms contact time and a delay of 5 sec for the CP-MAS experiments and 10 sec for the HPDEC experiments. 90° pulse lengths were 8 μsec for CP-MAS experiments and 12 μsec for the HPDEC experiments. Spin rates of 10 kHz were used to remove spinning sidebands from the region of interest.

Thermogravimetric analysis (TGA) were performed using a Polymer Laboratories TGA in air and nitrogen atmospheres with a flow rate of 10 ml/min. and with a heating rate of 10°C/min. Micrographs were obtained using a Jeol transmission electron microscope (TEM). Non-pyrolyzed samples were stained with ruthenium tetraoxide in order to improve contrast. A Fluke 77 multimeter was used to measure the resistivity of the foams across a two millimeter sample.

Effect of Pyrolysis Conditions

Much valuable information was gained prior to detailed analysis of these foams by visual inspection. Samples which were heated to too high an initial temperature tended to form black glassy carbon foams with large voids on the order of millimeters in size. At temperatures less than 350°C a "tanning" of the sample occurs. Between 350° and 500°C or short soak times, a char would form on the surface and the interior of the foam would have only discolored. Samples heated directly to 1,000°C tended to balloon up and were a shiny silver. The exception to this are the biphenyl foams which will be discussed later. Foams pyrolyzed at the optimum temperature in static air tended to be more velvety in appearance, although this "velvet" was not easy to abrade from the surface. These foams were robust in nature and had good mechanical properties although at this point measurements have not been made. For comparison, a high internal phase emulsion polystyrene/divinylbenzene foam was pyrolyzed under similar conditions as carbPS425. This carbon foam was fairy brittle and was easily abraded.

Table I. Conditions of Pyrolysis and Properties of Resulting Foams

Sample	BET Surface Area (m^2/g)	Weight Percent Char	Resistivity (ohms)
atmosphere		static air	
PS:DCX	1,023		∞
carbPS425	769	81.6	∞
carbPS450	58	79.2	∞
carbPS500	44	72.3	∞
carbPS425*	712	76.1	∞
carbPS425†	736	75.4	∞
BP:DCX	1,065		∞
carBP450	755	73.2	∞
m-TP:DCX	707		∞
carbTP450	524	70.5	∞
benzene:DCX	671		∞
carbenz500	484	77.7	∞
carbenz500/600	336	94.2§	2500
carbenz500/700	267	92.8§	30
carbenz500/800	250	93.1§	20
carbenz500/900	211	90.7§	4
carbenz500/1,000	208	89.3§	3
carbenz1,000	7.6	60.4	3
carBP450/1,000	18.7	90.4	3
carBP450/1,000¥	1,240	50.5	3
carBP1,000	13.1	55.2	2
carbTP425/1,000	24.6	87.4	3
carbTP425/1,000¥	174	45.1	3
carbTP1,000	2.2	50.9	2
atmosphere		air	
all	na	<1	
atmosphere		vacuum	
carbenz500	17	53.6	∞
carbPS425	28.3	47.4	∞
carBP450	18.5	55.2	∞
carbTP450	14.9	48.9	∞
atmosphere		nitrogen	
carbenz500	23.7	57.2	∞
carbPS425	26.8	46.8	∞
carBP450	32.3	52.8	∞
carbTP450	15.2	50.2	∞

* - heating rate = 5°C/min.
† - heating rate = 10°C/min.
¥ - second pyrolysis stage done in static air
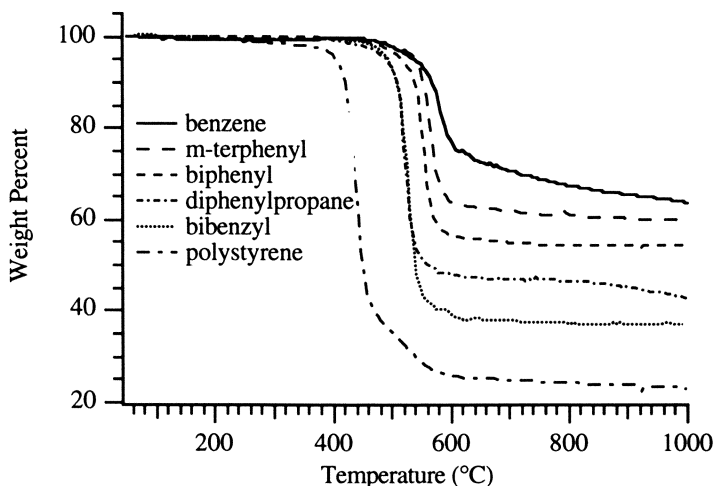§ - yield based on carbenz500

Figure 1. TGA of hypercrosslinked precursors.

Pyrolysis temperature was varied from sample to sample as seen in Table I. Initial attempts at pyrolysis was done at 500°C for all samples under vacuum. It appears that the optimum temperature for pyrolysis is related to the temperature at which the initial weight loss occurs in the TGA trace shown in Figure. 1. The closer the temperature is to this point, the more the precursor volatilizes leaving large voids in the foam. When the temperature is kept 25°C below this initial weight loss temperature there is uniform pyrolysis throughout the sample with a maximum retention of porosity. Much below this temperature there is an incomplete pyrolysis of the sample, even at longer soak times up to 24 hours. Although some Ambersorb resins are partially pyrolyzed (*28*), this avenue was not pursued. Incomplete pyrolysis was confirmed by both Fourier Transform Infrared (FTIR) analysis and NMR studies.

The atmosphere under which the pyrolysis was conducted was found to have a profound effect upon the properties of the resulting foam. The BET surface areas shown in Table I were at least an order of magnitude lower for all those samples that were pyrolyzed in either vacuum or nitrogen than those pyrolyzed in static air. Those that were heated in flowing air were reduced to ash. Degradation of crosslinked styrene/DVB leads to the formation of volatile by-products that are mainly styrene, but hydrogen, methane, ethylene, benzene, and toluene are also produced (*44*). As the samples are heated under a dynamic atmosphere the volatile compounds that result from degradation are then swept away from the foam. Whereas the volatiles that come off in a static atmosphere have the opportunity to redeposit themselves back onto the surface of the foam. Although there is a significant loss of surface area and porosity as the sample loses weight, the overall pore size distribution is retained. In order to clearly see this, one has to go to a log scale of the surface area as shown in Figure 2 for two carbonized benzene:DCX samples, one pyrolyzed in air and the other under a vacuum. Although the surface area for a given pore size is nearly two orders of magnitude lower for the vacuum pyrolyzed sample, the pore size distribution is comparable between 15 Å and 1,500 Å.

Heating rates of 1°, 5°, and 10°C/min. tended to provide foams with comparable surface areas and pore size distributions. The surface area for carbPS425, shown in Table I is a nominal 700 m²/g despite the difference in preparation times of
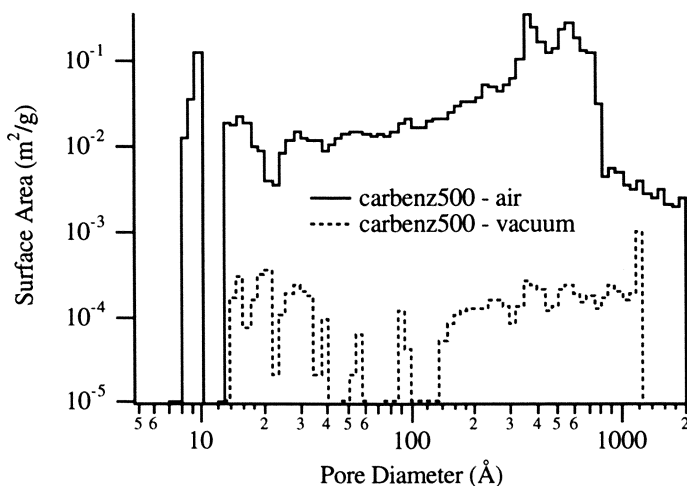
Figure 2. Pore size distributions for carbenz500 pyrolyzed under different atmospheres.

the carbonaceous foam. Similar behavior has is exhibited in the preparation of CMSfrom PVDC (*45*). CMS prepared with heating rates of 5° and 10°C/min. had pores which were nearly indistinguishable.

Two Stage Pyrolysis Preparation of graphitic carbon foams was also of interest. In order to do achieve graphitization, samples needed to be heated to temperatures in excess of 1,200°C. Although the temperature for graphitization could not be achieved in the furnace being used, it was of interest to investigate the dehydrogenation process of these materials. As mentioned earlier, samples that were heated to too high an initial temperature tended to form foams with very large pores. At these high initial temperatures the foam degrades at a rate where the degradation products volatilize rapidly enough to form these large pores at the expense of the initial architecture.

In an effort to pyrolyze these materials at higher temperatures, the hypercrosslinked precursor was first heated to a lower temperature where an optimum retention of pores was found. This generally involved pyrolyzing the foam in static air before subsequent high temperature pyrolysis. The use of multiple step temperature ramps is common in the preparation of CMS from PFA (*17*) or PVDC (*46*) to provide an optimum porosity. Similarly an oxidative, low temperature step is utilized to not only increase the porosity of the foam, but also to reduce shrinkage (*47*).

A series of carbenz foams was prepared, starting with carbenz500 pyrolyzed in static air. Benzene:DCX was initially chosen for high temperature pyrolysis due to its high char yield as exhibited by TGA. Carbenz500 retains over seventy percent of its porosity during the first pyrolysis step, as shown by retention of surface area in Table I. As the temperature of the second pyrolysis stage is increased from 600° to 1,000°C there is a gradual decrease in surface area from 484 m^2/g to 208 m^2/g. Char yield for these foams is high and weight loss alone does not account for the change in porosity. The DFT pore size distribution as a function of surface area shows a gradual decrease in the surface area for a given pore size with only a slight shift in overall distribution. Figure 3 shows transmission electron micrographs for benzene:DCX, carbenz500, and carbenz500/1,000. The white areas are the actual pores and the dark areas are
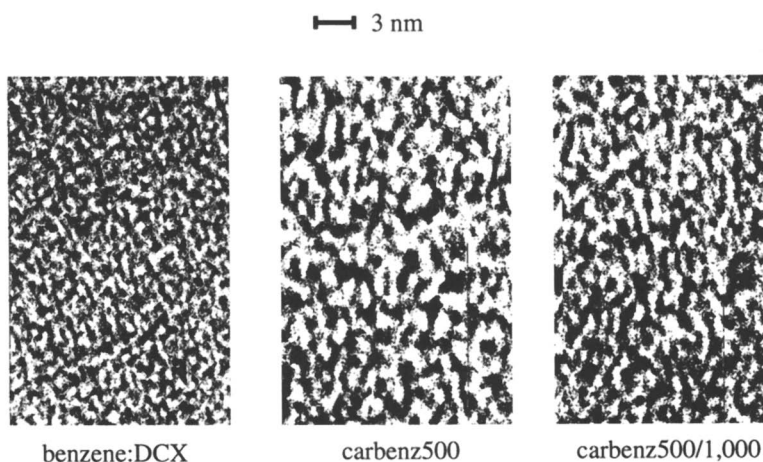
⊢—⊣ 3 nm

benzene:DCX   carbenz500   carbenz500/1,000

Figure 3. Transmission electrom micrographs of carbonized foams and
its precursor. (Scale bar = 3 nm for all micrographs)

either ruthenium tetraoxide stained foam or carbon foam.   Upon pyrolysis the size of
the pores increase in size, which is in agreement with nitrogen adsorption data. With
increasing temperature the pores decrease in size by both nitrogen adsorption and
TEM. This is due to a densification process that occurs a the carbon in the foams
undergo rearrangement. At temperatures above 500°C the aromatization process is
thermally driven by a loss of hydrogen thereby producing new carbon-carbon bonds.
As this process occurs there also is a loss in the sp^3 character of the system and an
increase in the sp^2 character. Further evidence of this is seen in the ^{13}C solid state
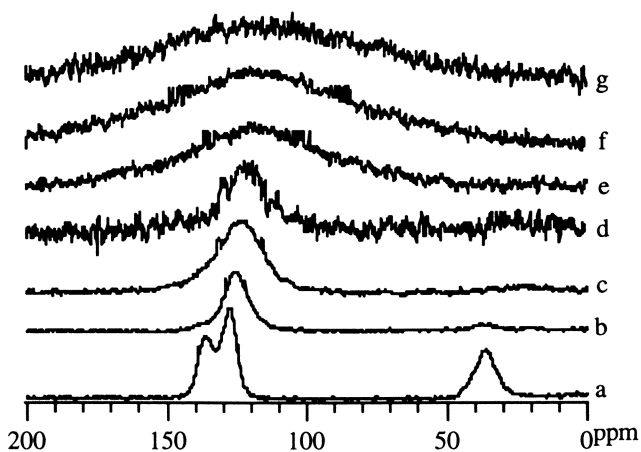spectra for the same series of foams, shown in Figure 4.

Figure 4. ^{13}C NMR spectra of: a) benzene:DCX, b) carbenz500,
c-g) carbenz500/600, 700, 800, 900, 1,000.

Acquisition of solid state NMR spectra was less than straight forward. As pyrolysis temperatures increased the conductance of the sample also increased. Not only was there a loss of protons to use for cross polarization purposes, but the signal was also being attenuated by the increased conductivity of sample. Spectra a-c were acquired using the CP-MAS technique with 1,000 scans. The number of scans was increased to 4,000 for the carbenz500/700 spectrum and also for the last two spectra where HPDEC was utilized. Sample response could be further enhanced by diluting the sample with a non-conductor, i.e. - glass beads.

There are three peaks in the spectrum of the starting material: 38 ppm, 128 ppm, and 138 ppm. The peak at 38 ppm can be attributed to the bridging methylene unit of the crosslinks. The latter two peaks are due to the aromatic moities of the foam, the upfield peak being a carbon with an attached proton, and the downfield peak a carbon attached to a bridging carbon. Two notable differences between the spectra of the starting material and the sample pyrolyzed at 500°C is the marked decrease in the intensity of peaks at 38 ppm and 138 ppm. Since these peaks correspond to carbons attached to hydrogen, this indicates that there is significant dehydrogenation occuring. Spectra obtained at lower temperatures still show a significant amount of hydrogen present in the system through 400°C. It is between 400° and 500°C that this dehydrogenation process occurs. Both the increase of aromaticity and the densification of the foam leads to the increase in conductance of the foam. Values for the conductance of these foams is given in Table I.

The hypercrosslinked biphenyl and its carbonized foams broke the trends observed in the other systems. The distributions for the biphenyl:DCX shown in Figure 5 is atypical for the hypercrosslinked system - a multimodal distribution with a maximum in the microporous regime of 10.4 Å and a maximum in the macroporous regime at 290 Å and 700 Å. Normally there is only one maximum in the macroporous region circa 700 Å to 1,000 Å, depending on the monomers used. As described earlier, the distribution for the vacuum pyrolyzed carBP450 is typical wherein the surface areas are two orders of magnitude lower with a fair retention of the pore size distribution. CarBP450 pyrolyzed in static air was the only low temperature foam to
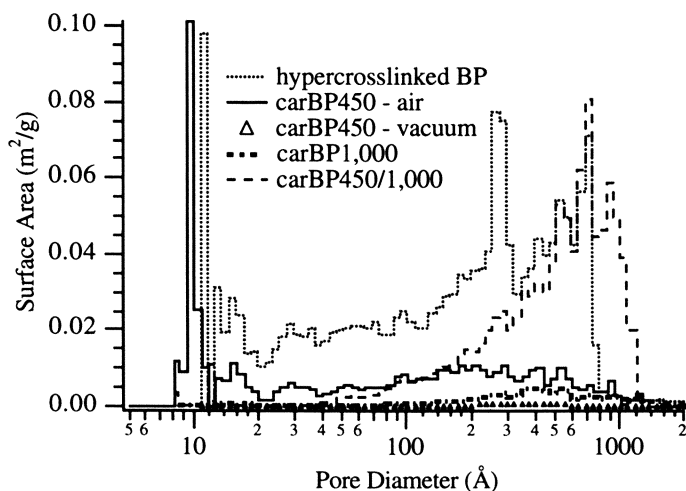

Figure 5. Pore size distributions for the hypercrosslinked biphenyl system.

show a decrease in the diameter of the micropores with a retention in surface area of the precursor. The corresponding decrease in the meso- and macropore surface area is typically observed during pyrolysis. The shift to larger pore diameters seen for carBP450/1,000 is typical during pyrolysis, however the retention of surface area is unusual. CarBP1,000 was the only sample to be ramped directly up to 1,000°C without the formation of a shiny silver balloon. This sample shrank only slightly and had a dull silver luster. The overall surface area and pore retention was greater than the sample heated to only 450°C in vacuum.

Conclusions

Hypercrosslinked polymers provide a matrix that is amenable to carbonization. Carbonaceous foams can be prepared with a wide variety of surface areas and pore sizes. These properties can be tailored not only by judicious choice of precursor but by pyrolysis conditions as well.

Acknowledgments

References

1. Sing, K.S.W.; Everett, D.H.; Haul, R.A.W.; Moscou, L., Pierotti, R.A.; Rouquerol, J.; Siemieniewska, T. *Pure Applied Chem.* **1985**, *57*, 603.
2. Foley, H.C. *Microporous Materials* **1995**, *4*, 407.
3. Fitzer, E.; Schaefer, W. *Carbon*, **1970**, *8*, 353.
4. Fitzer, E.; Schaefer, W.; Yamada, S. *Carbon*, **1969**, *7*, 643.
5. Walker, Jr., P.L.; Austin, L.G.; Nandi, S.P. In *Chemistry and Physics of Carbon*, Walker, Jr., P.L., Ed., Marcel Dekker, New York, NY, 1965, Vol. 2.
6. Mariwala, R.K.; Foley, H.C., *Ind. Eng. Chem. Res.*, **1994**, *33*, 607.
7. Kipling, J.J.; Sherwood, J.N.; Shooter, P.V.; Thompson, N.R. *Carbon*, **1964**, *1*, 321.
8. Spencer, D.H.J. In *Porous Carbon Solids*, Bond, R.L., Ed., Academic Press, London, 1967.
9. Kipling, J.J.; Wilson, R.B. *Trans. Farady Soc.*, **1960**, *56*, 557.
10. Kipling, J.J.; Wilson, R.B. *Trans. Farady Soc.*, **1960**, *56*, 562.
11. Dacey, J.R.; Thomas, D.G. *Trans. Faraday Soc.*, **1954**, *50*, 740.
12. Dacey, J.R.; Thomas, D.G. *Can. J. Chem.*, **1955**, *33*, 344.
13. Franklin, R.E. *Acta Crystallogr.*, **1950**, *3*, 107.
14. Franklin, R.E. *Proc. R. Soc. (London)*, **1951**, *A209*, 196.
15. Juntgen, H. *Carbon*, **1977**, *15*, 273.
16. Juntgen, H.; Knoblauch, K.; Harder, K. *Fuel*, **1981**, *60*, 817.
17. Mariwala, R.K.; Foley, H.C., *Ind. Eng. Chem. Res.*, **1994**, *33*, 2314.
18. Cabrera, A.L.; Zehner, J.E.; Coe, C.G.; Gaffney, T.R.; Farris, T.S.; Armor, J.N. *Carbon*, **1993**, *6*, 969.
19. Ohsaki, T.; Abe, S. *U.S. Patent 4,458,022*, **1984**.
20. Grant, R.J. *U.S. Patent 3,884,830*, **1975**.
21. Nandi, S.P.; Walker, Jr., P.L. *Fuel*, **1975**, *54*, 169.
22. Chihara, K.; Suzuki, M. *Carbon*, **1979**, *17*, 339.

23. Pekala, R.W.; Hopper, R.W. *J. Mater. Sci.,* **1987,** *22,* 1840.
24. Hulsey, S.S.; Poco, P.K. In *Novel Forms of Carbon,* Renschler, C.L.; Pouch, J.J.; Cox, D.M., Eds., MRS Symposium Proceedings Series ; Materials Research Society: Pittsburgh, PA, 1992; Vol. 270, 23.
25. Neely, J.W. *Carbon,* **1981,** *19,* **27.**
26. Winslow, F.H.; Baker, W.O.; Pape, N.R.; Matreyek, W. *J. Polym. Sci,* **1955,** *22,* 101.
27. Neely, J.W. *U.S. Patent 4,040,990,* **1975.**
28. Beasley, G.H.; Chong, B.P.; Ford, W. T.; Neely, J.W. *U.S. Patent 4,265,768,* **1981.**
28. Hager, J.W.; Lake, M.L. In *Novel Forms of Carbon,* op. cit., 29.
29. Dutta, D.; Hill, C.S.; Anderson, D.P. In *Novel Forms of Carbon II,* Renschler, C.L.; Pouch, J.J.; Cox, D.M.; Achiba, Y., Eds., MRS Symposium Proceedings Series ; Materials Research Society: Pittsbugh, PA, 1992; Vol. 349, 61.
30. Colton, J.S.; Suh, N.P. *Polym. Eng. Sci.,* **1987,** *27,* 493.
31. Colton, J.S.; Suh, N.P. *Polym. Eng. Sci.,* **1987,** *27,* 500.
32. Kumar, V.; Suh, N.P. *Polym. Eng. Sci.,* **1990,** *30,* 1323.
33. Grassie, N.; Meldrum, I.G. *Euro. Polym. J.* **1968,** *4,* 571 .
34. Patel,G.R.;Amin, P.T.; Patel,S.R. *J. Macromol. Sci. - Chem* **1982,** *A18(6),* 939 .
35. Grassie, N.; Gilks, J. *J. Polym. Sci: Polym. Chem.* **1973,** *11,* 1531 .
36. Davankov,V.A.; Rogoshin, S.V.; Tsyurupa, M.P. *US Pat. 3729457* **1969.**
37. Davankov,V.A.; Rogoshin, S.V.; Tsyurupa, M.P. *J. Polym. Sci.* **1974,** *47,* 95.
38. Steckle, Jr., W.P.; Mitchell, M.A.; Apen, P.G. *Polym. Materials Sci. Eng.,* **1996,** *74,* 344.
39. Steckle, Jr., W.P.; Mitchell, M.A.; Apen, P.G. In *Microporous and Macroporous Materials,* Lobo, R.F., et al., Eds.; MRS Symposium Proceedings Series ; Materials Research Society: Pittsbugh, PA, 1996; Vol. 431.
40. Brunauer, S.; Emmett, P.H.; Teller, E. *J. Am. Chem. Soc.* **1938** *60,* 309.
41. Horvath, G.; Kawazoe, K. *J. Chem. Eng. Japan* **1983** *16(6),* 470.
42. Barrett, E.P.; Joyner, L.S.; Halenda, P.P. *J. Am. Chem. Soc.* **1951,** *73,* 373.
43. Olivier,J.P.; Conklin, W.B.; Szombathely, M.V. *Stud. Surf. Sci. Catal.* **1994,** *87,* 81.
44. Hirasa, O. *Bulletin for Research Inst. for Polym. and Textiles,* **1976,** *112,* 11.
45. Barton, S.S.; Evans, M.J.; Harrison, B.H. *J. Colloid Interface Sci.,* **1974,** *49,* 462.
46. Adams, L.B.; Boucher, E.A.; Everett, D.H. *Carbon,* **1970,** *8,* 761.
47. Jenkins, G.M.; Kawamura, K. In *Polymeric Carbons,* 1976, Cambridge Univ. Press, Cambridge.

Preparation of Thermostable Rigid Foams by Control of the Reverse Diels–Alder Reaction During the Cross-Linking of Bis-nadimide Oligomers

L. Dutruch[1], M. Senneron[2], M. Bartholin[1], P. Mison[1], and B. Sillion[1,3]

[1] **Laboratoire des Matériaux Organiques à Propriétés Spécifiques, Centre National de la Recherche Scientifique, BP24–69390 Vernaison, France**
[2] **Institut Français du Pétrole, BP3–69390 Vernaison, France**

A new chemical approach using the polymerization of nadimide end-capped oligobenzhydrolimide (BBN) was found to produce rigid thermostable foams. Two BBNs with a theoretical molecular weight of 1000 and 1500 D were prepared. Under thermal curing (up to 300 °C), cyclopentadiene evolution takes place through a reverse Diels-Alder reaction during the gelation of the systeme (cross over of storage and loss moduli). To obtain good mechanical properties, BBNs were blended with 3% of linear thermostable polymers. Foams with density ranging between 50 to 400 kg/m^3 (3 to 25 lb/ft^3) were prepared. These materials exhibit low moisture uptake (2.5%) and an onset of decomposition at about 350 °C. Other interesting features of these materials are their insulating properties, non flammable character and good compressive strength up to 300 °C.

Various experimental approaches have been experimented to combine the thermal stability of the polyimide with a process leading to structural foams (1,2). Up to now, however, only linear polyimides have been used to prepare expanded materials according to different techniques, either based on chemistry or miscellaneous technologies.

The mechanical properties of such linear systems are limited by the polymer transitions. So, we aimed at obtaining expanded materials by using thermosetting polyimides. We found that during the curing of telechelic bis-nadimides, the cyclopentadiene which evolved from a side reaction can be used as a blowing agent.

The literature survey that follows covers briefly the two main ways used to prepare linear polyimide foams and the basic chemistry of end-capped nadimide oligomers used to develop our process.

[3]Corresponding author

37

Chemical reactions used for the preparation of polyimide foams

The cyclization of a polyamic acid can be carried out in solution by treatment with acetic anhydride and a tertiary amine. Oxalic acid introduced into the reaction medium is decomposed by acetic anhydride leading to carbon monoxide evolution which gives an insoluble foam (3).

The condensation of a tetracarboxylic dialkyl diester with a mixture of diamines in alcoholic solution gives a prepolymer powder after work up. Upon heating, a melt condensation takes place with water and alcohol evolution in the viscous medium to give the expanded material (4).

The reaction of a dianhydride with a diisocyanate leads to an unstable cyclic intermediate which evolves carbon dioxide during the gelation due to polyimide formation (5).

Copolyimides containing aromatic and aliphatic moieties can be obtained according to a substitution evolving ε-caprolactam during the melt condensation. This process was claimed for the production of expanded thermoplastic materials (6).

Linear polyimides carrying an hydroxyl group smoothly react with the tertiobutyl dicarbonate in γ-butyrolactone solution. The resulting solution of modified polyimide with a pending tert-butyl carbonate substituent is casted and the obtained film is dried. Upon heating to 250 °C, the carbonate group decomposes with evolution of carbon dioxide and isobutylene, both playing the role of blowing agent (7).

Some copolymers containing a thermostable polyimide block and a thermolabile block such as poly-α-methylstyrene or polypropylene oxide were prepared in solution and casted. During the film formation, a phase segregation takes place between the blocks. Upon heating the thermal decomposition of the labile block occurs to form low molecular weight products which evolve with formation of nanovoids in the films (8). Similar results were obtained when a labile phase was grafted on the polyimide backbone (9).

Polyimide foam formation using miscellaneous technologies

Syntactic foams were obtained when hollow glass microspheres were blended with a linear polyimide (10). Polyimide foams having non uniform density were chopped into flakes which were mixed with linear polyimide precursors. The blends were molded and cured to give another type of syntactic foams (11).

The thermal insulation and flame resistance of polyimide foams were improved by dispersion of inorganic particles like vermiculite or titane dioxide in the precursor (12).

An interesting approach is based on the impregnation of a reticulated thermally degradable foam such as polyurethane by a polyimide precursor in a mould. After curing of the polyimide, the reticulated thermolabile moiety was decomposed on heating below the degradation temperature of the polyimide. The low molecular weight products formed during decomposition of the polyurethane matrix are vaporized with formation of voids (13).

The formation of foams was also claimed by extrusion at 350 °C of a thermoplastic polyimide containing a blowing agent such as phthalic anhydride (14).

## Polymerization mechanism of nadimide end-capped oligomers

Since the seventies, telechelic imide oligomers with maleimide, nadimide or acetylene end caping groups were used as structural materials due to their better processability than the linear polyimide one (15). For example, bis nadimides (NAD) allow the preparation of composites with carbon fibers or clothes, which retain their mechanical properties up to 330 °C.

As early as 1971, Serafini *et al.* (16) suggested that the nadimide polymerization takes place through a reverse Diels-Alder (rDA) reaction forming maleimide (MAL) and cyclopentadiene (CDP) which could polymerize together. Later, Wilson *et al.* (17) and Ritchey *et al.* (18) confirmed the rDA mechanism but pointed out that CPD and MAL do not copolymerize ; they concluded that CPD reacts with NAD giving dicycloadducts (DCA), so the crosslinked network comes from the copolymerization of all insaturated species (MAL, NAD and DCA) (Scheme 1).

NAD   CPD   MAL

CPD   NAD   DCA

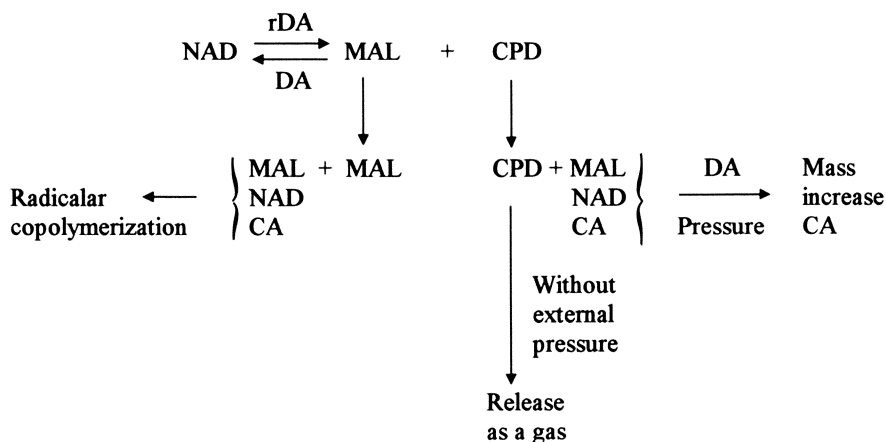Polymerization = MAL + NAD + DCA
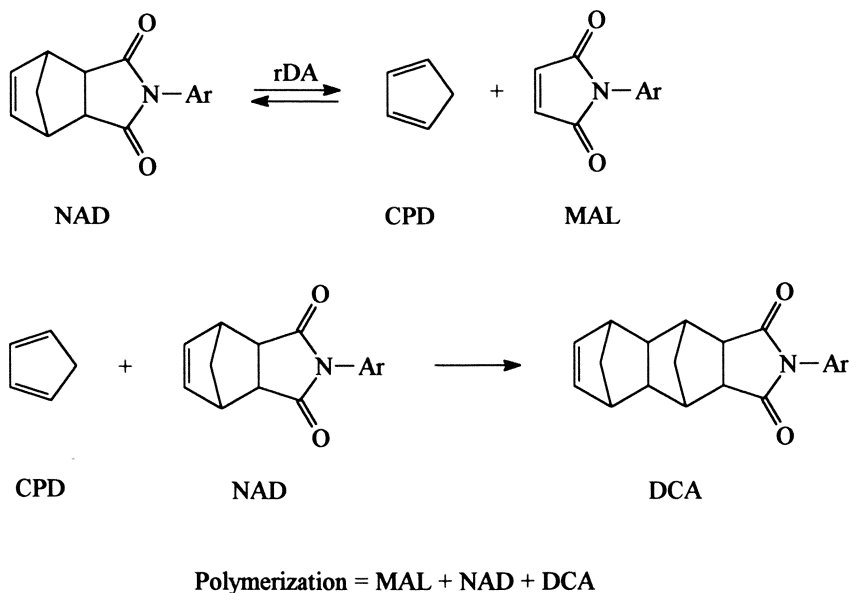
Scheme 1

The cyclopentadiene is a very low boiling point liquid and its controlled evolution during the nadimide thermal polymerization may act as a blowing agent. So, the thermal behaviour of the nadimide group was investigated in details in our laboratory. The rDA reaction occurs at temperatures as low as 160 °C (19) and is governing the endo (N) - exo (X) isomerization of the nadimide. The N-X isomerization starts as early as 180 °C even in the crystalline state (20). Mass spectrometry analyses allowed to determine the microstructure of a mononamide polymer obtained by curing at 310 °C under pressure (21). Each individual polymeric product contains MAL, NAD and polycycloadduct (PCA) (Scheme 2).
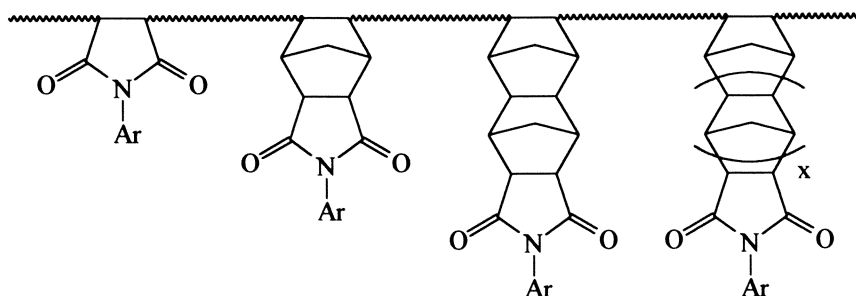
Scheme 2

From these results it was concluded that maleimide is always the polymerization initiator (Scheme 3).

$$\text{NAD} \underset{\text{DA}}{\overset{\text{rDA}}{\rightleftarrows}} \text{MAL} + \text{CPD}$$

Radicalar copolymerization ← { MAL + MAL / NAD / CA }   { CPD + MAL / NAD / CA }   → DA / Pressure   Mass increase / CA

Without external pressure

Release as a gas

Scheme 3

The first step is the rDA reaction. Reaction being carried out <u>under pressure</u> (in a sealed tube), the CPD recombines either with MAL or with NAD which is the major constituent of the medium ; but the CPD can also react with the produced cycloadducts leading to the polycycloadducts. Such a polydiene synthesis is limited by the radical polymerization initiated by maleimide (at around 200 °C) which is able to coplymerize in the molten state with all the cycloolefinic species available in the medium (Scheme 3).

In another respect, it was also established that at a given temperature, the CPD evolution is pressure dependent (20). The main conclusions of these studies are summarized in Table I.

According to these observations, a CPD evolution can be expected (as a function of both temperature and pression) during the melt polymerization <u>without external pressure</u> of an oligomeric bis nadimide.

Table I. Outstanding features of nadimide thermal polymerization mechanism

Temperature (°C)	Reaction features
160	rDA-DA equilibrium under kinetic control giving endo-nadimide alone (19)
180	rDA-DA equilibrium under thermodynamic control: formation of endo and exo nadimides (19) even in a crystalline state (20)
200	Maleimide coming from rDA initiates the polymerization process leading to the following structure $(MAL)_m (NAD)_n (CA)_p$ (21)
210	The cyclopentadiene may evolve with pressure dependent yields (20)

Experimental

Instrumentation

^{1}H NMR spectra were recorded on a Bruker DRX 400 using DMSO-d_6 solutions. Chemical shifts are given in ppm relative to internal tetramethylsilane (TMS). Size exclusion chromatography (SEC) analyses were carried out on a device equipped with a Waters 510 pump and a R 410 differential refractometer using THF as a mobile phase. The stationary phase was PSS gel mixed B (120 cm). Results are given relative to polystyrene standards. Thermal gravimetric analyses (TGA) were performed on a TG 209 Netzsch using 10-15 mg of the sample with a 10 °C.min^{-1} heating rate and in argon atmosphere. The complex viscosity (η^*) and shear modulus (G^*) were recorded on resin powders on a RMS 800 Rheometrics viscoelasticimeter equipped with two parallel plates. The sample thickness was 1.12 mm, the strain was 5 %, the rate was 2 rad.s^{-1} and heating rate was 10 °C.min^{-1}. The curves were recorded in the 200-330 °C temperature range. Thermomechanical analyses (TMA) were measured on TMA 40 Mettler. Heating rate was 5 °C.min^{-1} and penetrating strength was O.3 N. The scanning electron microscope (SEM) pictures were carried out with a JSM 35 Jeol at an accelerating voltage of 20 kV on various BBN foam specimens. Mechanical properties, such as compressive strength were measured using a 1175 Instron extensiometer. Flammability of the foams were determined according to the UL 94 standard.

Starting materials

Benzophenone tetracarboxylic dianhydride (BTDA) (Chemie Linz) treated with methanol at 50 °C for 4 hours gave a regioisomeric mixture of benzophenone tetracarboxylic diacid dimethylesters (BTDE). This mixture was hydrogenated using hydrogen and 5% palladium on charcoal (Engelhart) as a catalyst to form benhydrol tetracarboxylic diacid dimethyl esters (BHTDE) (mixture of isomers). Temperature was maintained below 30° C and the reaction was HPLC monitored and stopped when

about 95% of BTDE were transformed (*Ca.* 4 hrs). After filtration, the BHTDE was kept in solution, stored in a refrigerator and titrated before use.

4,4'-methylene diamiline (MDA) was used as received from BASF (reagent grade). Udel P 1700 N, a polyethersulfone was purchased from General Electric. 10312 Silicone, a polymethylphenyl siloxane was purchased from Rhône-Poulenc.

Preparation of α,ω-(oligobenzhydrolimide) bisnadimides of theoretical average molecular weight ($\overline{M}$) 1000 and 1500 D

The molecular ratio of the reactants were calculated for both theoretical molecular weight.

$\overline{M}$ = 1500 D	BHTDE	2.075 moles	M : 388
	MDA	3.075 moles	M : 198
	NE	2.00 moles	M : 196
$\overline{M}$ = 1000 D	BHTDE	1.047 moles	
	MDA	2.047 moles	
	NE	2.00 moles	

Nadic anhydride (Fluka) is dissolved into methanol (50% in weight) in a reactor equipped with a mechanical stirring and a nitrogen circulation. The solution was kept at 80° C for 4 hrs and after cooling the titrated solution of BHTDE was added. Then, the MDA was introduced, followed by the solvent (N-methyl pyrrolidone (NMP) or diglyme, concentration : 60 weight %). The solution was stepwise heated in order to remove methanol and finally kept at 140 °C (diglyme) or 160 °C (NMP). After cooling, the solution was poured into water and the precipitate filtered, washed five times with water. Powder drying was carried out in an oven under vacuum. Temperature and vacuum were stepwise increased to reach 160 °C and O.1 mbar respectively. Drying was monitored by ^{1}H NMR (total disappearance of the solvent proton signals at 3.3, 3.4 and 3.5 ppm for diglyme and 1.9, 2.2, 2.7 and 3.3 ppm for NMP.

For preparing the foams, BBNs were blended with 3 weight % of UDEL P 1700 N or 10312 SILICONE. The blending was performed in an NMP solution followed by precipitation in water and worked up as it was described for the unblended BBN.
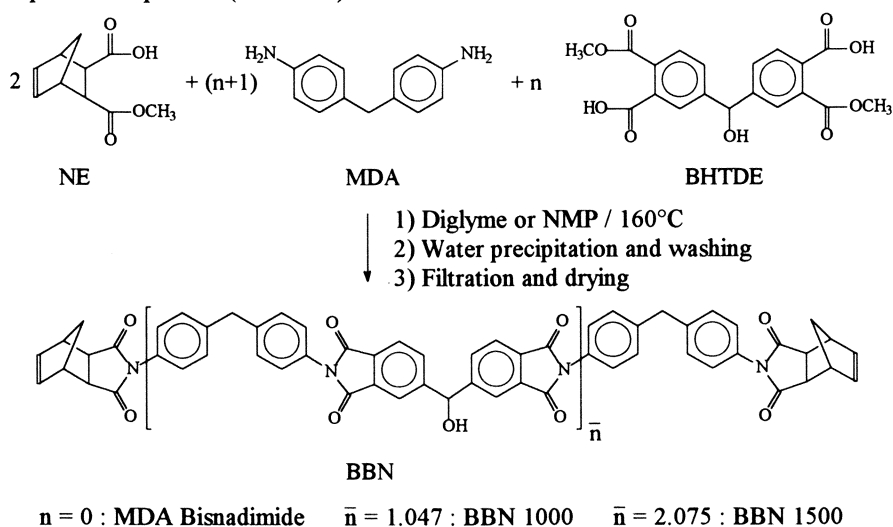
Safety

Preparation of BBN involves the 4,4'-diamino diphenylmethane (MDA) which must be handled according to the safety rules recommended for aromatic diamines. Toxical determination concerning the BBN 1500 were performed at International Center of Toxicology (CET) PO BOX 563 - 27005 EVREUX (France). Tests concerning skin sensitization, acute toxicity by dermal and oral route, primary eye irritation, reverse mutation (Ames test) allowed to conclude to the non-toxicity of BBN oligomers.

Results and Discussion

Bis-(oligobenzhydrolimides)-nadimide : preparation and characterization
The formation of expanded polymeric structure needs an optimal rheological behavior during the process. If the viscosity is too low, the foaming agent evolves without foaming effect ; if the viscosity is too high, the foaming agent does not evolve homogeneously. A thermosetting system creates an additional problem due to viscosity increase which is a function of the crosslinking extend. So a bis-nadimide candidate must exhibit a viscoelastic behavior when polymerization starts.

BBN is a soluble fully cyclized bis-nadimide which was used to develop high performance composites (22). BBN are obtained according to the following experimental process (Scheme 4).

NE   MDA   BHTDE

1) Diglyme or NMP / 160°C
2) Water precipitation and washing
3) Filtration and drying

BBN

n = 0 : MDA Bisnadimide $\bar{n}$ = 1.047 : BBN 1000 $\bar{n}$ = 2.075 : BBN 1500

Scheme 4

Benzophenone tetracarboxylic anhydride treated with methanol gave an isomeric mixture of dimethyl esters which was reduced by hydrogen using 5% palladium on charcoal as a catalyst. The regio-isomeric mixture of benzhydrol tetracarboxylic diacid dimethyl ester was then reacted with 4,4'-methylenedianiline and nadic acid monomethyl ester. The monomeric molar ratios were determined to obtain two oligomers with a theoretical polycondensation degree (n) of 2.075 (M : 1500 g/mol) BBN 1500 and 1.047 (M = 1000 g/mol) BBN 1000. The condensation and cyclization reactions were conducted in diglyme or N-methylpyrrolidone (NMP) solution with a 60 % (weight) concentration.

Structural characterization was done through NMR spectroscopy. Based on the signals of the methylene of MDA units, ^{1}H NMR spectroscopy allowed to determine the proportions of n = 0 and n = 1 species in the BBN resins. ^{1}H NMR spectrum of
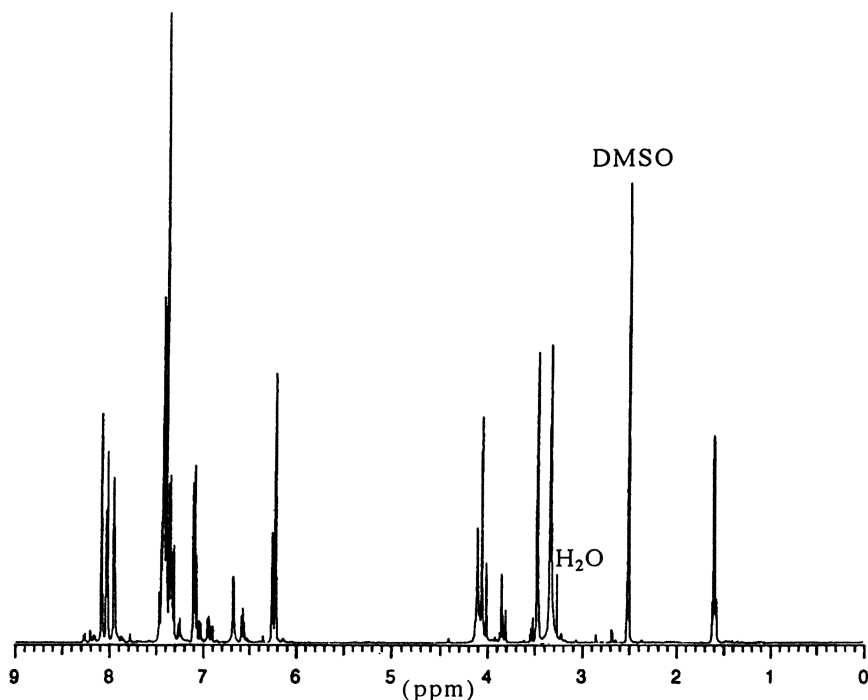
Figure 1: Dried BBN 1500 (Endo): ^{1}H NMR spectrum (500 MHz)

BBN 1500 showed that the oligomer mixture contains *Ca.* 40 % (molar) of bis-nadimide of MDA. The signal of the proton carried by the nadic groups allows to determine $\overline{M_n}$ (Figure 1).

Similar analyses were done with BBN 1000 (Figure 2).

These results were confirmed by the size exclusion chromatography (SEC) analyses which gave an $\overline{M_n}$ of 1492 for the BBN 1500 and an $\overline{M_n}$ of 860 for the BBN 1000 (Figure 3).

It was demonstrated from the thermogravimetric analyses (TGA) (coupled with a mass spectrometer) of the BBN 1500 powder (Figure 4) that the onset temperature of the cyclopentadiene evolution is around 270 °C and the maximum one is 300 °C.

The rheological profile of BBN 1500 powder obtained as a function of temperature (Figure 5) indicates a viscosity minimum around 275 °C and a crossover of the loss and storage module curves near 300 °C.

From these two kinds of measurements it is shown that the maximum rate of cyclopentadiene evolution is taking place at a temperature very close to the gel point one. So, such a controlled evolution of cyclopentadiene can be used for the preparation of foams.

H₂O

DMSO

x

x x

x residual NMP

ppm	8	7	6	5	4	3	2	1	0
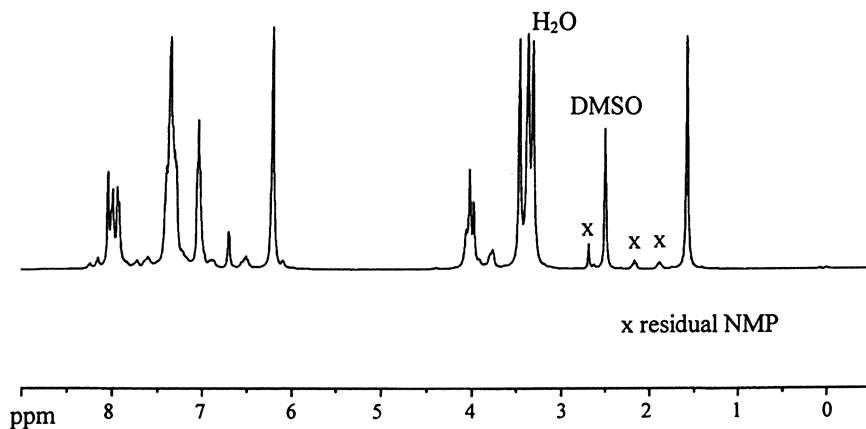
Figure 2: Dried BBN 1000 (Endo): ^{1}H NMR spectrum (400 MHz)

BBN 1500

$\overline{M}n$ 1377
$\overline{M}w$ 2471

$\overline{M}w/\overline{M}n$ 1.79

dN

34 35 36 37 38 39 40 41 42   Ur(ml)
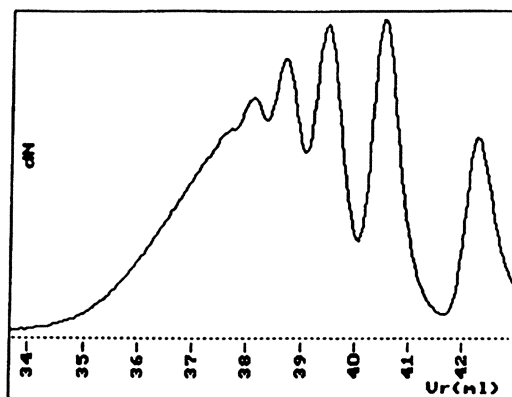
BBN 1000

$\overline{M}n$ 860
$\overline{M}w$ 1261

$\overline{M}w/\overline{M}n$ 1.47

dN

36 37 38 39 40 41 42   Ur(ml)
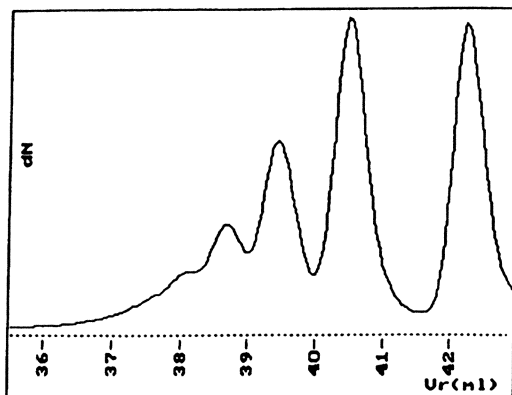
Figure 3: Size exclusion chromatography of BBN 1500 and BBN 1000
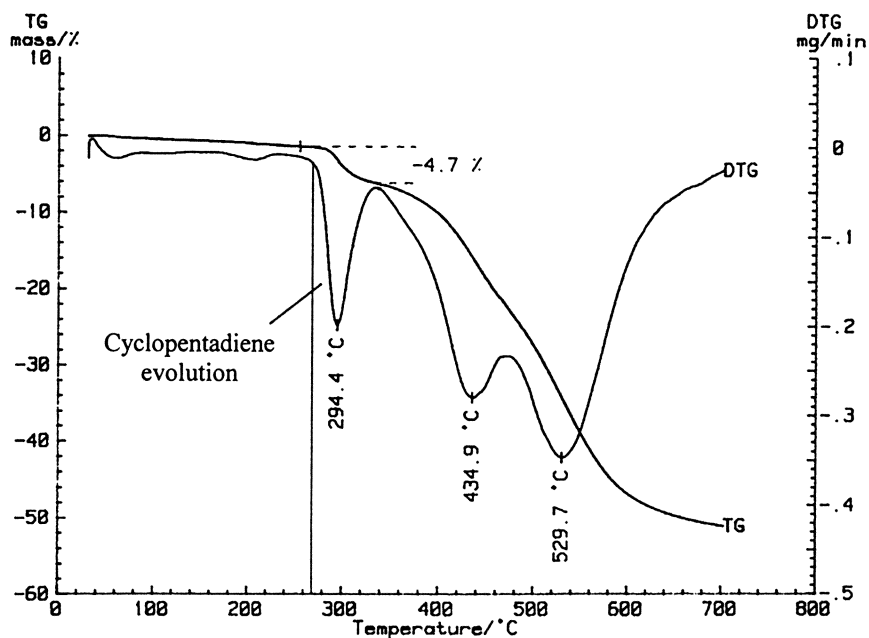
Figure 4: TGA and DTG analysis of BBN 1500
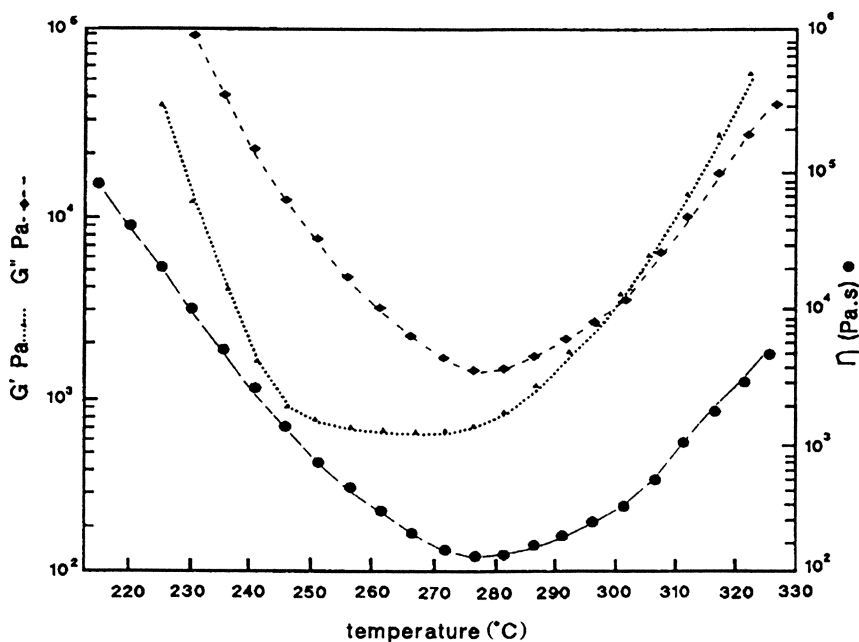
Figure 5: Rheological analysis of BBN 1500

Foam formulation and preparation

Foams were prepared in an aluminium mould (Figure 6). The weight of the powder and the volume of the mould control the foam density. The neat BBNs or the blended BBNs (with 3 weight % of UDEL or SILICONE) thoroughly dried were put on the bottom of the mould which is introduced into a preheated oven at 300 °C and left at this temperature for 7 hrs.

The foams prepared from the neat BBN 1500 and BBN 1000 were very brittle and it was not possible to measure any mechanical property. The bad toughness of the highly crosslinked rigid networks is a well known behavior. However, it was demonstrated that the fracture toughness of a crosslinked nadimide can be improved by blending with a linear aromatic polymer. The resulting semi-interpenetrated (semi IPN) network improves the mechanical properties without detrimental effect on the thermal stability (23).

This concept was applied for the foam preparation but in order to avoid an important increase in the melt viscosity, both thermoplastic polymers (UDEL and SILICONE) were used at low concentration. Viscosities determined at 264 °C are given in Table II.

It can be pointed out that introduction of linear polymers does not affect significantly the melt viscosity. On the other hand, the lower viscosity of the BBN 1000 can be adjusted by a precure at 255 °C (below the cyclopentadiene evolution).

Foams properties

Different foams with a density ranging from 50 to 400 kg/m^3 (3 to 25 lb/ft^3) were prepared from BBN 1000 and BBN 1500 blended with a polyether sulfone or a polysiloxane.

Aluminium plates
4 mm thick

Aluminium angle
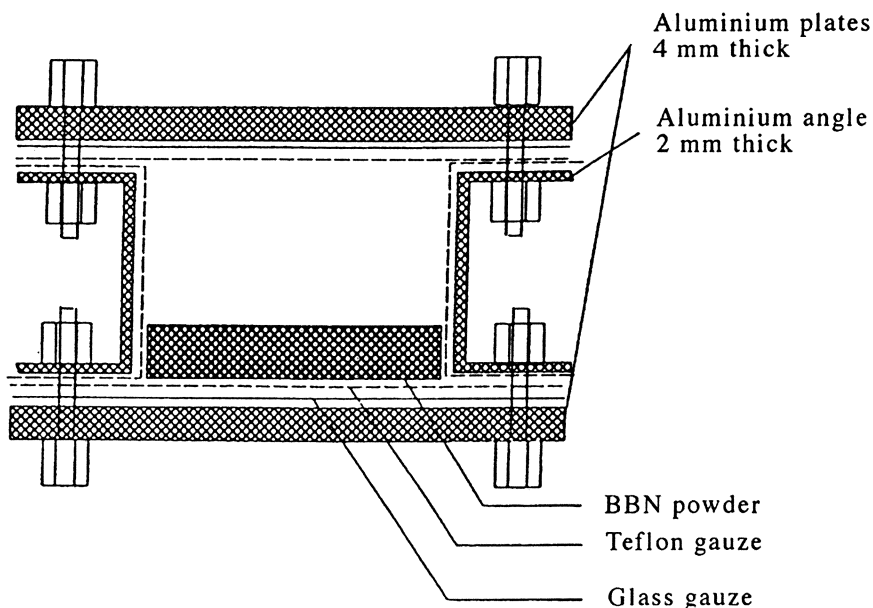2 mm thick

BBN powder

Teflon gauze

Glass gauze

Figure 6: Mould used to prepare BBN foams

Table II. BBN 1000 and BBN 1500 melt viscosity before curing and glass transition after curing

BBN type	Added linear polymer	Viscosity at 264 °C	Viscosity after precure at 255 °C (MPa.s⁻¹)		Foam glass transition after curing[1]
	(weight %)	(MPa.s⁻¹)	1.5 hrs	4 hrs	(°C)
1500	-	300	-	-	300-310
1000	-	5	-	-	320-330
1500	UDEL P1700N (3%)	380	-	-	310
1500	Silicone 10312 (3%)	160	-	-	310
1000	Silicone 10312 (3%)	5	80	300	320

[1] 300 °C for 7 hrs

The morphologies of the foams can be observed by scanning electron microscopy. In Figure 7 is shown the picture of three foams with different densities : the cell size distribution is more homogeneous for the highest foam density. For that foam, the average diameter cell size is in the range of 200 micrometers.

The foam glass transitions are given in Table II. For each system, only one Tg was observed ; however due to the low concentration of the linear polymer, it is not possible to assume that the bis-nadimide thermoset and the linear polymer are miscible. In another respect, as expected the lowest molecular weight BBN led to the foam with the highest Tg. The moisture uptake as a function of time (Figure 8) shows that the equilibrium is reached after less that 2 hrs and only 2.5% of water is absorbed. The same moisture uptake was observed for the BBN crosslinked powder. The water is fastly desorbed by heating, as shown by TGA determination (Figure 9) and the onset of decomposition occurs at about 350 °C. A similar behavior was observed for all types of foam coming either from BBN 1500 or BBN 1000. The thermal conductivity between 25 and 250 °C of the BBN 1500-UDEL foams are ranging from 0.05 to 0.11 W/(m.K).

A comparison of the compressive strength as a function of the density in the case of a BBN 1500 toughened either with UDEL or with SILICONE showed a similar behavior for both materials (Figure 10) and the foam with a density of 300 kg/m3 exhibits an interesting compressive strength up to 300 °C (Figure 11), probably due to the high Tg of the crosslinked BBN.

Density: 106 kg/m^3 Density: 140 kg/m^3
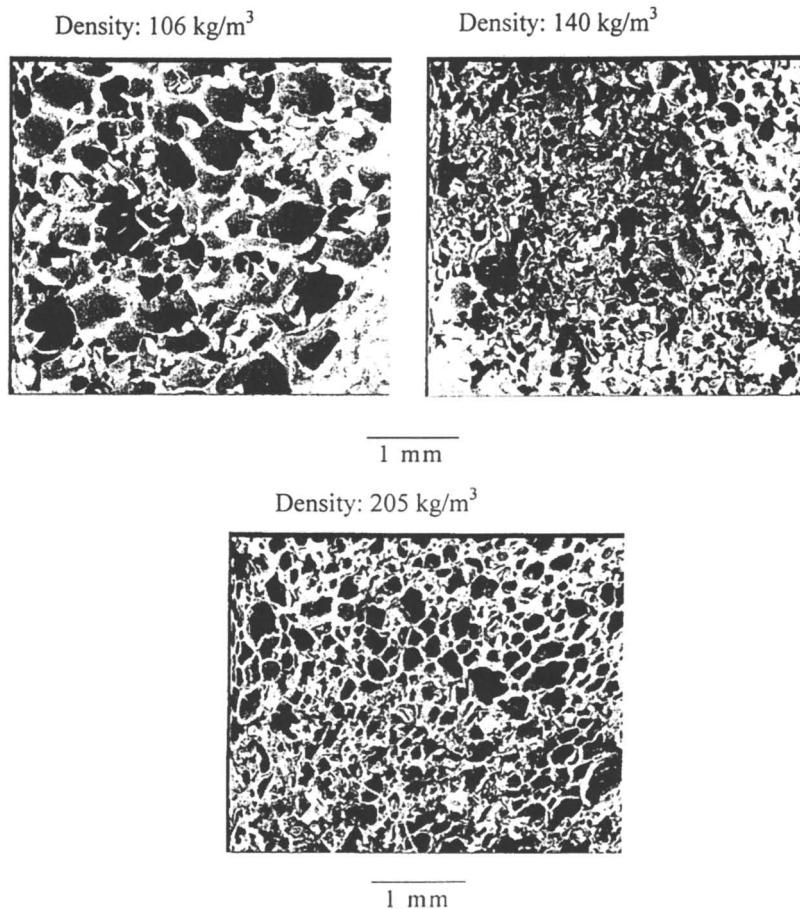
1 mm

Density: 205 kg/m^3

1 mm

Figure 7: Scanning electronic microscopy of various densities foams (3 % silicone 10312 BBN 1500)
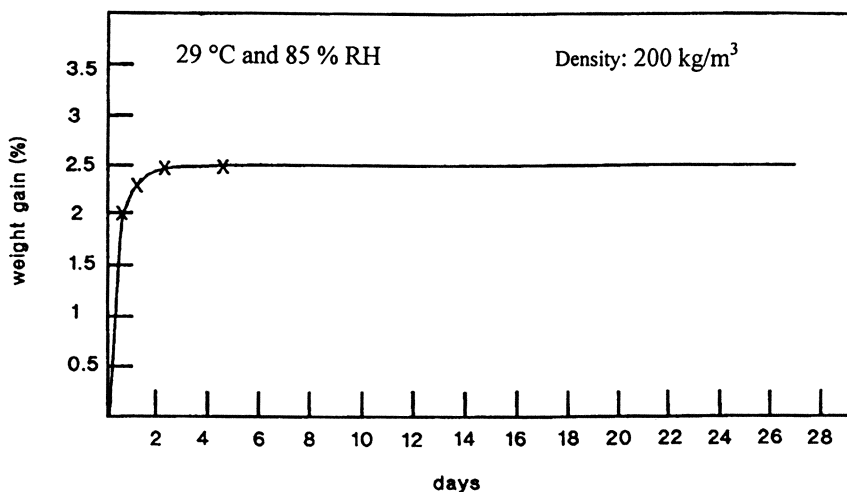
Figure 8: Moisture uptake versus time for 3 % silicone 10312 BBN 1500
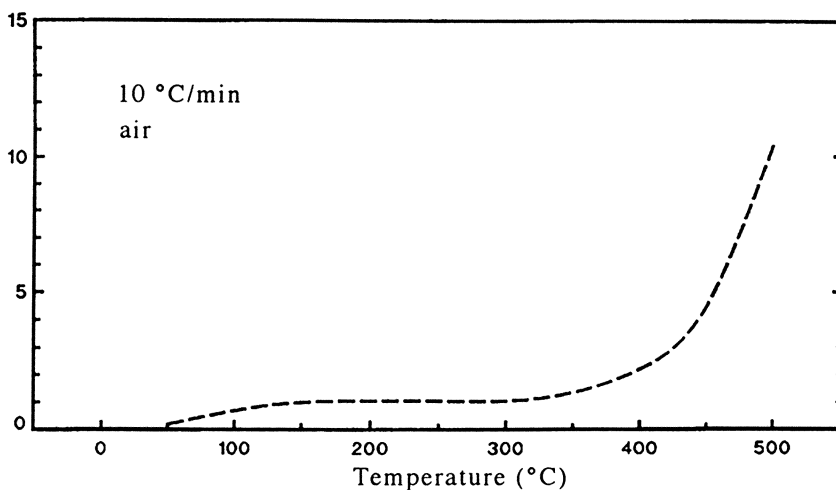
% weight loss

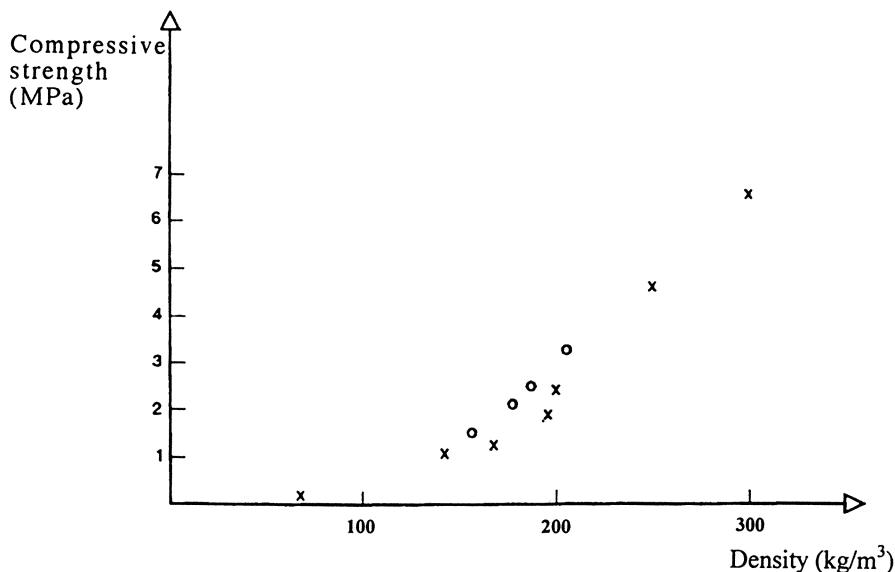Figure 9: Polyimide foam thermogravimetry of 3 % UDEL P1700N BBN 1500 foam (density: 200 kg/m^3)

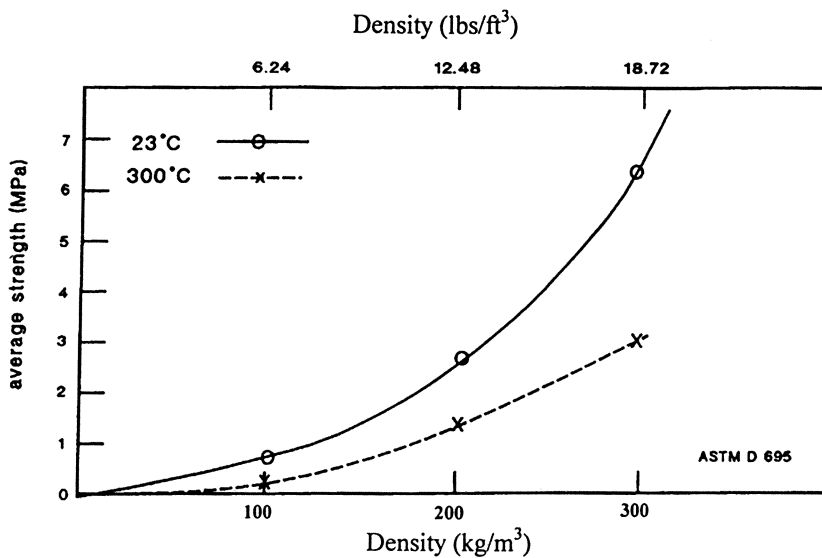Figure 10: Compressive strength versus density for 3 % UDEL P1700N (o) and 03 % silicone 10312 (x) BBN 1500 foams

Figure 11: Compressive strength versus density at 23 °C (o) and 300 °C (x) for 3 % silicone 10312 BBN 1500 foams
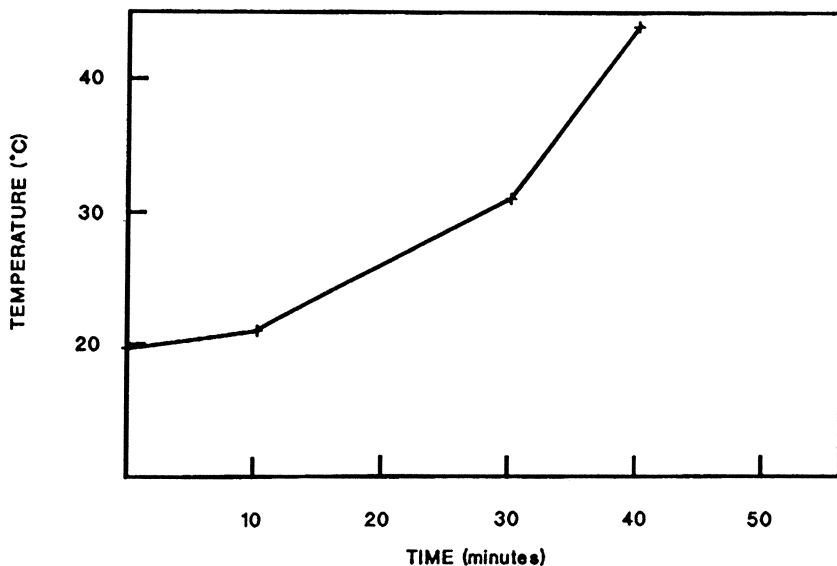
Figure 12: 3 % silicone BBN 1500 foam (density: 300 kg/m^3): backside sample temperature versus time (flame distance 135 cm)

The flame proof character and the insulating properties of a material with a density of 300 kg/m^3 was evidenced, using the following test : a 6 cm thick specimen was put in front of a burned flame at 850 °C ; after 40 min the face in front of the flame was black, but unburned, and the backside temperature was only 40 °C (Figure 12). Using the same conditions, a phenolic foam gave similar results.

Conclusions

The polymerization features of the nadimide end-capped benzhydrolimide oligomers offer the possibility of preparing thermostable crosslinked foams. A small quantity of gazeous cyclopentadiene produced by a side reaction evolves during the gelation of the network and plays the role of an *in situ* generated blowing agent.

The foams were prepared according to a very simple process based on the heating of a powder containing 97 % of BBN and 3 % of linear polymer. The density of the foam is only governed by the weight of the precursor and the volume of the mould.

The non-flammable foams exhibit nice insulating character and retain their mechanical properties up to 300 °C.

References

1. Hardy, E.E.; Saunder, J.H. In *New high temperature resistant plastic foams*; Frisch K.C.; Saunder J.H.,Eds.; Marcel Dekker, New York, New York, **1973**, chapter 14
2. Ashida, K.; Iwazaki, K. In *Handbook of plastic foams;* Landrock, A.H.,Ed.; Noyes Publication, Park Ridge, New Jersey, **1995**, pp 117-120
3. Hendrix, W.R. *U.S. Patent* 3249561 , **1968**
4. Gagliani, J. ; Supkis, D. *Acta Astronautica,* **1980,** *7,* 653
5. Roger, R.W. *U.S. Patent* 3772216, **1973**
6. Gagliani, J.; Long, J. *U.S. Patent* 4394464, **1983**
7. Sillion, B.; Rabilloud, G.; Garapon, J.; Gain, O.; Vallet, J. In *Low dielectric constant materials -Synthesis and application in microelectronics;* Lu, T.M.; Murarka, S.P.; Kuan, T.S.; Ting, C.H.,Eds.; Material Research Society ; Pittsburgh, Pennsylvania ; **1995,** *381,* pp 93-104
8. Carter, K.R.; Cha, H.J.; Dipietro, R.A.; Hawker C.J.; Hedrick, J.L.; Labadie, J.W.; Mac Grath ,J.E.; Russel, T.P.; Sanchez, M.I.; Swanson, S.A.; Wolksen, W.; Yoon, D.Y. In *Low dielectric constant materials - Synthesis and application in microelectronics;* Lu, T.M.; Murarka, S.P.; Kuan, T.S.; Ting, C.H.,Eds.; Material Research Society ; Pittsburgh, Pennsylvania ; **1995,** *381,* pp 79 - 91
9. Jayaraman, S.; Srinivas, S.; Wikes, G.L.; Mac Grath, J.E.; Hedrick, J.L.; Wolksen, W.; Labadie, J. *Polymer Preprints,* **1994,** *35(1),* 347
10. Farrissey, W.J.; Rauch, K.W., *U.S. Patent* 4077922, **1978**
11. Hill, F. *U.S. Patent,* 4923651, **1990**
12. Hill, F. *U.S. Patent,* 4978690, **1990**
13. Hill, F. *U.S. Patent,* 5135959, **1992**
14. Ezawa, H.; Nakakura, T.; Watanabe, T.; Tsushima, H. *Eur. Patent Appl.* E.P. 376592, **1990**
15. Sillion, B. In *Comprehensive Polymer Science*; Eastmond, G.C.; Ledwith, A.; Russo, S.; Sigwalt, P., Eds ; Pergamon Press, Oxford, U.K., **1988**, *Vol. 5,* pp 499 - 532
16. Serafini, T.T.; Delvigs, P. *Appl. Polym. Symp.*, **1973**, *22,* 89
17. Hay, J.N.; Boyle, J.D.; Parker, S.F.; Wilson, D. *Polymer,* **1989,** *30,* 1032
18. Wong, A.C.; Garroway, A.N.; Ritchey, W.H. *Macromolecules,* **1981,** *14,* 832
19. Bertholio, F.; Mison, P.; Pascal, T.; Sillion, B. *High Performance Polym.,* **1993,** *5,* 47
20. Laguitton, B.; Mison, P.; Pascal, T.; Sillion, B. *Polym. Bull.,* **1995,** *34,* 425
21. Damerval, V.; Mison, P.; Sillion, B. *4th European Tech. Symp. on Polyimide and other high performance polymers ;* Abadie, M.J.; Sillion, B., Eds; **1996,** in press
22. Malinge, J.; Rabilloud, G.; Sillion, B.; Garcin, C.; Bardin, I.; Berthier, J.M. In *Looking ahead for material and processes*; Bossu, J.; Briens, G.; Lissac, P., Eds., Elsevier; Amsterdam, Nederland, **1987**, p 455
23. Pascal, T.; Sillion, B. In *Advances in interpenetrating polymer networks;* Klempner, D.; Frisch, K.C.,Eds; Technomic, Lancaster, Pennsylvania, **1994,** *Vol. 4,* pp 141 - 190

Chapter 5

Extruded Polyester Foams

Kishan C. Khemani

Research Laboratories, Eastman Chemical Company, 200 South Wilcox Drive, Kingsport, TN 37662

An overview of the physical aspects of the fundamental requirements for extrusion foaming a polyester resin is presented along with a discussion of the various proven methods as reported in the literature. This is followed by a discussion of some newer methods of rendering polyesters foamable developed in more recent years. These include the use of monomeric and polymeric branching agents, and of polymeric concentrates containing monomeric branching agents. For foamed polyesters, the extractable issue which is particularly relevant for food packaging applications, is also addressed and some ways to reduce the level of these extractions / migrations of the additives in the food items are discussed and demonstrated.

Polyester foams have been the subject of intense curiosity and discussion for over a decade now. As evidenced by increased research and development activity in several academic and industrial institutions, interest in this field has been steadily growing.

Polyesters such as poly(ethylene terephthalate) (PET) have a much higher density (e.g. about 1.33 g/cc) than many other polymers. Therefore, it is desirable to be able to foam polyester materials to decrease the weight of molded parts, films, sheets, food trays, and the like. These foamed articles would also have better insulating properties than unfoamed articles. Interest in Polyester foam is also driven by its potential in niche markets (particularly in the food packaging industry) which require potential recyclability and high-temperature capabilities that the unfoamed polyesters provide. Such markets could include current CPET (crystallized PET) markets (which has lately seen volume erosions to other packaging products such as the coated paperboard), the deli and meat tray markets requiring ovenability and microwavability, the bake-in packaging market (for muffins, doughnuts, pizzas, cakes etc.), and more recently in the modified and controlled atmosphere packaging markets (for improving the shelf lives of fresh meats, salads, fruits, vegetables, baked goods and pre-cooked pastas etc.). It is estimated that the total market potential for foamed

54

polyester in food packaging may be a moderate 15-20 million pounds per year (*1*). Other markets such as the automotive and the construction industries is a distinct possibility as well, but may be hard to penetrate due to the presence of other well established products such as foamed polystyrene, polyurethane, polyvinyl chloride, polyethylene, phenolics and ABS. For the sake of discussion in this paper, two specific product grades may be arbitrarily defined as the medium density polyester foam (having a density reduction of 20-55%, i.e. to 0.6-1.1 g/cc) and the low density polyester foam (having a density reduction of 55-98%, i.e. to 0.03-0.6 g/cc). Of course, different markets would require one or the other of these grades of foams, and/or an intermediate grade, or even a combination thereof, as in a co-extruded or laminated foamed article.

An additional point of interest and importance for polyester foams, made for food packaging applications in particular, is that these foamable compositions should be made with any added additives which either do not extract at all or are extracted in extremely low levels into the packaged food products under the intended use conditions and thus meet the established regulatory guidelines. Obviously, such leaching or migration of any chemicals into the food items is extremely undesirable.

Background

General Difficulties. The task of extrusion foaming of any polymeric material is not easily achieved. It is difficult to foam polyesters in particular because of their crystalline nature, low melt viscosity and low melt strength. The polyester melt is thus incapable of effectively retaining the bubbles of an expanding blowing agent. The high melting points of polyesters is an additional disadvantage, since they do have a known propensity to thermal (Scheme 1) (*2-7*) and/or thermo-oxidative degradation (Scheme 2) (*8-11*) at very high processing temperatures (temperatures of 260-290°C is typically used for the extrusion processing of most polyesters). The ultimate outcome of all of these degradation routes is the loss of molecular weight and the formation of the various by-products identified in these two schemes. It is therefore desirable to be able to provide polyester compositions which are more stable and could be foamed easily and preferably using the conventional foaming systems.

How Does One Approach? Scheme 3 summarizes the overall resin, nucleation, blowing agent, as well as equipment (extruder, die and screw) requirements for producing a polymeric foam via the extrusion process (*12*). Some important Thermoforming and Recycle/Regrind issues are also captured in this comprehensive scheme. Under each heading is listed what are considered the attributes necessary for successful extrusion foam production. The key properties of the foam which are directly affected by the materials/processing requirements are listed under the subtitle Foam Responses. This scheme shows that extrusion foam production and processing is at best a very complex operation. The material requirements are obviously central to the whole foaming issue and will be dealt with in some detail for polyesters and copolyesters in this chapter, following a brief discussion of the other necessary parts of a foaming technology such as the cell nucleators, blowing agents and of course, the equipment.
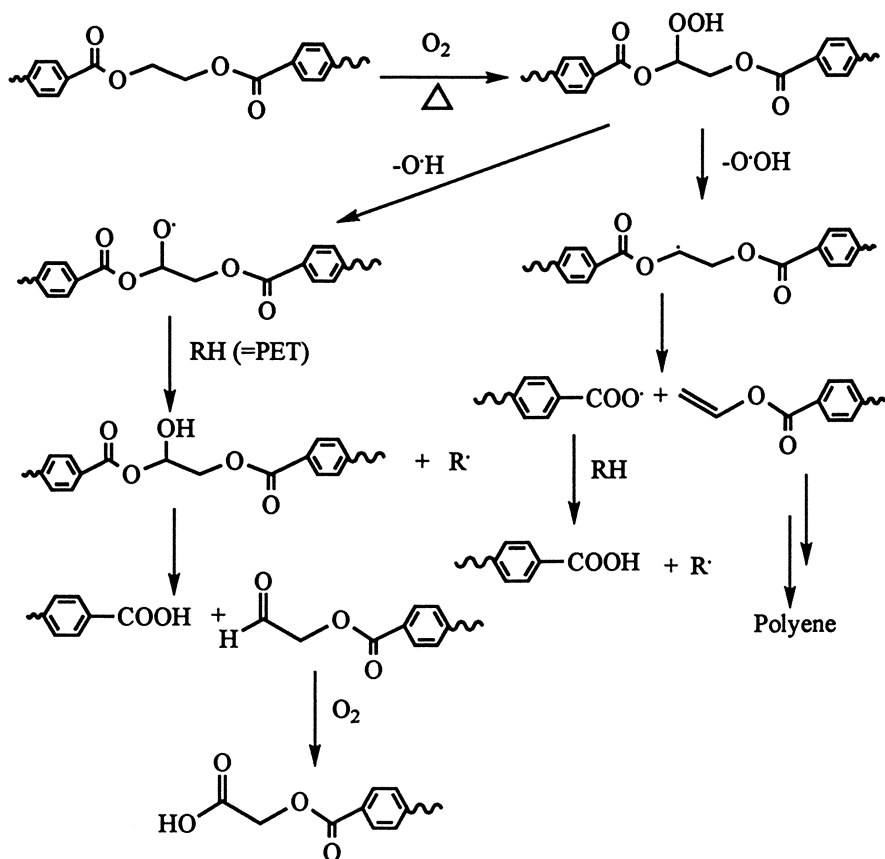
Degradation at the end of a chain:
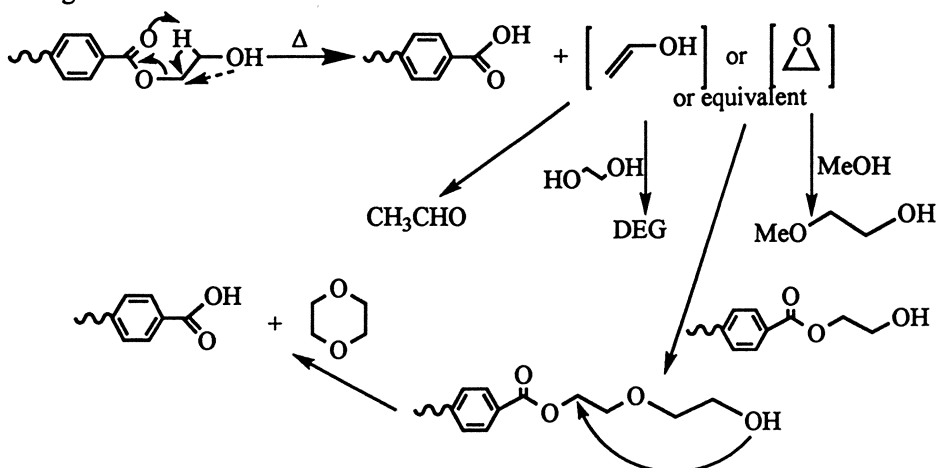
Degradation in the middle of a chain:

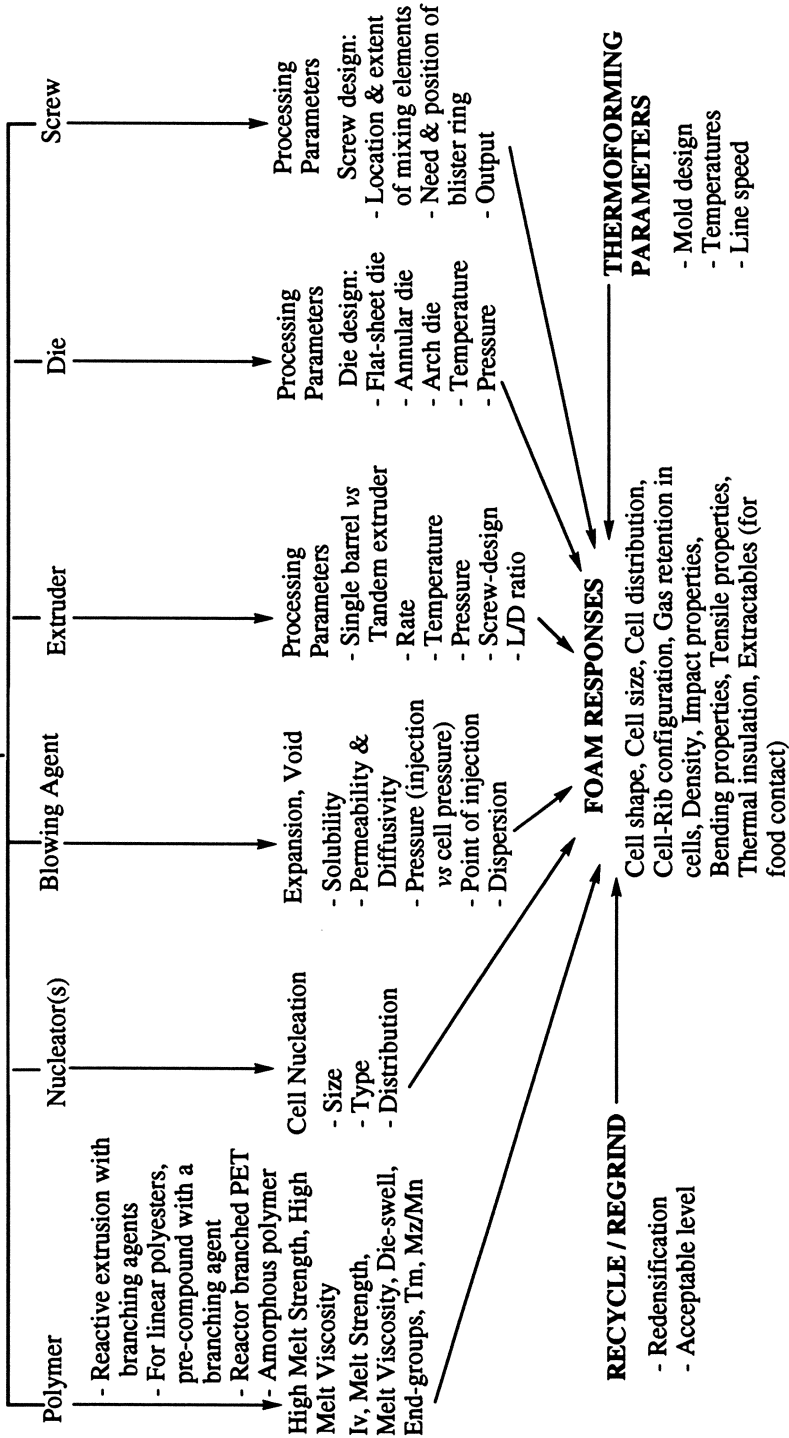EG or DEG or their half-esters or H_2O etc.
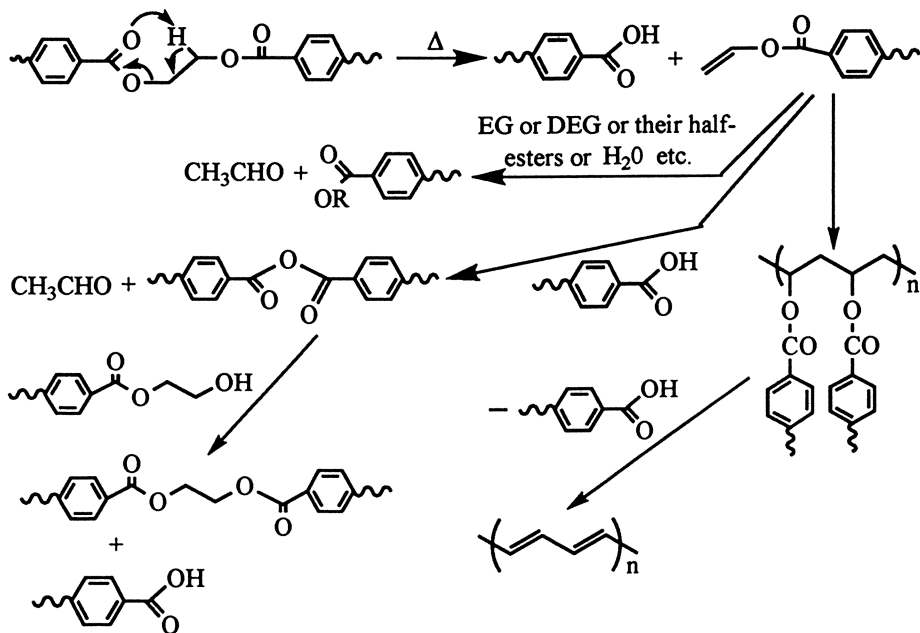
Scheme 1: Thermal Degradation routes for Polyesters

Scheme 2: Thermo-Oxidative degradation of Polyesters

Scheme-3: How to make extruded polymeric foam?

Polymer
- Reactive extrusion with branching agents
- For linear polyesters, pre-compound with a branching agent
- Reactor branched PET
- Amorphous polymer

High Melt Strength, High Melt Viscosity

Iv, Melt Strength, Melt Viscosity, Die-swell, End-groups, T_m, M_z/M_n

Nucleator(s)

Cell Nucleation
- Size
- Type
- Distribution

Blowing Agent

Expansion, Void
- Solubility
- Permeability & Diffusivity
- Pressure (injection *vs* cell pressure)
- Point of injection
- Dispersion

Extruder

Processing Parameters
- Single barrel *vs* Tandem extruder
- Rate
- Temperature
- Pressure
- Screw-design
- L/D ratio

Die

Processing Parameters

Die design:
- Flat-sheet die
- Annular die
- Arch die
- Temperature
- Pressure

Screw

Processing Parameters

Screw design:
- Location & extent of mixing elements
- Need & position of blister ring
- Output

THERMOFORMING PARAMETERS
- Mold design
- Temperatures
- Line speed

FOAM RESPONSES

Cell shape, Cell size, Cell distribution, Cell-Rib configuration, Gas retention in cells, Density, Impact properties, Bending properties, Tensile properties, Thermal insulation, Extractables (for food contact)

RECYCLE / REGRIND
- Redensification
- Acceptable level

Cell Nucleators. The shape, size and distribution of the voided cells in the foam is a direct consequence of the type, size, and distribution of the cell nucleator used in foam production, and thus the choice of the cell nucleator is very important. It is especially so due to the fact that the physical properties of the foam are heavily governed by its cellular structure. Some examples of cell nucleators more commonly used in the foam industry are microfine talc, TiO_2, fumed silica etc.. Chemical blowing agents are also often used in conjunction with the gaseous blowing agents, since their decomposition by-products act as *in-situ* nucleation sites often resulting in finer cellular structure in the final product.

Blowing Agents. Choosing the right blowing agent gas is important. The three key properties to consider with respect to the resin being foamed are the solubility, permeability and diffusivity of the gas in the polymer being foamed under the foam processing conditions. Other factors to be considered include the location of the gas injection port, the gas injection pressure and its ease of dispersion in the melt, and the operating extruder pressure. The combination of all of these factors dictates the equilibrium conditions in the gas laden melt at the extrusion temperature. Suitable physical blowing agents for foaming of polyesters include inert gases, such as N_2, CO_2; volatile hydrocarbons having boiling points between -40°C to +45°C, such as propane, butane and *i*-pentane; and, HFC's and HCFC's. Mixtures of blowing agents can also be used. Blowing agents are typically used in small amounts ranging anywhere from 0.1 wt% to 5 wt% depending upon the required degree of foaming. Chemical blowing agents have also been used as discussed later in this chapter.

Equipment Considerations. The three most important parts of any foam extrusion technique commonly used to foam polymers include a suitable extruder, a screw and a die. Normally the desired attributes of a particular foam product would dictate certain specific equipment requirements. Some important processing parameters with respect to the extruder, screw and die are listed in Scheme 3.
A simple equipment set-up for a foam extrusion process consists of a single extruder, preferably one having a high length to diameter ratio (L/D of 30:1 or more), a liquid or gas blowing-agent injection system consisting of a pump or a pressurized gas cylinder with injector valves, a die to shape the foam, a cooling unit such as a mandrel and a take-up system to collect the extruded foamed product. In such a process typically a two-stage screw, and a flat-sheet die is used. A schematic of this set-up is shown in Figure 1. The polymer and desired additives are metered-in at the feed section of the extruder. The polymer composition is melted and mixed in the transition section of the screw and the blowing agent is injected. The polymeric melt containing a specific mixed-in ratio of dissolved and dispersed blowing agent, which depends on several factors including the type of resin and blowing gas, temperature, pressure and other specific extrusion conditions, is then extruded through the die. Upon exiting the die, the melt expands, and the foam sheet is optionally shaped, cooled and collected. The temperature profile on the extruder is chosen such that the polymer is in a molten state prior to the injection of the blowing agent. The temperatures of the extruder zones past the gas-injection port, the (optional) static mixer section and the die, are generally set at the cooler side so as to allow for adequate cooling of the gas-laden melt prior to exiting the die, which is necessary for cell expansion without coalescence. The flat sheet die permits only a two dimensional
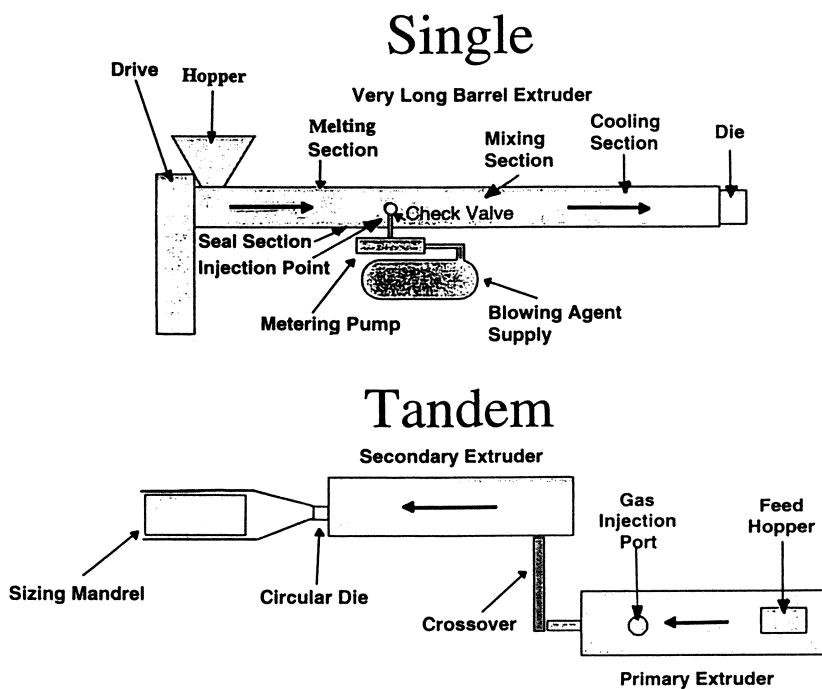
Single

Tandem

Figure 1. Schematics of single barrel and tandem foam extruders.

expansion of the extrudate and thus limits the degree of foaming achievable by this process. There has been some talk about using an arch die (a half moon shaped die) and a cooling mandrel with this set-up for obtaining an improved degree of foaming.

From foam industry point of view, however, a more commonly used foam extrusion process employs two extruders operating in tandem. An annular die is normally used with this set-up. A schematic is shown in the lower half of Figure 1. In this process the polymer and any additives are melted and mixed in a primary extruder, which is typically equipped with a high shear mixing screw. The gas or liquid blowing agent is injected near the end of this primary extruder. The melt/blowing agent composition is then transferred by means of a static heated tube generally referred to as the crossover section, to the feed section of the secondary extruder. The main purpose of this secondary extruder is to cool the gas-laden melt to an optimum melt temperature and pressure while transferring it to the annular die for foam formation without cell-coalescence. For this reason, typically the secondary extruder is of a much larger diameter than the primary extruder. A cooling mandrel is used immediately past the die to rapidly quench the expanding melt. The use of the annular die and the cooling mandrel allows for a three-dimensional expansion of the extrudate in a controlled manner, thereby allowing for the production of foams of very low densities. The extruded and expanded circular foam tube is typically slit at one (or two) point(s) and rolled-up as one (or two) foam sheet(s) using conventional take-up systems. The tandem extruder set-up normally allows for excellent control of process variables, and its use is the industry standard for making very low density polystyrene foams.

For either of these two processes, the key to any polymeric foam processing is to find and control the processing window in the terms of composition, temperatures and pressures etc., such as to avoid the foaming to occur inside the extruder or the die. This is necessary to obtain good surface quality in the foam sheet or article. If foaming is allowed to occur within the equipment, then the outcome is generally a very rough surface texture due to extensive corrugation and cell ruptures. In an ideal situation the clear unfoamed gas-laden melt extrudate can be visually seen immediately outside the die lips for a fleeting moment just before it starts to foam and turns opaque.

Polyester and Copolyester Foams

As mentioned above and also shown in Scheme 3, most semi-crystalline polyesters are generally at a disadvantage from melt strength and melt viscosity point of view. To get around this deficiency, one needs to consider either reactive extrusion with branching agents or the use of a pre-branched resin.

However, there have been reports of foaming very high molecular weight polyesters (inherent viscosity of 0.95 dl/g or more) to an upper medium density range using external cell nucleating agents and a gaseous blowing agent (e.g. nitrogen) (*13*). A slightly different approach uses a moderate inherent viscosity (0.73 dl/g) polyester which is first reinforced with glass- fiber via melt-compounding and then foamed using chemical blowing agents (*14*). There is also another report in the literature where small amounts of a polycarbonate is melt blended with a high molecular weight polyester, and then the polycarbonate is thermally decomposed to release gaseous blowing agents (CO_2, CO) *in-situ* whereupon foaming of the polyester occurs to yield
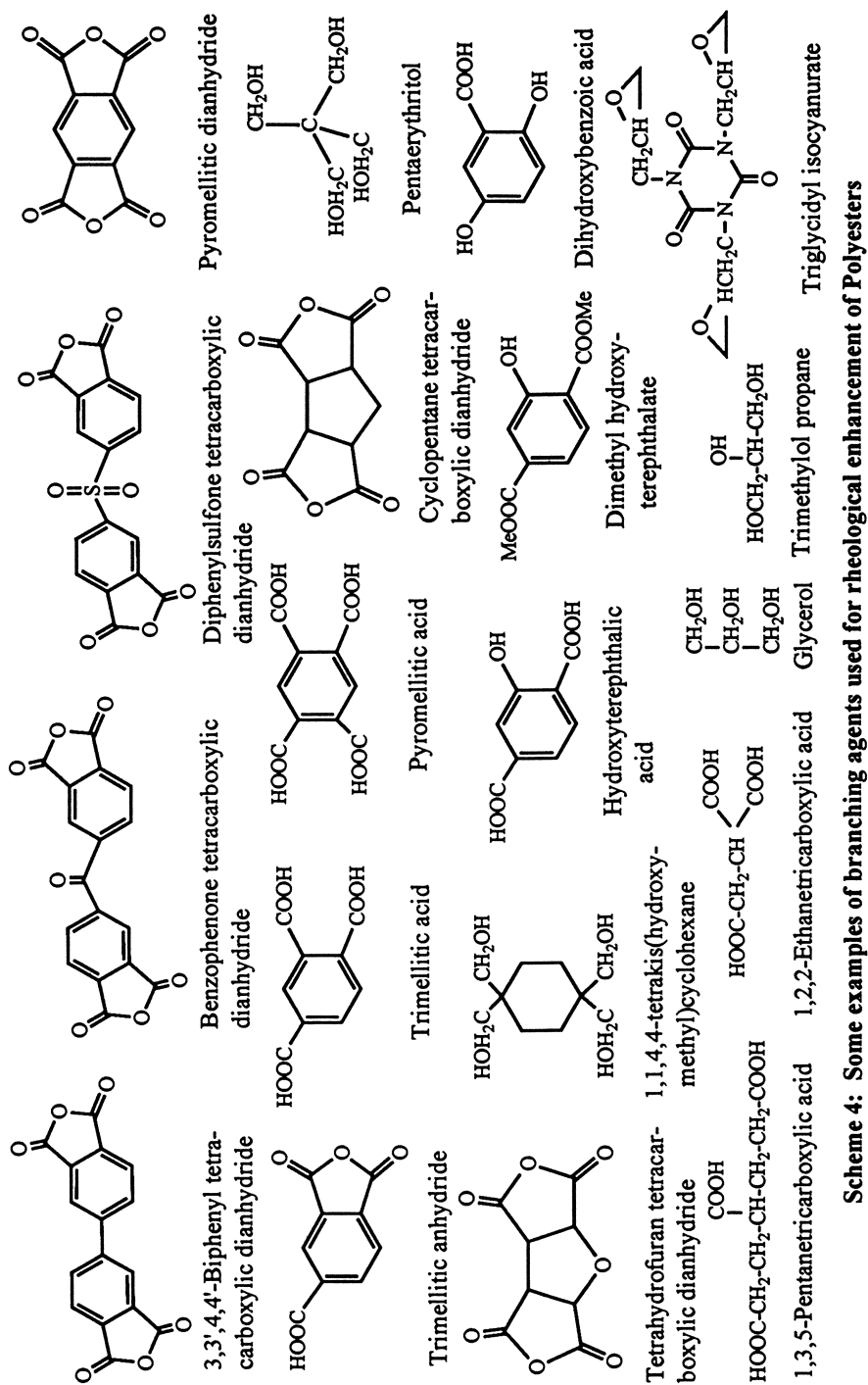
a medium density foam (*15*). Unbranched polyesters blended with elastomers have also been foamed to some extent using chemical and physical blowing agents; the elastomers reportedly help in the foaming due to their substantial stretchability and deformability (*16-17*).

Amorphous polyesters, such as Eastman Eastar PETG 6763 copolyester, also have much better rheological properties and thus may also be foamed readily to a low or medium density foam using chemical and/or physical blowing agents without any branching treatments. Eastman Eastar PETG is a glycol modified copolyester, which is a clear amorphous polymer with a glass transition temperature of about 81°C as determined by DSC. Thus it has been reported that the commercially available organic acid - carbonate salt containing chemical blowing agents work well with this copolyester as it is much more tolerant to the water by-product generated from it (*18*), as compared to most of the other semi-crystalline polyesters and copolyesters. Normally the water molecule hydrolyzes the ester linkage of polyesters at the high (processing) temperatures and results in a reduction of the molecular weight due to chain cleavage. A scanning electron micrograph of a medium density PETG foam sample foamed using Hydrocerol HK40B, an organic acid - carbonate salt type chemical blowing agent, is shown in Figure 2 (*19*) (the small cell diameter obtained by this process is notable). There is one report, however, which even discusses the use of these same types of chemical blowing agents with linear semi-crystalline polyesters in the presence of polycarbonate polymers, which reportedly counteracts the water-related degradation in the polyesters to allow successful production of foamed polyester fibers (*20*). Use of other types of chemical blowing agents such as, 5-phenyltetrazole, isatoic anhydride, azodicarbonamide, p-toluenesulfonyl semicarbazide etc., which do not evolve water by-product, with linear polyesters to produce medium density foams have also been reported (*21-23*).

Polystyrene is another very good example of an amorphous polymer capable of producing good quality low and medium density foams without the use of any branching agents, and several billion pounds of polystyrene foam is produced worldwide each year.

As mentioned previously, the melt rheological deficiencies of linear semi-crystalline polyesters can generally be substantially improved by branching. During the past several years, as a result of research and development work at several academic and industrial institutions (see below and references *24-46*), it has been found that the polyester polymers can be foamed in the presence of physical and/or chemical blowing agents when combined with branching agents (for increased melt viscosity and melt strength) and cell nucleators.

Monomeric Branching Agents. The use of multifunctional (having two or more functional groups) organic anhydrides, epoxides and isocyanates as branching agents to enhance the physical properties of polyesters for the production of thick-walled shaped articles by injection-molding has been reported as far back as 1971 (*24*). A listing of several such branching agents used in more recent years for the purpose of foaming polyesters is given in Scheme 4; however, only a few representative examples are listed here and the reader is encouraged to look-up individual references, *24-39*, for a more comprehensive list. As seen in Scheme 4, most commonly used monomeric branching agents include tri- and tetra- carboxylic acids and anhydrides such as trimesic acid, pyromellitic acid, trimellitic anhydride and pyromellitic

Pyromellitic dianhydride

Pentaerythritol

Dihydroxybenzoic acid

Triglycidyl isocyanurate

Diphenylsulfone tetracarboxylic dianhydride

Cyclopentane tetracarboxylic dianhydride

Dimethyl hydroxyterephthalate

Trimethylol propane

Benzophenone tetracarboxylic dianhydride

Trimellitic acid

Pyromellitic acid

Hydroxyterephthalic acid

Glycerol

1,2,2-Ethanetricarboxylic acid

3,3',4,4'-Biphenyl tetracarboxylic dianhydride

Trimellitic anhydride

Tetrahydrofuran tetracarboxylic dianhydride

1,1,4,4-tetrakis(hydroxymethyl)cyclohexane

HOOC-CH₂-CH₂-CH-CH₂-CH₂-COOH

1,3,5-Pentanetricarboxylic acid

Scheme 4: Some examples of branching agents used for rheological enhancement of Polyesters
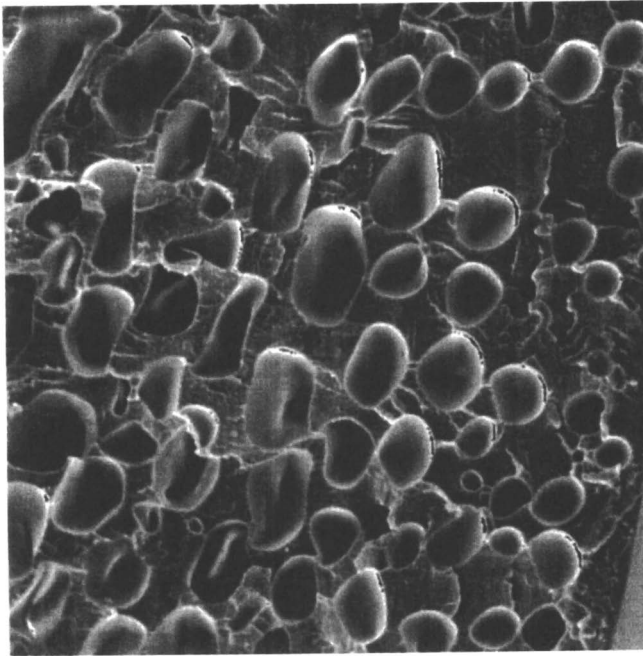
Figure 2. Scanning Electron Micrograph of a medium density PETG foam sheet (density = 0.82 g/cc) (1 cm = 20 microns).
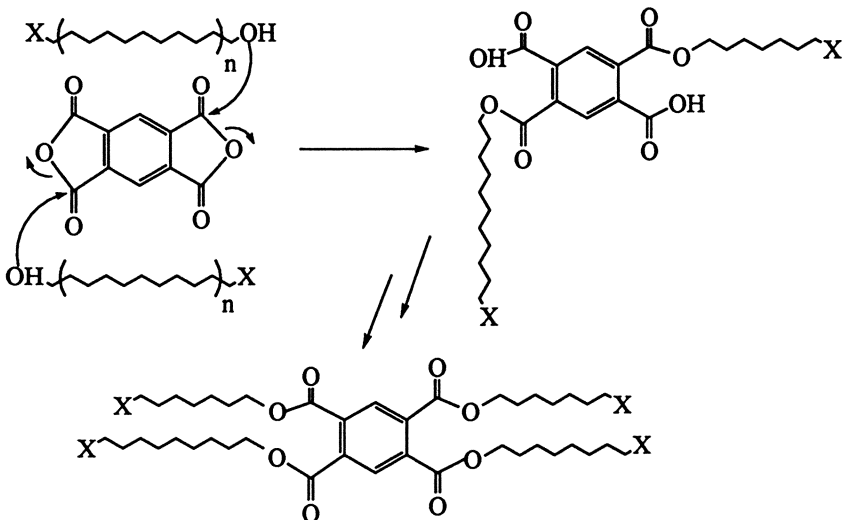
Scheme 5: An example of the branching caused in Polyesters by PMDA

dianhydride, or polyols such as trimethylolpropane and pentaerythritol, or a hybrid of hydroxyl and carboxyl functional groups, or a polyepoxy compound.

These branching agents provide polyesters with increased melt viscosity and melt strengths. Building of the polyester melt viscosity and melt strength with such a branching agent can be easily achieved by incorporating them in the polyester matrix by either of the following methods: (a) in a reactor during the polyester production, or (b) by a combination of melt compounding and/or solid-stating techniques, or (c) by reactive extrusion using an extruder. Several examples of each of these can be found in the literature as discussed below. Some such reports mention the use of branching agents such as trimellitic acid, pyromellitic acid (or their esters and anhydrides), pentaerythritol, tris(2-hydroxyethyl)isocyanurate etc. in a reactor to produce a branched polyester with enhanced rheology and foamability (*25-28*). Similar branching agents have also been used in a combination of melt-blending and solid-stating approach (method (b) above) to essentially accomplish the same sort of results by imparting a level of branching in a linear polyester and thus improving its melt strength and melt viscosity, and rendering it foamable (*29-31*). The last reactive extrusion approach (method (c)) has also been explored intensively and there are several reports in the literature which discuss using several of the above mentioned multifunctional monomeric branching agents either in the powder form (*32-34*) or in the form of concentrates in a polyester resin itself (*35-36*). One report even suggests that a PET/polyanhydride composition is ideally suited for the recycling of PET waste into panels of rigid foam (*37*). Along with the branching agents, use of hydroxyalkyl trimellitic imides as comonomers have also been reported to further enhance the mechanical and thermal properties of the polyesters produced (*38*). Epoxy functional group containing branching agents of different varieties are also described in the literature (*39-40*).

All of these various approaches convert the linear polyester into a partially branched polyester. The branching action is a result of several reaction steps which include the direct reaction of the polymer end-group with the branching agent, and subsequent glycol transfer and transesterification reactions. Examples of this using pyromellitic dianhydride and triglycidyl isocyanate as the branching agents are shown in Scheme 5 and Scheme 6 respectively.

These branched polyesters have the melt strength and melt viscosity needed to facilitate in cell formation which is initiated by an external cell nucleator, and in the expansion necessary for density reduction during foaming. Additionally, in most instances these modified resins also have an increased melt stability as well as improved hardening and crystallization kinetics.

As mentioned in the introduction section, any foamable polyester composition intended for use in food packaging applications should have very low (preferably zero) levels of free or unreacted branching agent in order to avoid adverse leaching or extraction into the food products per established regulatory compliance requirements. Although there has been some conscious effort to address this issue (see for example, references *35-36* and the following sections of this paper), much more work is needed to satisfactorily allay these genuine concerns. An obvious and easy solution to this issue might be to co-extrude or laminate a thin solid skin layer of unbranched and unfoamed food grade polyester onto the surfaces of such foamed packaging products. As discussed in some detail below, the other approaches might be to use polymeric branching agents where chain entanglements prevent them from migrations and
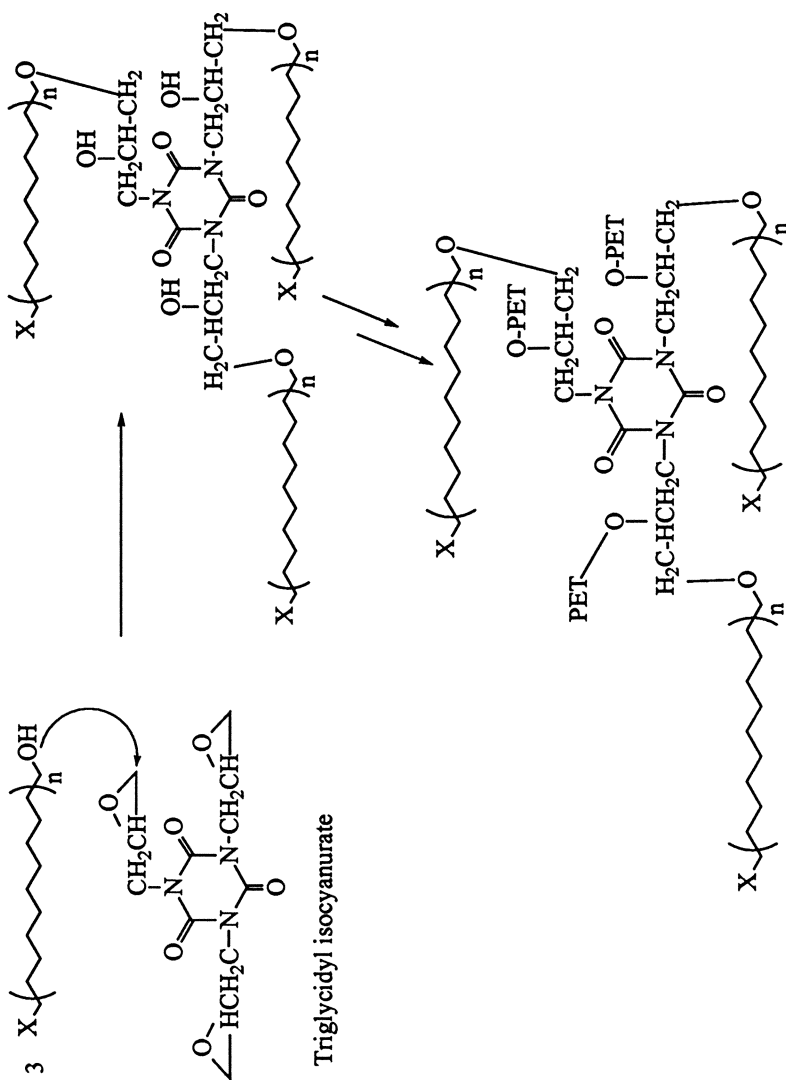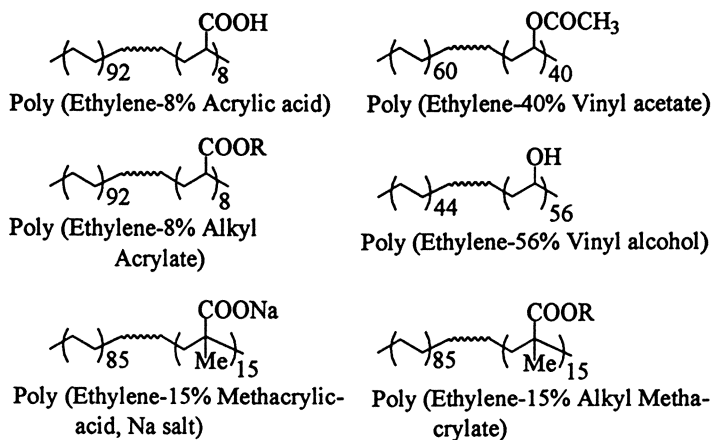
Scheme 6: An example of the branching caused in Polyesters by Triglycidyl isocyanate

extractions, or to use polymeric concentrates where (apparently) better control of the branching agent reactivity ensures that all molecules are bound to the polymeric chains and thus are rendered immobile.
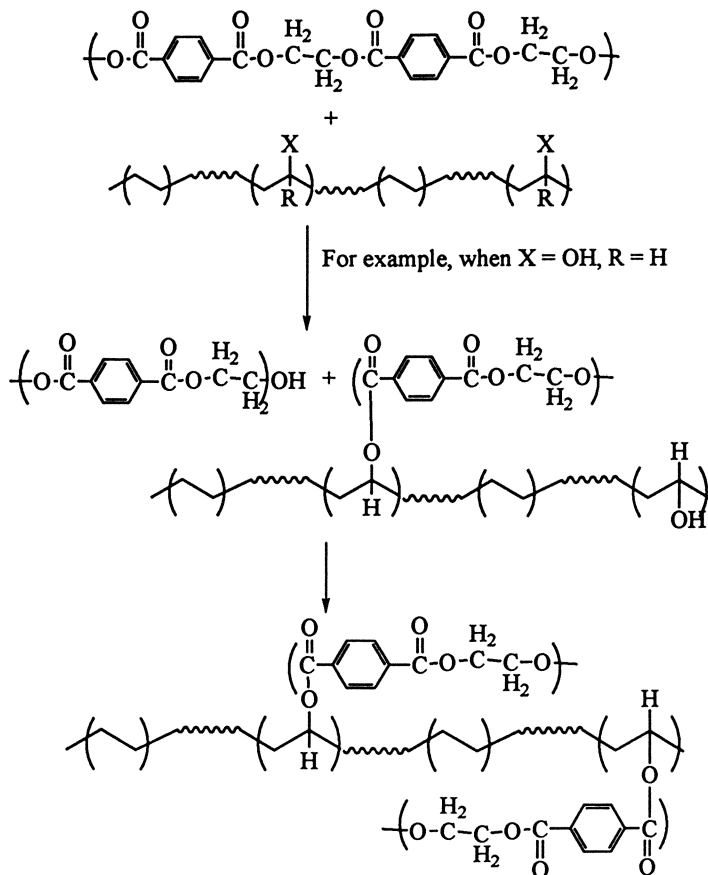
Polymeric Branching Agents. It has been reported in the literature that olefinic polymers containing anhydride functional groups can be used with advantage to foam polycarbonates and polyesters using chemical blowing agents (*41-42*).   Another report makes use of aromatic polymeric branching agents to impart branching in linear polyesters via transesterification reactions; thus the co-polycarbonate of bisphenol-A and methyl-2,4-dihydroxybenzoate, for example, have been used, where the ester side group is reportedly mainly responsible for the branching action (*43*).

As part of an effort in polyester foams, we have also evaluated the use of polymeric branching agents such as the copolymers of ethylene with one of the following functional comonomers: acrylic acid, methacrylic acid, alkyl acrylates, alkyl methacrylates, vinyl alcohol, etc. (*44*). Examples of such polymers are shown in Scheme 7. A combination of melt compounding and solid state polycondensation (i.e. method (b) mentioned above) is used to accomplish the branching reactions of the ethylene copolymers with the polyesters forming branched polymeric polyesters which exhibit increased melt viscosity and melt strengths, and have significantly improved foamability. As mentioned above, the branching action here is also a result of several reaction steps which include the direct reaction of the polymer end-group with the branching agent, and subsequent glycol transfer and transesterification reactions (examples of this are shown in Schemes 8 and 9).

Thus the process for achieving this involves drying and melt compounding the ethylene copolymer with the polyester in an extruder at temperatures in the range of 260°C to 290°C. Either a single screw extruder with mixing elements or a twin screw extruder can be used. The extrudate is cooled and pelletized. These pellets are then processed in a solid state polycondensation unit by circulating an inert gas, such as nitrogen, through the pellets at temperatures in the range of about 200°C to 230°C. The solid state polycondensation reaction is continued until the inherent viscosity (IV) of the polymer blend reaches a value of >0.75 dl/g. The branched polyester has a zero-shear melt viscosity (ASTM D4440) of above 5000 poise at 280°C and a melt strength (ASTM D3835) of above -50%, which are typical values for some linear polyesters. Depending upon the level and type of the ethylene copolymer used and the extent of solid-state polycondensation reaction, a polyester treated in the above manner may have melt viscosities in the range of 20,000 to 100,000 poise and melt strengths in the range of -25 to +30%. The combination of melt compounding and solid state polymerization is employed because polymerization in the melt phase to high MW polyesters is significantly limited by the substantial increase in melt viscosity of the branched polyesters. The melt eventually reaches a melt viscosity that is difficult to handle. In conventional extruders used for melt compounding, generally not enough time lapses to allow for sufficient branching reactions to occur when using the aforementioned polymeric branching agents. The resulting polymer is a ready-to-use branched polyester that is in a convenient pellet form for processing into medium or low density foamed end products.   Such branched polyesters may then be mixed with external cell nucleating agents and gaseous blowing agents in an extruder during foam processing. Typical examples of cell nucleating agents are talc and TiO_2, and of gas blowing agents are nitrogen, HFC's, HCFC's, etc.. We are

COOH
Poly (Ethylene-8% Acrylic acid)

OCOCH₃
Poly (Ethylene-40% Vinyl acetate)

COOR
Poly (Ethylene-8% Alkyl Acrylate)

OH
Poly (Ethylene-56% Vinyl alcohol)

COONa
Poly (Ethylene-15% Methacrylic-acid, Na salt)

COOR
Poly (Ethylene-15% Alkyl Methacrylate)

Scheme 7: Some examples of ethylene copolymers

+

For example, when X = OH, R = H

Scheme 8: An example of the branching caused by ethylene copolymers
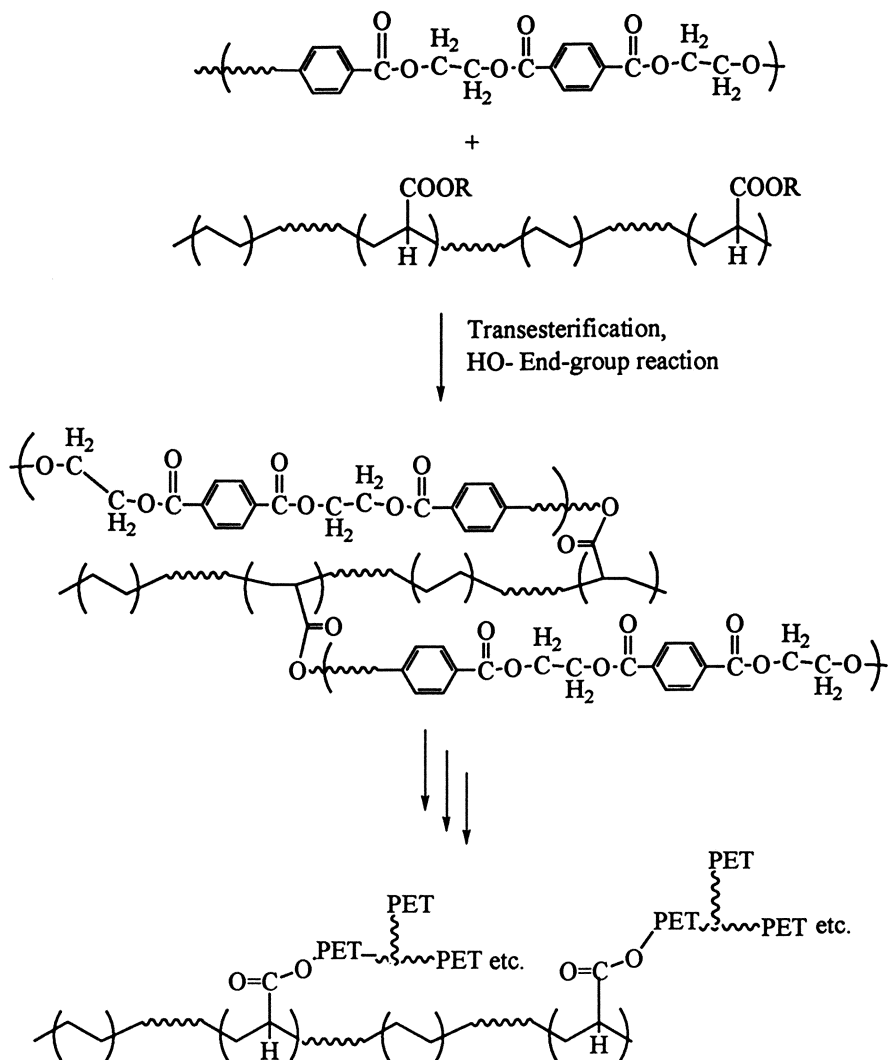
Scheme 9: An example of the branching caused by ethylene copolymers

currently in the process of conducting extraction studies to check migrations/ extractions of these additives into approved food simulating solvents.

Polymer Concentrates Containing Branching Agents. In yet another approach, we have also developed several pre-compounded polymeric concentrates which contain multifunctional reactive branching agents similar to the anhydrides and epoxides listed in Scheme 4, and cell nucleating agents (*45-46*). These concentrates are designed for convenience and can be easily used with any polyester or copolyester via the reactive extrusion technique in order to enhance rheological properties for foaming using externally injected gaseous blowing agents. Additionally, we have also found that some of these concentrates produce foamed articles which have very low levels of unreacted or free branching agents present in them (*46*).

These concentrates can be easily made by a melt-compounding process and used as an additive in a polyester (e.g. Eastman PET 12440) for preparing a branched polyester composition having a cell nucleator and increased melt strength and melt viscosity, improved foamability, and an almost negligible level of the unreacted branching agent. This approach in essence comprises of (a) the melt compounding of a carrier resin such as a polyolefin with a cell nucleating agent and a branching agent, and (b) blending the concentrates produced in (a) with the polyester in an extruder followed by the injection of a gaseous blowing agent to produce low or medium density foams. The branched polyester resulting from the use of these concentrates has a zero-shear melt viscosity of above 5000 poise at 280°C and a melt strength of above -50% which, as mentioned above, are typical values for some linear polyesters. Depending upon the level and type of the concentrate used, a polyester/concentrate melt blend may have melt viscosities in the range of 20,000 to 200,000 poise and melt strengths in the range of -5 to +60%.

The foamed trays prepared from such polyester/concentrate compositions have been subjected to extraction tests using food simulating solvents and were found to contain less than 15 ppb of the unreacted and extractable additives. In order to illustrate this more clearly, a summary of some representative data points from our work is tabulated in Table I. In this table, the foam PET samples studied were prepared using Eastman PET 12440 (IV 0.70 dl/g). This table lists the extraction data for several of our foam tray samples made using the foam concentrates. The foam trays produced in these examples were subjected to a complete extraction testing protocol for evaluation of compliance with European Union (EU) regulations for global (total) migration, antimony (Sb) migration, and branching agent (BA) migration into food simulating solvents. The test protocol also provides for evaluation of BA migration into food simulating solvents consistent with Food and Drug Administration (FDA) guidelines (1988 Recommendations for Chemistry Data for Indirect Additive Petitions). The calibration limit of our analytical procedure for the test of extractable BA in food simulating solvents is 15 parts per billion (ppb).

Experiment 1 in Table I was conducted using a foam tandem extruder (3.5" Primary and 4.5" Secondary Extruders, of L/D ratio of 30/1 each) and an annular die. A pelletized polypropylene concentrate containing 20 wt% branching agent (pyromellitic dianhydride) was used along with the Eastman PET 12440. The foamed PET sheet made by this equipment was thermoformed in a subsequent step to prepare the foam trays used in this extraction study. Details of this experiment are given in the experimental section. Experiment 2 through 7 also used similar polymeric

Table I. Extraction results for polyester foam trays

Expt. No.	Equipment Used	European Union (EU) and FDA — Oven Cooking						FDA — Oven Reheat			FDA — Oven Cooking		
		3% AcOH (100°C/2h)			HB 307 (175°C/2h)			10% EtOH (100°C/2h)			10%(8%)EtOH (121°C/2h)		
		TM mg/kg	Sb mg/kg	BA mg/kg	TM mg/kg	Sb mg/kg	BA mg/kg	TM mg/kg	Sb mg/kg	BA mg/kg	TM mg/kg	Sb mg/kg	BA
LIMITS:		60	.01	.05 mg/kg (50 ppb in-food)	60	.01	.05 mg/kg (50 ppb in-food)			50 ppb in-food			50 ppb in-food
1 (6, 7)	Tandem, annular die	.11	.0	ND	13	.00	ND				1.3	.06	ND
2	Single barrel, 30" flat sheet die	.21	.0056	ND	26.2	.0012	.018 (20)	.46	.011	ND	1.23	.053	ND
3	Single barrel, 30" flat sheet die	.27	.0054	ND	24.5	.0009	.025 (27)	.60	.012	ND	1.27	.054	ND
4	Single barrel, 30" flat sheet die	.24	.0075	ND	36.9	.00	.018 (20)	.62	.015	ND	1.61	.07	ND
5	Single barrel, 30" flat sheet die	.25	.0074	ND	33.5	.00	.025 (27)	.72	.020	ND	1.37	.09	ND
6	Single barrel, 30" flat sheet die	.27	.0084	.012 (14)	27.9	.00	ND	.63	.018	ND	2.19	.084	.013 (14)
7	Single barrel, 30" flat sheet die	.25	.0078	ND	23.6	.00	ND	.63	.018	ND	1.87	.082	ND

Notes: (*1*) BA = branching agent; ND = none detected; TM = total migration based on UV measurement for terephthaloyl moieties. (*2*) mg/kg based on EU factor of 6 dm^2/kg. (*3*) ppb in-food based on FDA factor of 10 g food/in^2. (*4*) For AcOH and HB 307 oil, trays were filled with 100 ml(g) of the simulants. The contact area was 1.34 dm^2/100 ml simulant. (*5*) For 8% and 10% EtOH, 1/2 dm^2 (7.75 in^2) strips were exposed to 50 ml in pressure cells. 50 ml/dm^2 (15.5 in^2) for calculations (double side). (*6*) 8% EtOH was used for this sample. (*7*) For 3% AcOH and HB 307 oil, the contact area for 100 g of the food simulant for this sample was 1.8 dm^2.

concentrates, but a single barrel sheet extruder (3.5" extruder having a L/D ratio of 24/1) modified for N_2 gas injection was used instead of the tandem extruder. Experiments 2 and 3 used an effective branching agent concentration of 0.15 wt%, and were conducted to study the effect of adding regrind to the system. This was done by adding 30% unfoamed-regrind (typical for the foam industry) into each pass along with the virgin PET and the foam concentrate in experiment 3; a total of five-passes were made through the extruder. During the 5th pass, N_2 gas was injected into the extruder to make the foamed sheet. The remaining experiments in this table were done using low (experiments 4 & 6) and high (experiments 5 & 7) levels of a foam concentrate made on a 83 mm Werner and Pfleiderer trilobe twin screw extruder; the effective branching agent level was 0.15 and 0.20 wt% respectively. Experiments 6 & 7 used the same concentrates as experiments 4 & 5, except that they were aged for two months at room temperature under ambient conditions. The objective of these experiments was (a) to check to see the scalability of the concentrate manufacturing process, (b) to set the upper and lower limits of the level of foam concentrate expected to be used to make foam PET, and (c) to see the effect of aging on the efficacy of the concentrate. As the data shows, for all of these runs (1 through 7), the branching agent migration was either undetectable or within the allowed limits, and the trays complied with total (global) migration and antimony (Sb) migration as well.

Scanning electron micrographs of some PET foam sheet samples made in experiment 1 are shown in Figures 3-5. As can be seen the cellular structure is fairly uniform, evenly distributed and consists of closed cells in all three samples produced which ranged in sheet thickness from 45 to 68 to 110 mils (1 mil = 1/1000 inch), and had densities of 0.26, 0.24 and 0.30 g/cc respectively.

The Recyclability Question?

As mentioned in the introduction section, one of the attractive features of the polyester foam might be its potential recyclability, as is well known for unfoamed polyester products used in several applications. However, the question remains whether a post-consumer, foamed and branched polyester containing branching agents and other additives can really be recycled with ease using existing polyester recycle streams? The possibility of redensifying foamed polyester parts by grinding, followed by methanolysis to breakdown the polymer chains back into monomers is a distinctly feasible solution since the technology to do so for unfoamed polyesters is currently available; however, this has not been proven to work for foamed branched polyesters. Clearly, much more work needs to be done to truly explore these and other options before anything can be stated with certainty.

Summary

This article provides a comprehensive overview of the physical aspects of the fundamental requirements for foaming a polyester resin, and a review of the various proven methods of foaming polyesters as reported in the scientific and patent literature over the past several years. This is followed by a discussion of the newer results, which include the use of monomeric and polymeric branching agents, and of polymeric concentrates containing reactive branching agents (for reactive extrusion)

for rendering the polyesters foamable. The concerns around the leaching and extraction of any additives from foamed polyester packaging trays intended for use in food packaging applications is also discussed. Preliminary results from our laboratories have shown that some viable methods of producing foamed polyesters include the use of polymeric branching agents and the polymeric concentrates, and also that the adverse migrations/extractions of the additives into the food products may be curtailed by these approaches as well.

Experimental

Inherent viscosity (IV) is measured in a 60/40 solution of phenol/tetrachloroethane at a concentration of 0.5 gram polymer per 100 ml, at 25°C. Molecular weight was measured by size exclusion chromatography (SEC) (or gel permeation chromatography, GPC). Melting point, % crystallinity, etc. were measured using a differential scanning calorimeter (DSC) at a scan rate of 20°C per minute. Densities of the foamed samples were measured using a pycnometer.

The polymeric concentrates discussed in the text were made at Eastman Chemical Company by melt compounding using either a 30 mm Werner and Pfleiderer co-rotating twin screw extruder or a co-rotating 83 mm Werner and Pfleiderer trilobe twin screw extruder.

Melt strength was measured according to ASTM D3835 at 280°C by extruding the molten polymer downward at a shear rate of 20 second^{-1} through a capillary die 0.1 inch in diameter and 0.25 inches long, using an Instron rheometer and allowing the extrudate to fall freely. The diameter of the end of a six inch length of extrudate, measured from the orifice of the die, is measured. The percent melt strength is then determined from the formula: (D - 0.1)/0.1 x 100, where D is the diameter, in inches, of the extrudate supporting a six inch length of extrudate. If D is less than 0.1 inch (the die diameter), the melt strength is a negative number since there is no increase in the diameter of the extrudate. If D is greater than 0.1 inch, the melt strength is a positive number. For instance, if D was 0.2 inch, then the Melt Strength would be +100%.

Melt viscosity was measured according to ASTM D4440 at 280°C and 10% strain. Dynamic frequency sweep tests were run using a Rheometrics RMS 800 mechanical spectrometer to generate plots of the complex viscosity (η^*) vs. oscillation frequency (rad/sec). The zero shear viscosity (η_0) was then estimated for each sample using the Cross model (*47*) in the Rheometrics software (where it is referred to as the Ellis model).

For illustration, details of polyester foam extrusion (Experiment 1/Table I) using a tandem foam extruder and an annular die are given below:
Poly(ethylene terephthalate), PET 12440 (IV 0.70), supplied by Eastman Chemical Company, was dried at 149 °C for 6 hours (to a dew point of -40°C) in a portable Walton Stout desiccant dryer. It was then fed through the main feed hopper of a Battenfeld Gloucester tandem foam extrusion line consisting of a 3.5" primary and a 4.5" secondary extruders (L/D ratio of 30/1 each), a 3.5" diameter annular die attached to the end of the secondary extruder, an additive pellet feeder, and an additive powder feeder attached to the feed throat of the primary extruder. An injection port capable

of injecting a blowing agent under high pressure into the polymeric melt was located near the end of the primary extruder. The blowing agent used in this example was an environmentally friendly hydrofluorocarbon gas, 1,1-difluoroethane (DuPont, 152A). The extruders, the crossover zone and the annular die were heated to various temperatures (°C) through their entire length as noted below:

Primary 3.5" Extruder Zone 1		229
Primary 3.5" Extruder Zone 2		284
Primary 3.5" Extruder Zone 3		281
Primary 3.5" Extruder Zone 4		276
Primary 3.5" Extruder Zone 5		270
Primary 3.5" Extruder Zone 6		266
Screen Changer Body		262
Screen Changer Slide		262
Crossover		295
Secondary Seal		79
Secondary 4.5" Extruder	Zone-1	248
Secondary 4.5" Extruder	Zone-2	249
Secondary 4.5" Extruder	Zone-3	249
Secondary 4.5" Extruder	Zone-4	247
Annular Die	Zone-1	254
Annular Die	Zone-2	251
Annular Die Adapter		248
Annular Die Melt Temperature		244

The foam concentrate was fed into the feed throat of the primary extruder using the pellet additive feeder attachment at a rate of 1 wt%. Powder talc (from Polar Minerals Inc., product # 9102, median particle size 2-3 microns) was also fed into the feed throat of the primary extruder using the powder feeder attachment at a rate of 0.3 wt%. Other relevant extrusion conditions and parameters were as follows:

Pressures (psi):

3.5" Extruder	2000-2200
Crossover zone	2000
4.5" Extruder	1600
Blowing agent injection pressure	3630

Drive Conditions:

3.5" Extruder	62 rpm / 84 amps
4.5" Extruder	12.4 rpm / 29 amps
Polymer output	316 lb/hour
Blowing agent injected	1.0 lb/hour

Under these conditions, the composition described above extruded with the desired characteristics needed to produce good foam. The foam coming out of the annular die had a dry hand and good melt strength so that it could be readily stretched over a 16 1/4" diameter water cooled mandrel (21°C). The foam was slit, and the sheet trimmed to 48" width and collected. The foam produced had a density of 0.26

g/cc at a thickness of 45 mils, an IV of 0.76 dl/g, and a weight average molecular weight of 76130 and a Mz/Mn ratio of 10.38. It had a crystallinity of 4.56% as measured by DSC. Scanning electron microscopy showed the cell structure to be well formed with all cells being closed. The average cell size was approximately 200-500 microns in diameter in the machine direction and 100-200 microns in diameter in the transverse direction (Figure 3).

The foam PET sheet produced above was thermoformed into foam trays (8.5x6.5x2 inches) using an Irwin thermoformer equipped with a heated matched mold. Typical forming conditions were as given below:

Oven Temperatures (°C):

	zone-1	zone-2	zone-3	zone-4
Top	257	255	255	256
Bottom	255	255	255	255

Top/Bottom	Near Side	288/260
Top/Bottom	Far Side	311/267
Top/Bottom	Radd	305/266
Top/Bottom	Pre-heat	260/272

Line speed: 10.9 cycles per minute

The foam trays produced had a crystallinity of 28.6%, and weight average molecular weight and Mz/Mn ratio of 74714 and 9.20 respectively. The increase in crystallinity from 4.56% in the foam sheet to 28.6% in the thermoformed tray is noteworthy since low sheet crystallinity is desirable for ease of thermoforming, and the high tray crystallinity is also desirable for needed structural integrity and thermal stability.

The thickness and density of the foam sheet produced responded well to changes in the extrusion line-speed and the level of the blowing gas. Two other foam sheet samples of different thickness' (68 mils and 110 mils) were also collected and analyzed by SEM and shown to have similarly well formed closed cell structure (Figures 4 and 5).

The procedure for the evaluation of foamed polyester trays for total migration and extractable branching agent and Sb in food simulating solvents and thus their compliance with FDA as well as European Union guidelines is briefly described below (this test was conducted by Eastman's Regulatory Compliance Testing laboratory).

Extractions and Analyses for Migration and Compliance Testing of Foam Samples:
Extractions:
In a typical procedure, three foam trays were filled with 100 ml of 3% acetic acid/water and covered with a sheet of Teflon. A temperature probe was added to one tray. The trays were placed in a pressure cooker with a 15 psi pressure regulator until the temperature reached 100°C. The regulator was then removed and the temperature maintained for 2 hours at 100°C. After 2 hours, the samples were removed from the pressure cooker, cooled to room temperature, and poured into clean rinsed flasks.
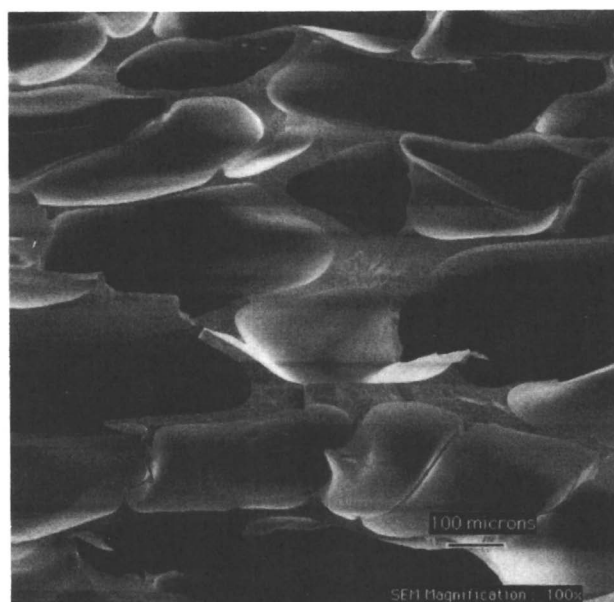
Figure 3. Scanning Electron Micrograph of low density Polyester foam sheet (density = 0.26 g/cc; sheet thickness = 45 mils).
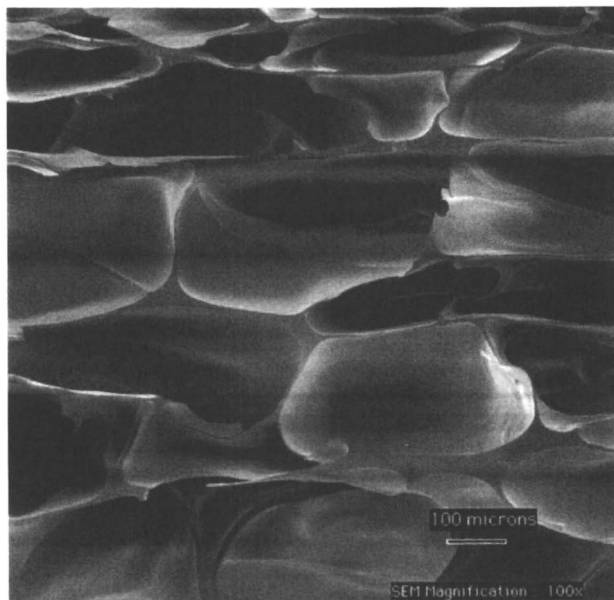
Figure 4. Scanning Electron Micrograph of low density Polyester foam sheet (density = 0.24 g/cc; sheet thickness = 68 mils).
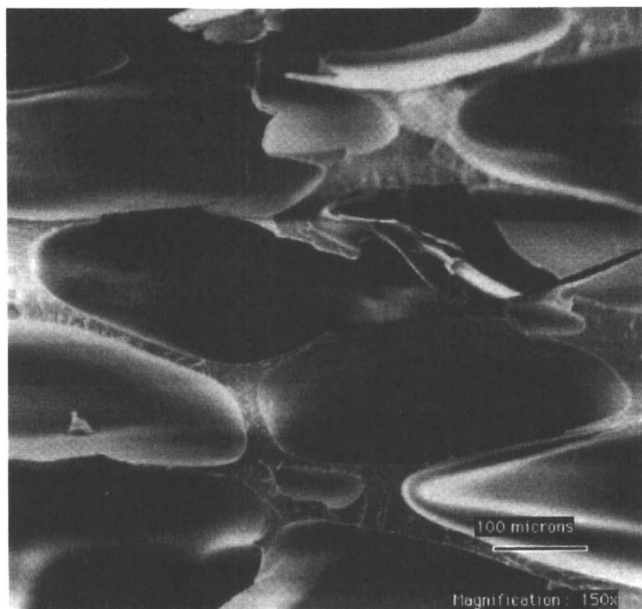
Figure 5. Scanning Electron Micrograph of low density Polyester foam sheet (density = 0.30 g/cc; sheet thickness = 110 mils).

Teflon pressure cells were used for the 8% ethanol/water extractions. The bottom part from four foam trays were cut into 1/2 dm^2 (7.75 in.^{2}) sections. The 1/2 dm^2 sections were cut into 8 strips of about 1 in.^{2}, placed in pressure cells with wire spacers, and filled with 50 ml of solvent. The pressure cells were placed in a pressure cooker with a 15 psi pressure regulator. After the pressure reached 15 psi (121°C), the samples were heated for 2 hours, removed from the oven, cooled to room temperature and poured into clean rinsed flasks.

Foam trays (four) filled with 100 g of HB 307 oil were placed in an oven at 175°C. It took about 2 hours for the oven temperature to recover to 175°C. The samples were then heated for 2 hours, removed from the oven, and the oil poured into flasks.

Area of Trays Exposed to Solvents: The area of the trays exposed to 100 ml of solvents were determined by cutting a section of trays exposed to 100 ml, weighing and comparing to the weight of a 4 in.^{2} section of the tray. For strips cut from trays for the 8% Ethanol extractions in (b) above, both sides of the strips were used in calculating the area of exposure.

Analyses:

Total Migration Into Food Simulants: Total migration of polymer species into the food simulants was determined by UV/VIS analyses of the extracts.

Branching agent and TPA in Food Simulants: The migration of the branching agent and TPA into the food simulants was determined by HPLC using a UV detector.

Antimony (Sb) in Food Simulants: Antimony migration into the food simulant was determined by ICP/MS.

Acknowledgments

References

1. Unpublished market research data, Eastman Chemical Company.
2. Marshall, I.; Todd, A. *Trans. Faraday Soc.*, **1953**, *49*, 67.
3. Hovenkamp, S. G.; Munting, J. P. *J. of Polymer Science*, **1970**, *8, Part A-1*, 679.
4. Jabarin, S. A.; Lofgren, E. A. *Poly. Engg. & Science*, **1984**, *24, No. 13*, 1056.
5. Goodings, E. P. *Soc. Chem. Ind. (London)*, **1961**, *Monograph#13*, 211.
6. Zimmermann, H. *Faserforschung und Textiltech*, **1962**, *13*, 481.
7. Allan, R. J. P.; Forman, R. L.; Ritchie, P. D. *J. Chem. Soc.*, **1955**, 2717.
8. Buxbaum, L. H. *ACS Polymer Preprints*, **1967**, *8*, 552.
9. Buxbaum, L. H. *Angew. Chem.*, **1968**, *80*, 225.
10. Buxbaum, L. H. *Angew. Chem. Int. Ed.*, **1968**, *7*, 182.
11. Yoda, K.; Tsuboi, A.; Wada, M.; Yamadera, R. *J. of Applied Polymer Science*, **1970**, *14*, 2357.
12. Khemani, K. C.; McConnell, R. L. *Polymer Preprints*; Publisher: American Chemical Society, Washington D.C., **1996**, *Vol. 37, No. 2*; 793; Khemani, K. C.; McConnell, R. L. *Advanced Materials: Development, Characterization, Processing,*

and Mechanical Behavior; Ed. T. Nicholas; Publisher: American Society of Mechanical Engineers, New York, **1996**, *Vol. 74*, 191.

13. Cheung, T. M.; Davis, C. L.; Prince, J. E. *US patent* 4,981,631 **(1991)**; Assignee: The Goodyear Tire & Rubber Company.

14. Fox, D. W. *US patents* 4,280,005 **(1981)**; 4,351,911 **(1982)**; Assignee: General Electric Company.

15. Huggard, M. T. *US patents* 4, 462,947 **(1984)**; 4,466,933 **(1984)**; Assignee: Mobil Oil Corporation.

16. Labar, R. A. *US patent* 4,152,495 **(1979)**; Assignee: Rohm and Haas Company.

17. Subramanian, P. M.; Tice, C. L. *US patent* 5,128,202 **(1992)**; Assignee: E.I. Du Pont de Nemours and Co..

18. Anonymous Research Disclosure *Derwent WPI*, **1994**, CC No. RD362028, Abstracted WPI Acc No. 94-232080/28.

19. Khemani, K. C.; Boone, G. D.; Lane, B. G. Unpublished results, Eastman Chemical Company.

20. Vischer, A. *US patent* 5,124,098 **(1992)**; Assignee: Hoechst Aktiengesellechaft.

21. Matsumura, S.; Inata, H. *US patent* 4,419,308 **(1983)**; Assignee: Teijin Ltd..

22. Hammer, H.; Kircher, K. *US patent* 4,728,673 **(1988)**; Assignee: Bayer Aktiengesellschaft.

23. Allen, R. B.; Avakian, R. W. *US patent* 4,683,247 **(1987)**; Assignee: General Electric Company.

24. Dijkstra, A. J.; Goodman, I.; Reid, J. A. W. *US patent* 3,553,157 **(1971)**; Assignee: Imperial Chemical Industries Ltd..

25. Edelman, R.; Berardinelli, F.M.; Wissbrun, K.F. *US patent* 4,234,708 **(1980)**; Assignee: Celanese Corporation.

26. Borman, W. F. H.; Kramer, M.; Reilly, E. P. *US patent* 4,419,485 **(1983)**; Assignee: General Electric Company.

27. Yatsu, T.; Nakano, T.; Hinooka, T. K. *US patent* 4,692,506 **(1987)**; Assignee: Mitsui Petrochemical Industries Ltd..

28. Muschiatti, L. C. *US patents* 5,229,432 **(1993)**; 5,391,582 **(1995)**; Assignee: E.I. Du Pont de Nemours and Co..

29. Borman, W. F. H. *US patent* 4,132,707 **(1979)**; Assignee: General Electric Company.

30. Al Ghatta, H. A. K.; Severini, T.; Astarita, L. *US patents* 5,362,763 **(1994)**; 5,422,381 **(1995)**; Assignee: M. & G. Richerche S.p.A..

31. Ghisolfi, G. *US patent* 5,243,020 **(1993)**; Assignee: Phobos N.V..

32. Leslie, J. P.; Lane, C. A.; Grant R. P. *US patents* 4,145,466 **(1979)**; 4,176,101 **(1979)**; Assignee: Rohm and Haas Company.

33. Hayashi, M.; Amano, N.; Taki, T. *US patents* 5,000,991 **(1991)**; 5,134,028 **(1992)**; Assignee: Sekisui Kaseihin Kogyo Kabushiki Kaisha.

34. Hayashi, M.; Amano, N.; Taki, T.; Hirai, T. *US patent* 5,110,844 **(1992)**; Assignee: Sekisui Kaseihin Kogyo Kabushiki Kaisha.

35. Rotter, G. E.; Melquist, J. L.; Chiang, W.; Tsai, B. C.; Kelly, J. J. *US patents* 5,288,764 **(1994)**; 5,340,846 **(1994)**; Assignee: Amoco Corporation.

36. Chen, S. Y.; Chiang, W.; Melquist, J. L.; Pauer, C. A.; Rotter, G. E.; Tsai, B. C. *US patent* 5,536,793 **(1996)**; Assignee: Amoco Corporation.

37. Smith, H. V.; Trevitt, E. W. WO 90/10667 **(1990)**; Assignee: TISSLAN S.A..

38. Tung, W. C. T.; Floyd, M. E. *US patent* 4,910,290 (**1990**); Assignee: The Goodyear Tire and Rubber Company.

39. Inokuchi, N.; Fukumoto, T.; Mori, Y. *US patent* 4,284,596 (**1981**); Assignee: Teitin Ltd..

40. Okamoto, K. T. *US patent* 4,999,388 (**1991**); Assignee: General Electric Company.

41. White, R. J.; Krishnan, S.; Siebourg, W. J. *US patent* 4,737,523 (**1988**); Assignee: Mobay Corporation.

42. White, R. J.; Krishnan, S. *US patents* 4,751,250 (**1988**); 4,837,243 (**1989**); 4,851,453 (**1989**); Assignee: Mobay Corporation.

43. Rosenquist, N. R.; Bostick, E. E. *US patent* 5,064,914 (**1991**); Assignee: General Electric Company.

44. Khemani, K. C.; McConnell, R. L. *US patents* 5, 482,977 (**1996**); 5,519,066 (**1996**); Assignee: Eastman Chemical Company.

45. Khemani, K. C.; Mercer, J. W.; McConnell, R. L. PCT/US94/10640, WO 95/09884 (**1995**); US 94/10640 has recently been granted to Eastman Chemical Company.

46. Khemani, K. C.; Juarez-Garcia, C. H.; Boone, G. D. Patent applications filed; US Serial No. 08/532208 has recently been granted to Eastman Chemical Company.

47. Hieber, C. A.; Chiang, H. H. *Polymer Eng. Science*, **1992**, *32*, No. 14, 931.

Chapter 6

Polyisocyanurate Foams Modified by Thermally Stable Linkages

K. Ashida[1], K. Saiki[2], J. Goto[2], and K. Sasaki[2]

[1]Polymer Institute, University of Detroit Mercy, 4001 West McNichols Road, P.O. Box 19900, Detroit MI 48219
[2]Nippon Polyurethane Industries Company, Limited, 440 Akiba-cho, Totsuka-ku, Yokohama 245, Japan

Urethane-modified polyisocyanurate foams have inherently higher flame retardation and thermal stability than those of urethane foams. However, they still have disadvantages of relatively high flammability , low thermal stability, and high smoke generation due to the labile urethane linkages. In this study, thermally more stable linkages than the urethane linkages, e.g., amide, imide and carbodiimide linkages were examined for improving these disadvantages. The resulting foams exhibited significant improvement in the above properties. In addition, zero ODP physical blowing agents consisting of halogen-free azeotropes were examined.

The isocyanurate linkage (Figure 1) is formed by the cyclotrimerization of isocyanate groups, and has inherently higher thermal stability than that of the urethane linkage. However, unmodified polyisocyanurate foams have inherent disadvantage by being extremely friable. In particular, their high friability makes it impossible to handle them in practical applications.Therefore, the crosslink density of the foams should be reduced by incorporating urethane linkages by the addition of polyols as modifiers [1]. A general formula of modified isocyanurate foams is illustrated in Figure 2. Since 1966, a number of R & D efforts were focused on urethane-modified isocyanurate foams. Two primers of isocyanurate foams have been published [2, 3]. The modifiers which appeared in the literature are summarized in Table I, in which " X " represents modifiers   The linkages for modification include urethane [1], amide [1,9,10] , imide [4,9], carbodiimide
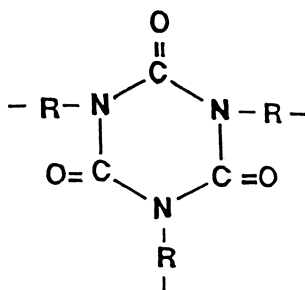
Figure 1. Isocyanurate Linkage.
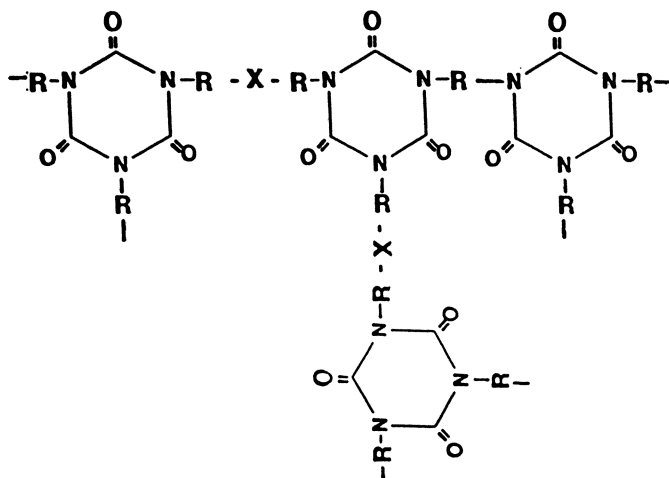
Figure 2. Modified Isocyanurate Foams.
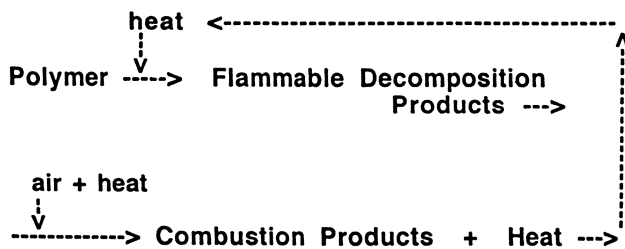
Figure 3. Combustion Mechanism.

[5,8] , oxazolidone [6] and substituted urea [7] linkages in which urethane linkages are most widely employed for producing commercial products.

Urethane-modified isocyanurate foams have better flame retardance and thermal stability than urethane foams.

The thermal stability and smoke generation of the urethane-modified isocyanurate foams are not quite satisfactory because the urethane linkage has a labile hydrogen atom, and therefore the linkage dissociates easily at about 200 °C to the original components, i.e., polyisocyanates and polyols .,These monomers can be ignited at elevated temperature in the presence of air , according to the combustion mechanism shown in Figure 3.

The research philosophy in this study is based on a hypothesis that the higher the thermal stability of polymeric linkages, the less the generation of flammable gases which result in low combustibility, and that the higher the thermal stability, the lower the smoke generation.

This paper , therefore, will present an evaluation of thermally stable modifiers, such as carbodiimide , imide , and amide linkages. In this study, the following abbreviation will be used. U-PIR : Urethane-modified isocyanurate foams, CD-PIR: carbodiimide-modified isocyanurate foams, I-PIR: imide-modified isocyanurate foams, A-PIR : amide-modified isocyanurate foams, and PUR : urethane foams.

Experimental

1.) Carbodiimide-Modified Polyisocyanurate Foams (CD-PIR).

1.1. Raw Materials

A polymeric isocyanate (polymeric MDI , NCO% : 31.2%), carbodiimide-forming catalyst [1-phenyl-3-methyl-2-phospholene-1-oxide, (PMPO)], isocyanate trimerization catalysts, [quaternary ammonium carboxylate, (DABCO TMR-2)], potassium 2-ethylhexanoate, (DABCO K-15), and 1,3-5,-tris(dimethylaminopropyl)sym-hexahydrotriazine, (Toyocat TRC)], silicone surfactant, [poly(dimethyl siloxane-oxyalkylene- block copolymer , DC-137], and a physical blowing agent, $CCl_2F - CH_3$, (HCFC-141b) , were used.

1.2. Foaming Procedures

The one step process employed for preparing modified polyisocyanurate foams was as follows; Into a paper cup, a polymeric MDI and a silicone surfactant were charged and then a carbodiimdie-forming catalyst and an isocyanate trimerization catalyst were added using microsyringes. After the catalysts were added, the mixture was immediately stirred for 7-10 seconds at about 2000 rpm. using a high shear stirring paddle, and allowed to foam in the paper cup. The foams

Table I. Modifiers for Isocyanurate Foams

Modifier	Resulting Linkage	Structure
Polyol	Urethane	-NH-CO-O-
Polycarboxylic acid	Amide	-NH-CO-
Carboxylic dianhydride	Imide	CO -R N- CO
(catalyst only)	Carbodiimide	-N=C=N-
Polyepoxide	Oxazolidone	-NH-CH$_2$-CH- O=C O R
Poly-sec.amine	Urea	-N-CO-NH-

Table II. Comparison Between Unmodified Polycarbodiimide Foam and Unmodified Polyisocyanurate Foam

Formulation (pbw)	1	2
Polymeric MDI	25.	25.
DC-193	0.4	0.4
PMPO	1.0	0.
Dabco TMR-2	0.	0.4
HCFC-141b	0.	5.0
Reaction Profile		
Cream time, sec.	60.	70.
Gel time, sec.	1,400.	110.
Rise time, sec.	>3,600.	185.
Foam Properties		
Density, kg/m^3	19.4	28.5
Cell size	coarse	fine
Closed cell content,%	5.0	90.0
Friability, % wt. loss	20.0	100.

were post cured for 2 days under ambient conditions before testing. Similar procedures were used for preparing other types of modified polyisocyanurate foams.

   The two step process consists of the first step of prepolymer preparation and the second process of mixing foaming ingredients . The prepolymers were prepared by the reaction of a modifier with an excess amount of polyisocyanate. The preparation conditions are described in respective chapters.

   This process was preferably used for preparing CD-PIR foams and adipic acid modified A-PIR foams.

1.3. Foam Testing

   The smoke density was determined by the ASTM D-2843-70 using the XP-2 smoke chamber. The Butler chimney test was used for determining surface flammability according to ASTM D-3014-76. The friability test was conducted according to ASTM C-421, and the oxygen index was determined by ASTM D-2863-77. The flame penetration test was conducted by the method according to the Bureau of Mines Report of Investigation # 6366 (1964).

1.4. Results and Discussion

   A comparison of an unmodified carbodiimide foam (Formulation #1) and an unmodified isocyanurate foam (Formulation #2) are shown in Table II. The unmodified carbodiimide foam exhibited a low closed cell content and a low friability. In comparison, the unmodified polyisocyanurate foam exhibited a high closed cell content and extremely high friability.

   CD-PIR foams were prepared by both the one step and the two step processes. A one step process formulation and the foam properties obtained are listed in Tables III and IV. Table III shows a comparison of various catalysts. In the one step process, low density foams were obtained without the addition of blowing agents, because the carbodiimide linkage formation is accompanied by the simultaneous generation of carbon dioxide gas. Table IV exhibits the effect of component temperature of CD-PIR by the one step process. A   component temperature of 40 -60 $^\circ$C gave a desirable foaming profile, and the resulting foams exhibited outstanding flame retardance in terms of the Butler Chimney test and superior low-friability, but the closed cell content was low due to the generation of carbon dioxide gas in the low viscosity components. Therefore, the prepolymer (two step) process was attempted to solve this disadvantage.

   A two step process formulation and the foam properties obtained are shown in Table V. In the two step process, HCFC 141b was added as physical blowing agent. Both the carbodiimide linkage and the isocyanurate linkage are thermally stable, and therefore, modification by these linkages provides more thermally stable

Table III. Effect of PMPO & Cyclotrimerization Catalysts on Physical Properties of CD-PIR ** Foams, (One Step Process)

Formulation (pbw)	1.	2.	3.	4.	5.
Polymeric MDI (1)	25.	25.	25.	25.	25.
PMPO (2)	0.36	0.67	1.44	1.44	1.44
DC-193 (3)	0.4	0.4	0.4	0.4	0.4
Dabco TMR-2 (4)	0.12	0.12	0.12	0.	0.
Dabco K-15 (5)	0.	0.	0.	0.12	0.
Toyocat TRC (6)	0.	0.	0.	0.	1.0
Reaction Profile					
Cream time,sec.	60.	35.	18.	14.	14.
Gel time, sec.	120.	115.	110.	80.	90.
Rise time, sec.	172.	155.	135.	120	155
Foam Properties					
Density, kg/m^3.	47.3	33.3	27.2	30.6	27.4
Cell size	fine	fine	fine	fine	fine
Closed cell, %	6.9	6.8	14.7	29.3	15.3
Friability, % wt.loss	52.5	42.6	14.4	29.3	15.3
Butler Chimney, % wt.retained	96.4	96.0	91.8	93.1	85.7
Oxygen index	28.5	28.0	27.5	27.5	25.0

Note:
(1) %NCO: 31.2   , (2) 1-Phenyl-3-methyl-2-phosphorene-1oxide
(3) Silicone surfactant, (4) Quaternary ammonium carboxylate (5) Potassium 2-ethylhexanoate
(6)1,3,5-tris(dimethylaminopropyl)sym-hexahydrotriazine
 **   Carbodiimide-modified polyisocyanurate

Table IV. Effect of Component Temperature of CD-PIR * Foams on Foam Properties (One Step Process)

Formulation (pbw)	1	2	3
Polymeric MDI	25.	25.	25.
PMPO	0.25	0.25	0.25
DC-193	0.4	0.4	0.4
Dabco K-15 **	0.12	0.12	0.12
Component -			
Temperature,^{o}C	25.	40.	60.
Reaction Profile			
Cream time, sec.	86.	16.	10.
Gel time, sec.	100.	30.	20.
Rise time,sec.	120.	36.	28.
Foam Properties			
Density, kg/m^3	44.4	41.1	34.0
Cell size	fine	fine	fine
Friability, % wt.loss	33.3	24.0	20.0
Butler Chimney,			
% wt. retained	97.6	97.9	97.7

*   Carbodiimide-modified polyisocyanurate
**   Potassium 2-ethylhexanoate

Table V. CD-PIR * Foams by the Two Step Process

Formulation (pbw)	1	2	3	4
%NCO, Prepolymer	29.2	26.7	23.2	19.3
Polymeric MDI,	25.	25.	25.	25.
DC-193	0.4	0.4	0.4	0.4
Dabco TMR-2	0.4	0.4	0.4	0.4
HCFC-141b	4.5	4.5	4.5	4.5
Foam Properties				
Density, kg/m^3	28.5	28.0	27.3	29.8
Cell size	coarse	fine	fine	fine
Closed cell,%	56.1	93.4	82.4	15.8
Friability, %wt.loss	100	50.0	45.5	41.5
Butler Chimney,				
% wt. retained	98.6	94.1	95.3	95.7
Oxygen index, %	29.5	27.5	27.5	27.0

*   Carbodiimide-modified polyisocyanurate
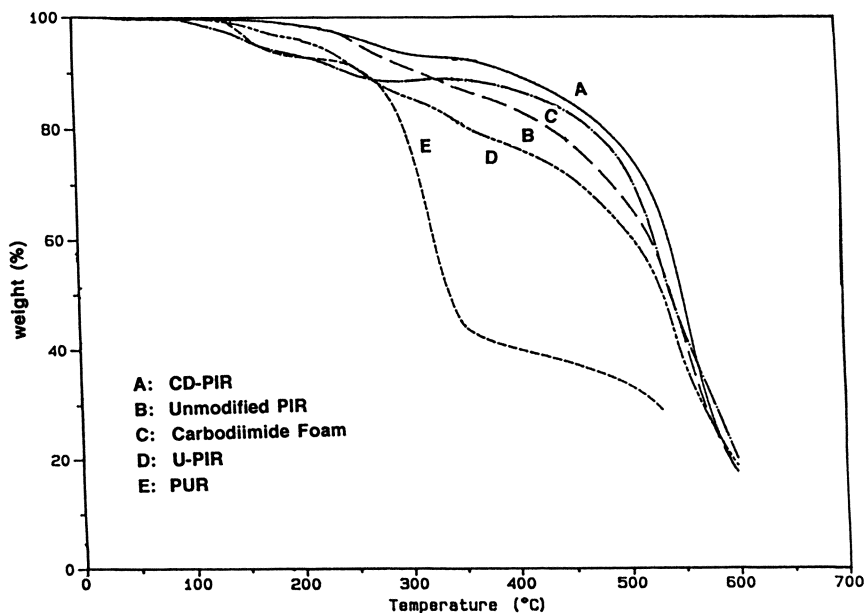
Figure 4. TGA Profiles of Various Foams
(Reproduced with permission from K.Saiki, K.Sasaki and
K. Ashida, J. Cellular Plastics, Vol.30, No.5, Figure 1)
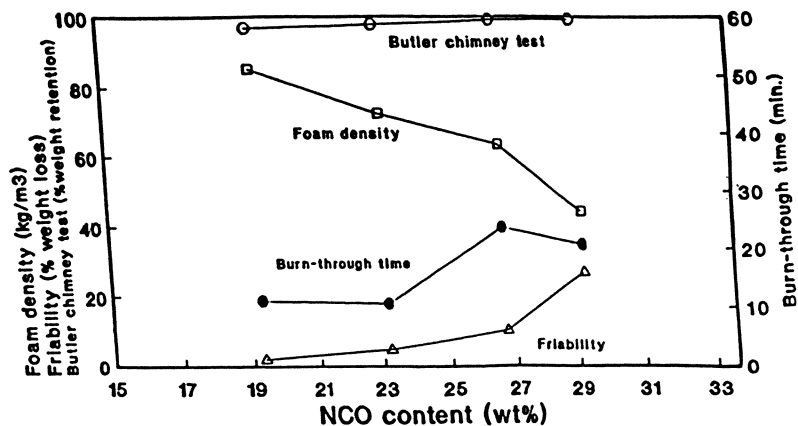
Figure 5. Relationship Between NCO% vs. Foam Properties.
(Reproduced with permission from K.Saiki, K.Sasaki and
K. Ashida, ibid: Vol.30, No.5, Figure 2)

foams than the U-PIR foams. Figure 4 shows a thermal stability comparison of CD-PIR foam, unmodified PIR foam, U-PIR foam (NCO / OH equivalent ratio = 30) and a PUR foam by means of TGA. The four kinds of modified foams, except PUR foam, exhibited superior thermal stability.

Figure 5 shows the relationship between NCO% of prepolymers vs. foam properties. The foams were prepared with the addition of carbodiimide-forming catalyst and without the addition of a physical blowing agent, i.e. the foams were blown by the carbon dioxide generated in the simultaneous formation of carbodiimide linkages by the condensation reaction of isocyanate groups. Therefore, the higher the NCO content of the prepolymers , the higher the CO_2 generation , and therefore,the lower the foam density. It should be noted that the resulting foams exhibited outstanding weight retention determined by the Butler chimney test. according to ASTM D-3614, and low flame penetration (burn through) time.according to Bureau of Mines test (Report # 6366)

Figure 6 shows a significant difference in smoke density between the CD-PIR foam and the U-PIR foam.

2) Amide-Modified Isocyanurate Foams.(A-PIR Foams)

2-1. Raw Materials: The modifiers used in this study are adipic acid, dimer acid (Hystrene 3695, Witco Chemical) and a ketimine prepared by the reaction of 2-heptanone and hexamethylenediamine. The trimerization catalysts employed were quaternary ammonium 2-ethylhexanoate in dipropylene glycol (Dabco TMR , Air Products) , N,N',N"-tris(dimethylaminopropyl)-sym-
-hexahydrotriazine (Toyocat TRC), and potassium acetylacetonate (Kacac) in ethylene glycol. The silicone surfactant employed was DC-193 and the physical blowing agent for the two step process was HCFC-141b. The polymeric isocyanate used had an NCO content of 31.2 % . The isocyanate-terminated amide prepolymers were prepared as follows: adipic acid was dissolved in THF,
mixed with an excess of polymeric MDI (NCO / COOH = 10/1) and reacted at 80 - 90 $^{\circ}$C until the carbon dioxide generation ceased. After the reaction was completed , the THF was removed by distillation.

2-2. Foam Preparation and Testing

The one step process was carried out as follows: Polymeric isocyanate, modifiers and surfactants were hand-mixed at room temperature. In this process, adipic acid as modifier did not give good foams because it was insoluble in the foam ingredients. Dimer acid and a ketimine were used as liquid state modifiers in this process. After the catalysts were added to the mixture, it was stirred for 10 seconds and poured into a paper cup. The cup was put in an oven at about 70 $^{\circ}$C to
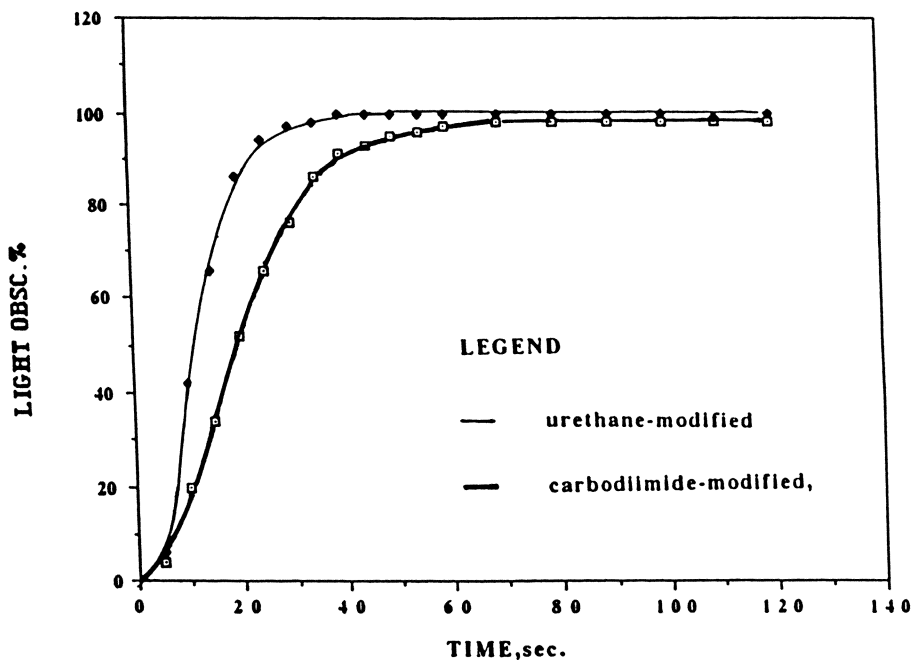
Figure 6. Smoke Density Comparison.
          (Reproduced with permission from K.Saiki, K.Sasaki and
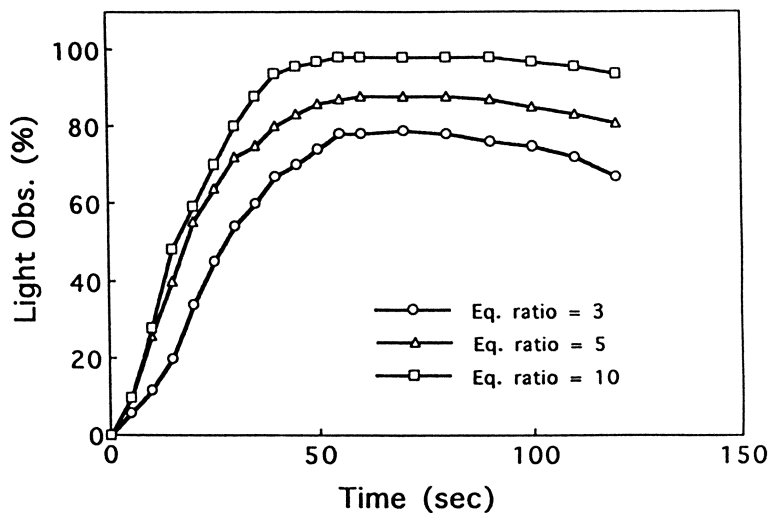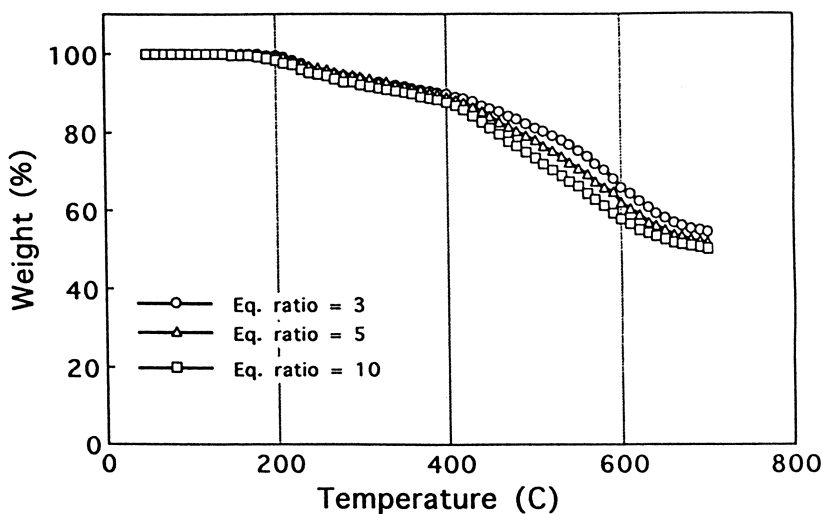   K. Ashida , ibid: Vol.30, No.5, Figure 3)
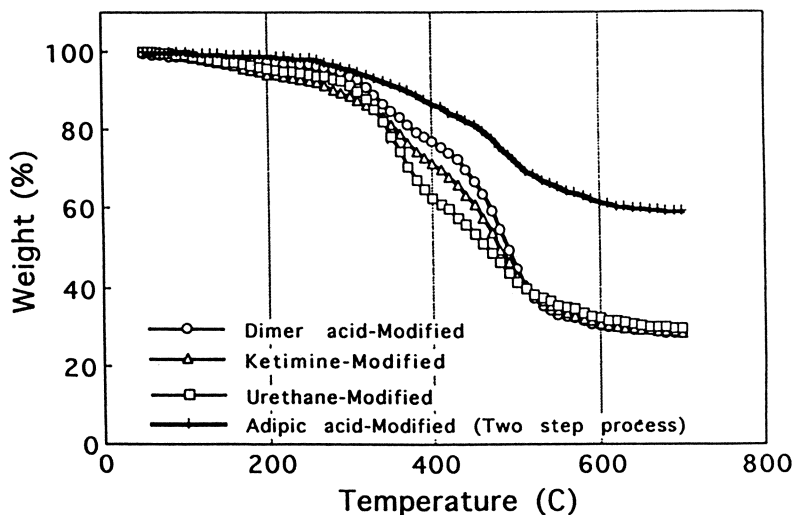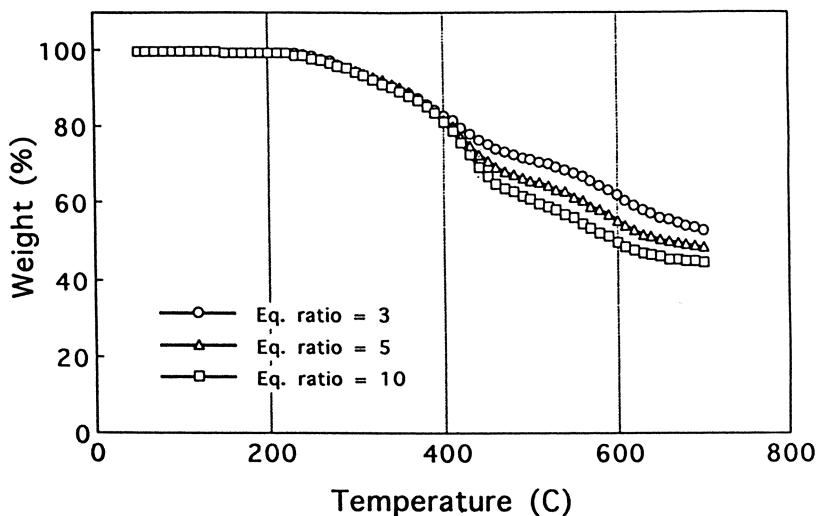

Figure 7. TGA Profiles of Modified Isocyanurate Foams.
          (Reproduced with permission from J. Goto, K. Sasaki, and
          K. Ashida, ibid: Vol. 31, No.6, Figure 1)

accelerate the reaction. The resulting foam was post-cured at 120 °C for 24 hours.

2.3. Results and Discussion

The above-mentioned liquid modifiers did not impart satisfactory fire resistant to the A-PIR foam properties due to the relative large hydrocarbon chains.

The two step process was carried out as follows: Adipic acid was reacted in excess amount of polymeric isocyanate to produce NCO-terminated amide-containing prepolymers,as explained in Section 2-1. The prepolymers were then cyclotrimerized in the presence of the physical blowing agent, HCFC-141b.

The TGA profiles of various A-PIR foams are shown in Figure 7 in which adipic acid -modified isocyanurate foam , prepared by the two step process, exhibited outstanding thermal stability. Figure 8 shows smoke densities of various A-PIR foams. The two step process formulation employed and physical properties of the resulting foams are shown in Table VI. The resulting foam exhibited high flame retardance and low friability.

3)   Imide-Modified Isocyanurate Foams (I-PIR Foams)

3-1.   Raw Materials

BTDA (3,3'4,4'-Benzophenone tetracarboxylic dianhydride) was used as modifier for imide-modified isocyanurate foams. The trimerization catalysts employed were N,N',N''-tris(dimethylaminopropyl)-sym-hexahydrotriazine (Toyocat TRC) and the imide-forming catalyst employed was Kacac(potassium acetylacetonate in ethylene glycol).

3-2.   Results and Discussion

Foams were prepared by the one step process at 120 °C using the formulations shown in Table VII. Neither solvents nor physical blowing agents were used. Outstanding smoke suppression was observed as shown in Figure 9 It is interesting to note that a lower equivalent ratio of NCO / anhydride of I-PIR foams exhibited better smoke suppression. Similarly, better thermal stability in terms of TGA profile was obtained as shown in Figure 10. These results suggest that the imide linkage has higher thermal stability than the isocyanurate linkage.

4)   Imide- / Carbodiimide-Modified Isocyanurate Foams
(I- / CD--PIR Foams)

The title foams were prepared by the reaction of polymeric MDI with 3,3',4,4'-benzophenone tetracarboxylic dianhydride (BTDA) at 120 °C in the presence of a cyclotrimerization catalyst ; 1,3,5-tris(dimethylaminopropyl)-s-hexahydrotriazine (Toyocat TRC), and a carbodiimide catalyst ; 1 -phenyl-3-methyl-2-phospholene-1-oxide (PMPO. The formulations employed are shown in
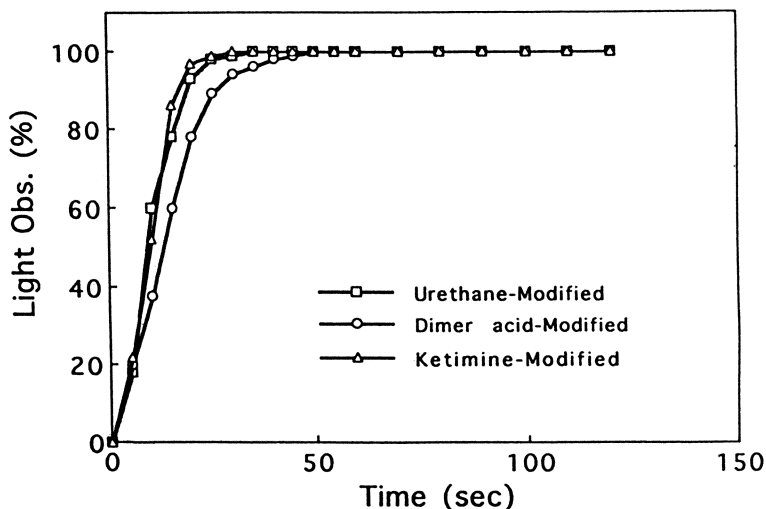
Figure 8. Smoke Densities of Modified Isocyanurate Foams (Eq.ratio : 5)
(Reproduced with permission from J. Goto, K. Sasaki, and
K. Ashida, ibid: Vol. 31, No.6, Figure 2)

Table VI.   A-PIR * Foams by the Two Step Process

Formulation (pbw)

Amide-prepolymer * *	100.
DC-197	2.0
Toyocat TRC	1.6
HCFC-141b	15.0

Reaction Profile

Cream time,sec.	36.
Gel time, sec.	68.
Rise time,sec.	195.
Tack free, time, sec	118.

Foam Properties

Density, kg/m3	32.8
Cell size	fine
Butler Chimney,%wt.retained	94.0
Friability, %wt.loss	30.6

----

    *   Amide-modified polyisocyanurate
    * *   NCO / COOH = 10.

Table VII.   I-PIR * Foams by the One Step Process

Formulation (pbw)	1	2	3
Polymeric MDI	100	100	100
BTDA (1)	40.1	24.1	12.0
DC-197	2.8	2.5	2.2
Equ.ratio,(NCO/anhydride)	3.0	5.0	10.0
DC-197	2.8	2.5	2.2
Toyocat TRC (2)	2.8	2.5	2.2
Kacac (3)	2.8	2.5	2.2
Reaction Profile			
Gel time, sec.	390	335	292
Rise time,sec.	516	482	450
Foam Properties			
Density, Kg/m3	31.1	37.0	49.9
Cell size	coarse	fine	fine
Butler Chimney, %wt.retained	91.9	92.0	95.0
Friability, %wt.retained	46.8	43.6	42.0
Closed cell content,%	60.9	77.4	95.4

* Imide-modified polyisocyanurate
(1)   3,3',4,4'-Benzophenone tetracarboxylic dianhydride
(2)   1,3,5-Tris(dimethylaminopropyl)sym-hexahydrotriazine
(3)   Potassium acetylacetonate in ethylene glycol

Figure 9. Smoke Densities of Imide-Modified Isocyanurate Foams.
(Reproduced with permission from J. Goto, K. Sasaki, and
K. Ashida, ibid: Vol. 31, No.6, Figure 3)

Figure 10. TGA Profiles of Imide-Modified Isocyanurate Foams.
(Reproduced with permission from J. Goto, K. Sasaki, and
K. Ashida, ibid: Vol. 31, No.6, Figure 4)

Table VIII. The modifier, BTDA, is a fine powder having a melting point of 225°C, and does not react at room temperature. Therefore an elevated temperature was employed for the reaction.

The properties of the resulting foams are shown in Figures 11 and 12, respectively. Similar to the I-PIR foams, the I- / CD- PIR foams exhibited greater smoke suppression than the other modified-isocyanurate foams. However, the I- / CD-PIR foams had higher friability and a very low closed cell content.This might be due to the generation of large amounts of carbon dioxide in the simultaneous formation of both the imide and carbodiimide formation.

5)   Overall Comparison of Foams

Figure 13 shows an overall comparison of three foam properties (Butler weight retention, tumbling friability, and % closed cell content) of four kinds of modified isocyanurate foams,i.e, U-PIR, A-PIR, I-PIR and I-/ CO-PIR foams. Based on the results shown in this figure, the overall properties of the A-PIR foam seem to be the best.

6)   Zero ODP, Halogen-free Azeotropes as Blowing Agents for PIR Foams

Due to the ozone depleting potential in the stratosphere , CFCs have been phased out. Alternative physical blowing agents candidates under evaluation are HFCs (hydrofluorocarbons), C_5-hydrocarbons and halogen-free azeotropes [11, 12] . In this study , an azeotrope consisting of n-pentane / methyl formate was used as a blowing agent. The formulation and physical properties of foams are shown in Table IX. A comparison of the Butler chimney tests between an azeotrope "A-22" :(n-pentane/methyl formate) blown foam and a CFC-11 blown foam is shown in Figure 14 to demonstrate the influence of the proposed blowing agent on the foam flammability.

Conclusions

Thermally stable linkages, e.g., amide, imide, and carbodiimide linkages were used as modifiers in place of urethane linkages for isocyanurate foams .The resulting foams exhibited better properties with regards to Butler Chimney weight retention and TGA profile than those of urethane-modified isocyanurate foams. In addition, amide-modified isocyanurate foams prepared by the prepolymer process could meet the requirements for high closed cell content,low smoke generation ,and low friability for building insulation materials. Therefore, it could be concluded that

Table VIII.   I- / CD-PIR * Foams by the One Step Process

Formulation (pbw)	1	2	3
Polymeric isocyanate	100	100	100
BTDA **	40.1	24.1	12.0
Equiv.ratio,NCO/anhydride.	3	5	10
DC-197	2.8	2.5	2.2
Toyocat TRC	2.8	2.5	2.2
PMPO	1.4	1.2	1.1
Reaction Profile			
Gel time, sec.	635	485	401
Rise time,sec.	719	710	804
Tack free time,sec..	699	555	638
Foam Properties			
Density, kg/m3	26.3	23.2	20.2
Cell size	fine	fine	fine
Butler Chimney,			
%wt.retained	93.1	92.0	91.4
Friability, % wt.loss	81.8	82.7	70.3

*   Imide / carbodiimide-modified polyisocyanurate
**   3,3',4,4'-benzophenone tetrcarboxylic dianhydride

Figure 11. TGA Profiles of Imide/Carbodiimide Modified Isocyanurate Foams.
(Reproduced with permission from J. Goto, K. Sasaki, and
K. Ashida, ibid: Vol. 31, No.6, Figure 5)
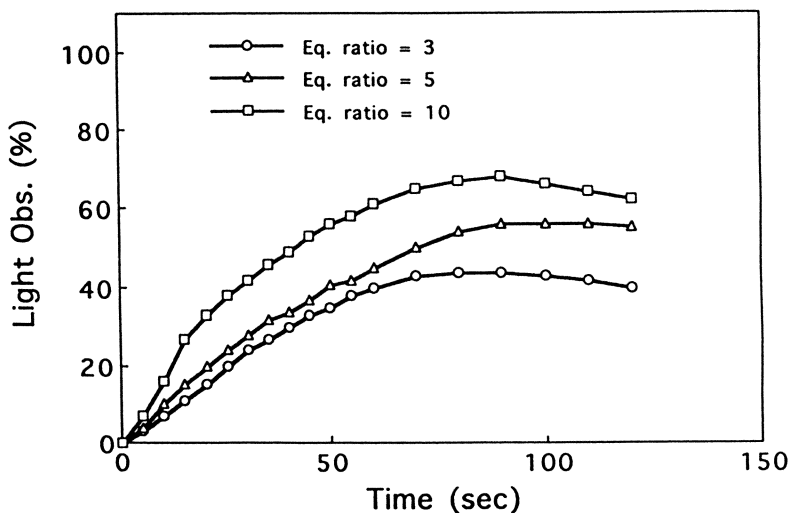
Figure 12. Smoke Densities of Imide/Carbodiimide-Modified Isocyanurate Foams.
(Reproduced with permission from J. Goto, K. Sasaki, and
K. Ashida, ibid: Vol. 31, No.6, Figure 6)

% BUTLER WT. RETENTION

% TUMBLING FRIABILITY

% CLOSED CELL CONTENT
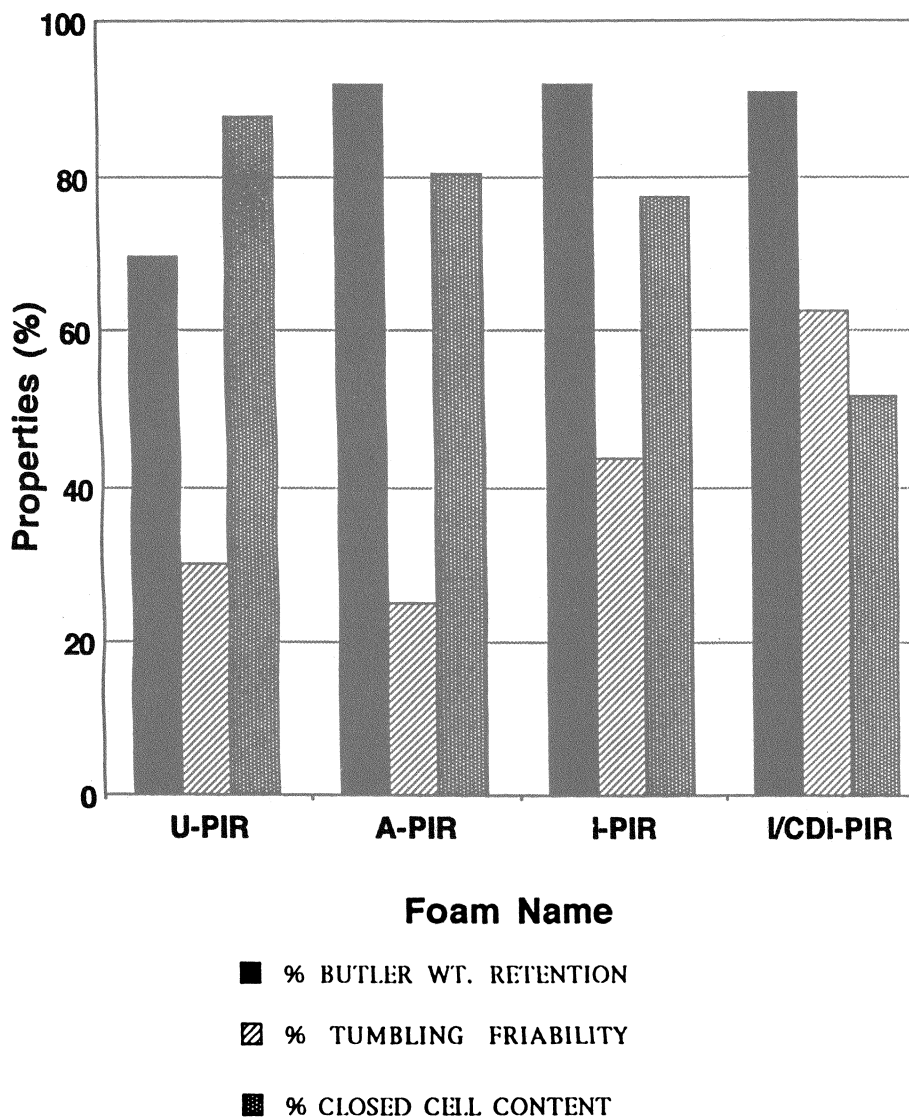
Figure 13. Overall Comparison of Modified Isocyanurate Foams.
(Reproduced with permission from J. Goto, K. Sasaki, and
K. Ashida, ibid: Vol. 31, No.6, Figure 7)

Table IX   PIR Foams Blown with Physical Blowing Agents

Formulation (pbw)	1	2	3	4
PAPI 580	100	100	100	100
Pluracol TP440	19.8	9.9	6.6	6.6
DC-193	1.5	1.5	1.5	1.5
Dabco TMR-2	1.5	1.5	1.5	1.5
CFC-11	0	0	0	16.6
n-Pentane	3.8	3.8	3.8	0
Methyl formate	4.1	4.1	4.1	0
NCO/OH ratio	5	10	15	15
Foam Properties				
Density, kg/m3	39.1	38.8	37.7	36.1
Friability, %wt.loss	17.3	20.1	23.5	21.7
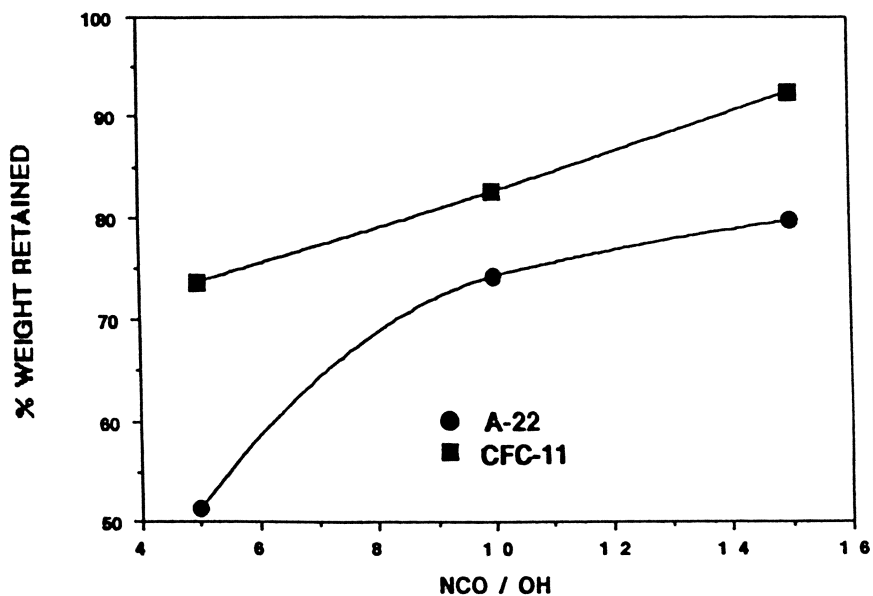
Figure 14. Butler Chimney Flammability
(Reproduced with permission from K. Ashida, K. Morimoto, and A. Yufu, ibid. Vol.31, No.4, Figure 27.)

amide-modified isocyanurate foams are the best foams among the modified foams investigated.

Novel physical blowing agents having zero ODP, i.e., halogen-free azeotropes used for preparing urethane-modified isocyanurate foam were deserved to have only slightly lower weight retained in the Butler Chimney Flammability Test.

References
1.   Ashida, K, Yagi,T. ,French Patent 1 511 865 (to Nisshinbo)
      1967
2.   Ashida, K.; Polyisocyanurate Foams, Chapter 6 of "Handbook of
      Polymeric Foams and Foam Technology" , (pp. 95 - 134) ;
      D. Klempner and K. C.Frisch. Eds. , Hanser Publishers, (1991) .
3.   Ashida,K. , Thermosetting Foams, Chapter 3 of " Handbook of
      Plastic Foams ", (pp. 11-183) ; A. Landrock , Ed; Noyes Publishers,
      (1995)
4.   Grieve,R.L.(to Upjohn Co.), U.S.Pat. 3,644,234 , 1972.
5   Bernard,D.L. Doheny,A.J. (to Mobay Chem..) Belg. Pat. 723,151 1967
6.   Ashida, K. and Frisch, K.C.*J.Cellular Plastics*, Vol. 8, p. 160 **1972**
7.   Scott,R.V.House,D.W.,Gattuso,M.J.& Ashida,K., Frisch,K.C.Klempner,
      D.Mahdi,S. and Parekh, C., *Proceedings of the SPI-34th Annual
      Technical/Marketing Conference*, October 21-24, 1992, New Orleans,LA,
      p.331.
8.   Saiki, K. Sasaki, K. and Ashida,K.   *J. Cellular Plastics* Vol. 30, No.5,
      1994, p. 470.
9.   Goto,J.Sasaki,K.and Ashida,K., *J. Cellular Plastics*, Vol. 31, No.6,
      1995 , p. 548.
10.   Zhang, Z. and Ashida, K., *Proceedings of the Polyurethane 1995
      Conference,*   Sept. 26-29, 1995, Chicago, p.234.
11.   Ashida,K. Morimoto, K. and Yufu,A. , *J. Cellular Plastics*, Vol. 31,
      No.4, **1995**, p.330.
12.   Ashida, K. *Proceedings of 1995 International CFC and Halon Alternatives
      Conference & Exposition.* October 21-23, 1995, Washington , D.C.,
      p.438.

Chapter 7

Microcellular Foams

Vipin Kumar and John E. Weller

UW–Industry Cellular Composites Consortium, Department of Mechanical Engineering, Box 352600, University of Washington, Seattle, WA 98195

Microcellular polymers refer to closed cell thermoplastic foams with an extremely large number of very small cells. Typically, one hundred million or more bubbles nucleate per cm^3 of polymer, and each cell is of order 10 μm in diameter. These materials were first produced in the early 1980's with the objective of reducing the amount of polymer used in mass produced items, and have the potential to revolutionize the way thermoplastic polymers are used today. Microcellular plastics have been produced from a number of polymers and can be produced with densities ranging from 3 to 99 percent of the density of the solid material, offering engineers a new range of properties for design. Microcellular foams possess improved fatigue life and energy absorption characteristics as well as a high specific strength. It is expected that these materials will be utilized in a wide variety of applications in the next century.

Imagine solid polymers replaced by microcellular polymers with 20 to 40 percent reduction in material without compromising their function or required strength. Also look forward to composite microcellular materials with layers of solid and cellular materials designed to offer optimum mechanical and thermal properties and a minimal use of polymer. Created by processes without using any chemicals that are harmful to the environment, such materials may well become widely used by the turn of the century!

Microcellular polymers are closed cell plastic foams with a bubble densities in excess of 100 million bubbles per cm^3 and diameters of order 10 μm. The idea to introduce very small bubbles in plastics by gas nucleation was originally advanced by Professor Nam P. Suh (*1*) of the Massachusetts Institute of Technology around 1980 as a means to reduce the cost of many mass produced plastic items. The rationale was that if bubbles smaller than the critical flaws that already exist in plastics could be introduced in sufficient numbers, then the material density could be reduced while maintaining the essential mechanical properties.

The basic microcellular process is a two-step process shown in Figure 1. In the first step, the polymer sample is saturated by a pressurized, non-reacting gas in a pressure vessel. Over time, the polymer absorbs the gas, and eventually become saturated. When the polymer is saturated, it will not absorb any more gas, and the gas is distributed uniformly throughout the polymer. Typically, it takes several hours to several days for a thin polymer sheet to become saturated. Of course, the amount of time required to satu-

101
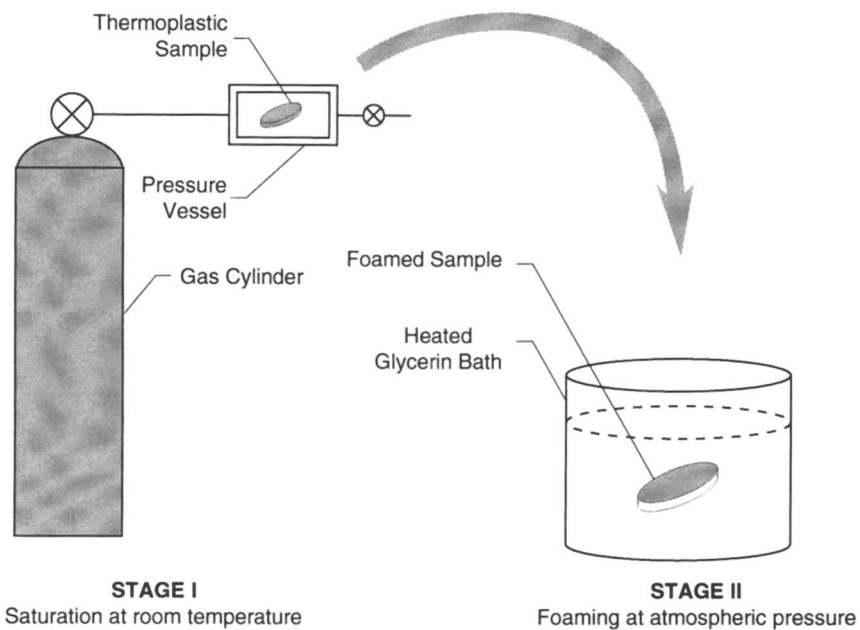
Figure 1. Schematic of the microcellular process: (a) saturation of polymer with gas at room temperature; (b) bubble nucleation and growth at atmospheric pressure.

rate the polymer depends on the polymer itself, its diffusivity, its thickness, the satura-
tion temperature, and sometimes the gas pressure.

   This saturation step is usually carried out at room temperature since the solubil-
ity of most gases is higher at lower temperatures. Higher saturation temperatures may be
employed however, to accelerate the diffusion of gas in the polymer. After the polymer
has become saturated, it is removed from the pressure vessel and then foamed. In the
second step of the process, the saturated sample is heated to the foaming temperature,
which is close to the glass transition temperature of the virgin polymer. During this stage
a large number of bubbles nucleate and grow. Bubble growth is controlled by holding the
specimen at the foaming temperature for a certain length time. This time is commonly
referred to as the foaming time. Since the growth rates of bubbles near the glass transi-
tion temperature are relatively low, it is possible to arrest the bubble growth in a control-
lable manner by quenching the foam in a low temperature bath.

   Figure 2 shows scanning electron micrographs of a number of polymers foamed
by this process. The microcellular structure for all of these foams is very homogenous,
and the bubbles are typically between 5 to 25 µm in diameter. One exception is the PET
foam, where the bubbles are an order of magnitude larger. The average bubble size in all
microcellular foams is strongly influenced by the number of bubbles that nucleate, which
in turn is a function of the concentration of gas in the sample after saturation. The den-
sity of the foams can be controlled by choosing an appropriate gas saturation pressure,
and using a suitable foaming time and temperature. These parameters are specific to a
given gas-polymer system, and for the most part must be determined experimentally.

   Figure 3 shows scanning a scanning electron micrograph of a polystyrene sample
showing the full specimen cross section. This sample was originally 0.40 mm thick and
grew to a thickness of 0.65 mm after foaming. This example shows that thin sections of
polymers normally made from solid polymer can indeed be foamed by the microcellular
process (7).

Overview of Microcellular Polymers

The basic microcellular process outlined above has been successful with a number of
amorphous polymers, and semicrystalline polymers with low levels of crystallinity. Some
of these gas-polymers systems are discussed below.

Polyvinyl Chloride (PVC). Microcellular PVC foams have been produced by Kumar
and Weller (2) using carbon dioxide as the nucleating gas. Bubble densities in the range
10^7-10^9 per cm^3 of polymer were achieved, and foams with relative density (density of
the foam divided by the density of the polymer) in the range 0.15 to 0.94 have been
produced. The sorption data for carbon dioxide in PVC (2) shows that for 2 mm thick
specimens of a rigid PVC formulation saturated at 4.8 MPa and room temperature, the
gas concentration at equilibrium is approximately 75 mg of carbon dioxide per gram of
PVC, or about 7.5 percent by weight. Thus a very high concentration of gas molecules
exists in the polymer matrix at saturation. As a result, there is significant plasticization
of the polymer, and the glass transition temperature drops from 78.2 °C for original PVC
to an estimated 14 °C upon saturation (2). Bubble nucleation and growth is therefore
possible at very moderate temperatures, at or below the glass transition temperature of
the original polymer. In the case of PVC, the lowest temperature at which microcellular
foam was produced was 14 °C

   Figure 4 shows the range of relative densities for the family of microcellular PVC
foams produced by heating the saturated PVC specimens to different temperatures. The
lowest density foams (15 to 20 percent of the solid PVC density) are produced in the
100-115°C temperature range. Note the nearly linear variation of foam relative density
with foaming temperature in the range 56°C to 105°C, demonstrating that the foam den-
sity can be simply and accurately controlled by controlling the temperature to which the
saturated plastic is heated.
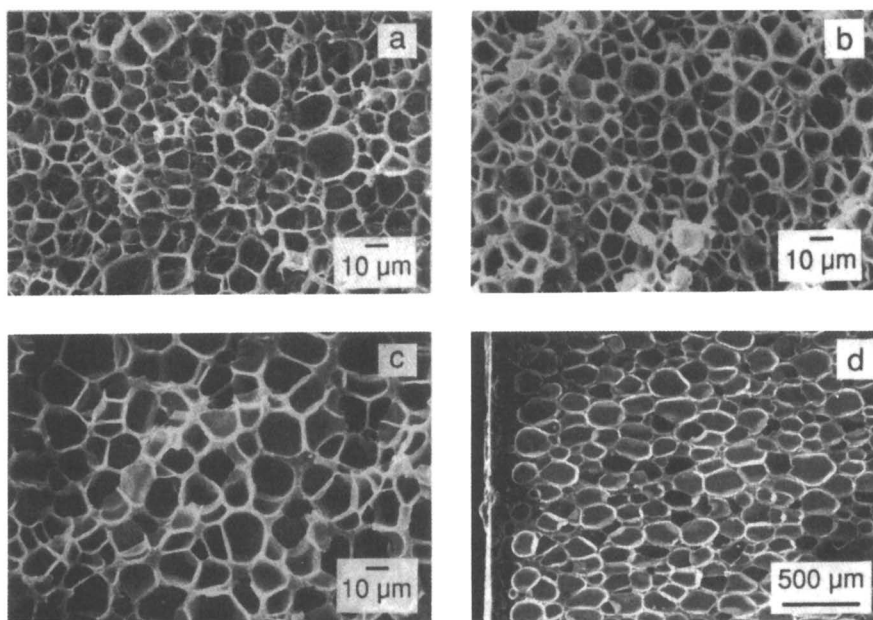
Figure 2. Scanning electron micrographs showing examples of the structure created by the microcellular process: (a) PVC; (b) polycarbonate; (c) ABS; and (d) PET.
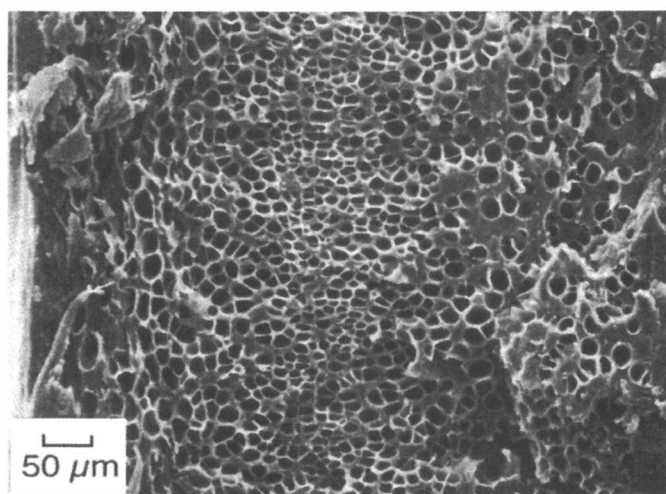
Figure 3. Overall view across a polystyrene sample originally 0.40 mm thick (7). The thickness after foaming was 0.65 mm.

Polycarbonate (PC). Creation of microcellular structure in polycarbonate was first reported in 1990 by Kumar, Weller and Hoffer (*3*). Carbon dioxide, due to its high solubility in polycarbonate, was used to achieve very high bubble nucleation densities in the range $1\text{-}10 \times 10^9$ per cm^3 of polymer. Sorption data shows an equilibrium gas concentration of approximately nine percent by weight at a saturation pressure of 4.8 MPa. The number of bubbles nucleated was found to increase exponentially with increasing gas saturation pressure. A family of microcellular polycarbonate foams has been produced ranging in density from 10 to 99 percent of the density of solid polycarbonate.

Weller (*24*) has conducted a detailed characterization of the PC-CO_2 system. The density of microcellular polycarbonate foams as a function of the foaming temperature for various saturation pressures is shown in Figure 5. Again, we see a linear relationship, suggesting that the foaming temperature is a critical parameter for controlling the density of the microcellular foams, and thus an effective means of in-process control of foam morphology. The data in Figure 5 is discussed further in the section on mechanical properties.

Polystyrene (PS). Microcellular polystyrene has been studied by a number of investigators (*1,6,7,8,9,10,15*). Martini et al. (1) produced microcellular polystyrene with cells in the 5-25 mm range and void fractions of 5 to 30 percent. Using higher nitrogen pressures for saturation, Kumar (10) extended the void fraction range to 80 percent. This was possible because the number of bubbles increased exponentially with saturation pressure, allowing for lower density foams to be produced while keeping the average bubble diameter in the microcellular range.

Polyethylene Terephthalate (PET). Kumar and Gebizlioglu (*11*), and Baldwin and Suh (*12*) have applied the microcellular process to foam PET using carbon dioxide. The results with PET have been most interesting. It has been found that with sufficiently long exposure to high pressure carbon dioxide, PET begins to crystallize. The resulting PET foams have a significantly higher crystalline content, and although mechanical property data is not yet available, these foams appear to be much stronger than microcellular foams from other polymers at comparable relative densities.

PETG. The most recent addition to the family of polymers successfully processed by the microcellular process is PETG *(22,23)*. Relative densities of three percent and higher have been achieved using carbon dioxide for bubble nucleation, see Figure 6. An interesting observation in CO_2-PETG system is the relatively high foaming temperature to which the process appears to be stable. In Figure 6, the highest temperature at which foam was produced is 120 °C, which is nearly 40 °C above the T_g of PETG. By comparison, in Polycarbonate-CO_2 system, the process becomes unstable at 160 °C, about 10 °C above the T_g of polycarbonate.

Mechanical Properties of Microcellular Polymers

The available mechanical property data on microcellular foams is expected to increase as the number of researchers and our understanding of the processing characteristics of different gas-polymer systems grows. However, the data available so far is quite limited except for a few select systems. The results to date show that these novel materials offer many properties that were not previously available from either conventional foams or solid polymers. In many cases, the properties are improved over those of conventional foams, and in some cases a particular property may be better than that of the original, solid material.

The polycarbonate - CO_2 system has received a great deal of attention since a wide range of processing conditions have been documented *(24)*. Figure 5 shows the
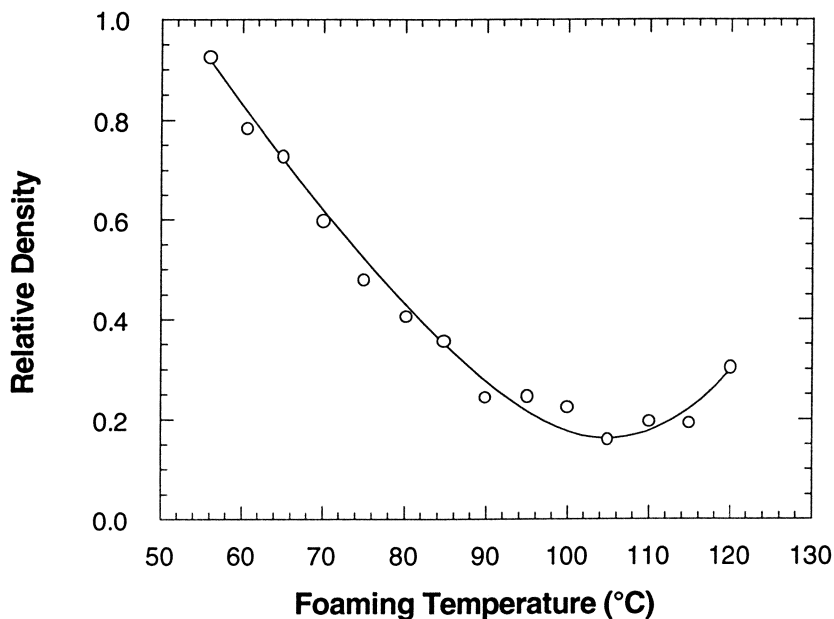
Figure 4. Plot of PVC foam relative density as a function of foaming temperature for specimens saturated with carbon dioxide at 4.8 MPa (2)
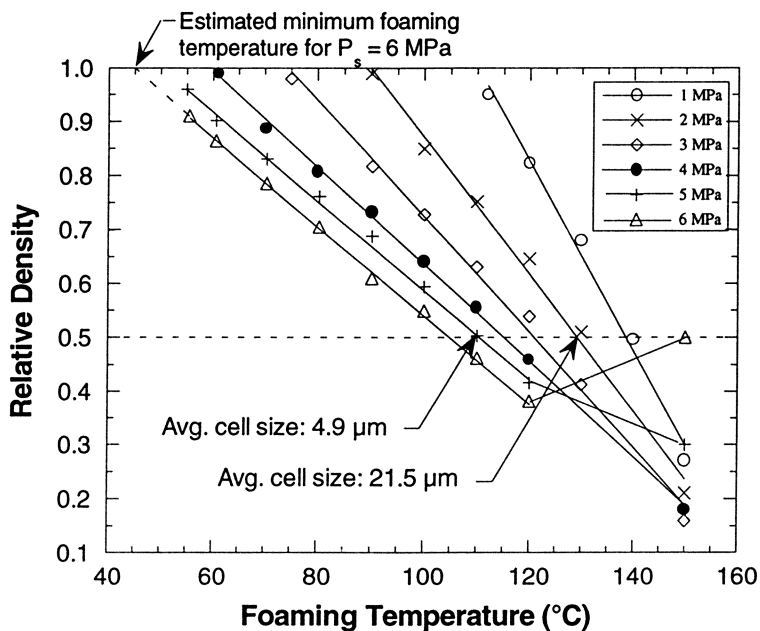
Figure 5. The steady state process space for the polycarbonate-CO_2 system.

steady state process space for PC-CO$_2$ system, where steady state refers to the state where all cell growth has completed. This figure illustrates the wide range of relative densities that can be produced in this system and the numerous processing conditions that can be employed. These different processing conditions can be used to produce foams that have the same relative density and different average cell size. For example, a sample could be saturated at 5 MPa and foamed at approximately 100 °C or it could be saturated at 1 MPa and foamed at 140 °C to produce a foam of the same density. The possibility of producing these foams is illustrated by the horizontal dashed line in Figure 5. For the two processing conditions discussed above, a relative density of approximately 0.5 will be produced. In addition, foams of different average cell size are produced as illustrated by the two indicated data points, which have the same relative density and cell sizes of approximately 5 μm and 22 μm. The ability to produce foams of the same density and different cell size has opened the possibility to explore the effect of cell size on the properties of microcellular materials.

The strength of microcellular foams is nearly proportional to the foam density. Figure 7 shows the relative tensile strength of several microcellular foams and some structural foams as a function of the relative density. For this plot, the relative tensile strength was computed by dividing the strength of the foam by the strength of the unprocessed material. The relative tensile strength of microcellular foams appears to be marginally better than the strength of conventional foams. It is interesting to note that microcellular foams of relatively small thicknesses retain strengths similar to structural foams which have far thicker cross-sections. When compared to the rule of mixtures line, the data for all microcellular foams is slightly lower than this prediction. All of the microcellular data is significantly higher however, than the line representing the commonly used relative density squared model *(25)*.

The tensile modulus of several microcellular foams is shown in Figure 8 . Here results are shown from Weller *(24)* who tested microcellular PC, microcellular ABS, and microcellular PET; Kumar and VanderWel *(14)*, where microcellular PC was tested; and Waldman *(15)* who tested microcellular PS. All of the relative modulus values shown in this figure were computed by dividing the modulus of the foam by the modulus of the best estimate of the matrix material. For the amorphous polymers, PC, ABS, and PS, the modulus of the matrix material was taken as the modulus of the original, unprocessed material. In the case of PET the properties were taken as those of the CO$_2$ crystallized material (see *(24)*). The error bars in this figure represent the relative standard deviation. Figure 8 also shows a plot of the Mori-Tanaka model, adapted for foams *(24)*

$$\frac{E_f}{E_m} = \frac{\left(\dfrac{\rho_f}{\rho_m}\right)}{\left(\dfrac{\rho_f}{\rho_m}\right) + 2\left(1 - \dfrac{\rho_f}{\rho_m}\right)} \tag{1}$$

where

E_f	=	modulus of the foam (MPa)
E_m	=	modulus of the matrix material (MPa)
ρ_f	=	density of the foam (g/cm^3)
ρ_m	=	density of the matrix material

For all of the microcellular systems, the Mori-Tanaka model can be used to predict the relative tensile modulus over a wide range of relative densities.

Waldman *(15)* tested the toughness of several microcellular polystyrene foams and found that the toughness increases nearly 400 % as a result of the enhanced craze
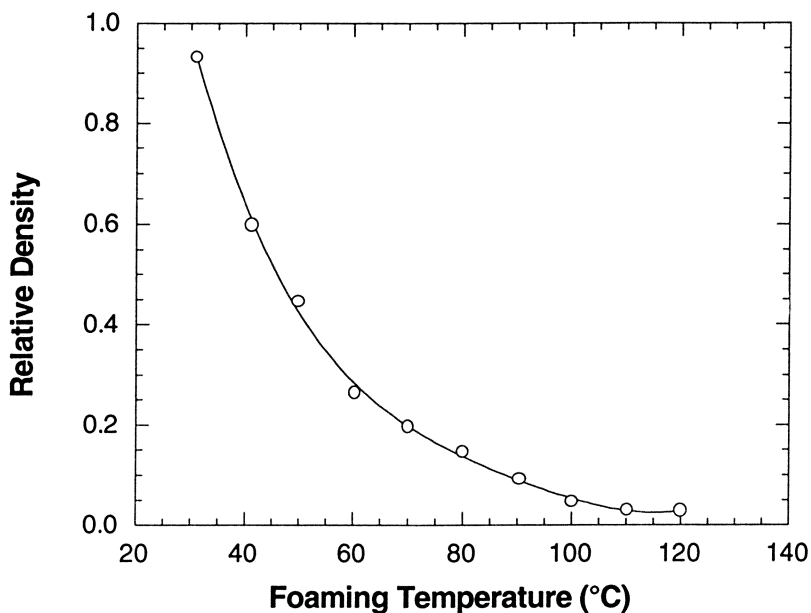
Figure 6. Relative density as a function of foaming temperature for PETG saturated at 4.8 MPa (700 psi).
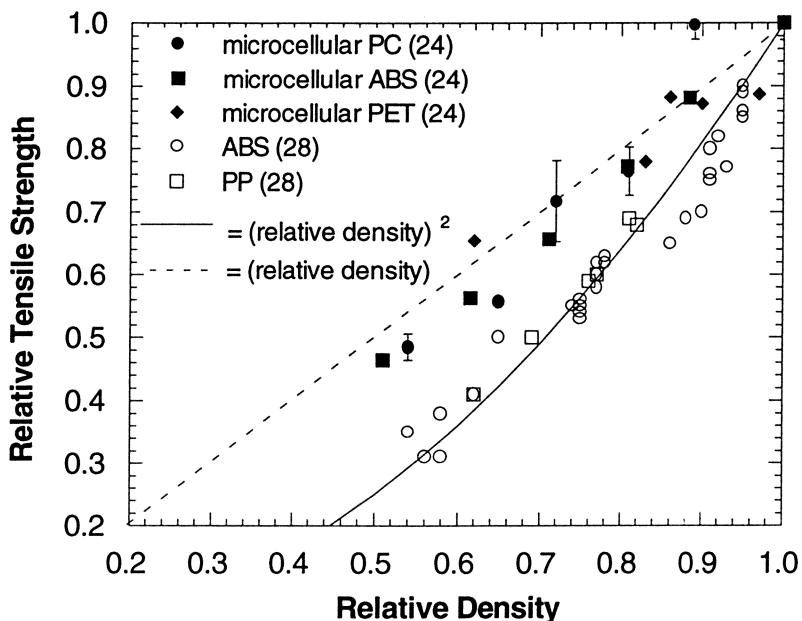
Figure 7. Plot of relative tensile strength of microcellular foams and some structural foams as a function of relative density (24).

initiation by the voids. Collias and Baird (*26*) repeated Waldman's experiments and performed several others, trying to show that the microcellular structure actually increased the toughness of the material. They concluded that the toughness of microcellular polystyrene only increases <u>marginally</u> over the original material. They also found that the presence of nitrogen gas in the polymer significantly affects the tensile toughness; the toughness was improved in the presence of nitrogen, and then decayed as the gas diffused from the polymer.

In 1993, Wing and Kumar presented work on the creep response of polycarbonate and microcellular polycarbonate (*27*), the first time-dependent study on microcellular foams. They found that CO_2 residing in the matrix can have a significant effect on the creep/creep recovery of microcellular foams. In addition, even after all of the measurable gas had left the matrix, it was found that the creep response continued to change as the specimen aged. Changes in behavior were observed for periods up to 60 days after all of the gas had diffused from the matrix, 90 days following removal of the material from the pressure vessel. Schapery's theory was applied successfully to characterize the time dependent response of both PC and microcellular PC.

Seeler and Kumar (*16*) have performed extensive studies regarding the fatigue life of microcellular polycarbonate foams. Stemming from the original rationale for developing microcellular foams, it has long been hypothesized that properties like fatigue life should be significantly improved in microcellular foams due to crack blunting by the voids. Fatigue data from some of their experiments are shown in Figure 9. The unfoamed material in this figure represents tests performed on unprocessed, virgin polycarbonate. Data at other relative densities are microcellular PC foams, and show similar behavior to the solid material. Specimens with a relative density of 0.90 (approx. 10% reduction in density) show the same fatigue life as the solid polymer for nominal stresses between 25 and 45 MPa. The fatigue life of the 0.97 relative density foam exceeds that of the solid polymer by an order of magnitude at a nominal stress of approximately 30 MPa. Thus the introduction of a microcellular structure by the solid-state process appears to increase the fatigue life of very high relative density polycarbonate foams. This phenomenon should be investigated in other gas-polymer systems.

Innovations in Microcellular Processing

Initially it was believed that the bubble nucleation in the microcellular process is caused by the supersaturation of the polymer (*1, 6*). Kumar (*7*) showed that the reduction in the solubility of the gas with temperature can provide a very significant driving force for bubble nucleation even without creating supersaturation condition. Thus an alternative to the process shown in Figure 1 would be to saturate the polymer at a certain temperature and pressure (this could be room temperature or an elevated temperature) and then raise the temperature of the polymer to cause bubble nucleation while maintaining the gas pressure at the level used for saturation. This principle has been employed by Park and Suh (*17*) to create a microcellular structure in extruded filament. This advance is a significant step toward production of microcellular polymers in a continuous process.

A thermoforming process to produce microcellular parts was developed by Kumar (*7, 18*). In this process a polymer sheet saturated by gas is thermoformed using a heated mold. Thus the shape of the part is achieved first, and the foaming is completed later. This process can be readily adapted to produce microcellular components by thermoforming from a plastic sheet. Figure 10 shows a picture of a microcellular polystyrene container produced by this process.

A skin of unfoamed polymer can be created on the microcellular foam by letting the gas diffuse out of the surface layers prior to foaming (*19*). This simple modification to the original process is illustrated in Figure 11. In the region where the gas concentration in the polymer drops below the minimum concentration needed for nucleation C*, bubbles do not nucleate when the polymer is heated resulting in an unfoamed skin. The
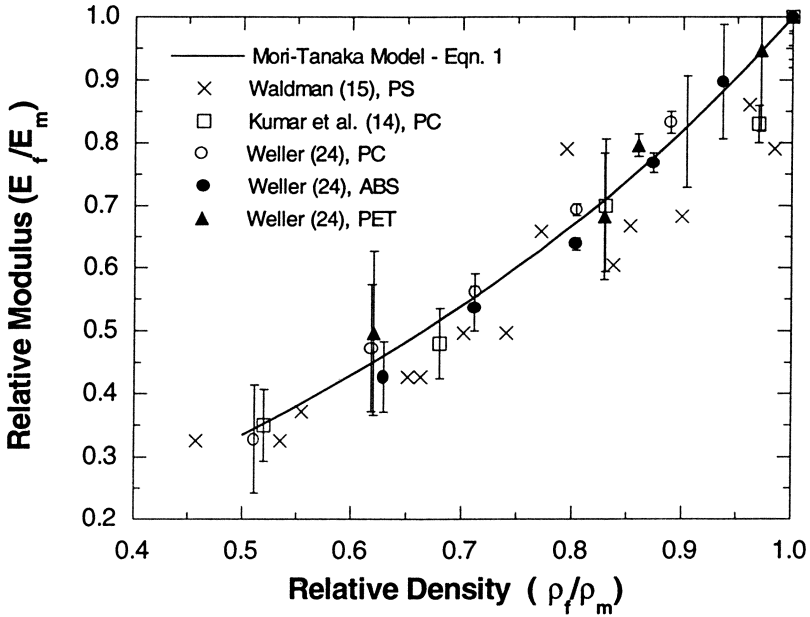
Figure 8. Plot of relative tensile modulus of several microcellular foams as a function of the relative density. The solid line is the Mori-Tanaka prediction (Eqn. 1) *(24)*.
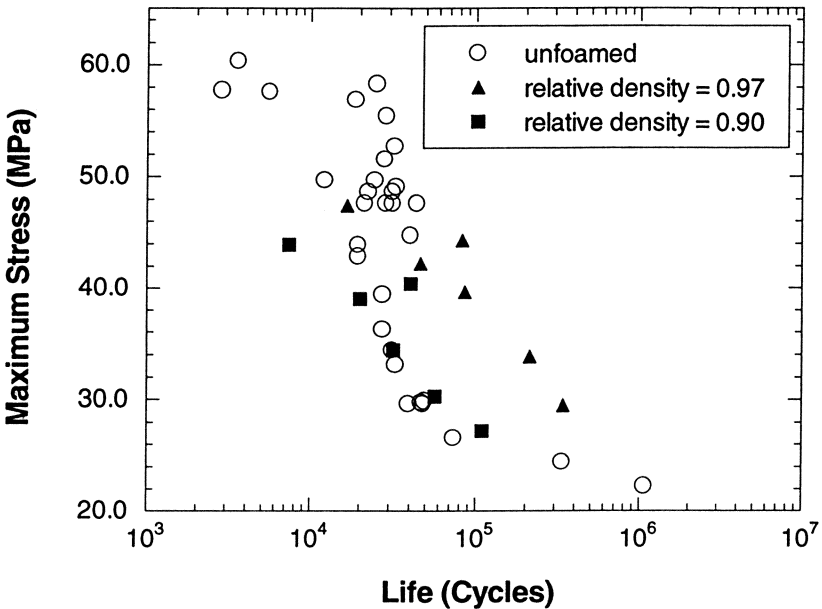
Figure 9. Fatigue life of high relative density microcellular polycarbonate foams *(16)*.
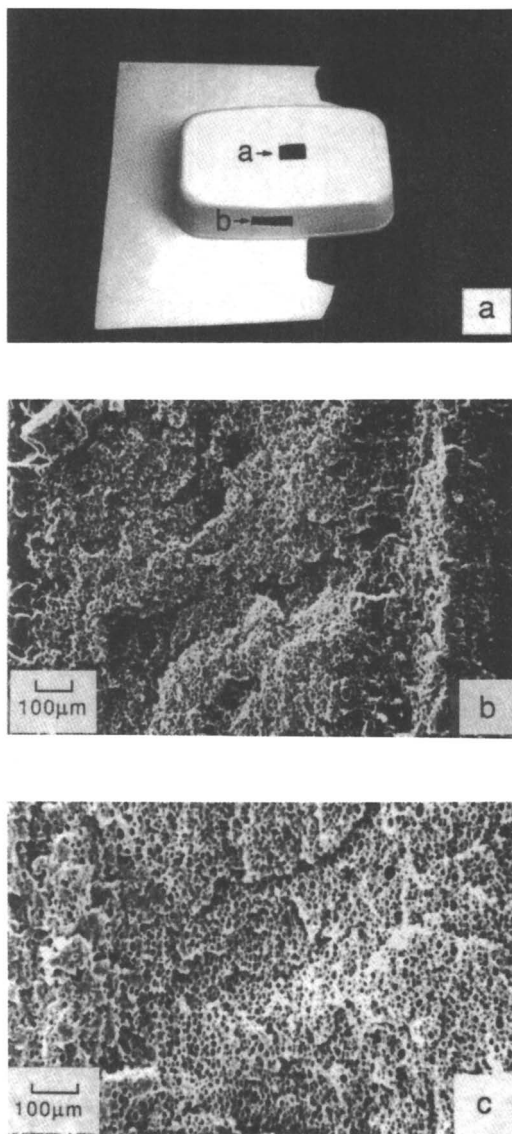
Figure 10. Example of a microcellular part made by a modified thermoforming process: (a) photograph of a microcellular container; (b) scanning electron micrograph of a sample from container bottom; (c) from the container wall. The average cell size is approximately 7 μm *(18)*.
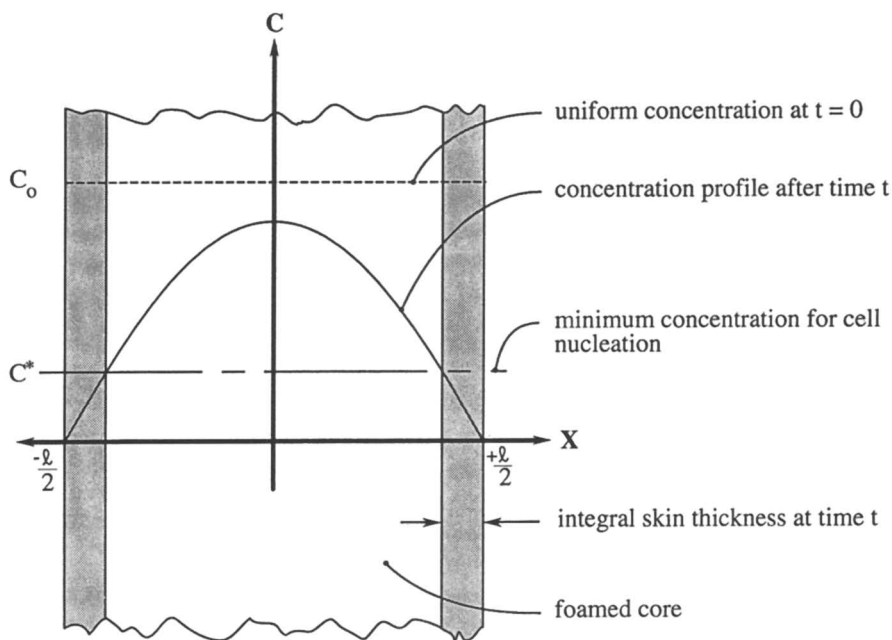
Figure 11. Schematic showing development of a skin region as a function of gas desorption time. C* is the minimum concentration needed for bubble nucleation *(19)*.

(a)

(b)
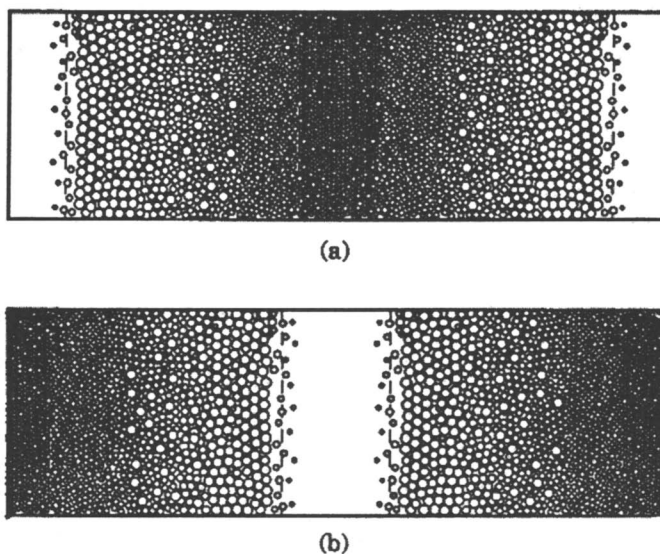
Figure 12. Illustration of control of microstructure: (a) schematic of foamed core with solid skin produced by the process shown in Figure 11; (b) schematic of an inverted structure with a foamed skin and a solid core *(21)*.

thickness of this solid skin can be easily controlled by monitoring the time allowed for gas desorbtion and the foaming temperature. Thus microcellular foams with an engineered skin/core structure can be created for applications where the solid material or foamed material alone cannot be used. In PET foams a crystalline skin integral to the foam core can be produced (*11*) creating a cellular composite material with higher specific strength.

Research on nondestructive evaluation of the microcellular structure, and on development of sensors for in-process control of the microstructure has been initiated (*20, 21*). The controllability of microstructure is illustrated in Figure 12. These structures have been realized by Holl (*21*) by control of the gas concentration profile in the specimen. These advances point to the possible creation of composite structures designed to deliver engineered mechanical and thermal properties with minimal use of polymeric materials.

Impact of Microcellular Polymers

There is a recognized need for minimizing the consumption of our natural resources. Further, there is an increased awareness that in processing our natural resources, the environment must be protected. Microcellular processes and materials address both of these concerns, and are therefore likely to strongly impact the way plastics are used in the future.

Wherever solid plastics are used today, there is the potential of significant reduction in the amount of material used by employing microcellular plastics. The savings in material and transportation costs could potentially be very significant for a number of plastic items. In aircraft, for example, the weight saving by use of microcellular plastics could significantly enhance payload efficiency. Although the mechanical property data available so far is limited, there is an indication that materials produced by this process could show improved toughness and fatigue life over solid plastics. In the future, it is expected that these materials will be used in a number of applications (e.g. packaging, automotive, home construction, toys, aerospace, medical prostheses, telecommunications, to name a few). As no harmful chemicals are used in the microcellular process, it is likely that microcellular polymers will replace many cellular polymers now produced by processes that damage the environment. The ability to control the microstructure and create composite structures will greatly increase the range of applications of these materials. We expect that by the turn of the century, the engineering and commercial potential of these novel materials will begin to be realized.

Acknowledgments

References

1. Martini J. E.; Waldman F. A.; Suh N. P.; *SPE Technical Papers* **1982**, *Vol. 28*, pp 674-676.
2. Kumar V.; Weller J.E *International Polymer Processing* **1993**, *Vol. 13*, pp 73-80.
3. Kumar V.; Weller J. E.; Hoffer H. Y. *Processing of Polymers and Polymeric Composites*, Vol. MD-19, ASME: New York, 1990, p 197-212.
4. Durril P.L.; Griskey R.G. *AIChE Journal*, **1969**, *Vol.15*, pp 106-110.
5. Kumar V.; Weller J. E., *Journal of Engineering for Industry*, **1993**, *Vol. 116*, pp 413-421.

6. Colton, J. S. *The Nucleation of Thermoplastic Microcellular Foam*, Ph.D. Thesis, Mechanical Engineering., MIT, 1985.
7. Kumar V. *Process Synthesis for Manufacturing Microcellular Thermoplastic Parts: A Case Study in Axiomatic Design*, Ph.D. Thesis, Mechanical Engineering, MIT, 1988.
8. Ramesh N. S.; Kweeder J. A.; Rasmussen D. H.; Campbell G. A. *SPE Technical Papers*, **1992,** *Vol. 38,* pp 1078-1081.
9. Kweeder J. A.; Ramesh N. S.; Campbell G. A.; Rasmussen, D. H. *SPE Technical Papers*, **1991,** *Vol. 37,* pp 1398-1400.
10. Kumar V.; Suh N. P. *SPE Technical Papers*, **1988,** *Vol. 34,* p 715.
11. Kumar V.; Gebizlioglu O. S. *SPE Technical Papers*, **1991,** *Vol. 37,* pp 1297-1299.
12. Baldwin D. F.; Suh N. P. *SPE Technical Papers*, **1991,** *Vol. 37,* p 1300.
13. Vanderwel M., *Microcellular Polycarbonate: Characterization of Microstructure and Mechanical Properties*, M.S. Thesis, University of Washington, 1991.
14. Kumar V.; Weller J. E.; VanderWel, M.; Seeler K. A. *Journal of Engineering Materials and Technology*, **1993,** *Vol. 116,* pp 439-445.
15. Waldman, F.A., *The Processing of Microcellular Foam,* S.M. Thesis, Mechanical Engineering MIT, 1982.
16. Kumar V.; Seeler K. A. *Journal of Reinforced Plastics and Composites*, **1993,** *Vol. 12,* pp 359-376.
17. Park C. B.; Suh N. P., In *Cellular Polymers*; Editors, V. Kumar; S.G. Advani; MD Vol. 38, ASME, New York, 1992; pp 69-91.
18. Kumar V.; Suh N. P., *Polymer Engineering and Science*, **1990,** *Vol. 30,* pp 1323-1329.
19. Kumar V.; Weller J. E *SPE Technical Papers*, **1992,** *Vol. 38,* pp 1508-1512.
20. Garbini J. L.; Holl M.; Kumar V.; Murray W. M.; Jorgensen J. E. *SPE Technical Papers*, **1992,** *Vol. 38,* p 1519.
21. Holl M. *Dynamic Analysis, Measurement, and Control of Cell Growth in Solid State Polymeric Foams*, Ph.D. Thesis, University of Washington, Seattle, 1995.
22. Kumar, V.; Eddy, S.; Murray, R. *SPE Technical Papers*, **1996,** *Vol. 42,* pp 1920-1925.
23. Kumar, V.; Eddy, S.; Murray, R. *Polymer Preprints,* American Chemical Society, **1996,** Vol.37, pp 779-780.
24. Weller, J. E. *The Effects of Processing and Microstructure on the Tensile Behavior of Microcellular Foams*, Ph. D. Thesis, University of Washington, Seattle, 1996.
25. More, D. R.; Couzens, K. H.; and Iremonger, M. J *Journal of Cellular Plastics*, **1974,** *Vol. 10,* pp 135-139.
26. Collias, D. I.; Baird, D. G. *Polymer Engineering and Science*, **1995,** *Vol. 34,* pp 1167-1177.
27. Wing, G. T.; Pasricha, A.; Tuttle, M.; Kumar, V *Polymer Engineering and Science*, **1995,** *Vol. 35,* pp 663-670.
28. Wendle, B. C. *Engineering Guide to Structural Foam*, Technomic, Westport, CT, pp 92-97.

Chapter 8

A Strategy for the Suppression of Cell Coalescence in the Extrusion of Microcellular High-Impact Polystyrene Foams

Chul B. Park, Amir H. Behravesh, and Ronald D. Venter

Department of Mechanical and Industrial Engineering, University of Toronto, 5 King's College Road, Toronto, Ontario M5S 3G8, Canada

This article describes a strategy for suppressing the coalescence of cells during shaping in continuous processing of microcellular plastics. Microcellular plastics are foamed polymers characterized by a cell density greater than 10^9 cells/cm^3 and fully grown cell size on the order of 10 μm. Since the invention of microcellular plastics in a batch process, research has focused on cost-effective, continuous processing of these materials. The basic approach to the production of microcellular structures is to continuously form a polymer/gas solution, to nucleate a large number of bubbles using rapid pressure drop, to shape a nucleated polymer/gas solution under pressure, and to induce a volume expansion to desired expansion ratio. Successful completion of these steps in extrusion will manufacture microcellular foamed plastics with a high cell population density. The critical issue to be dealt with in this article is how to prevent the deterioration of the nucleated cell-density via cell coalescence, which vigorously occurs in a shear field during shaping while the nucleated cells are growing. An effective strategy for preventing the cell coalescence is established and some critical experiments are then presented which verify the concept of preserving the high cell population density in a shear field.

Microcellular plastics are characterized by cell sizes in the range of 0.1 to 10 micrometers, cell densities in the range of 10^9 to 10^{15} cells per cubic centimeter, and specific density reductions in the range of 5 to 95 percent. The concept for microcellular plastics was created by Suh (Suh, N.P., MIT-Industry Polymer Processing Program, Private Communication, 1980.) in response to industrial need for reducing materials cost for certain polymer products without compromising mechanical properties. The central idea was to create a large number of bubbles,

115

smaller than the pre-existing flaws in a polymer. Typically, microcellular plastics exhibit high Charpy impact strength (i.e., up to a five-fold increase over unfoamed plastic (*1-5*), high toughness (i.e., up to a five-fold increase over unfoamed plastic (*5-7*), high stiffness-to-weight ratio (i.e., three to five times larger than unfoamed material), high fatigue life (i.e., up to a five-fold increase over unfoamed plastic (*8-9*)), high thermal stability (*10-11*), low dielectric constant, and low thermal conductivity (Glicksman, L., Notes from MIT Summer Session Program 4.10S Foams and Cellular Materials: Thermal and Mechanical Properties, Cambridge, MA, June 29-July 1, 1992). Because of these unique properties, a large number of innovative applications of microcellular plastics can be imagined. These include food packaging with reduced material costs, airplane and automotive parts with high strength-to-weight ratio and acoustic dampening, sporting equipment with reduced weight and high energy absorption, insulative fibers/filaments for fabric, molecular grade filters for separation processes, surface modifiers for low friction, and biomedical materials. Additionally, since hydrocarbons and chlorofluorocarbons (CFCs) are not used, the processing of microcellular plastics would be an environmentally friendly replacement for some conventional foams.

Over the past decade, substantial research and development have been conducted to gain knowledge about the physical phenomena governing microcellular processing and the properties of microcellular polymers. This knowledge has lead to the implementation of batch processes (*12-16*), and some significant structure and property characterization studies have been performed as well (*3-12, 17-18*). However, continuous manufacturing processes have not been developed extensively. Kumar and Suh (*19-21*) developed a semi-continuous process using a modified thermoforming process. Park and Suh (*22,23*), Park et al. (*24-26*), and Baldwin et al. (*27*) demonstrated an extrusion process for microcellular plastics using a simple filament or sheet die. Further research and development need to be conducted to develop continuous processes that can cost-effectively manufacture microcellular plastics.

Background on Microcellular Plastics Processing

Invented in 1981, microcellular plastics have been produced using a thermodynamic instability of a polymer/gas system to promote a large bubble density in a polymer matrix. Microcellular plastics processing involves the following three basic steps to utilize such a thermodynamic instability: a) polymer/gas solution formation, b) microcell nucleation, and c) cell growth. These steps are basic to microcellular processing and are applied to both batch processes and continuous manufacturing processes.

Typically, the polymer/gas solution formation is accomplished by dissolving an inert gas, such as carbon dioxide or nitrogen, into a polymer matrix under a high pressure. This creates a solution having a high gas concentration (typically 5 to 20 percent gas by weight) in the polymer matrix. The solution formation is governed by gas diffusion in the polymer. Diffusion processes are typically slow, resulting in long cycle times. A number of techniques can be used to expedite the solution formation process. Increasing gas pressure increases the local gas concentration

which increases the diffusion rate.   Increasing the temperature also increases the diffusivity.

The next phase of microcellular processing involves subjecting the polymer/gas solution to a thermodynamic instability to nucleate microcells. This is achieved by lowering the solubility of the solution by controlling the temperature and/or pressure. The system now seeks a state of lower free energy which results in the clustering of gas molecules in the form of cell nuclei. The formation of cell nuclei provides a relatively small mean free distance for the gas molecules in solution to diffuse through before reaching a cell nucleus (i.e., the gas phase). As the gas diffuses into the cells, the free energy of the system is lowered.   The cell nucleation process can occur homogeneously throughout the material or heterogeneously at high energy regions such as phase boundaries (*28*). In the ideal case, nucleation occurs instantaneously.   The cell nucleation process is very important in microcellular plastics production in that it governs the cell morphology of material and to a large extent, the properties of the material.

When the cells are nucleated, they continue to grow as available gas diffuses into cells, provided little resistance is encountered.   The cells grow and reduce the total polymer density as the gas molecules diffuse into the nucleated cells from the polymer matrix (a distance on the order of 10 microns). The rate at which the cells grow is limited by the diffusion rate and the stiffness of the viscoelastic polymer/gas solution. If the stiffness of the matrix is too high, cell growth is extremely slow. In this case, the solution temperature can be increased to lower the matrix stiffness. In general, the cell growth process is controlled primarily by the time allowed for the cells to grow, the temperature of the system, the state of supersaturation, the hydrostatic pressure or stress applied to the polymer matrix, and the viscoelastic properties of the polymer/gas solution (*29*).

Microcellular polymers were first produced in a batch process (*1*). In this process, a polymer sample is first placed in a high pressure chamber where the sample is saturated with an inert gas (such as CO_2 or N_2) under high pressure at ambient temperature.   Then, a thermodynamic instability is induced by rapidly dropping the solubility of gas in the polymer. This is accomplished by releasing the pressure and heating the sample.   This drives the nucleation of a myriad of microcells, and the nucleated cells continue to grow leading to the foam expansion. One of the disadvantages of the batch process is a very long cycle time required for the gas saturation in the polymer since the diffusion rate is very low at the ambient temperature.

In order to overcome this shortcoming, a cost-effective, continuous microcellular process has been developed in extrusion (*22-27*). In this process, a much shorter time is needed for the saturation of polymer with gas. When the polymer is melted in the extrusion barrel, a metered amount of gas is delivered to the polymer melt. The injected gas diffuses into the polymer matrix at a much higher rate because of a convective diffusion induced in the extrusion barrel at an elevated temperature (*22*). The formation of a uniform solution of polymer and gas is essential in microcellular processing since undissolved gas pockets can generate undesirable large voids. This can be achieved by the complete dissolution of gas in the polymer melt using a diffusion enhancing device (*22*). Microcell nucleation is promoted in a rapid-pressure-drop nucleating nozzle by a thermodynamic instability
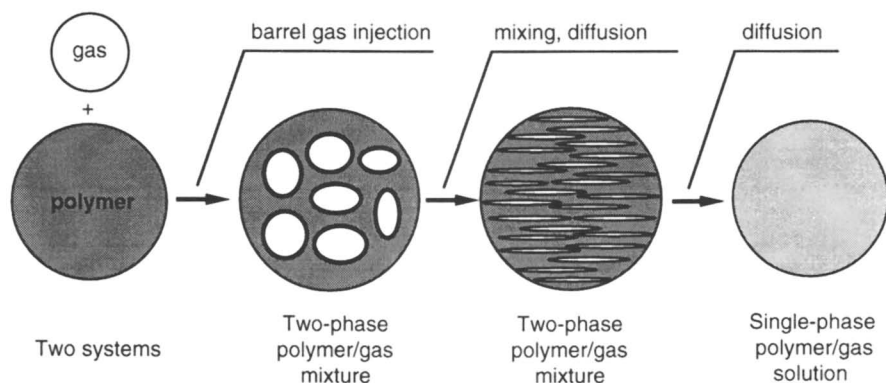
Figure 1.   Morphology Change of Polymer/Gas System in Solution Formation Process. Reproduced with Permission from Ref. 23. Copyright 1996 Polymer Engineering and Science.

Table I. Estimated Solubility of CO_2 in Polymers at 200°C and 27.6 MPa (4,000 psi).

Polymer	CO_2 weight gain (%)
PE	15
PP	12
PS	12
PMMA	15

SOURCE: Reproduced with Permission from Reference 23. Copyright 1996 Polymer Engineering and Science.

(*23,24*). The nucleated bubbles continue to grow to a desired final size during shaping and at the die exit.

Formation of a Single-Phase Polymer/Gas Solution (*22,23*)

One of the critical steps in the continuous production of microcellular plastics is the creation of a polymer/gas solution at industrial processing rates. Figure 1 shows the morphology change of polymer and gas system in the solution formation process. Initially, a soluble amount of gas is injected into a polymer melt stream, forming a two-phase polymer/gas mixture. Then, the large injected gas bubbles are broken into smaller bubbles and stretched through shear mixing. Eventually, the gas diffuses into the polymer matrix, forming a single-phase solution.

Estimation of Gas Solubility in Polymers at Elevated Temperatures and Pressures. Only a soluble amount of gas should be injected into the polymer melt stream. Excess gas would result in the formation of undesirable voids in the melt. Such voids could be detrimental to the cell structure. The existence of voids suppresses homogeneous nucleation because the gas molecules preferentially diffuse to larger cells (*30*), resulting in the formation of hollow cavities in the final product.

In order to inject only a soluble amount of gas into the polymer matrix, the solubilities of CO_2 in various polymers were estimated at 200°C and 27.6 MPa (4,000 psi), which are a typical processing temperature and pressure, respectively. Shim and Johnston's work (*31*, Johnston, K.P., University of Texas at Austin, Private Communication, 1993) suggested that the logarithm of the CO_2 solubility in polymers at elevated pressures is well correlated to the density of CO_2 up to 30 MPa for a constant temperature. Durril and Grieskey's data (*32,33*) was used to derive this correlationship, and the solubilities of CO_2 at 27.6 MPa (4,000 psi) were extrapolated from this correlationship. The estimated solubilities are summarized in Table I. The solubilities of CO_2 in many polymers are approximately 10% by weight.

Estimation of Gas Diffusivity in Polymers at Elevated Temperatures. The diffusivity of gas in a polymer was also investigated to determine the processing time required for the formation of a single-phase polymer/gas solution. In general, the gas diffusivity in a polymer changes with temperature, pressure, and gas concentration (*32-35*). Since the diffusivity increases as the temperature increases, the rate of gas diffusion is enhanced by processing the mixture at a high temperature. Therefore, compared to room temperature, the gas diffusion rate for the polymer mixture is increased in the heated extrusion barrel.

Only limited data was available for gas diffusion in polymers at high temperatures (*32-34*). The estimated diffusivities are summarized in Table II. At 200 °C, a typical diffusivity of CO_2 and N_2 in a thermoplastic is approximately 10^{-6} cm^2/sec, which is two orders of magnitude greater than a typical diffusivity, 10^{-8} cm^2/s, at room temperature (*34*).

Convective Diffusion in Extrusion. When a metered amount of gas is delivered to the polymer melt stream, the formation of a uniform and homogeneous single-phase solution from the two-phase mixture is accomplished through gas diffusion. Because

Table II. Estimated Diffusivity of CO_2 in Polymers at Elevated Temperatures.

Polymer	D of CO_2 (cm^2/s)	
	at 188°C [*]	at 200°C [†]
PS	-	1.3×10^{-5}
PP	4.2×10^{-5}	-
PET	-	2.6×10^{-6}
HDPE	5.7×10^{-5}	2.4×10^{-5}
LDPE	-	1.1×10^{-4}
PTFE	-	7.0×10^{-6}
PVC	-	3.8×10^{-5}

[*]   Durril and Griskey (*32,33*)
[†]   van Krevelen (*34*)

SOURCE: Reproduced with Permission from Reference 23. Copyright 1996 Polymer Engineering and Science.
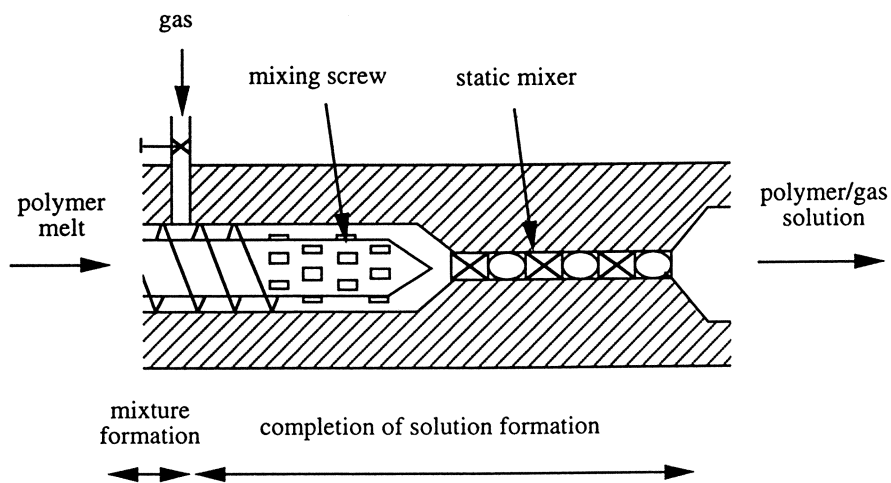
Figure 2.   Polymer/Gas Solution Formation in an Extrusion Barrel.

the gas diffusion is a very slow process, a technique for rapid solution formation was developed in order to produce microcellular plastics at industrial processing rates. The basic strategy for rapid solution formation was to induce convective diffusion.

It was rather difficult to analyze the mixing behavior of the two-phase mixture and the flow fields of each phase because the volume of the gaseous phase diminishes in size as the gas molecules diffuse into the polymer matrix (*22,23*). Since the diffusion phenomenon strongly depends on mixing behavior, the analysis of the mass transfer phenomena of diffusion is also complicated. Therefore, the diffusion of gas into the polymer matrix during extrusion may not be completely analyzed.

Despite the complication of modeling the dynamic behavior of the mixture of the two fluids, the diffusion rate is greatly enhanced when the diffusion source is also moving. As the degree of mixing increases, more polymer melt is brought into contact with the source of the high gas concentration which increases the effect of convective diffusion. This convective diffusion effect is enhanced through an increase in the interfacial area per unit volume, a reduction of the diffusion distance, and a redistribution of the local gas concentration profile in the polymer matrix. In addition, since the diffusion rate strongly depends on the mixing behavior, the diffusion time can be controlled by varying the degree of mixing.

The concept of convective diffusion has been effectively utilized to enhance the diffusion rate in an extrusion barrel. One technique for rapid solution formation using convective diffusion employed laminar mixing in the molten polymer shear field. Since the mixing accomplished by the simple screw motion was limited, efforts were also made to enhance the mixing effectiveness by introducing various mixing sections in the extruder (*37,38*). The idea behind the mixing section was that reorientation of the mixture during processing would enhance the effectiveness of shear mixing. Using the mixing section, the diffusion time decreased due to the enhanced degree of mixing. Figure 2 shows a schematic of the convective diffusion device developed in this study.

A fundamental study has been carried out to estimate the striation thickness of polymer and gas in an extruder and the required processing time for the solution formation. An order of magnitude analysis (*22*) predicts that the solution formation will be completed in 20 seconds when the polymer/gas system is fully mixed and the striation thickness is 45 μm. Therefore, continuous solution formation has been achieved in extrusion systems without substantially decreasing the processing rates. However, it should be noted that if the amount of gas injected is more than the solubility at the processing condition, then the solution formation could not be completed. In addition, due to the limited available CO_2 diffusivity data for high concentration at elevated temperatures, the concentration-dependent nature of the diffusivity could not be accounted for in this order of magnitude analysis. In order to develop a better model of the continuous formation of a single-phase polymer/gas solution, fundamental research on the diffusivity and the solubility of a gas at high temperatures and pressures, and the polymer/gas mixing behavior in the mixing elements should be carried out.

Microcellular Nucleation Device: a Rapid Decompressive Element (23,24)

The next critical step in the continuous production of microcellular plastics is the promotion of high bubble nucleation rates in the polymer/gas solution. The process requires that the nucleation cell density be large enough so that the fully grown cells are microcellular. The key to producing a microcellular nucleation density is a very high nucleation rate. High nucleation rates have been produced by batch processes using a thermodynamic instability of the polymer/gas system. In order to use a thermodynamic instability in a continuous process, a rapid drop of gas solubility in the polymer must be induced in the polymer/gas system. Since the solubility of a gas in a polymer decreases as the pressure decreases, a thermodynamic instability can be induced when the polymer/gas solution is subjected to a rapid pressure drop. Based on this strategy, a suitable rapid-pressure-drop element consisting of a nozzle has been devised as a continuous microcellular nucleation device, which allows a rapid pressure drop in the flowing, viscous fluids. The developed rapid-pressure-drop element has been proved to be effective in promoting microcell nucleation (23,24).

Shaping and Cell Growth (27)

To date, the studies on the continuous processing of microcellular plastics have centered around the nucleation in the filamentary extrusion (22-26). Little work has been conducted to study the cell growth phenomenon in the continuous microcellular processing. Baldwin et al. (27) carried out a preliminary study on the shaping and cell growth control in microcellular extrusion processing. Because of the difficulty of inducing a rapid pressure drop for microcell nucleation at the die exit, it was proposed that the nucleation of the microcells be controlled independently in the first stage of the die by rapidly dropping the pressure of the polymer/gas solution using a nozzle, and the shaping and cell growth be controlled in the second stage of the die. Baldwin et al. proposed to use a high pressure to suppress the premature growth in the shaping die and to prevent the bubbles from being stretched along in the shaping direction. Based on this strategy, they demonstrated the feasibility of the concept of shaping a nucleated polymer/gas solution under high pressure to prevent the distortion of the bubbles, and successfully produced 2 mm thick filament and 1mm thick sheet with a microcellular foamed structure. However, the volume expansion ratios of the extruded foams were relatively low (less than two times) and the coalescence of nucleated cells was observed to a large extent. It was expected that when the cells were controlled to be further grown, the cell coalescence problem would be severer and a much less cell-population density would be obtained. Therefore, an effective strategy for preventing the coalescence of nucleated cells needs to be established to preserve the high cell-population density obtained in the nucleating nozzle before a large expansion of microcellular foams is attempted to achieve. This article focuses on the development of an effective strategy to prevent the cell coalescence during shaping in microcellular extrusion processing.

A Strategy for Suppression of Cell Coalescence

The proposed scheme of the independent nucleation control in extrusion may not guarantee that the final cell density of produced foams will be high enough to be microcellular if the cell coalescence occurs. When the nucleated cells grow and come in contact with each other, the contiguous cells tend to coalesce because the total free energy will be reduced through the coalescence of cells (*39*). It may be noted that the shear field generated during the shaping process tends to stretch nucleated bubbles and this will further accelerate the cell coalescence (*27*).   When the cells are coalesced, the initial nucleated-cell-density will be deteriorated. In other words, although a microcellular nuclei density (higher than 10^9 cells/cm^3) has been achieved by the independent control of cell nucleation via a rapid pressure drop, the final cell density of produced foams might not be microcellular when the cell coalescence occurs. As a result, the mechanical and thermal properties of the foam products will be deteriorated as well. In order to prevent the deterioration of the properties and to fully utilize the unique properties of microcellular plastics, the cell coalescence should be effectively suppressed.

Although Baldwin et al. attempted to prevent the cell coalescence in the die by pressurizing the nucleated polymer solution during shaping, the extruded foam structure showed that many adjacent cells were coalesced each other and the cell density was deteriorated (*27*). Maintaining a high pressure in the shaping section to prevent the premature cell growth right after the cell nucleation was believed to be a good strategy because the nucleated cells could not grow under high pressure. However, considering the difficulty of maintaining a high back pressure in the shaping die for the case of large cross section of extrudated foam, it may not be realistic to prevent the cell coalescence by controlling the pressure alone in the shaping die.

One way of suppressing the cell coalescence is to increase the melt strength of the polymer by lowering the temperature (*40,41*). The melt strength by definition may be considered as a degree of resistance to the extensional flow of the cell wall during the drainage of polymer in the cell wall when the volume expansion takes place. Therefore, the cell wall stability will increase as the melt strength increases (*41*). It is expected that the melt strength of polymer can be enhanced by branching, cross-linking, temperature reduction, control of molecular weight and molecular weight distribution, and blending of polymers and compatibilization of blends (*40*). In this research, it is proposed that the processing temperature be controlled to increase the melt strength and to prevent the cell coalescence in the shaping and cell growth processes. It is expected that the increased melt strength due to the lowered melt temperature will effectively suppress the coalescence of cells and the high nucleated-cell density obtained at the microcellular nucleation device will be substantially maintained. The idea of increasing the melt strength to prevent the cell coalescence at the die exit (or at the die lip) has been well utilized in the conventional foam processing, particularly in the low density foam production (*41,42*). However, the temperature control has not been extensively used in the microcellular processing. It was the purpose of this research to investigate the feasibility of the temperature control for preventing the cell coalescence, and thereby preserving the high nucleated-cell density in the microcellular extrusion processing.
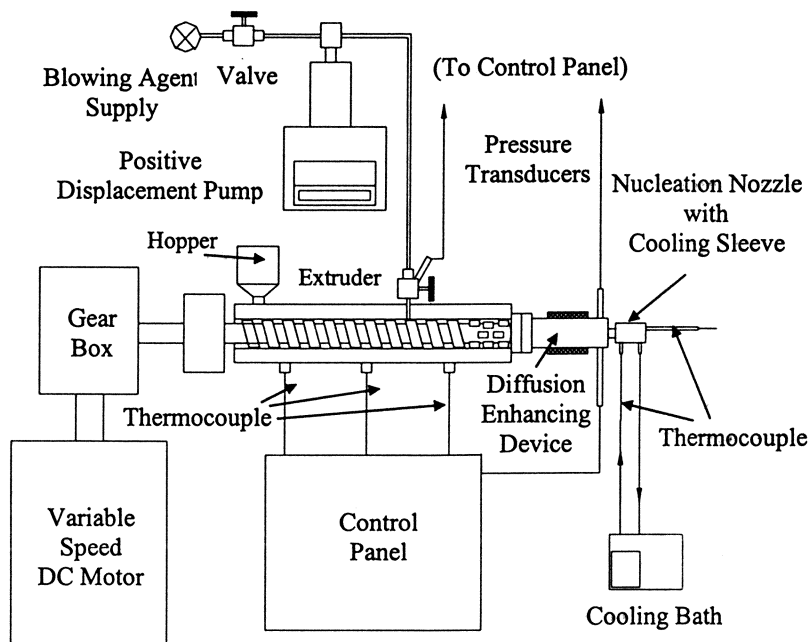
Figure 3.   Schematic of the Overall Experimental Equipment.
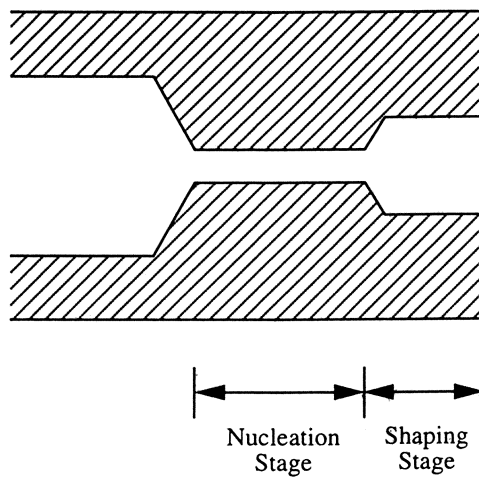
Figure 4.   Schematic of the Nucleating and Shaping Device.

Experimentation

The feasibility of suppressing the cell coalescence in the microcellular extrusion foam processing was examined experimentally. Figure 3 shows a schematic of the experimental setup used in this study. It consisted of a 5 hp DC motor, a speed reduction gearbox, a 3/4" extruder (C.W. Brabender 05-25-000), a positive displacement pump, a diffusion-enhancing device containing static mixers (Omega Model FMX8441S), a nucleation nozzle, a cooling sleeve, and a hot-oil circulating bath (Grant Model W6-KD). Figure 4 shows a schematic of the filament dies used in the experiments which consisted of two stages: nucleating nozzle and shaping section. High impact polystyrene (HIPS, Novacor 3350) was used as the polymer material. The blowing agent used in this study was CO_2 (Matheson, Commercial grade) and a positive displacement pump was utilized to inject the blowing agent into the polymer melt at a desired rate. In all the experiments, the amount of injected CO_2 was maintained as 5% by weight.

Three sets of critical experiments were carried out. In the first experiment, only the nucleating nozzle was attached as the die without any shaping section as in the previous studies (*23,24*). In this experiment, the cell nucleation took place when the polymer/gas solution experienced a rapid pressure drop in the nozzle and the nucleated cells continued to grow in the air after the extrudate exited the nucleating nozzle. In the second experiment, a shaping section was attached further to the nucleating nozzle and the nucleated cells were induced to grow in the shaping section. In the both the first and second experiments, the die temperature was maintained 200°C. In the third experiment, a shaping section was also attached to the nucleating nozzle. However, the die temperature in the experiment was significantly lowered down to 125°C. Because of the increased resistance in the die at the low temperature, the length of the nucleating nozzle was reduced from 10.2 mm (0.4 inch) to 2.5 mm (0.1 inch) to maintain the same processing pressure of 28 MPa (4000 psi) as in the first and second experiments. The dimension and the processing temperature of each nozzle are presented in Table III.

Results and Discussion

Figure 5.a shows the microstructure of the foam obtained when no shaping section was attached to the nucleating nozzle (Experiment 1). The cell population density in this case was 1×10^{10} cells/cm^3. Since the processing temperature was very high (200°C), it was observed that some adjacent cells were coalesced. Figure 5.b shows the microstructure of the foam obtained from the second experiment where a shaping section was attached to the nucleating nozzle. The cell population density was dramatically reduced to 2×10^8 cells/cm^3 while the cell coalescence was highly promoted by the shaping section. Finally, Figure 5.c shows the microstructure of the foam obtained from the third experiment in which a shaping section was also attached but the processing temperature was significantly lowered.   The cell-population density in this case was found to be 5×10^9 cells/cm^3, indicating that cell density was substantially maintained by suppressing the cell coalescence through the reduction in the melt temperature.

Table III. Nozzle Specifications and the Melt Temperatures Used in the Experiments

	Nucleation stage		Shaping stage		Melt temperature
	Diameter (mm)	Length (mm)	Diameter (mm)	Length (mm)	(°C)
Experiment 1	0.46	10.16	-	-	200
Experiment 2	0.46	10.16	1.52	10.16	200
Experiment 3	0.46	2.54	1.52	10.16	125
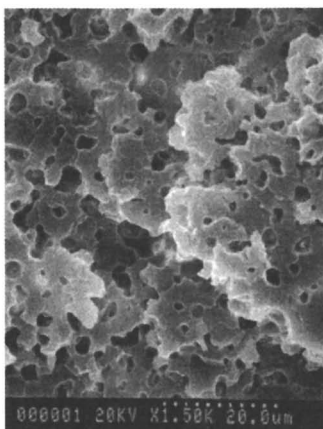
(a) Experiment 1.
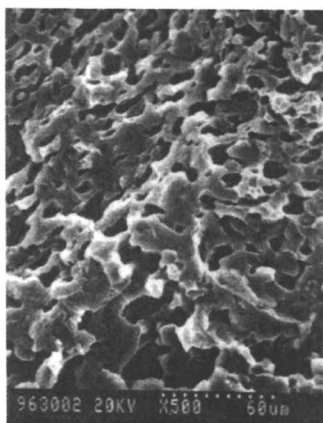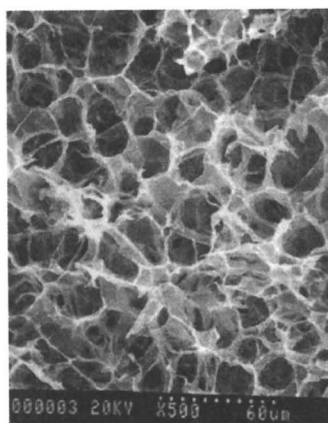
(b) Experiment 2.   (c) Experiment 3.

Figure 5.   Microstructure of the Foams at Three Various Processing Conditions.

In the first experiment, the bubble coalescence was observed to some degree because of the high melt temperature. The cell density obtained in this experiment, 1×10^{10} cells/cm^3, agreed to the previous results (*8,9*). When the shaping section was added to the die, the cell density was dropped to 2×10^8 cells/cm^3. This implies that the cell coalescence was vigorously occurring in the shaping section at the high temperature after a large cell density was achieved at the nucleating nozzle. If we assume that 1×10^{10} cells/cm^3 were nucleated in the nozzle as in the other experiments (*23,24*), we may conclude that around 50 bubbles were coalesced into a single bubble in the shaping section. It was believed that the shear field generated in the shaping section caused this vigorous coalescence of cells. In the third experiment, the temperature of the die was lowered significantly. Surprisingly, the cell density was very high and the cell coalescence was substantially prevented by decreasing the temperature. Because the melt strength increases as the temperature decreases (*40*), it may be concluded that the increased melt strength by lowering the temperature prevented the cell coalescence despite the shear field during shaping. This experimental result confirmed that the previously proposed scheme of independently controlling the cell nucleation, followed by controlling the shaping and the cell growth, can be effectively utilized in the microcellular extrusion foam processing. In addition to pressurizing the nucleated polymer/gas solution, the melt temperature can be significantly lowered to prevent the cell coalescence in the shaping section of the die. This processing scheme offers a tremendous advantage over the conventional foam processing of simultaneously inducing nucleation and growth at the die exit via a pressure drop because it is practically difficult to promote a very high pressure drop rate required for microcellular nucleation (on the order of 1 GPa/s) (*24*) at the normal die exit.

Summary and Conclusions

This paper describes a strategy to effectively suppress the cell coalescence during shaping in the microcellular extrusion foam processing of HIPS. In the microcellular extrusion processing, a high nucleated-cell density is achieved by rapidly dropping the pressure in the first section of the die. However, the high nucleated cell density needs to be preserved in the shaping section, and lowering the melt temperature down to 125°C turned out to be a good strategy for preventing the cell nucleation in the microcellular processing of HIPS.

The experimental studies conducted in this paper lead to the following conclusions:

- The presence of a shear field generated in the shaping section significantly promoted the cell coalescence at a high temperature which resulted in the deterioration of the cell density in the microcellular extrusion foam processing.
- The cell coalescence was effectively suppressed by cooling the melt significantly in the shaping section. It is believed that the increased melt strength due to the lowered temperature exerted a strong influence in

preventing the cell coalescence and preserving the high nucleated cell density of HIPS foams.

References

1. Martini, J.; Waldman, F.A.; Suh, N.P. *SPE ANTEC Tech. Papers* **1982**, 28, 674.
2. Doroudiani,.S.; Park, C.B.; Kortschot, M.T. *SPE ANTEC Tech. Papers* **1996**, 42, 1914.
3. Matuana, L.M.; Park, C.B.; Balatinecz, J.J. In *Cellular and Microcellular Materials*; Kumar, V; Seelaer, K.A., Eds.; ASME: New York, NY, 1996; pp 1-16.
4. Collias, D.I.; Baird; D.G.; Borggreve, R.J.M. *Polymer* **1994**, 25, 3978-3983.
5. Collias, D.I.; Baird, D.G. *Polym. Eng. Sci.* **1995**, 35, 1178-1183.
6. Collias, D.I.; Baird, D.G. *Polym. Eng. Sci.* **1995**, 35, 1167-1177.
7. Baldwin, D.F.; Suh, N.P. *SPE ANTEC Tech. Papers* **1992**, 38, 1503.
8. Seeler, K.A.; Kumar, V. ASME, *Cellular Polymers* **1992**, MD-Vol. 38, 93.
9. Seeler, K.A.; Kumar, V. *J. Reinforced Plast. Comp.* **1993**, 12, 359-376.
10. Shimbo, M.; Baldwin, D.F.; Suh, N.P. *Proc. Amer. Chem. Soc., Polymeric Materials: Sci. Eng.* **1992**, 67, 512.
11. Shimbo, M.; Baldwin, D.F.; Suh, N.P. *Polym. Eng. Sci.* **1995**, 35, 1387.
12. Martini-Vvedensky J.E.; Suh, N.P.; Waldman, F.A. *U.S. Patent 4473665* **1984**.
13. Yoon J.R.; Suh, N.P. *Polymer Composites* **1985**, 6, 175.
14. Colton J.S.; Suh, N.P. *U.S. Patent 5160674* **1992**.
15. Cha, S.W.; Suh, N.P.; Baldwin, D.F.; Park, C.B. *U.S. Patent 5158986* **1992**.
16. Cha, S.W.; Suh, N.P. *SPE ANTEC Tech. Papers* **1992**, 37, 1527.
17. Kumar, V.; Weller, J.E. *SPE ANTEC Tech. Papers* **1991**, 37, 1401.
18. Ramesh, N.S.; Kweeder, J.A.; Rasmussen, D.H.; Campbell, G.A. *SPE ANTEC Tech. Papers* **1992**, 38, 1078.
19. Kumar, V. Ph.D. Thesis, Department of Mechanical Engineering, Massachusetts Institute of Technology, Cambridge, MA, **1984**.
20. Kumar, V.; Suh, N.P. ASME, *Mechanics of Plastics and Plastic Composites* **1989**, AMD-Vol. 104, 321.
21. Kumar, V.; Suh, N.P. *Polym. Eng. Sci.* **1990**, 30, 1323.
22. Park, C.B.; Suh, N.P. ASME Trans. *J. Manuf. Sci. Eng. (J. Eng. Ind.)* **1996**, 118, 639-645.
23. Park, C.B.; Suh, N.P. *Polym. Eng. Sci.* **1996**, 36, 34-48.
24. Park, C.B.; Baldwin, D.F.; Suh, N.P. *Polym. Eng. Sci.* **1995**, 35, 432-440.
25. Park, C.B.; Baldwin, D.F.; Suh, N.P. In *Cellular and Microcellular Materials*; Kumar, V.; Sealer, K.A., Eds.; ASME: New York, NY, 1994, MD-Vol. 53, pp 109-124.
26. Park, C.B.; Baldwin, D.F.; Suh, N.P. *Res. Eng. Des.* **1996**, 8, 166-177.
27. Baldwin, D.F.; Park, C.B.; Suh, N.P. *Polym. Eng. Sci.* **1996**, 36, 1446-1453.
28. Colton, J.S.; Suh, N.P. *Polym. Eng. Sci.* **1987**, 27, 500.
29. Baldwin, B.F.; Suh, N.P.; Shimbo, M. ASME, *Cellular Polymers* **1992**, MD-Vol. 38, 109.

30. Martini, J. S.M. Thesis, Department of Mechanical Engineering, Massachusetts Institute of Technology, Cambridge, MA, **1982**.
31. Shim, J.-J.; Johnston, K.P. *A.I.Ch.E. Journal* **1991**, 37, 607.
32. Durril, P.L.; Griskey, R.G. *A.I.Ch.E. Journal* **1966**, 12, 1147.
33. Durril, P.L.; Griskey, R.G. *A.I.Ch.E. Journal* **1969**, 15, 106.
34. Van Krevelen, D.W. *Properties of Polymers*; Elsevier: New York, NY, 1980.
35. Vieth, W.R. *Diffusion in and through Polymers: Principles and Applications*; Hanser Publishers: New York, NY, 1991.
36. Bird, R.B.; Stewart, W.E.; Lightfoot, E.N. *Transport Phenomena*; 1960; pp 592-625 and pp 642-652.
37. Erwin, L. *Polym. Eng. Sci.* **1978**, 18, 572-576.
38. Raunwendaal, C. In *Mixing in Polymer Processing*; Raunwendaal, C., Ed.; Marcel Dekker, Inc.: New York, NY, 1991; pp 129-240.
39. Saunders, J.H. In *Handbook of Polymeric Foams and Foam Technology;* Klempner, D.; Frisch, K.C., Eds.; Hanser Publishers: New York, NY, 1991; 575.
40. Goyal, S.K. *Plastics Engineering* **1995**, Feb., 25-28.
41. Frisch, K.C.; Saunders, J.H. *Plastic Foams;* Marcel Dekker: New York, N.Y., 1972, Vol. 1.
42. Jacob, C.; Dey, S.K. *SPE ANTEC Tech. Papers* **1994**, 1964-1971.

Chapter 9

Effect of Silicone Surfactant on Air Flow of Flexible Polyurethane Foams

Xiaodong D. Zhang, Christopher W. Macosko, and H. T. Davis

Department of Chemical Engineering and Materials Science, University of Minnesota, 421 Washington Avenue Southeast, Minneapolis, MN 55455

Grafted copolymers which consist of a polydimethylsiloxane backbone and poly(ethylene oxide-co-propylene oxide) pendant groups are used as surfactant to stablize the bubbles in flexible polyurethane foam. The final properties such as air flow through the foam are significantly affected by the structure of the silicone surfactant used. Foams in which only the surfactant was changed provide a relationship between surfactant structure and foam air flow. Air flow of the foam increased as the polysiloxane backbone length of the surfactant decreased. Air flow of the foam increased as the polyether branch frequency of the surfactant increased. The drainage rate of cell windows and the foam top skin breaking time are shown to have significant effect on percentage of open cell windows. Both cell window drainage rate and top skin blow-off time are affected by silicone surfactant structure. Basic surface chemistry measurements such as surface tension, dynamic surface tension and dynamic light scattering method are used to characterize the surfactant properties.

The addition polymerization reaction of diisocyanates with alcohols was discovered by Professor Dr. Otto Bayer and co-workers in 1937 (1). This discovery set up the fundamental chemistry for the polyurethane industry. Polyurethanes are characterized by their repeating urethane linkages (-NH-CO-O) formed by the reaction between an isocyanate group (-N=C=O) and a hydroxyl group (-OH). Depending on the starting material, a range of products from soft flexible foam through semirigid and rigid foam to molded foam or elastomers can be achieved. Of all the polyurethane products, flexible polyurethane foam has the largest production and is most widely used.

Silicone-polyether graft block copolymers are used as surfactants in flexible polyurethane foaming systems (2, 3). In the absence of these surfactants, a foaming urethane will experience catastrophic coalescence and eventually cause foam collapse. These surfactants are efficiently adsorbed at the air/liquid interface and thus may have great impact on cell opening/window rupture in polyurethane foam. Percentage of ruptured cell windows in cured foam is shown to be affected by the silicone surfactant structure in the foam formulation. In other words, the silicone surfactant structure has

a great impact on openness of the final foam product, which is directly related to the air flow of the foam. Many physical properties of a flexible polyurethane foam are highly affected by its air flow (*4*). However, air flow is a hard property to control in industry because the effect of surfactant is not elucidated. Understanding the role of silicone surfactant during foaming, especially its effect on air flow of the final foam product can be helpful in designing new surfactant and obtaining flexible polyurethane foams with desired physical properties.

Designed Surfactant Series and Resulting Foam Air Flow

A series of surfactants was synthesized to vary surfactant backbone length and polyether branch percentage. The structure of the surfactants is shown in Figure 1. The nomenclature of the structure is also shown in Figure 1. (D+D') represents the length of the siloxane backbone, D'/(D+D') represents the percentage of polyether branches. Foams were made with these surfactants. Formulation of the foams is listed in Table I.

Table I.   Formulations for air flow test   **Unit: pphp[a]**

Formulation	weight (gram)
Voranol 3137[b]	100
water	4.0
Dabco 33LV[c]	0.30
Dabco T-9[d]	**0.20**
Silicone Surfactants[f]	**1.0**
Voranate T-80[e]index	110

[a]Parts per hundred parts polyol (by weight).
[b]1000 equivalent weight triol containing 13% ethylene oxide, 87% propylene oxide and all secondary hydroxyl groups (Dow Chemical).
[c]33% triethylenediamine in dipropylene glycol (Air Products).
[d]Stabilized stannous octoate (Air Products).
[e]An 80:20 mixture of 2,4- and 2,6-toluene diisocyanate (Dow Chemical)
[f]Structures of the surfactants are described in Figure 1.
SOURCE: Adapted from ref. 6.

Air flow measurement is used to evaluate the openness of the foam, since a linear relationship between the two has been found (Figure 2). A cell window is considered open if the window is totally missing. If there are there pin-holes on a window, then it is considered partially open. Air flow of the foams was measured according to ASTM D 3574. Foam specimens 50x50x25 mm in size were cut out from the top and bottom part of the buns in the buckets with a 50x50 surface perpendicular to blow direction. The specimens were prepared so that the upper surface of the top specimens was leveled with the shoulders of the buns and the lower surface of the bottom specimen was 25 mm distant from the bottom. In Table II, foam air flow as well as cell opening time are listed for foams made with the designed surfactants.

  An increase in polyether branch percentage tends to increase air flow (Figure 3a). The surfactants with the smallest polyether branch percentage D'/(D+D') made the foam collapse or produced foam with lower air flow. Silicone surfactants with very low percentage polyether branches act as defoamers. There is an important balance balance between the defoamer and the silicone foam stabilizer with a higher percentage of polyether branches. Actually, the foam did not collapse when the concentration of

$$(CH_3)_3SiO-(SiO)_b-(SiO)_{b'}-Si(CH_3)_3$$

with CH_3, CH_3 above and CH_3, R below.
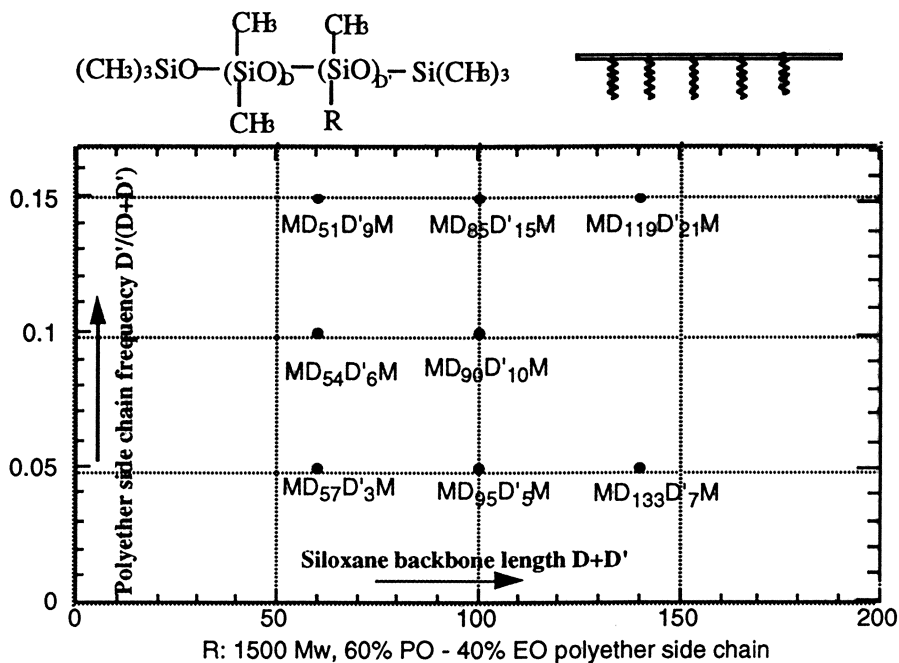
Figure 1. Structure of designed surfactant series.

M = CH$_3$ D = (CH$_3$)$_2$Si-O   D' = (CH$_3$)RSi-O,

Plot Y-axis: Polyether side chain frequency D'/(D+D'); X-axis: Siloxane backbone length D+D'; values from 0 to 200. Data points labeled: MD$_{51}$D'$_9$M, MD$_{85}$D'$_{15}$M, MD$_{119}$D'$_{21}$M (at 0.15); MD$_{54}$D'$_6$M, MD$_{90}$D'$_{10}$M (at 0.1); MD$_{57}$D'$_3$M, MD$_{95}$D'$_5$M, MD$_{133}$D'$_7$M (at 0.05).

R: 1500 Mw, 60% PO - 40% EO polyether side chain
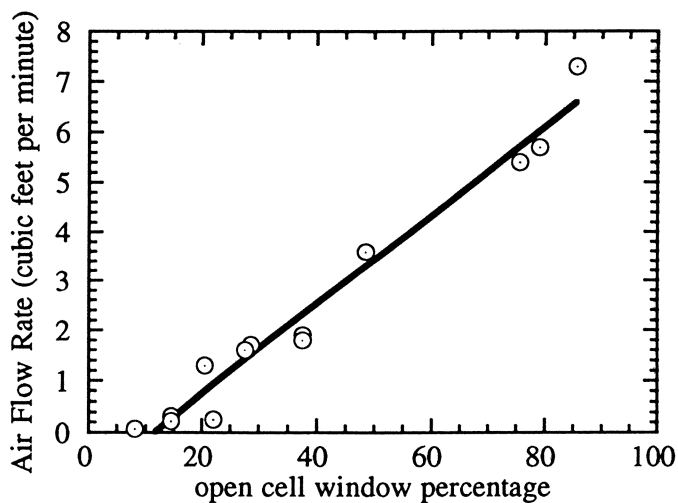
Figure 2. Air flow as a function of effective fraction of open cells (p$_{eff.}$).

Plot Y-axis: Air Flow Rate (cubic feet per minute) 0 to 8; X-axis: open cell window percentage 0 to 100.

$$p_{eff} = \frac{N_{open} + (1/2)N_{part.}}{N_{open} + N_{part.} + N_{pin.} + N_{closed}}$$
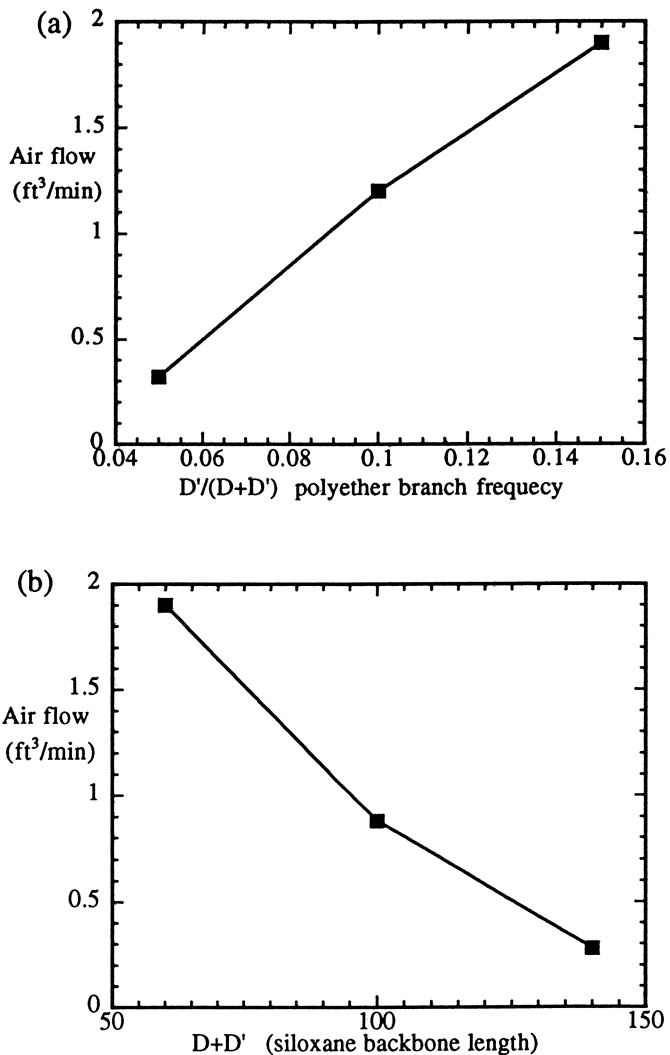
Figure 3(a). Effect of polyether percentage of surfactant on foam air flow. D+D'=60
3(b). Effect of siloxane backbone length of surfactant on foam air flow. D'/(D+D')=0.015

$MD_{95}D'_5M$ type surfactant was increased to 2 pphp. The reason the foam had lower air flow is not clear.

In the series of $D'/(D+D') = 0.15$, larger $D+D'$ (longer siloxane chain) produced lower air flow (Figure 3b). This result may be caused by the slower drainage of film containing longer siloxane chain surfactant, since a large surfactant tends to give a higher surface viscosity (5). Slower drainage causes thicker films and will lead to fewer open windows (6).

Table II. Time to internal cell opening (t_0), blow-off time (t_1, time at hole formation on top skin of the foam bun) final foam bun height and airflow with different surfactant structures

Surfactant	t_0 (sec)	t_1 (sec)	Foam height (mm)	Air Flow (CFM) Top / Bottom
$MD_{54}D'_6M$	-	79	202	1.3 / 0.37
$MD_{51}D'_9M$	75	77	177	2.2 / 1.9
$MD_{95}D'_5M$	-	75	191	0.33 / 0.33
$MD_{90}D'_{10}M$	75	79	215	1.8 / 0.4
$MD_{85}D'_{15}M$	-	80	209	1.8 / 0.88
$MD_{119}D'_{21}M$	76	85	220	1.5 / 0.28

SOURCE: Adapted from ref. 6.

The silicone surfactant structure has a great impact on many factors in foaming urethane. Some of these factors such as drainage rate of the cell windows and top skin strength of the foam bun are believed to have a significant effect on the cell opening event. Drainage rate will determine the thickness of cell windows at onset of cell opening. Top skin strength can control the visual blow-off time. Cell opening event is shown to be a continuous process between the onset of cell opening and the visual blow-off rather than a sudden event. Both drainage and top skin strength are affected by the surfactants used. These effects will be discussed in the next two sections.

Effect of Cell Window Drainage

During foaming, the bubbles initially introduced by mechanical mixing will grow. As the volume fraction of the gas bubbles exceeds 74%, the spherical bubbles will begin to distort into multisided polyhedra and cell windows are formed. As the reaction proceeds, the cell windows will get thinner by drainage and by the biaxial extension caused by bubble expansion. Due to capillary forces, the liquid pressure inside the Plateau borders will be lower than in the cell windows (Figure 4). This pressure difference will cause cell window thinning by sucking liquid from the windows into the struts. The silicone surfactant added can retard cell window drainage. Different surfactant structures will have different abilities to retard drainage, resulting in a distribution of different cell window thickness at time of cell opening.

Theory of thin liquid film drainage   Liquid in thin films will drain into the Plateau border by the Plateau border suction (Figure 4). For films with a partially mobile surface, drainage will cause movement of the surface layer and a surfactant surface concentration gradient will be generated. The surfactant surface concentration gradient will cause a surface tension gradient along the surface that will retard the film drainage. This effect is called Gibbs-Marangoni effect and is reviewed by Scriven and Sternling (7). The surface tension gradient can be affected by the diffusion of the surfactant along the surface as well as the diffusion of the surfactant from the bulk.

Thus the surface rheological properties of the film such as surface viscosity becomes important since they will affect the surface diffusion of the surfactant. The drainage can be obtained by solving the Navier-Stokes equations under the lubrication approximation accounting for the mobile surface (8, 9).

$$V_0 = -\frac{dh}{dt} = \frac{h^3 \Delta p}{24\eta R^2} \left[\sum_{n=1}^{\infty} \frac{(6\eta + \eta_s k_n^2 Mh)J_2(\lambda_n)}{(6\eta + 6M + \eta_s k_n^2 Mh)\lambda_n^3 J_1(\lambda_n)} \right]^{-1} \tag{1}$$

where h is film thickness, η is bulk viscosity, R is radius of the film and p is the capillary pressure; J_0, J_1 and J_2 are Bessel functions; eigenvalues λ_n are solutions of equations $J_0(\lambda_n)=0$, and $k_n = \lambda_n/R$. The surface mobility of the film is expressed by surface viscosity η_S and the mobility parameter M. The mobility parameter M compares the contribution of bulk and surface diffusion to the Marangoni effect and is defined as the following (8, 9):

$$M = -\frac{3D\eta}{\gamma\left(\frac{\partial\gamma}{\partial c}\right)_0} \left[1 + \frac{2D_s\left(\frac{\partial\Gamma}{\partial c}\right)_0}{Dh} \right] \tag{2}$$

where D and D_s are the bulk and surface diffusion coefficients of the surfactant respectively. C is the surfactant concentration in the bulk; γ is the surface tension and Γ is the surface excess concentration of the surfactant on the air/liquid interface.

The analysis for drainage rate in a thin liquid film with constant area is shown in the above section. In polyurethane foaming system, the area of the cell window increases as bubbles grow. Radius and thickness of the film are changing due to the bubble expansion, making drainage calculation even more complicated. Although drainage rate at any instant can be estimated by equation 1 and this relation can be integrated with respect to time to predict film thickness at cell opening time, the parameters in equation 1 are difficult to obtain during foam expansion.

However, equation 1 does tell us what factors contribute to film drainage. In general, the surfactant changes the drainage rate of thin liquid film by affecting the surface condition of the air/liquid interface. Surfactants with different structure will give different surface conditions. Dynamic surface tension, surfactant diffusivity in bulk solution and on surface of a thin film, surface coverage of surfactant as well as surface rheology of the thin film will be affected by the surfactant structure. Our previous work showed that the silicone surfactant does not affect reaction kinetics (6). So the bulk viscosity of the liquid material during foaming should be the same for foams made with different surfactants. Since liquid viscosity profiles are the same for formulations with different surfactants, drainage rate should be mainly affected by surfactant surface coverage and surface viscoelasticity (10, 11). Surfactant surface coverage is important since it can determine surface tension of the films during foaming and change surface viscosity as well. Surface viscoelasticity is important for surface flow of surfactant and boundary conditions for drainage flow. As foam expands, cell windows will expand and more surface is generated. Surfactant will move to the liquid/gas interface during the expansion. Surfactants can move from the surface along the struts into surface of cell window driven by the surface tension gradient. Surface

Plateau's Border (strut)

Drainage Flow

h
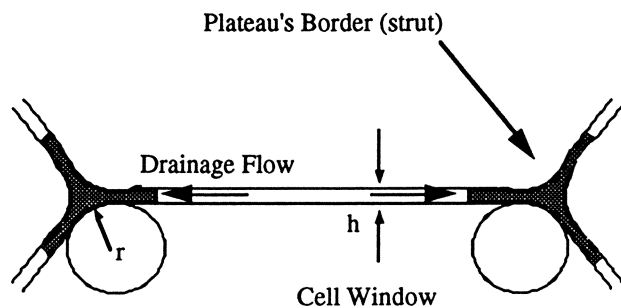
Cell Window

Figure 4. Diagram of drainage in a cell window.
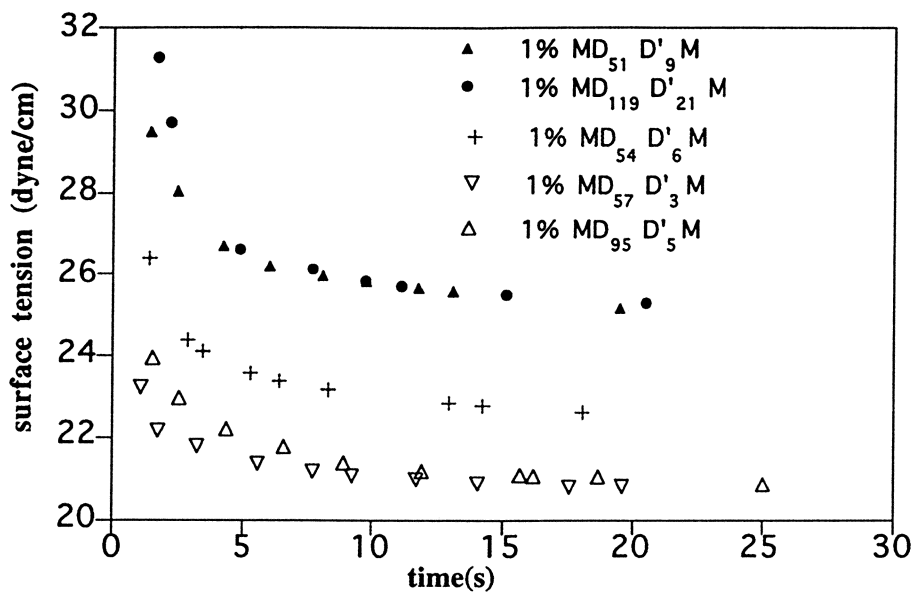
Figure 5. Dynamic surface tension of different surfactant solutions.

viscoelasticity can affect the surface flow rate of the surfactant. Both surface flow rate of surfactant and drainage flow rate will be affect by the surface viscoelasticity of the cell window.

Surfactant property measurements   Experiments were performed to characterize the designed surfactant series. These experiments will provide information about surfactant performance with different structures. The goal is to relate surfactant structures to the drainage rate discussed in the previous section.

Surface Tension Measurements   Surface tension measurements were made by the Wilhelmy method using a digital tensiometer K10ST from Kuss Instrument [12]. Surfactant solution in polyol Voranol 3137 with concentration ranging from 0.0001wt.% to 10 wt.% were measured. Prior to each run the surface tension of pure water was measured. Samples were prepared at least 48 hours before the measurements. Concentrations used in this experiment were prepared by serial dilution with polyol. Static surface tension shows that the equilibrium surface excess concentration of all the listed surfactants are approximately the same (see Table III).

Table III. Surfactant surface coverage result

surfactant	$MD_{119}D'_{21}M$	$MD_{85}D'_{15}M$	$MD_{51}D'_9M$	$MD_{54}D'_6M$	$MD_{57}D'_3M$
nm^2/molecule	2.98	2.91	3.11	2.43	2.55

All surfactants have surface density of 2.43 - 3.11 nm^2/molecule. Static surface tension method measures the thermodynamic equilibrium surface coverage concentration. However, foaming reaction is quite rapid and it is very unlikely to get equilibrium surface coverage. Thus the mobility of different surfactants need to be investigated.

Dynamic Surface Tension Measurements   Dynamic surface tension measurements were made by the drop weight method [12]. 1wt.% surfactant solution in polyol is put in a burette with a grounded tip of inner diameter of 1mm and outer diameter of 3.93 mm. Twenty drops were collected; their mass and time to fall were recorded. Dynamic surface tension results are shown in Figure 5. If the drops are formed very fast, then surface tension will be high due to insufficient amount of surfactant on the interface. As time increases, the surface tension will approach static surface tension value by an exponential decay function,

$$\gamma - \gamma_{equilibrium} = (\gamma_{solvent} - \gamma_{equilibrium}) * exp(-kt) \qquad (3)$$

where γ is the dynamic surface tension at time t, $\gamma_{equilibrium}$ is surface tension value at equilibrium and mobility coefficient k is decay coefficient for the exponential decay function. The mobility coefficient k represents how fast the surfactant moves. It is seen that the mobility coefficient decreases as percentage of polyether branches increases. However, backbone length does not show any significant effect on mobility coefficient k (Figure 6b). The dynamic surface tension data implies that the mobility of the surfactant will increase as ether branch frequency decreases (Figure 6a). Higher mobility means the surfactant can diffuse to the interface faster and have a higher excess interface concentration. Higher surface concentration of the surfactant may
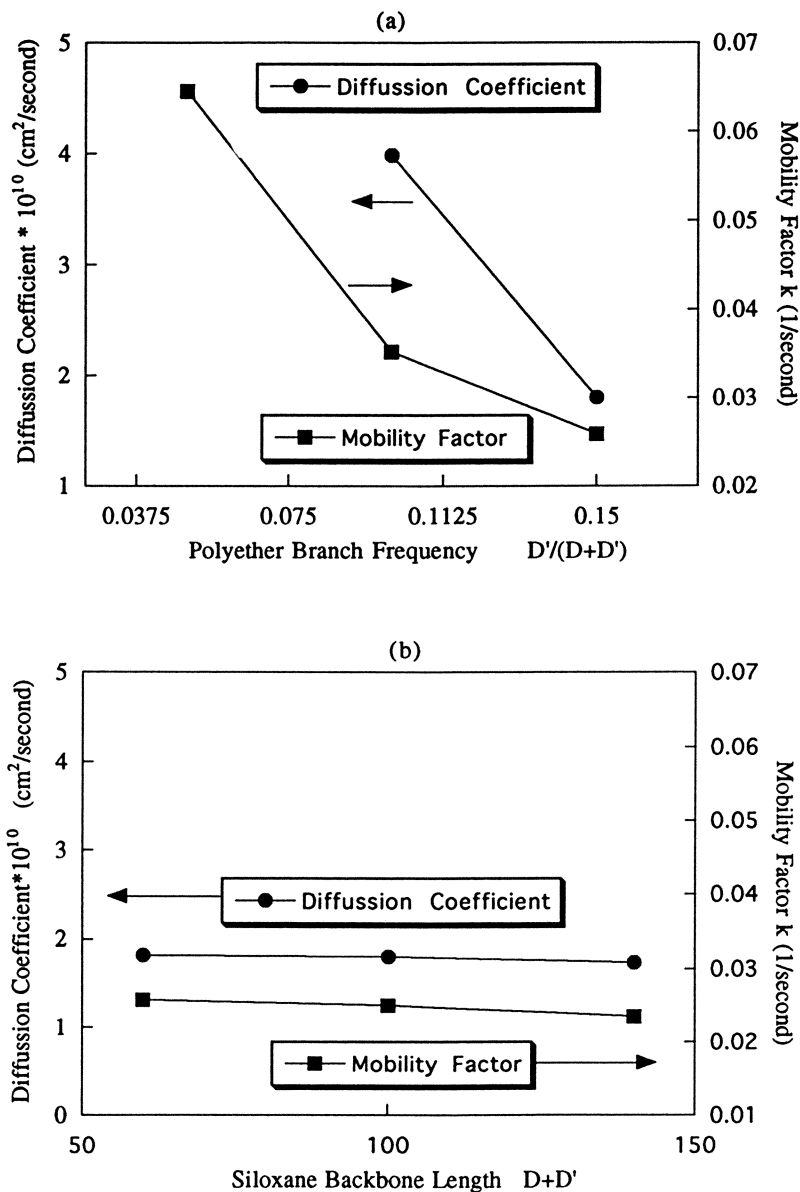
Figure 6(a). Effect of polyether percentage of surfactant on surfactant mobility. D+D'=60
6(b). Effect of siloxane backbone length of surfactant on surfactant mobility. D'/(D+D')=0.015

cause higher surface viscosity and retard drainage flow further. Thus, surfactants with low polyether branch percentage have stronger stablization ability and the resulting polyurethane foam will be more closed. Therefore, the trend for surfactants with different polyether branch percentages observed in air flow measurements can be explained by the mobility of the surfactants.

Dynamic Light Scattering The mobility of different surfactant were confirmed by a dynamic light scattering experiment [13]. Dynamic light scattering or Photon Correlation Spectroscopy measurements employed a Brookhaven Instrument Company Model BI-9000AT Digital Correlator. The correlation function is measured for relaxation time ranging from 1 microsecond to 1s. Results were analyzed on a separate computer with software CONTIN which uses non-linear regularized inverse Laplace transformation to obtain relaxation time distribution. Samples were filtered with a 0.45 micrometer filter 24 hours before measurements. The characteristic relaxation time was found by software CONTIN which uses non-linear regularized inverse Laplace transformation. The diffusion coefficients were calculated from the characteristic relaxation time and shown in Figure 6 along with the mobility coefficients determined by dynamic surface tension method. The diffusion coefficient is directly related to the mobility of the surfactant. Again, the mobility is shown to increase as the percentage of the polyether branch on the siloxane backbone decreases. The results for surfactants with 5% polyether branches were not shown since they were cloudy and large aggregation, or more likely, phase separation occurs. This phase separation may be the reason that foams having surfactant with 5% polyether branches tend to collapse. Compound with only the backbone of the surfactant is called silicone oil, and is a commercial defoamer. Backbone length did not show a significant effect on surfactant mobility.

Effect of Top Skin Strength of the Foam Bun

Foam formation occurs with a high exotherm. As the temperature of the foam bun gets higher, heat will be lost from the top skin of the foam bun to ambient air. As a result of the heat loss, temperature at the top skin is lower than that of the center. This lower temperature profile will yield slower reaction kinetics. Thus there will be less carbon dioxide generated in the top skin than at the center of the bun. The gas diffusion to the ambient air will be fast at the top skin as well. As a result, the top skin will be a dense, low gas fraction layer (*15*).

It is shown that during foaming, the cell windows inside the bun will open before the visual blow-off time, that is, the time when the top skin of the foam bun is open (*14*). After cell opening occurs, the material inside the foam bun stiffens and pressure will build up by generated carbon dioxide. At this time the top skin is still liquid, and as pressure reaches a certain value, carbon dioxide gas will break the top skin and the pressure inside the foam will approach atmospheric pressure (*15*). Surfactant can change the yield stress for liquid foams. Thus the strength of the top skin is affected by surfactant. Formulations with different surfactants will then have different blow-off time.

Effect of Skin-breaking Time on Foam Air Flow To show skin-breaking time has great effect on air flow rate, an experiment is designed. One set of foams were made with 3 pphp (part per hundred part polyol) surfactant 53RMG7 (containing MD$_{85}$D'$_{15}$M and polyether) and skins were manually broken at different time with a glass stir bar. Air flow resistance of these foams were then measured. The top specimen in the second set of experiments were cut 13 mm below the shoulder of the bun to reduce the effect of mechanical breaking by manual blow-off.
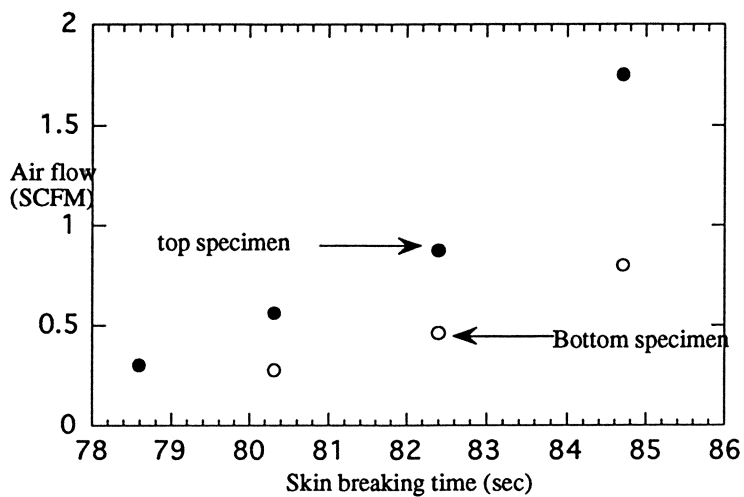
Figure 7. Skin breaking time (manual blow-off time) vs. air flow for foams made with 3pphp surfactant A (containing MD₈₅D'₁₅M and polyether).

Data in Figure 7 were obtained by manually breaking the top skin at different time after internal cell opening. It can be seen that air flow increases significantly as skin-breaking time increases. Since surfactant can affect top skin strength and change blow-off time, the effect of surfactant on air flow can also be controlling strength of the top skin.

Yield Stress of Liquid Foam   In polyurethane foams, the visual blow-off time is determined by the strength of the liquid top skin layer of the foam bun. It is generally agreed that liquid foams have a yield stress (*16, 17*). The foam will experience elastic deformation under stress below the yield stress. However, when the yield stress is reached, the cells (ie. bubbles) will gain flow ability. Thus the yield stress of the top skin will determine the internal gas pressure needed to break the liquid top skin layer. The yield stress of liquid foam can be expressed as the following (*16*):

$$\tau_y = \frac{\alpha\gamma}{d} \qquad (4)$$

where α is a dimensionless coefficient based on the gas fraction of the foam, γ is the surface tension and d is bubble diameter. So three factors will change yield stress, gas fraction, surface tension and bubble size. Dynamic surface tension at visual blow-off time is determined by surfactant added. Surfactant is also shown to be able to affect the gas diffusion through the cell windows (*18*), which can change both bubble size and gas fraction. Surfactant structure and properties will then determine the top skin strength of the foam and visual blow-off time.

Conclusion

Air flow of the foam product is seen to be affected by the structure of the surfactant used. It is observed that as the backbone of the surfactant increases, air flow will decrease; as the polyether branch percentage increases, air flow will increase. It is shown that both drainage rate and strength of the top skin have effect on air flow.
Thin film drainage literature is reviewed. Surfactant can affect drainage rate of thin liquid film by affecting the surface condition of the air/liquid interface. Structure of silicone surfactant will determine the dynamic surface tension, surfactant bulk and surface diffusion coeffecient as well as surfce rheology of the thin film.   Some surfactant property measurements were performed to relate surfactant structure to its surface properties. Static surface tension shows that the surfactant surface coverage of the air/liquid interface is the same for surfactant with different structures.   Using dynamic surface tension and dynamic light scattering method, it is shown that surfactant with lower polyether percentage has higher mobility and can move to the surface faster and retard drainage more. So surfactant with lower polyether percentage will often result in lower air flow.
Top skin strength of the foam bun is shown to affect air flow as well. The strength of the top skin is represented by its yield stress. The top skin yield stress can determine the skin breaking time of the foam bun. For the same formulation, foam air flow is shown to decrease as skin-breaking time decreases. The surfactant can affect the yield stress of the top skin layer and affect the skin-breaking time.
However, no explanation were found for air flow trend observed for surfactants with different backbone length. It is suspected that backbone length of the surfactant can change the surface viscosity. Experiments to directly measure surface viscosity and drainage rate of surfactant solution will be carried out in the future.

Acknowledgments

References

1. Bayer, O. *Mod. Plast.* **1947**, *24*, 149.
2. Rossmy, G. R.; Kollmeier, H. J.; Lidy, W.; Schator, H.; Weimann, M. *J. Cell. Plast.* **1977**, *13 (1)*, 26.
3. Woods, G. W. *Flexible Polyurethane Foams, Chemistry and Technology*; Applied Science, New Jersey; 1982, pp. 68-72.
4. Jones, R. E.; Fesman, G. *J. Cell. Plast.* **1965**, *1 (1)*, 200.
5. Owen, M. J.; Kendrick, T. C.; Kingston, B. M.; Lloyd, N. C. *J. Colloid Interface Sci.* **1968**, *24*, 135.
6. Yasunaga, K; Neff R. A.; Zhang X. D.; Macosko, C. W. *J. Cell. Plast.* **1996**, *32*, 427.
7. Scriven, L. E.; Sternling, C. V. *Nature* **1960**, *187*, 186.
8. Prud'homme, R. K.; Khan, S. A. *Foams* ; Marcel Deckker, Inc., New York, 1996.
9. Ivanov, I. B.; Dimitrov, D. S. *Colloid. Polymer. Sci.* **1974**, *252*, 982.
10. Rao, A. A; Wasan, D. T.; Manev, E. D. *Chem. Eng. Commun.* **1982**, *15,* 63.
11. Baets, P. J. M.; Stein, H. N. *Langmuir* **1992**, *8*, 3099.
12. Adamson, A. W. *Physical Chemistry of Surfaces*, Wiley, New York; 1990.
13. Ford, N. C., Jr. *Dynamic light scattering:applications of photon correlation spectroscopy*, R. Pecora Ed.; Plenum, New York; 1985.
14. Neff, R. A.; Macosko, C. W. *Proceeding of the SPI Polyurethanes Technical/Marketing Conference,* Boston, MA, 1994, 386.
15. Yasunaga, K.; Zhang, X. D.; Macosko, C. W. *J. Cell. Plast.*, in press.
16. Princen, H. M. *J. of Colloid Interface Sci.* **1983**, *91*, 160.
17. Princen, H. M. *J. of Colloid Interface Sci.* **1985**, *105(1)*, 150.
18. Ronteltap, A. D.; Prins, A. *Colloids and Surfaces* **1990**, *47(1)*, 285.

Chapter 10

Polymer Structure Development During Reactive Processing: In Situ Studies of a Cellular, Multiphase Block Copolymer

Michael J. Elwell[1], Anthony J. Ryan[2], Henri J. M. Grünbauer[1], and Henry C. van Lieshout[1]

[1]Urethanes Polymers Research and Development, Dow Benelux N.V., Herbert H. Dow Weg, Postbus 48, 4530 AA Terneuzen, Netherlands
[2]Manchester Materials Science Centre, University of Manchester Institute of Science and Technology, Grosvenor Street, Manchester M1 7HS, United Kingdom

In-situ studies of polymer structure development during the reactive processing of water-blown, flexible copoly(urethane-urea) foams are presented. Time-resolved FT-IR spectroscopy, synchrotron small angle X-ray scattering and dynamic rheometry techniques were employed, under forced-adiabatic conditions. FT-IR spectroscopy was used to monitor the the polymerization reactions. FT-IR spectroscopy indicated that the microphase separation transition (MST) occurred at a critical conversion of isocyanate functional groups and followed the kinetics associated with nucleation and growth. Synchrotron small angle X-ray scattering was used to probe the kinetics of the reaction-induced phase transformation process, its mechanism(s), the length scales and architecture of the resultant polymer morphology. Microphase separation was observed to occur at a critical conversion of isocyanate functional groups; and followed the kinetics associated with spinodal decomposition. Dynamic rheometry was used to monitor the rheological properties associated with the evolving morphology. Four main regions of rheological development during the formation of polyurethane foam were identified. The emphasis is directed at how these techniques complement each other to provide an overall view of polymer structure development.

Each day 85% of the world's population sits on upholstered furniture that derives its cushioning from flexible polyurethane foam; a cellular, multiphase block copolymer. In addition to furniture and bedding, other application areas for flexible polyurethane foam include automotive and packaging. Of the total amount of urethane chemicals used world wide, the amount that contributes to the production of flexible polyurethane foam is by far, the greatest.

143

For a material that has found such widespread use in our society, little is understood as to how the polymer morphology evolves, and more importantly, how it can be controlled during reactive processing, to improve the performance of the material. The aim of this article is to provide the reader with the scientific understanding available today, behind what remains for many, a "black art".

The morphology of a polymer, derived from either a thermoplastic or thermosetting polymer, is inherently controlled by the thermal history that it experiences during the transformation from the liquid state (e.g. melt) to solid polymer. In order to control how the polymer morphology evolves, an understanding of the molecular response(s) of the polymer or evolving polymer (depending on the processing route) to changes in temperature is essential. For some thermoplastic polymers, (such as polyolefins and polyamides), a polymer in granular form is processed (*1-3*). The material is transformed from granules/pellets (solid), to polymer melt (liquid) to the final polymer artefact. However, for some thermoplastics (e.g. thermoplastic copolyurethanes) and many thermosetting polymers (such as RIM non-linear copolyurethanes, IPN's, epoxies) the situation is somewhat different. Here, monomers/oligomers (liquid) undergo polymerization coupled with phase separation, vitrification, crystallisation, chemical gelation and combinations of these (depending on the particular system) to yield the eventual solid polymer article (*4,5*).

The reactive processing of water-blown flexible polyurethane foam is a good example of this. Flexible polyurethane foam is formed by the simultaneous reaction of a diisocyanate with polyether polyol and water. These two exothermic reactions lead to the formation of a segmented block copoly(urethane-urea), of the $-(H_m S)_n-$ type, where H_m represents the polyurea hard segment with degree of polymerization m, and S is the poly(ether-urethane) soft segment: n is the degree of polymerization of the block copolymer. This is blown into a foam by the co-generation of carbon dioxide gas evolved from the water-isocyanate reaction. As the polymerization proceeds, the core of the rising foam bun becomes self-insulated by the surrounding polymerising mixture creating, in effect, a quasi-adiabatic environment. Previous reaction kinetic studies during foam formation with both toluene diisocyanate (TDI) and methylene diphenyl diisocyanate (MDI) are documented in the literature (*6-10*). 'Post-mortem' analyses (*11-13*) of the final morphology present in flexible polyurethane foams has shown that they exhibit a microphase separated morphology similar to that of segmented urethane/urethane-urea elastomers.

The development of morphology during foam formation is complex (*8,10*). As the chemical reactions proceed, the chain lengths of all polymeric moieties increase giving rise to an increase in the degree of polymerization, N. In addition, the interaction parameters (c) characterising the miscibilities between such moieties can also change as a consequence of the increase in N. Such changes in c and N, (more specifically, the product cN) can give rise to the system crossing thermodynamic boundaries which results in a transition from an initial homogeneous (disordered) state to a microphase separated (ordered) state (*14,15*). The resultant morphology is determined by the competition between the kinetics of polymerization and microphase separation (*10,14,15*). Understanding the complex competition between polymerization, microphase and/or macrophase separation, and the solidification

process(es) require the use of *in-situ*, time-resolved analytical methods. *In-situ* studies regarding both the reaction kinetics and development of polymer structure in both flexible and rigid polyurethane foam are sparse (*8,10,16-18*). Model reactions have been employed previously to investigate the reaction kinetics in urethane systems (*19-26*). As far as we are aware, there are only six studies in the literature where model reaction systems have been employed to study the development of polymer morphology in urethane foams (*6,27-31*).

Equally important, are the reaction conditions that are imposed upon the system during the *in-situ* analysis. Early studies of structure development in flexible polyurethane foam; especially the kinetic processes involved, ignored the importance of the thermal process history (*27-29,32-34*). This led to erroneous results and misinterpretation of the kinetics data obtained. Only when it was realised that analytical investigations had to be conducted under forced-adiabatic conditions, was further progress made in the understanding of structure development during foam formation (*6-10,17,31,35*)

In-situ investigations: the analytical tools

Monitoring the reaction kinetics during a fast bulk copolymerization, where several chemical changes occur simultaneously, requires the use of time-resolved FT-IR spectroscopy. This technique has the capability to analyse fast polymerization reactions (reaction times $\leq$ 10 s) and monitor several chemical changes simultaneously; such as the decay in concentration of a component monomer, the concomitant increase in concentration of product(s) and any environmental/structural changes in the nature of those products. Its use in the study of polyurethane systems (linear and non-linear elastomers, and flexible and rigid foams) has been well demonstrated (*5-10,16,31-35*).

In multiphase polymer systems (e.g. flexible polyurethane foam), probing the phase separation kinetics requires the use of a time-resolved scattering technique such as synchrotron small angle X-ray scattering (SAXS) (*17*) or small angle light scattering (SALS), depending upon the length scales of the evolving polymer structure. In the early stages of the polymerization process which evolve flexible polyurethane foam, the material is a combination of homopolymer, block copolymers and monomers. The final structured material is predominantly a multiblock copolymer (*6,10,17*). Scattering studies of phase separation kinetics in multiblock copolymers are not common (*10,17,18,36-45*).

During reactive processing as the polymer morphology develops, the macroscopic properties associated with the *evolving* morphology will change. Clearly, from the standpoint of polymer processing, knowing at which point in the cycle time the evolving material has achieved sufficient stiffness (modulus) to be de-moulded, is important. It is only by understanding how the morphology and rheological properties associated with it, evolve during reactive processing, can control and improvement in materials properties be achieved (*5,14,15*). In order to obtain macroscopic property information (e.g. stiffness) during polymer formation, time-resolved rheological techniques are necessary (*46-56*). Despite the widespread applications of cellular polymers, very little information is presented in the literature on the development of the foamed polymer's rheological characteristics. The nature
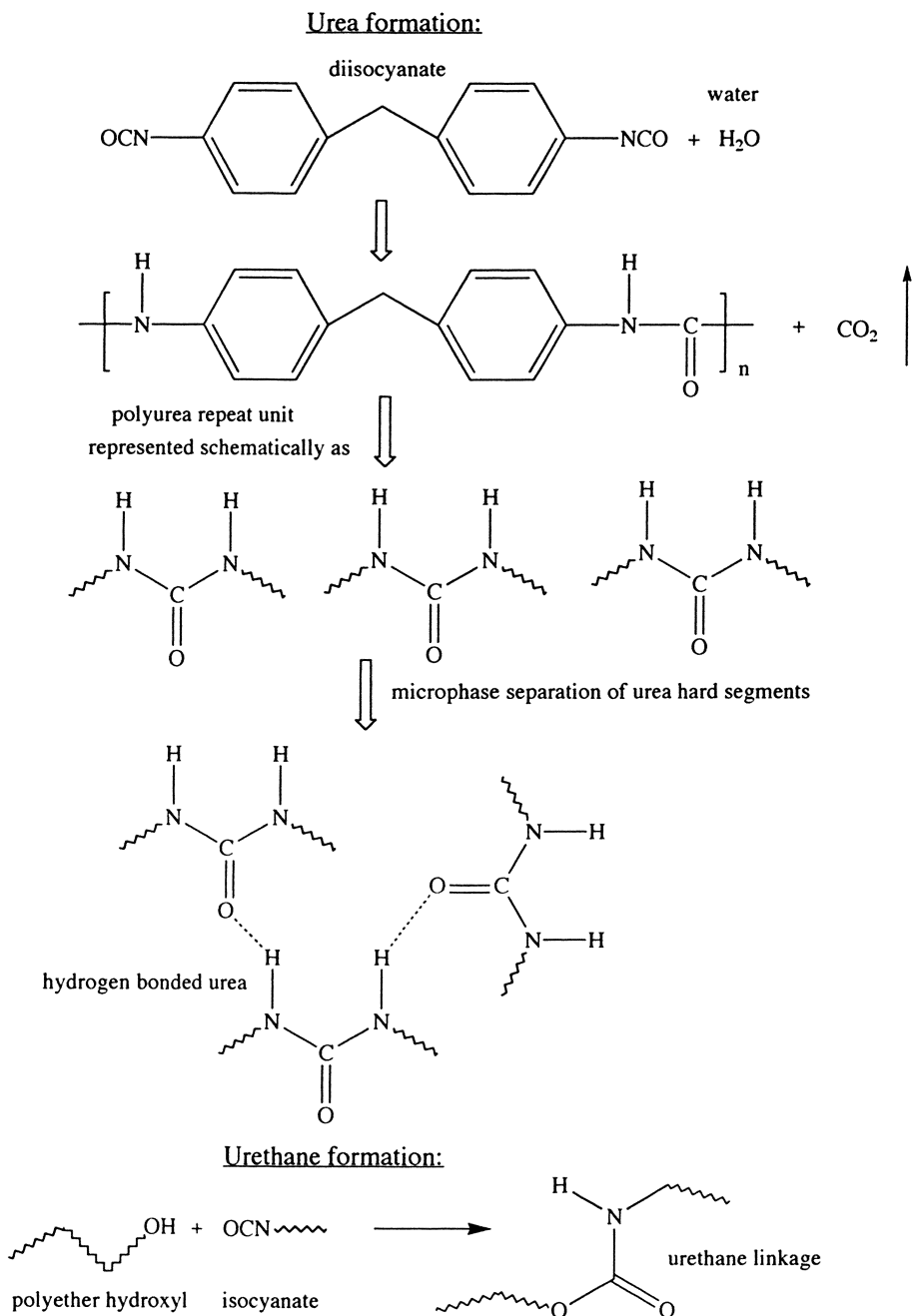
Figure 1. Schematic representation of the reaction chemistry taking place during polyurethane foam formation.

of the foaming reaction is the reason for the absence of a suitable, reliable rheological instrument capable of handling the unique challenge associated with a reacting, foaming polymer. Much of the work that has been previously reported on reacting foam (*57-59*) was conducted under isothermal conditions. The first step towards an adiabatic rheometer was made by Mora et al. (*53,54*). A temperature controlled rheometer plate was designed and employed by Elwell et al. (*10,35*). This type of temperature controlled rheometer plate has been further developed by Neff and Macosko (*60,61*).

Evolution of structure in flexible polyurethane foam

This article deals specifically with *in-situ* studies of polymer structure development during the reactive processing of water-blown, flexible copoly(urethane-urea) foams based on MDI.

FT-IR Spectroscopy. Figure 1 shows the basic reaction chemistry that takes place during foam formation (*9,18,31,43*). The isocyanate-polyether hydroxyl reaction generates the urethane group, whilst the isocyanate-water reaction generates polyurea and carbon dioxide. The isocyanate absorption band occurs at approximately 2300-2270 cm^{-1} in the mid infra-red spectrum. The decay in the intensity of this absorbance can be used to monitor the conversion of isocyanate functional groups during the reaction. The evolution of urethane, soluble urea and hydrogen-bonded urea species during the polymerization can be followed by monitoring the carbonyl region of the mid infra-red spectrum (*6-10,16,18,27-33,41,43*). Several absorbances that occur in the carbonyl region have been assigned to specific functional groups, interactions and types of hydrogen bonding (*6-8,10,27-33*).

Figure 2 (a,b) shows the wide range of information available from *in-situ* FT-IR spectroscopy (*9,10,18,31,43*). Figure 2 (a) is a three dimensional plot of the isocyanate absorbance, versus frequency, versus time (*31,43*). It shows clearly the decay in the intensity of the isocyanate absorbance with time. Each spectrum was recorded at 6 second intervals. Figure 2 (b) shows a similar three dimensional plot for the corresponding carbonyl region; illustrating the evolution of urethane, soluble urea and hydrogen-bonded urea (*31,43*). It is apparent that urethane (≈ 1730 cm^{-1}) and soluble urea (≈ 1715 cm^{-1}) evolve early in the reaction. These two reactions take place simultaneously: not sequentially, as early research had suggested (*32-34*). It is also apparent that there is an induction time prior to the evolution of hydrogen-bonded urea (≈ 1654 cm^{-1}).

It is possible to correlate the isocyanate conversion calculated from the decay in the isocyanate absorption with time, and that calculated from normalisation of the reaction exotherm (*6,8-10,18,31,43,53,60,61*). Figure 2 (a) compares isocyanate conversion calculated from the forced-adiabatic spectroscopy data (open symbols) with that calculated from the normalisation of the foam reaction exotherm (solid line). Figure 2 (b) shows representative plots of normalised soluble urea (1715 cm^{-1}, open symbols) and hydrogen-bonded urea (1654 cm^{-1}, closed symbols) versus
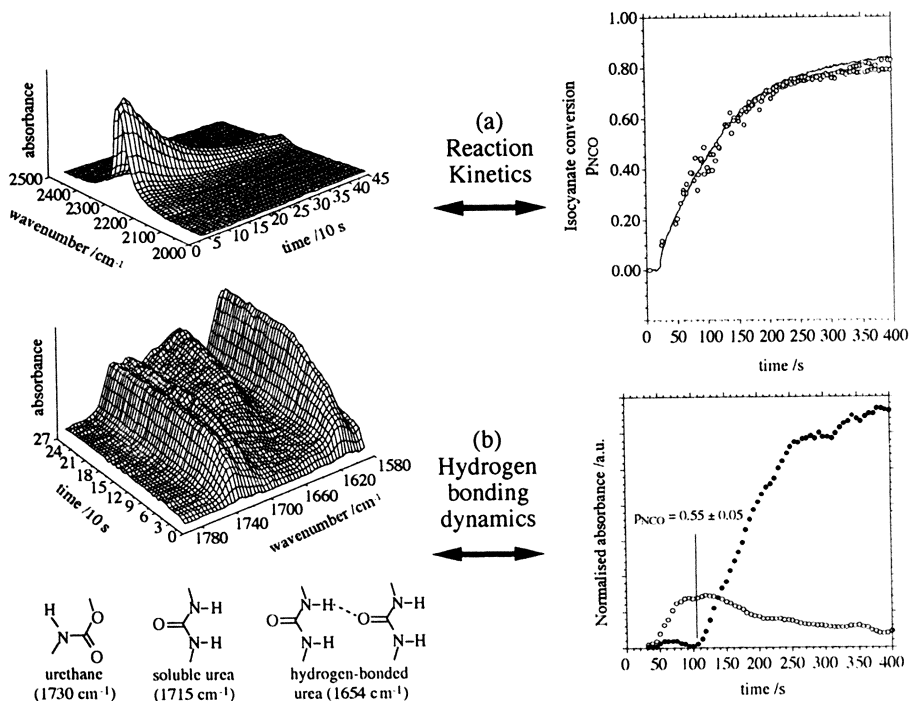
Figure 2. The wide range of information available from *in-situ* FT-IR spectroscopy for a low water content formulation.

(a) *Copolymerization kinetics.* Three dimensional plot of the isocyanate absorbance ($\sim$2270 cm^{-1}), versus frequency, versus time showing the decay in the intensity of the isocyanate absorbance and the correlation between the isocyanate conversion, p_{NCO}, calculated from the decay in the isocyanate absorption with that calculated from normalisation of the reaction exotherm.

(b) *Hydrogen-bonding dynamics.* Three dimensional plot for the corresponding carbonyl region, and normalised soluble urea (open symbols, 1715 cm^{-1}) and hydrogen-bonded urea (closed symbols, 1654 cm^{-1}) versus time. The microphase separation transition (MST) is indicated. (Adapted from refs. 10,17,43.).

reaction time (*9,10,18,31,43*). The soluble urea and hydrogen-bonded urea absorbance bands were normalised against isocyanate conversion. The normalisation is carried out because the probe (carbonyl) concentration is directly proportional to conversion. The normalisation removes the change in concentration effect. The microphase separation transition (MST) is indicated and is taken as the point at which there is an acceleration in the hydrogen-bonded urea and a depletion in the soluble urea (*5,6,8,50,52*). At the MST, the system becomes both chemically and spatially heterogeneous, and this separates functional groups.

It has been observed (*9,10*) for polyether polyol systems, that across a broad range of water concentrations, the conversion of isocyanate functional groups at the MST remains approximately constant at p_{NCO} = 0.55 ± 0.05. Thus, the critical isocyanate conversion at which the local number average hard segment sequence length, N_H, reaches N_{Hcrit}, is approximately 55 ± 5% conversion of isocyanate functional groups. This corresponds to an average hard segment sequence length of 1.1-1.5 units (*10,31*). In order to understand more fully the reaction chemistry and subsequent structure development processes during foam formation; model foaming reactions employing a mono-functional polyether have also been investigated (*27-29,31,43*). In foam formulations which commonly employ a nominally, tri-functional polyether polyol, this component has been substituted for a mono-functional polyether (or monol) of the same chemical composition as the polyether polyol (i.e. effectively one arm of the polyether polyol). This eliminates the presence of urethane covalent crosslinks and enables the effect of their absence on the structure development processes to be established. The presence of covalent crosslinks has been shown to delay the onset of microphase separation (*8,31,43*). Furthermore, water has been replaced by deuterium oxide as the blowing agent. Replacing water with deuterium oxide as the blowing agent, results in a shifting of the soluble D-urea and associated D-urea absorbance peaks to lower wavenumbers (*6,8,30,31*) This facilitates further exposure of the urethane absorbance peak; which maybe partly obscured by the soluble urea peak when water is used. This enables the presence of hydrogen-bonded urethane species to be probed, as a result of the large reduction in the extent of peak overlap.

Synchrotron SAXS. Figure 3 shows the plethora of information attainable from time-resolved, synchrotron small angle X-ray scattering studies during the polymerization reaction to evolve flexible polyurethane foam (*17,18,43*). Density changes, length scales structure, microphase/macrophase separation transitions, mechanisms of phase separation and effective diffusion coefficients of particular moieties during phase separation are readily accessible. Illustrated in Figure 3 are; a representative set of time-resolved SAXS data that have been collected during foam formation (at 2 second intervals) for a high water content formulation (*17*) (for the purpose of clarity, only every fourth time-frame is shown), the change in sample density during the polymerization for a low water content formulation (*17*), how the structure and corresponding interparticle scattering distance (or interdomain spacing), *d*, evolves for a high water content formulation (*17*), relative invariant, Q', (a measure of the degree of microphase separation) versus reaction time (*17*), interpretation of the mechanism of phase separation from the density corrected, scattered intensity, *I* (*q,t*), as a function of time and finally, evaluation of the

effective diffusion coefficient, D_{eff}, of the polyether soft-segment (polyol system) for both high and low water content formulations (*17,18,43*).

The three dimensional surface plot of intensity, $I(q,t)$, versus scattering vector, q, versus time, t, shows that in the early stages of the reaction, there is a homogeneous liquid present. At the microphase separation transition (MST), there is the first appearance of a scattering maximum and the intensity of this peak continuously increases. Eventually, the growth slows down and the peak intensity becomes approximately constant. This is after the expanding foam has reached the Berghmans point (*62*); where microphase separation is intercepted and arrested by vitrification of the phase that is richer in hard segment. The maximum in $I(q)$ suggests the presence of structure with periodic electron density within the sample. For this foaming system (*17*), the maximum in $I(q)$ occurs at $q \approx 0.05$ Å^{-1} giving an interdomain spacing of 126 Å. As will be apparent from the plot of $I(q)$ versus q, the position of the peak maximum, q^*, did not change during the structuring process for this system.

From the plot of relative invariant, Q', (a measure of the degree of microphase separation) versus reaction time in Figure 3, the onset of microphase separation is taken as 60 ± 2 seconds. This corresponds to an isocyanate conversion, $p_{NCO} = 0.54 \pm 0.02$ (*10,17,18,43*) The driving force for microphase separation is the thermodynamic incompatibility between the hard and soft-segment blocks (*14,15,38,41*). As polymerization proceeds, the degree of polymerization of the hard-segment, N_H, increases. At a particular conversion of isocyanate, viz. $p_{NCO} = 0.54 \pm 0.02$, the number average hard-segment sequence length reaches a critical value, the product cN_H is such that the system is no longer thermodynamically stable [i.e. D$G \geq 0$ and $(\partial^2 DG/\partial f_H^2) \leq 0$]. The polymerization has acted as a large thermodynamically driven quench. The depth of this quench will determine the mechanism by which microphase separation takes place.

The material that starts to form structure is a combination of homopolymer, block copolymers and monomers and is discussed in terms of a mixture (*17,18,43*). The final structured material is predominantly a block copolymer; and thus the data can also be analysed in terms of the time-dependent Ginzburg-Landau (TDGL) theory for microphase separation (*36,37,63*). Depending upon the route a mixture follows through phase space, two very distinct mechanisms of phase separation are observed; nucleation and growth, and spinodal decomposition (*14,64-66*). Spinodal decomposition can lead to the formation of non-equilibrium morphologies comprising of two interconnecting networks (physical or chemical). On the other hand, nucleation and growth will lead to a continuous phase/dispersed phase morphology (*64,65*). Both mechanisms have characteristic scattering signatures. The linearized theory of Cahn and Hilliard (*66*) predicts that the compositional fluctuations, and thus the scattered intensity have a maximum for a given wavelength. In the early stages of the decomposition, there is an exponential increase in the scattered intensity with time. The nucleation and growth process is not well defined in terms of a kinetic scattering theory. However, the scattered intensity should exhibit a monotonic decrease with increase in scattering vector. It has been shown previously (*67*) that the scattered intensity at a fixed angle increases
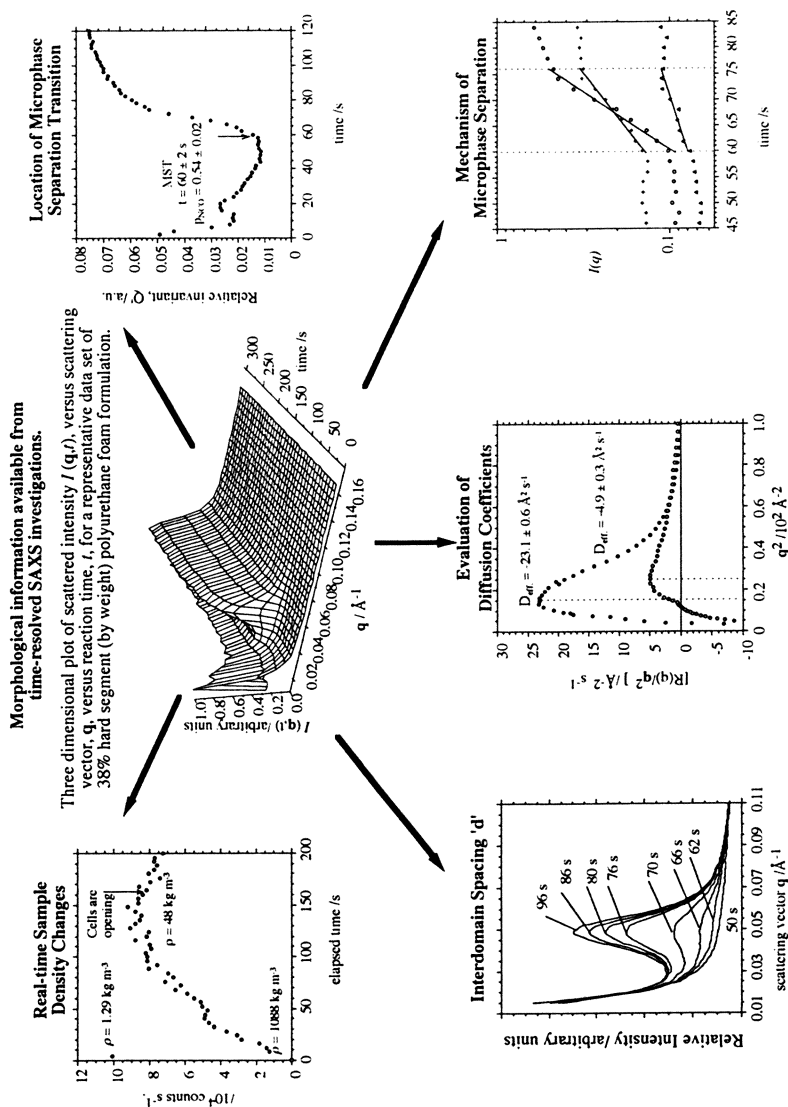
Figure 3. The plethora of information attainable from time-resolved, synchrotron small angle X-ray scattering studies during the polymerization reaction to evolve flexible polyurethane foam. (Adapted from refs. 17,43.).
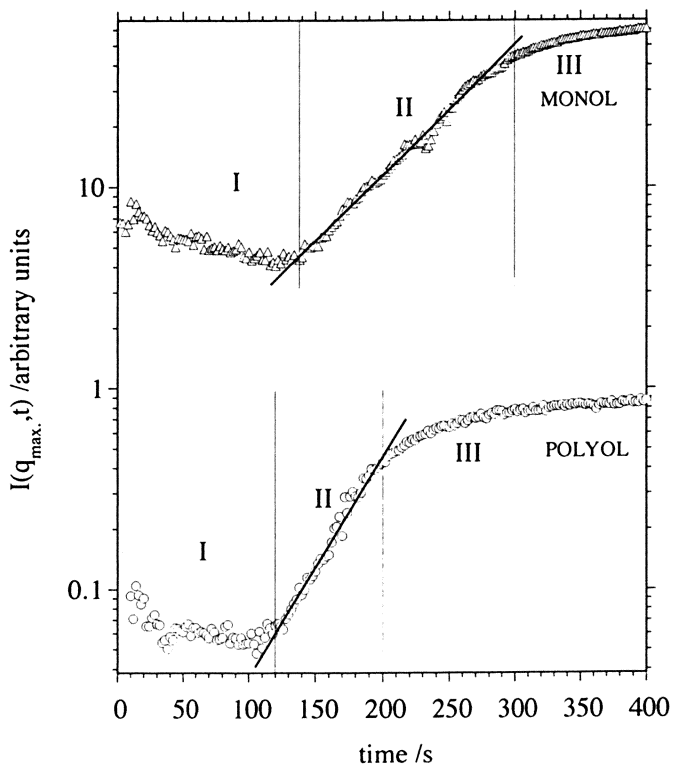
Figure 4. Plot of the density corrected, peak intensity, I ($q_{max.}$,t), versus time, t, for representative data sets of low water content polyether polyol and polyether monol formulations. The symbols are experimental data points and the solid line is a logarithmic fit (after Cahn and Hilliard (66). (Reproduced with permission from ref. 43. Copyright 1996 ACS.)

with the square of time for well characterised nucleation and growth systems. Figure 4 shows representative plots of the peak intensity, $I(q_{max}, t)$, as a function of time for a low water content polyether polyol formulation and a low water content polyether monol formulation, respectively (*43*). From the two curves, there appear to be three distinct regions of phase behaviour.

Region I. Homogeneous liquid mixture comprised of unreacted monomer, homopolymer, urea hard segment sequences and isocyanate tipped, polyether oligomers.

Region II. This is the microphase separation transition (MST). At the MST there is observed a rapid increase in the scattered intensity. There is a good fit of the data to an exponential increase in intensity with time. This is a characteristic of phase separation via spinodal decomposition (*66*). The slope of the line provides a measure of the amplification rate, $R(q)$, of the composition fluctuations (*37,63*).

Region III. The expanding foam has reached the Berghmans point (*62*) (onset of vitrification) and beyond this, the scattered intensity remains approximately constant.

For the case of the polyether polyol, vitrification of the hard segments freezes in the morphology at that time and results in a foam with an internal polymer morphology that comprises an interconnecting physical network of hydrogen-bonded urea hard segment sequences within *a crosslinked polyether-urethane* (*17,18,43*). For the case of the polyether monol system, the internal polymer morphology for the greater part is an interconnecting physical network of hydrogen-bonded urea hard segment sequences within *a polyether-urethane*, but dispersed within the interconnecting physical network of hydrogen-bonded urea hard segment sequences and polyether-urethane are isolated larger aggregates of hydrogen-bonded urea hard segment sequences (*31,43*). Figure 5 shows representative plots of the scattered intensity, $I(q,t)$, versus scattering vector, q, after 500 seconds of reaction for the polyol and monol systems (*43*). The rapid increase in magnitude of $I(q,t)$ at low values of q in the case of the monol, suggests the presence of larger dispersed particles. Furthermore, the level of phase separation in the monol system is higher than that in the polyol system.

To aid in the interpretation of the mechanism of phase separation, the scattering data taken during the reaction can be further analysed to obtain the composition amplification rate at discreet wave vectors, $R(q)$ (*37,63,67*). This is shown in Figure 3 (mechanism of microphase separation) for three different values of scattering vector, q (*17*). For microphase separation via spinodal decomposition, a plot of $R(q)/q^2$ (a measure of the thermodynamic driving force for phase separation, *10,17,18,37,43,63-68*) versus q^2 should exhibit a maximum at a finite value of q (*37,63*). Figure 6 shows a plot of $R(q)/q^2$ versus q^2 for a high water content polyether polyol formulation (*17,18,44*), a low water content polyether polyol formulation (*17,18,43,44*) and a low water content polyether monol formulation (*43*). From the peak in the curve, the effective diffusion coefficient, D_{eff}, of the polyether soft-segment (at high water content) was calculated to be -23.1 ± 0.6 $Å^2$ s⁻
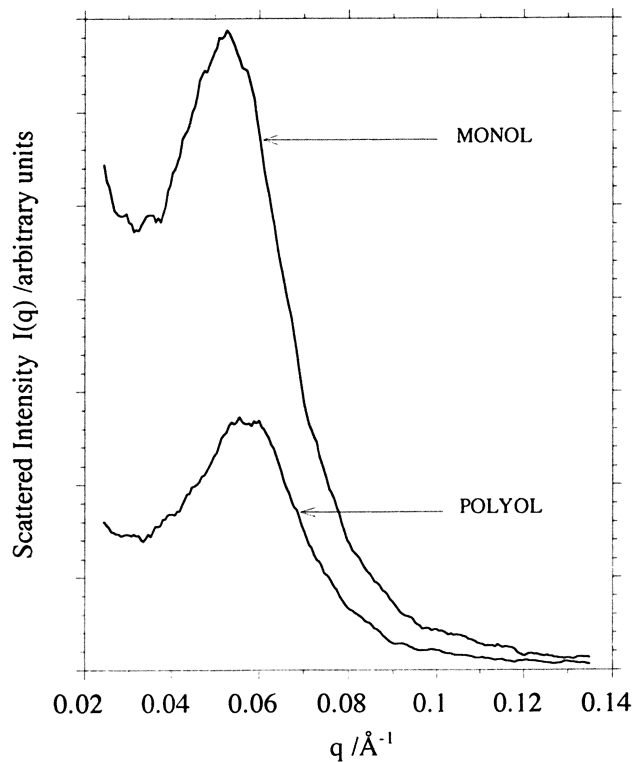
Figure 5. Plot of the scattered intensity, $I(q,t)$, versus scattering vector, q, after 500 seconds of reaction; for representative data sets of low water content polyether polyol and polyether monol formulations. (Reproduced with permission from ref. 43. Copyright 1996 ACS.)
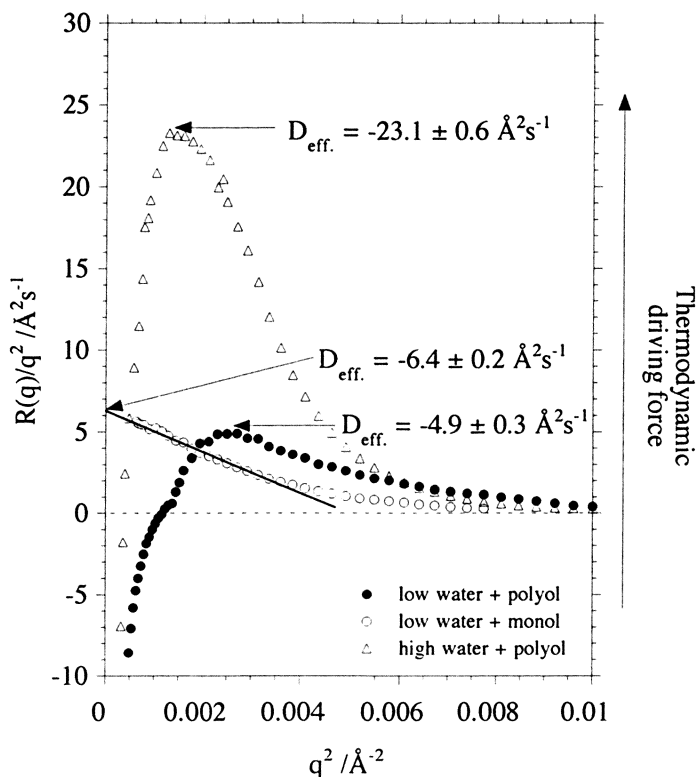
Figure 6. Plot of $R(q)/q^2$ versus q^2 for representative data sets of a high water content polyether polyol formulation ($\triangle$), a low water content polyether polyol formulation ($\bullet$) and a low water content polyether monol formulation ($\bigcirc$). (Adapted from refs. 17,43.).
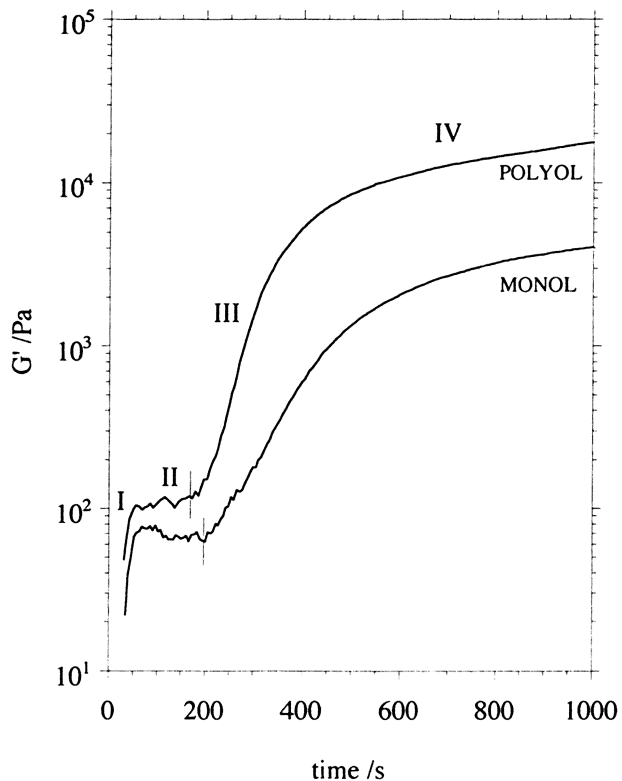
Figure 7. Plot of representative data sets of the elastic shear modulus, G', versus reaction time for low water content polyether polyol and polyether monol formulations.
(Reproduced with permission from ref. 43. Copyright 1996 ACS.)

[1] and the effective diffusion coefficient, D_{eff}, of the polyether soft-segment (at low water content) was calculated to be -4.9 ± 0.3 $\text{Å}^2 \text{s}^{-1}$. For the polyether monol formulation, no maximum in $R(q)/q^2$ versus q^2 is observed. The linear behaviour at low values of q can be extrapolated to $q^2 = 0$; allowing the effective diffusion coefficient, D_{eff}, of the polyether soft-segment (monol system) to be calculated. A value of -6.4 ± 0.2 $\text{Å}^2 \text{s}^{-1}$ was obtained for D_{eff}. This type of behaviour suggests that the monol system is similar to that of a macrophase separated polymer blend/mixture rather than a microphase separated block copolymer. Similar behaviour was observed by Bates and Wiltzius (*68*) for a mixture of protonated and deuterated poly(buta-1,4-diene). The major difference between the mono-functional and the nominally tri-functional based system, is that molecular connectivity exists between two microphases of the same type in the polyether polyol based systems.

Two important results emerge from the previous analysis described. Firstly, for the polyether polyol foaming systems (*17,18,43,44*), the microphase separation kinetics can be qualitatively described by the time-dependent Ginzburg-Landau model described by Hashimoto (*63*). This provides very strong evidence in favour of microphase separation proceeding via a spinodal decomposition type process during the foaming reaction. Secondly, as the water content is increased in the foam formulation; the driving force for phase separation increases. This is apparent from the values of the effective diffusion coefficients obtained. As the depth of the thermodynamic quench increases, so does the value of the effective diffusion coefficient. For the polyether monol foaming system (*31,43*), the scattering data strongly suggest that the mechanism is macrophase separation via a spinodal decomposition and that the final structured material is a macrophase separated mixture of diblock copolymer, homopolymer and monomers. This would suggest that the internal morphology of the foam derived from the polyether monol is for the greater part, similar to that derived from the polyether polyol, but dispersed within the interconnecting physical network of hydrogen-bonded urea hard segment sequences and polyether-urethane, are isolated larger aggregates of hydrogen-bonded urea hard segment sequences (*31,43*).

Dynamic rheometry. As the polymerization progresses, the reacting system undergoes the following transformations:
1) liquid oligomers Æ 2) homogeneous polymerising mixture Æ 3) foaming mixture of homopolymer, block copolymers, and monomers Æ 4) solidified, cellular block copoly(urethane-urea) foam.

Clearly, accompanying these transformations are changes in the rheological properties of the polymerising system. Mora et al. (*53,54*) and more recently Neff and Macosko (*60,61*) have identified four main regions of rheological development during the formation of polyurethane foam. Figure 7 shows representative plots of elastic shear modulus, G', versus reaction time for low water content polyether polyol and polyether monol foam formulations (*43*). Also indicated on the figures are the four regions of rheological development. However, the interpretation here is slightly different from that of Macosko et al. (*8,53,54,60,61*).

Region I: Bubble Nucleation. In this stage, the dissolved bubbles of air that were 'whipped' into the system during mechanical agitation act as nucleation sites for the carbon dioxide gas generated from the water-isocyanate reaction. These bubbles develop into a space filling network (*69*). The initial viscosity is determined by the monomer viscosity.

Region II: Liquid Foam and Microphase Separation. For the polyether polyol foam; at the end of region I the reacting mixture has an elastic shear modulus of approximately 100 Pa (G'>G") and shows solid-like behaviour which is a characteristic of liquid foams (*70,71*) For the polyether monol foam; the reacting mixture has an elastic shear modulus of approximately 60-80 Pa (G'>G"). The reacting mixture in both cases is still a low modulus gel that continues to expand as a result of the continued generation of carbon dioxide. The gel is formed from the interaction of closely packed bubbles. The liquid cell walls still have both low molar mass and viscosity. For the polyether polyol, microphase separation of urea hard segment sequences takes place (p_{NCO} = 0.54 ± 0.02) as evidenced from SAXS measurements (*17,18,43,44*) and infra-red measurements (*9,10,18,31,43*).

Beyond the MST, the foam modulus still remains approximately constant. For the polyether monol, macrophase separation of urea hard segment sequences takes place (p_{NCO} = 0.42 ± 0.02) as evidenced from SAXS measurements (*17,18,43,44*) and infra-red measurements (*9,10,18,31,43*). It has been reported, however, that the change in modulus associated with the MST of polyolefins (*72-74*) and in one case of a polyurethane (*75*), is of the order of a factor of two. There are three contributions to there being no apparent change in the modulus at the MST for both the polyol and the monol. Firstly, the material temperature is continuously changing (quasi-adiabatic). Secondly, the phase transition is not a particularly sharp one and is smeared even further by the polydisperse nature of the hard segment sequences. Finally, the polymer is at a volume fraction of $\approx$ 0.1 at the MST and it is estimated that the increase in modulus of the polymer at the MST would give rise to a change in the foam modulus of $\approx$ 2% (*43*).

Region III: Physical Gelation. For the polyether polyol foam, at the end of region II the isocyanate conversion is approximately 70 ± 1% (*10,18,43*). At the start of region III there is a large increase the elastic storage modulus, G', of approximately 2 decades. This increase in modulus results from microphase separation being intercepted and arrested by vitrification of the phase that is richer in urea hard segment. This is the Berghmans point (*62*). Towards the end of region II, cell opening occurs. For the polyether monol foam, at the end of region II the isocyanate conversion is of the order of approximately 69 ± 1% (*10,31,43*).

Region IV: Foamed Elastomer. In polyurethane foam, after cell opening has occurred, the reactions still continue but do so in a medium of increasing viscosity and stiffness. In this region, the foamed polymer reaches maximum temperature and modulus. The modulus of the foam in this region is dominated by the polymer modulus. Similar behaviour is seen in both polyether polyol and polyether monol foams, but in the monol, covalent crosslinks are absent. Dynamic rheological measurements probe the macrocopic behaviour of the sample. In the case of the

monol system, the lower and more erratic increase in modulus at the Berghmans point; and the lower overall value of the elastic shear modulus results from macrophase separation within this system. The macrophase separated aggregates of urea hard segment sequences are not connected to the physical network of hydrogen-bonded urea hard segment sequences, and as such, they do not contribute to the polymer modulus. Thus, the final value of the modulus of the foamed polymer is lower than that observed in the polyol based system (*43*).

In the polyether polyol systems, polymerization proceeds and from an early stage in the reaction there are isocyanate tipped polyether oligomers and urea hard-segment sequences present in the system (refer to Figure 2). The degree of polymerization of hard-segment, N_H, increases steadily and at $p_{NCO} = 0.54 \pm 0.02$, N_H reaches N_{Hcrit} ($N_{Hcrit} \approx 1.5$ units, *10*) and microphase separation takes place. Polymerization provides the quench, passing from the homogeneous (disordered) one phase region to the heterogeneous (ordered) two phase region. For the case of the polyol, the isocyanate conversion at the MST [$p_{NCO} = 0.54 \pm 0.02$] is higher than that for the monol [$p_{NCO} = 0.42 \pm 0.02$]. This behaviour can be predicted from the theory of block copolymer thermodynamics proposed by Leibler (*76*) and Benoit and Hadziioannou (*77*). For a diblock copolymer (the polyether monol system) $cN_{crit} \approx 10$, but for a multiblock (the polyether polyol system), $cN_{crit} \approx 15$. In the context of this article, the more covalent bonds that exist between dissimilar blocks, the higher the molecular weight obtained before ordering takes place. Put another way, as the polymer molecular weight increases, so does N_{Hcrit} (*38*). The microphase separated hard segments continue to grow and association of these urea hard segments occurs (*9,10,17,18,31,43*) (refer to Figure 2). At $p_{NCO} = 0.71 \pm 0.02$, microphase separation is intercepted and quickly arrested by vitrification of the phase that is richer in hard-segment (*9,10,18,31*). This phase has attained a composition with a $T_g \geq$ the temperature of the reacting system. It is the composition where liquid-liquid phase separation is intercepted and arrested by glass transition (*62*). Vitrification of the hard segments 'freezes in' the morphology at that time and results in a foam with an internal polymer morphology that comprises an interconnecting physical network of hydrogen-bonded urea hard-segment sequences within the crosslinked polyether-urethane (*10,17,18*).

In the polyether monol system, polymerization proceeds and in the early stages of the reaction there are isocyanate tipped polyether oligomers and urea hard-segment sequences present in the system (*10,31,43*). The degree of polymerization of hard-segment, N_H, increases steadily and at $p_{NCO} = 0.42 \pm 0.02$, N_H reaches N_{Hcrit} ($N_{Hcrit} \approx 1.05$ units), (*43*) and macrophase separation takes place (*10,31,43*) (refer to Figure 6). The macrophase separated urea hard segments continue to grow and association of these urea hard segments occurs. For the polyether monol system, the rate of association of urea hard segments is approximately 33 % faster than in the polyether polyol system. This evidence is provided by values obtained for the effective diffusion coefficients from the *in-situ* synchrotron SAXS measurements (refer to Figure 6). The very much faster rate of association of the urea hard segments and lack of connectivity, leads to the formation of aggregates of
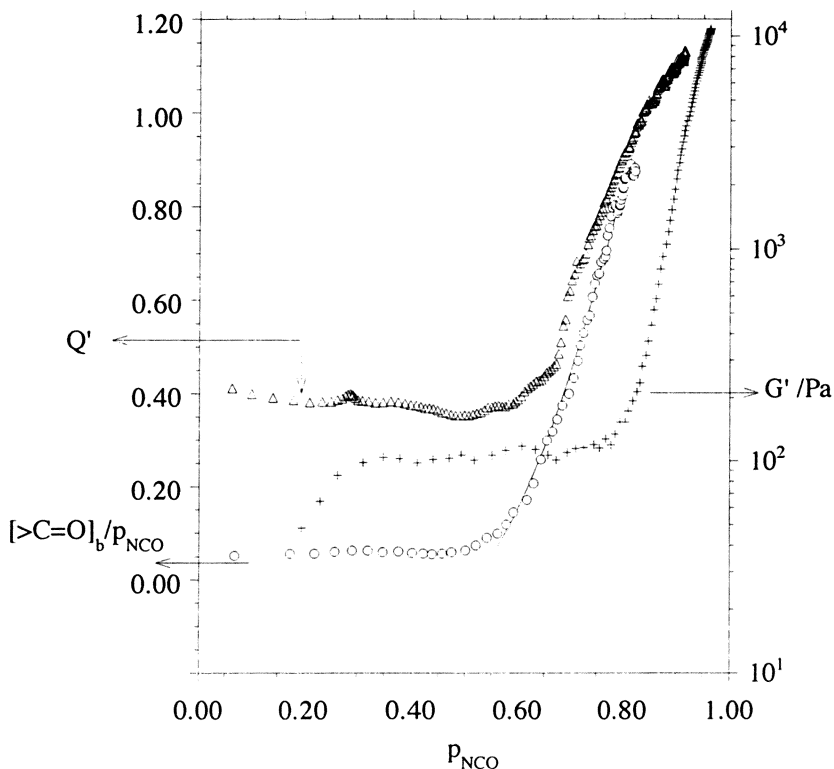
Figure 8. Comparison of the changes in the key structuring parameters as isocyanate conversion increases during the foaming reaction for a low water content polyether polyol formulation. SAXS relative invariant, Q', (Δ), Hydrogen-bonded urea carbonyl, $[>C=O]_b/p_{NCO}$, (O) and elastic storage modulus, G', (+). The curve through the hydrogen-bonded urea carbonyl data is a fit to: $[>C=O]_b/p_{NCO} = 1 - a[exp(p_{NCO}-b)^c]$ according to a pseudo-Avrami analysis; where a, b and c are fitting parameters. a is a rate constant, b is the conversion at the onset of hydrogen bonding and c is the phase-growth exponent.
(Reproduced with permission from ref. 43. Copyright 1996 ACS.)

urea hard segments. These aggregates are macrophase separated and not connected to the polyether via a urethane linkage.

At p_{NCO} = 0.69 ± 0.01, phase separation is intercepted and arrested by vitrification of the phase that is richer in hard-segment. The internal polymer morphology of the polyether-monol foam system is for the greater part, similar to that of the polyether-polyol foam system (*10,31,43*). Also dispersed within the interconnecting physical network of hydrogen-bonded urea hard-segment sequences and polyether-urethane are isolated, larger aggregates of hydrogen-bonded urea hard-segment sequences (refer to Figure 5).

The overall view of polymer structure development

In this chapter we have described how the techniques of FT-IR spectroscopy, synchrotron SAXS and dynamic rheometry can be used, to investigate *in-situ*, the development of polymer morphology during the reactive processing of flexible polyurethane foam. Each technique yields structural information of a different nature. The changes in the key structure parameters as isocyanate conversion increases can be summarized in a single diagram; and these are illustrated in Figure 8 for a low water content polyether polyol formulation (*10,18,43*). The same type of figure can also be constructed for the polyether monol system (*43*). It will be apparent that the SAXS relative invariant, Q', *appears* [within the limits of experimental error] to start to increase prior to the rapid growth in the concentration of hydrogen-bonded urea carbonyl species, $[>C=O]_b/p_{NCO}$. The growth of foam's elastic shear modulus, G', lags the growth of the relative invariant, Q', and the hydrogen-bonded urea carbonyl concentration, respectively. A simplified analogy to this discussion is that microphase separation is considered to be the 'closing of the door' on the system and the subsequent formation of the hydrogen bonds between the microphase separated urea hard segments is the 'turning of the door handle'; i.e. the hydrogen bonds fix the structure in place. This is then further locked in place by vitrification of the hard segments as the Berghmans point is crossed (*62*); i.e. the 'turning of the key'.

In order to provide a fundamental understanding of the competition between both polymerization and structure development processes; *in-situ* investigations *under routine processing conditions* are essential. It is only then, that the final properties of the material can be engineered by tailoring the starting chemistry and process thermal history accordingly.

Acknowledgements

Dr. Alan K. Schrock (The Dow Chemical Company, Freeport, Texas, USA) for presenting the paper at the ACS meeting in Florida, August 1996, at such short notice.

References

1. Young, R. J. ; Lovell, P. A. *Introduction to Polymers*; 2nd Ed.; Chapman & Hall: London, 1991.
2. Cowie, J. M. G. *Polymers: Chemistry & Physics of Modern Materials*; 2nd Ed.; Chapman & Hall: New York, 1991.
3. Billmeyer Jr., F. W. *Textbook of Polymer Science; 3rd Edition*; Wiley Intersience: New York, 1984.
4. Elias, H. G. *An Introduction to Plastics*; VCH Publishers: Weinheim, 1993.
5. Macosko, C. W. *RIM: Fundamentals of Reaction Injection Molding*; Carl Hanser Verlag: Munich, 1988.
6. Artavia, L. D.; Macosko, C. W. *J. Cell. Plast.* **1990**, *26*, 490.
7. Priester Jnr., R. D.; McClusky, J. V.; O'Neill, R. E.; Turner, R. B.; Harthcock, M. A.; Davis, B.L. *J. Cell. Plast.* **1990**, *26*, 346.
8. Artavia, L. D. Ph.D. Thesis, University of Minnesota, 1991.
9. Elwell, M. J. A.; Ryan, A. J.; Grünbauer, H. J. M.; Van Lieshout, H. C.; Thoen, J. A. *Prog. Rubb. Plast. Tech.* **1993**, *9*, 120.
10. Elwell, M. J. A. Ph.D. Thesis, Victoria University of Manchester, 1993.
11. Turner, R. B.; Spell, H. L.; Wilkes, G. L. **1988**, Proc. 28th SPI Annu.Tech./Mrkt. Conf., 244, Lancaster, PA, USA: Technomic Publishing Co.
12. Armistead, J. P.; Turner, R. B.; Wilkes, G. L. *J. Appl. Polym. Sci.* **1988**, *35*, 601.
13. Creswick, M. W.; Lee, K. D.; Turner, R. B.; Huber, L. M. *J. Elast. Plast.* **1989**, *21*, 179.
14. Ryan, A. J. *Polymer* **1990**, *31*, 707.
15. Ryan, A. J.; Stanford, J. L.; Still, R. H. *Plast. Rubb. Proc. Appl.* **1990**, *13*, 99.
16. Grünbauer, H. J. M.; Thoen, J. A.; Folmer, J. C. W.; Van Lieshout, H. C. *J. Cell. Plast.* **1992**, *28*, 36.
17. Elwell, M. J. A.; Mortimer, S.; Ryan, A. J. *Macromolecules* **1994**, *27*, 5428.
18. Elwell, M. J. A.; Ryan, A. J.; Grünbauer, H. J. M.; Van Lieshout, H. C. *Plast. Rubb. Proc. Appl.* **1995**, *23*, 265.
19. Wong, S. W.; Frisch, K. C. *Prog. Rubber Plast. Technol.* **1991**, *7*, 243.
20. Wong, S. W.; Frisch, K. C. *J. Polym. Sci., Part A: Polym. Chem.* **1986**, *24*, 2867.
21. Sorokin, M. F.; Shode, L. G.; Klochkova, L. V.; Finyakin, L. N. *Izv. Vyssh. Uchebn. Zaved., Khim. Khim. Tekhnol.* **1984**, *27*, 852.
22. Gus'kova, N. A.; Sorokin, M. F. *Deposited Doc.* **1978**, *VINITI 12*, 321.
23. Lipatova, T. E.; Bakalo, L. A.; Chirkova, L. I. *Sint. Fiz.-Khim. Polim.* **1978**, *23*, 74.
24. Metlyakova, I. R.; Shoshtaeva, M. V. *Sint. Fiz.-Khim. Polim.* **1976**, *18*, 48.
25. Borkent, G. *Adv. Urethane Sci. Technol.* **1974**, *3*, 1.
26. Grigor'eva, V. A.; Baturin, S. M.; Entelis, S. G. *Vysokomol. Soedin., Ser. A.* **1972**, *14*, 1345.

27. Rossmy, G. R.; Kollmeier, H. J.; Lidy, W.; Schator, H.; Wiemann, M. *J. Cell. Plast.* **1981**, *17*, 319.
28. Rossmy, G. R.; Kollmeier, H. J.; Lidy, W.; Schator, H.; Wiemann, M. *J. Cell. Plast.* **1977**, *13*, 26.
29. Rossmy, G. R.; Kollmeier, H. J.; Lidy, W.; Schator, H.; Wiemann, M. *J. Cell. Plast.* **1979**, *15*, 276.
30. Hocker, J. *J. Appl. Polym. Sci.* **1980**, *25*, 2879.
31. Elwell, M. J. A.; Ryan, A. J.; Grünbauer, H. J. M.; Van Lieshout, H. C. *Polymer* **1996**, *37*, 1353.
32. Merten, R.; Lauerer, D.; Dahm, M. *J. Cell. Plast.* **1969**, *5*, 262.
33. Hauptmann, G.; Dörner, K. H.; Pfisterer, G. **1980**, Proc. 5th SPI Annu.Tech./ Mrkt. Conf., 617, Lancaster, PA, USA: Technomic Publishing Co.
34. Bailey, F. E.; Critchfield, F. E. *J. Cell. Plast.* **1981**, *17*, 333.
35. Elwell, M. J. A. *Thermochimica Acta* **1995**, *269*, 145.
36. Hashimoto, T.; Kowsaka, K.; Shibayama, M.; Kawai, H. *Macromolecules* **1986**, *19*, 754.
37. Connell, J. G.; Richards, R. W.; Rennie, A. R. *Polymer* **1991**, *32*, 2033.
38. Ryan, A. J.; Willkomm, W. R.; Bergstrom, T. B.; Macosko, C. W.; Koberstein, J. T.; Yu, C. C.; Russell, T. P. *Macromolecules* **1991**, *24*, 2883.
39. Li, Y.; Gao, T.; Chu, B. *Macromolecules*, **1992**, *25*, 1737.
40. Chu, B.; Gao, T.; Li, Y.; Wang, J.; Desper, C. R.; Byrne, C. A. *Macromolecules* **1992**, *25*, 5724.
41. Bras, W.; Derbyshire, G.; Bogg, D.; Cooke, J. S.; Elwell, M. J. A.; Komanschek, B. U.; Naylor, S.; Ryan, A. J. *Science* **1995**, *267*, 996.
42. Wilkinson, A. N.; Naylor, S.; Elwell, M. J. A.; Draper, P.; Komanschek, B. U.; Stanford, J. L.; Ryan, A. J. *Polym. Comm., Polymer* **1996**, *37*, 2021.
43. Elwell, M. J. A.; Ryan, A. J.; Grünbauer, H. J. M.; Van Lieshout, H. C. *Macromolecules* **1996**, *29*, 2960.
44. Elwell, M. J. A.; Mortimer, S.; Ryan, A. J.; Bras, W. *Nuclear Instruments and Methods in Physics Reserach*, **1995**, *B 97*, 261.
45. Bogg, D.; Derbyshire, G.; Bras, W.; Cooke, J. S.; Elwell, M. J. A.; Naylor, S.; Ryan, A. J. *Nuclear Instruments and Methods in Physics Reserach*, **1995**, *B 97*, 261.
46. Mussatti, F. G.; Macosko, C. W. *Polym. Eng. Sci.* **1973**, *13*, 236.
47. Lipshitz, S. D.; Macosko, C. W. *Polym. Eng. Sci.* **1976**, *16*, 803.
48. Castro, J. M.; Macosko, C. W.; Perry, S. J. *Polym. Comm.* **1984**, *25*, 82.
49. Perry, S. J.; Castro, J. M.; Macosko, C. W. *J. Rheol.*, **1985**, *29*, 19.
50. Yang, W. P. Ph.D. Thesis, University of Minnesota, 1987.
51. Blake, J. W.; Yang, W. P.; Anderson, R. D.; Macosko, C. W. *Polym. Eng. Sci.* **1987**, *27*, 1238.
52. Yang, W. P.; Macosko, C. W. *Die Makromol. Chem., Macromol. Symp.* **1989**, *25*, 23.
53. Mora, E. MSc. Dissertation, University of Minnesota, 1991.
54. Mora, E.; Artavia, L. D.; Macosko, C. W. *J. Rheol.* **1991**, *35*, 921.
55. Malkin, A. Y.; Bolgov, S. A.; Begishev, V. P.; Mansurov, V. A. *Rheol. Acta.* **1992**, *31*, 345.

56. Griffiths, I. M.; Ryan, A. J.; Stanford, J. L. **1996**, Proceedings of the XIIth International Polymer Processing Society; Rheology and Rheometry, 43, Sorrento, Italy.
57. Bessette, M. D.; Sundstrom, D. W. *Polym. Process. Eng.* **1985**, *3*, 25.
58. Carriere, C. J.; Bank, D. H.; Christenson, C. P. *Polym. Eng. Sci.* **1992**, *32*, 426.
59. Nabata, Y.; Mamada, A.; Yamasaki, H. *J. Appl. Polym. Sci.* **1988**, *35*, 155.
60. Neff, R. Ph.D. Thesis, University of Minesota, 1995
61. Neff, R., Macosko, C. W. **1995**, Proc. SPI Polyurethane Conf., 344, Lancaster, PA, USA: Technomic Publishing Co.
62. Callister, S.; Keller, A.; Hikmet, R. M. *Makromol. Chem. Makromol. Symp.* **1990**, *39*, 19.
63. Hashimoto, T. *Macromolecules* **1987**, *20*, 465.
64. Olabisi, O.; Robeson, L. M.; Shaw, M. T. *Polymer-Polymer Miscibility;* Academic Press: New York, 1977.
65. Binder, K. In: *Phase Transformations in Materials*, Cahn, R. W., Haasen, P., Kramer, E. J., Eds.; Materials Science and Technology: A Comprehensive Treatment, VCH Publishers: Weinheim, 1991; Chapter 7, p 405.
66. Cahn, J. W.; Hilliard, J. *J. Chem. Phys.* **1958**, *28*, 258.
67. Lipatov, Y. S.; Grigor'yeva, O. P.; Kovernick, G. P.; Shilov, V. V.; Sergryeva, L. M. *Makromol. Chem.*, **1985**, *186*, 1401.
68. Bates, F. S.; Wiltzius, P. *J. Chem. Phys.* **1989**, *91*, 3258.
69. Kanner, B.; Decker, T. G. *J. Cell. Plast.* **1969**, *5*, 32.
70. Khan, S. A.; Schnepper, C. A.; Armstrong, R. C. *J. Rheol.* **1988**, *32*, 69.
71. Princen, H. M.; Kiss, A. D. *J. Coll. Int. Sci.* **1986**, *112*, 427.
72. Bates, F. S. *Macromolecules* **1984**, *17*, 2607.
73. Bates, F. S.; Rosedale, J. H.; Frederickson, G. H. *J. Chem. Phys.* **1990**, *92*, 6255.
74. Rosedale, J. H.; Bates, F. S. *Macromolecules* **1990**, *23*, 2329.
75. Ryan, A. J.; Macosko, C. W.; Bras, W. *Macromolecules* **1992**, *25*, 6277.
76. Leibler, L. *Macromolecules* **1980**, *13*, 1602.
77. Benoit, H.; Hadziioannou, G. *Macromolecules* **1988**, *21*, 1449.

Chapter 11

Imaging Open-Cell Polyurethane Foam via Confocal Microscopy

Rida Hamza[1], Xiaodong D. Zhang[2,4], Christopher W. Macosko[2], Robert Stevens[3], and Mark Listemann[3]

[1]Honeywell Technology Center, 3660 Technology Drive, Minneapolis, MN 55418
[2] Department of Chemical Engineering and Materials Science, University of Minnesota, 421 Washington Avenue Southeast, Minneapolis, MN 55455
[3]Air Products and Chemicals, Inc., 7201 Hamilton Boulevard, Allentown, PA 18195

Flexible polyurethane foam is based on a 3-dimensional cellular network. The mechanical properties of foam material depend upon cell structure and cell size distribution. In this work, we use laser confocal microscopy to image the foam cells and recover its 3-dimensional cellular network. Based on this technique we provide a statistical analysis and compare several foam samples. Confocal microscopic images are also used to visualize foam compression. Images for foam network structure under different mechanical compressions are also obtained. Limitations of confocal microscope are discussed and a new method - nuclear magnetic resonance imaging is proposed.

Polyurethane foam (PUF) is a widely used cushioning materials with a complex three-dimensional structure (Figure 1). It is well understood that the mechanical properties of the foamed material depends on cell structure and cell size distribution (1,2).

Recent attempts to characterize cell structure involved two dimensional image analysis (3). The conventional methods for foam imaging includes two-dimensional images obtained through either optical or scanning electron microscopy (SEM)(1). However, foam cells are multidimensional and resemble an interconnected polyhedron network. Hence accurate characterization of cell structure from such images faces many difficulties. In addition, conventional optical microscopy techniques require a thin slice of material. Using SEM, only the surface of the sample can be observed. In both scenarios, the imaged cells can be damaged during sample preparation.

A technique is therefore desired to image the foam in three-dimensions (3D), and observe undamaged material inside of a thicker sample. Three dimensional structural information can then be extracted for foam samples with different cell size distribution and different mechanical properties. To perform 3D image processing, practical solutions to display 3D images are required. There exists several image rendering techniques and commercial image processing software. However, none of these software appear practical for our application since they all require a large amount of memory to process complex 3D images and the memory requirement overcomes most of the systems limits. Automated algorithms for 3D reconstruction are under development with encouraging results especially in biomedical applications (5-7). However, none of these previous attempts was able to reduce the three dimensional image of a complex feature, such as foam, to a concise set of rules and procedures.

[4]Corresponding author

165
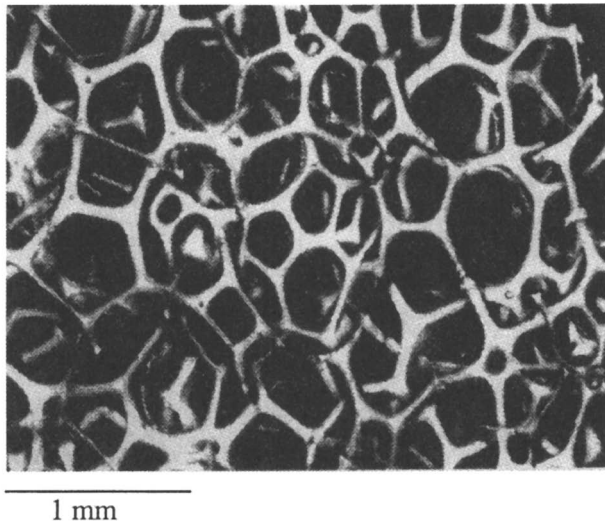
Figure 1. A typical PUF cellular structure: overlay of 23 confocal microscope 2D images (image size 37mm x 25mm).
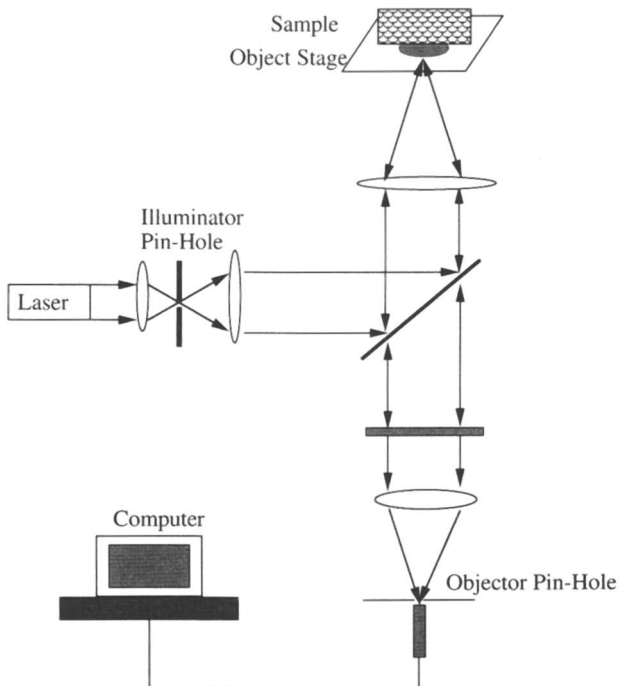
Figure 2. System diagram of Laser Confocal Microscope (LCM).

This is the goal of this work. A new technique, laser confocal microscopy is used for image acquisition to provide sharp 2D images used for 3D reconstruction.

2D Foam Image Acquisition Via Confocal Microscopy

Laser confocal microscopy (LCM) is used to collect two-dimensional images at different depths in foam samples. This technique is proved to be advantageous over the conventional techniques. Before we compare these techniques, we describe the size, type and preparation of our foam samples. The foaming process is an important issue in sample preparation which is, however, beyond the scope of this paper.

PUF Samples. Since the microscopy imagery is based on a laser light that excites *fluorescein*, a dye coding was necessary to image the foam cell network. When excited with a blue laser (496nm), *Fluorescein* emits at 518 nm. Foam samples (1 cm^3) were stained in a solution of 10 mg of fluoresceinamine in 5 ml of tetrahydrofuran. The portion of the sample observed in this experiment is about 3.7x2.5x2mm. For foam III (see Table I), this represents an average of 14 cells.

LCM Technique The Bio-Rad LCM, MRC600, was used to conduct all this work. This work is conducted using a different image acquisition approach. We collect PUF images using LCM. The LCM imagery is based on a laser light which passes through a barrier filter that selects the peaks to be used in exciting the fluorophone (see Figure 2). A dichroic mirror reflects the laser wavelength to the foam sample and allows returning wavelengths that are greater than a threshold value. For the PUF case, we use 510 nm wavelength as a threshold. The software package with this instrument has limited functionality except for noise smoothness, stacking images and making stereo pairs. Most of the images taken by the Bio-Rad LCM were of high quality and only few image processing operations were needed. Each image section had a resolution of 512 x 768 pixels, with 4.875μm/pixel. Figure 3 presents a sequence of frames captured at different scanning depths. These captured images are arranged accordingly to present the variations in the cellular network projection planes that will be used to detect information about the network. We varied the spacing between slices to focus on planes where more structural information resides. Due to out-of-focus planes shielding, (i.e. see Figure 3f), the maximum scanning depth was typically limited to 2mm.

In some applications, it is required to store these images for later analysis. In most cases, this is not reliable due to the tremendous space needed to store all these captured images. Instead of storing vast amount of possibly redundant images, shared image database can be provided to different analyzers.

Statistical Analysis The advantage of this imaging process concerns the possibility to analyze the PUF cellular network and relate its learned distributions to mechanical response of the sample. Using the software capabilities in the Bio-Rad LCM, Khoros modules (these modules are created from image process, signal processing and morphology tool boxes of Khoros), and some manual editing we were able to conduct a statistical analysis on three foam samples with different cellular sizes. Among the various statistical parameters possible from this imaging technique, the following statistical structural parameters have been selected: the mean μ_l and the standard deviation of the length of the struts σ_l, the number of vertices n_v, the number of windows n_w, and finally the means μ_i and standard deviations σ_i (i =a,b or c) of diameters a, b, and c, that define the elliptic dimension of a typical foam cell. All these statistics are based on a volume of 16.82mm^3. In Table I, three foam samples, having

(a)

(b)

(c)

(d)

(e)

(f)

1 mm
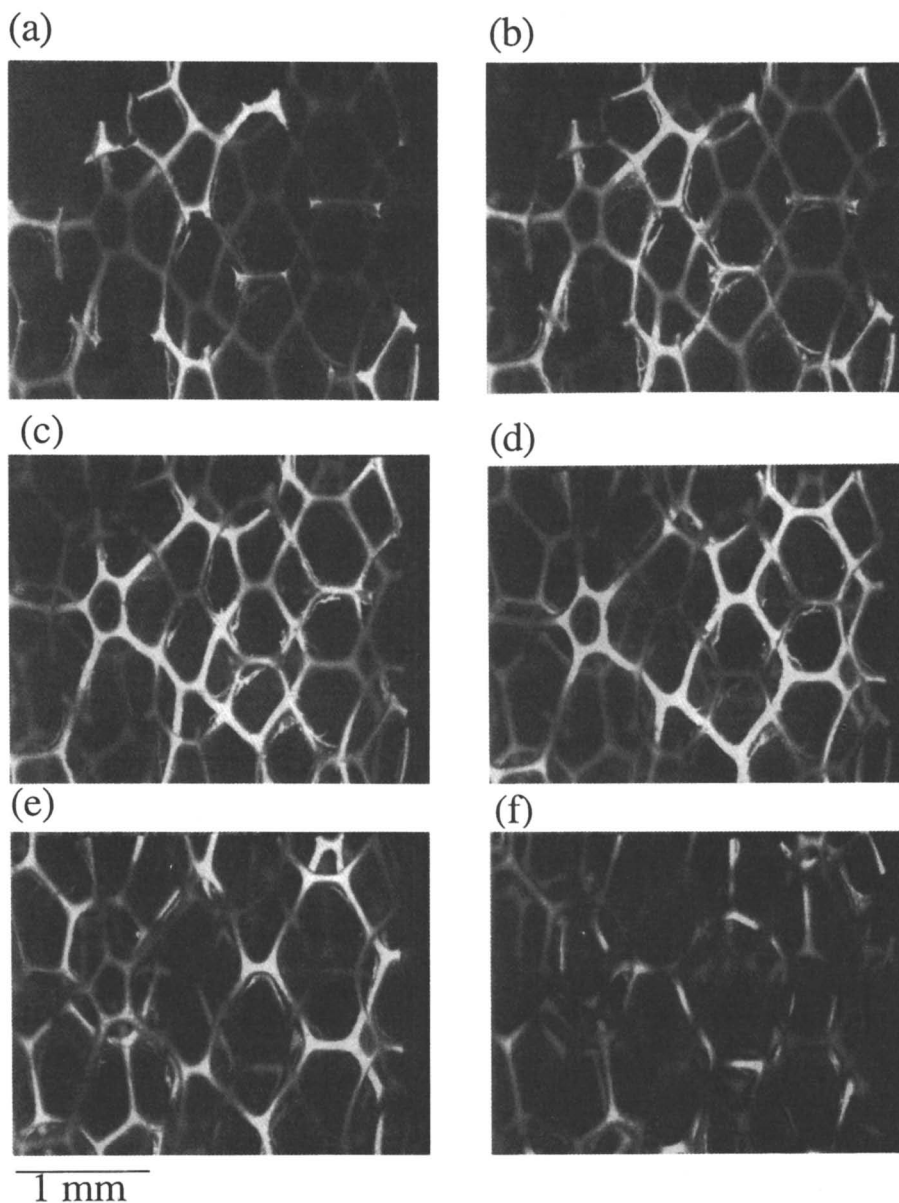
Figure 3. Confocal microscope images at increasing depth into the foam (image size 37mm x 25mm). (a) 114 µm; (b) 320 µm; (c) 812 µm; (d) 1400 µm; (e) 1720µm; (f) 1860 µm. A Kalman filter was applied on these images to smooth and smear out some of the background noise.

different cell sizes, were considered. Within the specified volume there were not enough cells to measure an accurate diameter standard deviation for foam I and II. It is worth noting that other statistics can be easily deduced from these measurements. Moreover, other statistical parameters, such as distributions of vertices, window surface and shape and cell volume were considered but found to be highly correlated with the provided list using Euler's law on the dependence of faces, vertices and cells. This list of parameters is sufficient to characterize the foam cellular distribution.

Table I. Statistical distribution of three foam samples with different cellular sizes: l - length of cell struts; n_w, number of windows in a cell; n_v - number of vertices in a cell; a, b, &c - diameters that define the elliptic dimension of a cell; μ, &σ - mean and standard deviation

Parameters	Foam I	Samples Foam II	Foam III
μ_l (μm)	577	407	230
σ_l (μm)	113	98	57
n_v	34	62	291
n_w	7	38	184
μ_a (μm)	1611	1003	351
σ_a (μm)	-	-	234
μ_b (μm)	1807	1210	398
σ_b (μm)	-	-	220
μ_c (μm)	1213	1200	370
σ_c (μm)	-	-	198

Imaging PUF Under Mechanical Force

The imaging approach introduced in the previous section can be used to visually demonstrate a variety of phenomena of foams. One example is the mechanical response of foam to constant rate compression test. Foam used in this test was prepared with 100g Voranol 3137 polyol, 52.6g TDI, 4g water, 1.5ml of silicone surfactant, 0.29 ml 33-LV amine catalyst and 0.12ml of T-9 tin catalyst. A 52mmx52mmx27mm piece of this foam was used in compression test. The compression test was performed at 240mm/min to 85% compression and then unloaded at the same rate on Instron machine at 25°C. Two load cycles were performed perpendicular to the 52x52mm surface and the mechanical response from the foam is shown in Figure 4 (*4*). Three stages are shown in the compression curve. Five images were taken to shown these stages. The images were taken on a different piece of foam that is fitted between to parallel aluminum plates by screw at the corners. Different levels of compression were achieved by changing position of the screws. Point A in Figure 4 and image A in Figure 5 is the foam without any compression. Since no stress is applied, all struts seems undeformed. At low compression, in this case less than 12%, the stress is proportional to the strain applied on the foam sample. Point B in Figure 4 has 7% compression. The corresponding image (Figure 5B) shows some struts were bent, and the bending is mainly on struts normal to the load
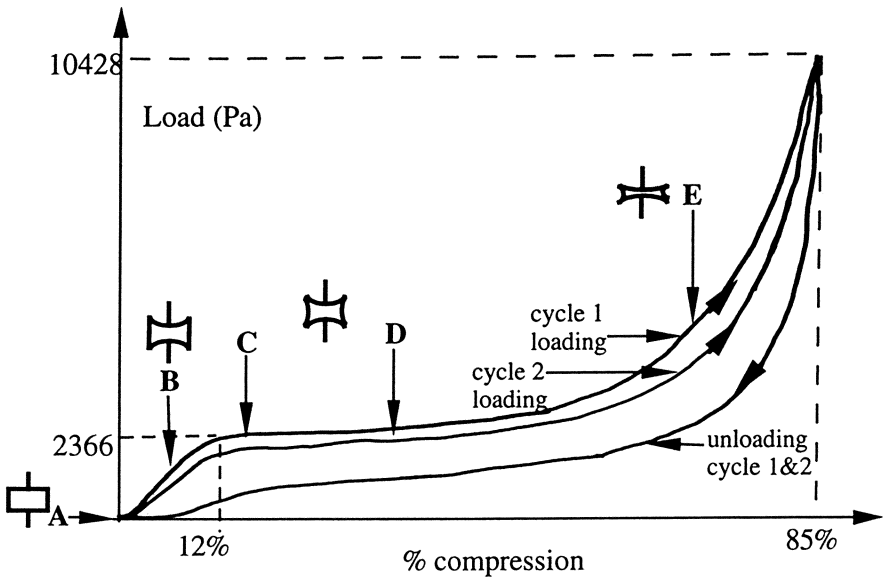
Figure 4. Compression stress-strain curve for foam sample. Compression rate 240mm/sec. Two loading cycles are applied.

IMAGES OF FOAM UNDER DIFFERENT DEGREE OF COMPRESSION
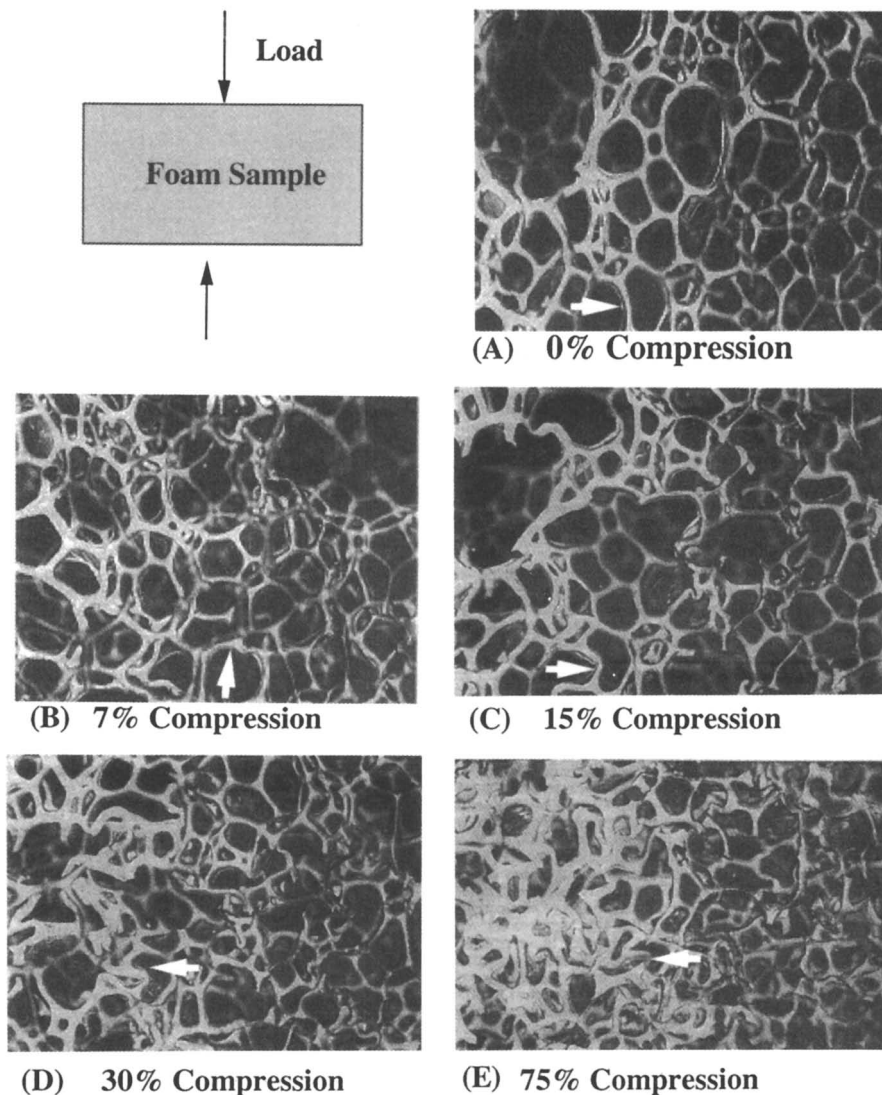
Figure 5. Confocal microscope images of foam under different levels of compression (image size 37 mm x 25 mm). Images A, C, D, E are from the same region. Image B is a different region.

direction. At about 12%, the initial straight line rise changes to the knee in the curve. This corresponds to a critical stress that causes the struts parallel to the load direction to buckle. Point C in Figure 4 has 15% compression, it is right after the buckling occurs. Buckling of struts perpendicular to the load direction can be observed in the corresponding image (Figure 5 C). As the extent of strain increases, the struts parallel to the load direction will buckle more. This can be seen in Figure 5 D, where the foam is at 30% compression. As the strain increases past 55% compression, a rapid rise in stress is observed in the compression curve.   Point E in Figure 4 has 75% compression.   The corresponding image (Figure 5E) shows that at this level of compression, the struts are interacting with each other rather than just buckling or bending.

PUF Cellular Network Recovery

The 3D reconstruction is an important constituent of pattern recognition as well as machine intelligence. The potential for better understanding the mechanical properties of the polyurethane foam based on its 3D cellular structures, leads to the necessity for carefully recovering its underling 3D model. To this end, several variations of 3D reconstruction algorithms have been proposed in literature (5)-(12) and references therein. In general, it seems that most of these existing algorithms are not capable of detecting shapes with significant protrusions (i.e. foam cellular network) and that a great many of them are not applicable to categories that exhibit complicated distributions in the feature space. In this framework, we present an alternative approach to recover the 3D polyurethane foam cellular structure from sequences of 2D LCM images.

Theoretical Solution   Before we present a practical solution, we outline the theoretical difficulties in supplying a numeric solution to the recovery of the 3D object model using only its 2D projection sequences.   Based on functional analysis and assuming that the cell network is represented by a continuous space function f(x,y,z), the network may be completely defined by its 3D *Radon transform*. The 3D Radon transform $F(\rho,\theta,\phi)$ associates function $f(\rho,\theta,\phi)$ with the set of its section planes $P(\rho,\theta,\phi)$ integrals, as follows

$$F(\rho,n) = \iint_{M \in P(\rho,n)} f(M) dM \qquad (1)$$

where (ρ,θ,ϕ) are the classical parameters of spherical coordinates, and **n** is the unit vector in the direction of (θ, ϕ). The integral in Equation (1) is evaluated at points M in plane $P(\rho,\theta,\phi)$, which has **n** as a normal vector. The cellular network can then be reconstructed by using the following inversion formula (13)

$$f(M) = \frac{1}{4\pi} \int_{\theta=0}^{\pi} \int_{\phi=0}^{\pi} \frac{\partial^2 F(\rho(M,\theta,\phi),\theta,\phi)}{\partial \rho^2} \sin\theta d\theta d\phi \qquad (2)$$

here $\rho(M,\theta,\phi) = $ **OM*n**; O is the space origin. The theoretical difficulty, linked up to the cellular geometry is to express a relation between the LCM imaging function and the 3D *Radon transform.*. Only the human vision system is capable to overcome this difficulty. While the human eye is able to integrate the 3D network; it is a difficult task to automate this integration to a computer system since the numeric solution is

difficult to formulate. In the following, we present a semi-automated approach which requires a certain amount of manual editing and human expertise.

Practical Solution   One of the key fact during the foaming process, is that gas bubbles nucleate throughout the liquid and grow as spheres until they interact and change to forms that resemble polyhedrons. These cells shapes can then be defined as part of Voronoi tesselations centered on the point of nucleation (*14, 15*). Based on this concept, we implemented an algorithm that searches for vertices of these cells. No assumption was made on the family of these cellular shapes, except each is centered on the point of the nucleation and obey Voronoi tessellation. It may be satisfactory to select a simplified set of models, defined by a finite number of vertices in a 3D space.

The first step of our approach is to process the LCM sectioning images to overcome background noise and sharpen edge contrast. An optional operation is to restore lost features in the images by means of the 2D Euclidean distance function. This restoring approach is well discussed in (*8, 16, 17*). Our technique is then to etch away all of the image features except for lines of pixels which represent the midlines of the edges and branching of the original cell projection on the working plane. Hence, the structural features are reduced to line segments. This set of consistent rules of fading and plating pixels is known as Skeletonization. A resulting image of this process is illustrated in Figure 6. Using a 3x3 kernel, we were able to identify the triple points of lines intersections, as shown in Figure 6. These points of intersections were taken as the cell vertices. This process was then repeated on all the sectioning images to obtain a complete set of foam sample vertices.

Notice that the process detected few other points that do not present real vertices. These extra points usually reside close to an actual vertex and hence does not have a major affect on our approximation procedure. Moreover, these extraneous vertices, can be eliminated by imposing more constrains on the kernel, used for detection. On the other hand, adding constrains to the kernel might miss few real vertices. The kernel used in Figure 6, did not exceed, in most scenarios, 5% of the entire set of real vertices as undetected vertices. Some of these procedures were developed using modules from the standard Khoros platform.   Based on manual editing, the algorithm then renders through these set of vertices to restore lost connectivities between the entire set of cell vertices. The algorithm then generates a relational database of edges, facets, and vertices. This data base is then fed into a developed software that generates the restored 3D cellular network. Figure 7 represents a holistic view of a recovered cellular network. Notice that few vertices are spaced in the network with no recovered struts. Two possible reasons that justify their existence. They might not represent real vertices and are generated based on a constrained kernel, or are due to the ambiguity in the imaging plane projection and shielding effect. If they represent real vertices, then their struts are perpendicular to the imaging planes and were not detected.

Discussion

In this framework, we present an approach to image and recover the 3D PUF cellular network. Using the laser confocal microscopy, we were able to capture most of the detailed information of the foam cellular network. This approach is proven to be more effective than conventional methods, in characterizing the foam cells. We were able to extract 3D structure of the cellular network and conduct a statistical analysis. As a result of this work, we were able to reconstruct a holistic 3D reconstruction of the cellular network of a given foam sample.   We conducted an approach (not fully automated) based on Voronoi technique and developed a software to display the 3D shape of this network.   One way to completely automate this proposed technique is by modifying the Voronoi algorithm (*18*) to account for the nonlinear bubble growth
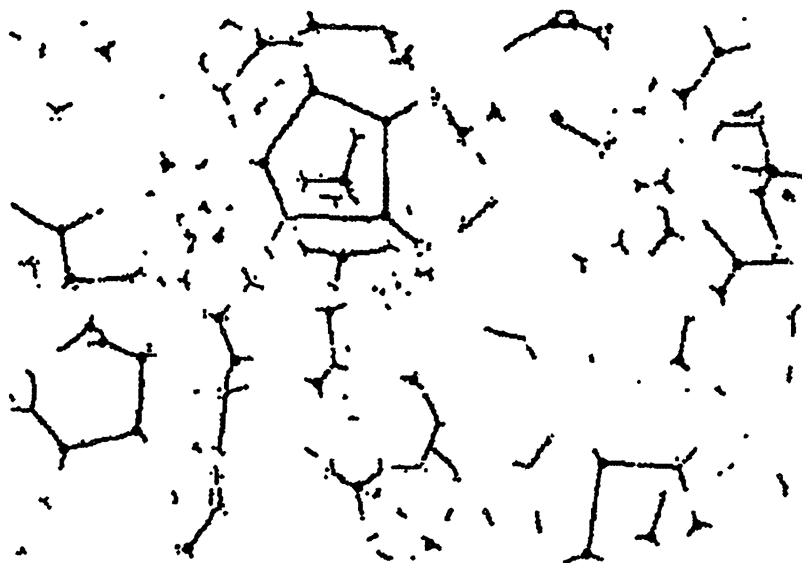
Figure 6. A skeletonized image to identify PUF cells vertices.
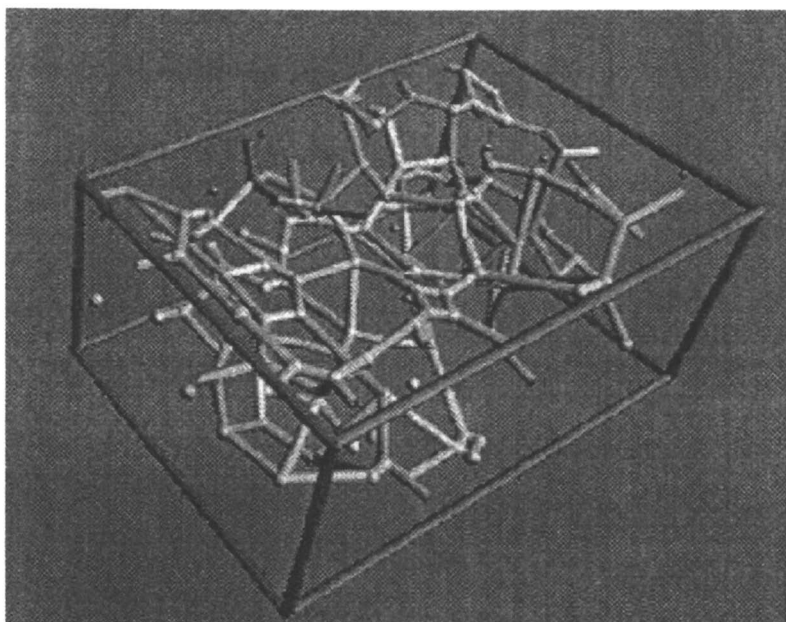
Figure 7. A 3D recovered PUF network.

rate. To better illustrate this idea, consider the case where the bubbles were uniformly distributed and cells had similar linear growth rate, then the foam network probably would have *Kelvin Bulk* structure which divides the space into cells with uniform faces. As seen in Figure 7, neither the *Kelvin Bulk* structure nor the *Rival Bulk* structure (a geometric model that reconstructs a unit space from a set of similar cells with non-uniform windows) proposed in (*19, 20*) would lend to foam cellular reconstruction. Indeed the distribution of the nucleation points must be assumed random. Nevertheless, a 3D fully automated reconstruction is possible if we include a weighting technique on the existing Voronoi algorithm. For future development, the approach will be based on an automated method of configuration and training which is capable of searching a large dimensional space of modules, constructed by the weighted Voronoi algorithm, and weighted parameters to produce the best image suites in each trained scenario, i.e., cell edges are weighted to simulate a foam structure projected into different angels. A least square algorithm can then be used to minimize the difference between the model and the actual 2D images. This technique was first developed to configure Automated Target Recognition (ATR) algorithms (*21*). The idea is to produce a self-adaptive system via the image context-based configuration and control. Based on an intensive training process, a software system employs the machine learning technique to correlate the different scenes of a foam network taken at different angles with the Voronoi algorithm adaptation (weighted Voronoi structures). An image database is then built to be used via a context capture tool to perform a selective perception that lead to most likelihood cellular model for the new imaged PUF.

A Different Approach - NMR Imaging

Confocal microscopy is proven to be more advantageous over the conventional microscopy method since it provides with sharper 2D images and can image foam structure up to 2 mm into the surface of the foam. However, from Figure 3f, we can see that the out-of-plane shielding is a seriously limit the quality of the image, many struts are partially hidden by the cell structure about the focusing plane. During image processing, these images with partial information can cause false detection of vertices. This is one of the reason in Figure 7, there are some vertices that are not connected to anything. Out-of-plane shielding effect is an inherent limitation of the confocal microscopy. With this problem existing, the original 2D images will not provide complete information about the cell network. The accuracy of the reconstructed 3D image is thus limited. Also, although the 2D images obtained by confocal microscope are sharper than images obtained by conventional method such as standard optical microscopy, they still show some out-of-plane images. This leads to an extra step in image process - eliminating the out-of-plane images. This extra step may give rise to some undesired artifacts such as losing some of the focus plane image patterns.

Nuclear magnetic resonance imaging (MRI) is a powerful technique that is widely used in clinics to image the structure of the human body, especially brain, cardiovascular system etc (*22*). It provides an alternative to obtain 2D foam images without out-of-plane shielding, since this method is based on response of certain nuclei under radio wave. The resulting images are depth independent. For example, Figure 8 is a 2D image of a large cell foam sample almost 3 cm under the surface. We can obtain sharp 2D images deep inside the foam without out-of-plane shielding effect. This MRI image is better focused than the images obtained by confocal microscopy. The MRI image is so sharp that it is similar to the skeletonized image of confocal microscopy (Figure 6), which is obtained after many steps of image processing. So if we used MRI to obtain the 2D images for 3D reconstruction, the 2D images will provides complete information about cell network and they are also easier to process.
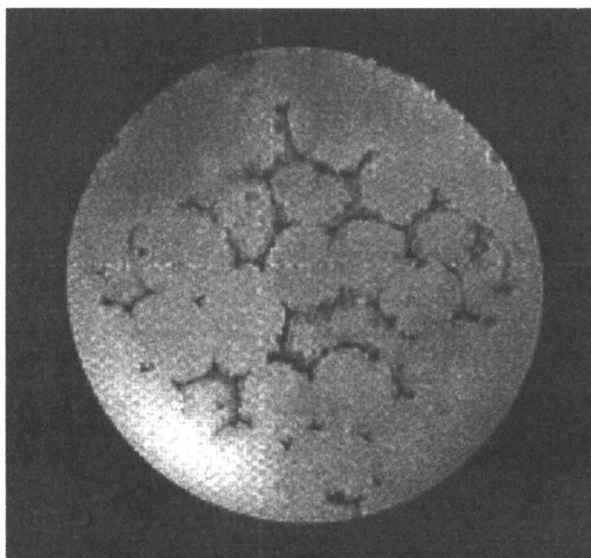
Figure 8. A 2D MRI (magnetic resonance imaging) image of foam material 3 cm under the foam surface.

The MRI technique even has the ability to scan the 3D image of the foam network directly (*23*). A 3D image acquisition script can be written and theoretical calculation shows that with 3D resolution of 25x25x25 μm, a 3D image acquisition of a 3x3x3 mm sample can be done in about four hours, which is much less than the time required to do the 3D reconstruction from 2D image series. We are currently writing the script and making required coil that will be used in 3D image acquisition.

Acknowledgments

References

1. Rhodes, M. B. In *Low Density Cellular Plastics: Physical Basis of Behavior*, Hillyard, N. C.; Cunningham, A. Eds.; Chapman & Hill: London, 1994, pp 56-67.
2. Rhodes, M. B.; Khaykin, B. *Langmuir* **1986**, *2*, 643.
3. Chaffanjon, P.; Verhelst, G. *Cellular Polymers* **1992**, Vol. 11, 2, 1.
4. Hilyard, N. C. In *Low Density Cellular Plastics: Physical Basis of Behavior*, Hillyard, N. C.; Cunningham, A. Eds.; Chapman & Hill, London, 1994, 226.
5. Minsoo, S. *Three Dimensional Object Recognition from Range Image*; Academic Press: New York, 1992.
6. Toga, A. W. *Three-Dimensional Neuroimaging*, Raven Press, New York, pp. 211-234, 1990.
7. Konig, D.; Carvajal-Gonzalez, S.; Downs, A.; Vassy, J.; Rigaut, J. *J. Microscopy* **1991**, *161*, 405.
8. Robb, R. A. *Three Dimensional Biomedical Imaging, Principles and Practice*, VCH Publishers: New York, 1993.
9. Meyer, F. *J. Microscopy* **1992**, *162*, 5.
10. Terzopoulos, D. *IEEE Trans. on Pattern Analysis and Machine Intelligence* **1988**, *4*, 417.
11. Kass, M.; Witkin, A.; Terzopoulos, D. *Proceedings of First International Conference on Computer Vision* **1988**, 321.
12. Malladi, R.; Sethian, J. A.; Vemuri, B. C. *IEEE Trans. on Pattern Analysis and Machine Intelligence* **1995**, *17*, 158.
13. Sire, P.; Grangeat, P.; Lemasson, P.; Melenne, P.; Rizo, P. *Materials Research Soc. Symp. Proceedings* **1991**, *217*, 129.
14. Gibson, L. J.; Ashby, M. *Cellular Solids: Structure and Properties*; Pergamon Press: New York City, 1988, pp. 10-41.
15. Moller, J. *Lectures on Random Voronoi Tesselation*; Spring-Verlag: New York City, NY, 1994.
16. Serra, J. *Image Analysis and Mathematical Morphology, Vol. 2 Theoretical Advance* ; Academic Press: London, 1988.
17. Serra, J. *Image Analysis and Mathematical Morphology*, Academic Press, London, 1982.
18. Medvedev, N. N. *J. Comp. Phys.* **1986**, *67*, 223.
19. Weaire, D.; Phelan, R. *Philosophical Mag.Letters* **1994**, *69*, 107.
20. Weaire, D.; Phelan, R. *Philosophical Mag. Letters* **1994**, *70*, 345.
21. Roberts, B.; Au, W. *Proceedings of SPIE*, Vol. 2496, April 1995.
22. Hammer, B.E.; Heath, C.A.; Mirer, S.; Belfort, G. *Bio/Technology* **1990**, *8*, 327.
23. Cenens, J.; Huis, R.; Chauvaux, B.; Dereppe, J. M.; Gratin, C.; Meyer, F. *Cellular and Microcellular Materials* **1994**, *53*, 29.

Chapter 12

A Perspective on Cell Morphology and Foam Properties

M. B. Rhodes

Chemistry Department, Graduate Research Tower, University of Massachusetts, Amherst, MA 01003

In spite of the difficulty regarding the true nature of cells in polymeric foams, it has long been advantageous to characterize foam samples with respect to their cell size. Although agreement is poor among the various methods in use, these measurements have a great validity when made with the understanding of their ultimate purpose. Precision and confidence levels are a function of the major objective of the measurement and play a significant role in dealing with the inherent variability of the foam cell population. The appropriate design of a measurement process will aid in establishing any correlation of cellular parameters with the physical properties of the foam. Computer interfaced methods, especially those of stereology, establish many of these correlations.

There continues to be an interest within the scientific community in investigations relating the bulk foam properties and the foam cellular morphology. This is despite the fact that there is much confusion regarding the interpretation of the data from such investigations. The resulting data are frequently questioned because of two experimental difficulties. The first is the use of different models to describe the "cell" and therefore agreement for a quantitative characteristic such as cell size is usually poor. The other experimental difficulty is the need to statistically accommodate the inherent non-Gaussian foam cell variability of the sample. Understanding both of these difficulties and their subsequent imposed limitations will guide the experimental design of any investigation and provide a useful perspective on the relationships existing between cell morphology and foam properties. A logical path for developing this perspective starts with examining the concept of the cell, critically surveys the manner by which cell morphology is quantitatively studied, and finally evaluates the significance of the cell measurements to foam properties.

Concept of the Cell

The concept of "the cell" in cellular structures carries different implications depending on the foamed material in question. However, whether one is dealing with coral reefs, bread, sponges, or polymeric foam, a simple description is initially applicable; namely, " a gas-in-a-liquid" or "a gas-in-a- solid". The gas phase is considered to be

178

the dispersed phase and the liquid or the solid is identified as the continuous phase. The gas phase will vary between fifty to over ninety percent, thereby resulting in a large interfacial area *(1)*. Consequently some foam systems are mainly concerned with stability, as in the aqueous surfactant systems. While stability plays an important role in the evolution of polymeric foams, there are other more permanent morphological features that enter into foam classification. One can identify the polymeric material, i.e., polyolefins, polystyrene, phenolic, polyurethane, etc. or imply structure-property relationships, as rigid versus flexible foams, or open versus closed cell foams. Recently studies have included systems which are microcellular in nature, and the means by which these systems are prepared can contribute significantly to their range of properties. Irrespective of the foam system under consideration, they almost always exhibit some common features or processes.

The initial geometry of the foamed polymer is characterized by the transition from that of the growing spherical gas bubble to volume filling phases with planar interfaces. These are illustrated in Figure 1.   Figure 1a shows the "klugelschaum" stage, Figure 1b illustrates the transition to the last stage shown in Figure 1c, the "polyederschaum" stage *(2)*. This latter figure also shows the presence of two very distinct features of the cell geometry that will play an important role in the stabilization of the cells and in the characterization of foam properties. These features are identified in the figure as the "lamellae" and the "Plateau borders". In spite of the final differences in appearance, polymeric foams are very similar to aqueous foams during this dynamic, non-equilibrium, heterogeneous stage. Benning stated " many thermoset systems behave like liquid aqueous foams in their initial stages of formation and stabilization before cure" *(3)*.

There is a specific geometry associated with individual cells that is common to all types of foams as a result of the equalization of forces. Observation shows that in two dimensional space, cells meet a point that gives an angle of 120 degrees, while in three dimensional space, this meeting point is the characteristic 109 degrees. Although these angular relationships will vary somewhat because of the need to accommodate irregular polyhedra into the three dimensional packing, the usual geometry that results is the pentagonal dodecahedron. While this may be a common geometric form in foamed systems, it is not a volume filling geometry. Measurements on many different types of foamed systems have shown that the most appropriate volume filling geometry is that of truncated octahedrons, having six square faces and eight hexagonal faces *(4,5)*. Even this structural form shows slight curvature of the faces.   In real samples of either natural or polymerized foamed systems, one finds a distribution of not only different types of polyhedra but also a distribution of cell sizes.   This results from the system, during its evolution, maintaining its stability through the interaction of various physical   chemical processes *(6)*. This final distribution of the cell shapes and sizes is an important characteristic of the properties of the foam system in its various applications *(7)*. Additionally this characteristic distribution also plays a significant role in establishing the validity of any measurement associated with cell morphology *(8)*.

Evolution of Cell Models

The evolution of cell models reflects the changing emphasis that has been associated with polymeric foams. This emphasis has usually been associated with a specific scientific discipline. Thus engineers interested in the mechanical properties of the foam, emphasized foam properties such as foam density, cell shape, symmetry of the cell structures, mean number of edges per face, mean number of faces per cell, largest cell size, shape anisotropy, etc. The colloid chemist described the foam in terms of an equation of state, involving free energy, surface area and surface tension. Scientists interested in the thermal properties of a foam emphasized cell diameters and window thickness.   Investigators pursuing the fundamental nature of foam cells were

Plateau Borders

(a)   (b)   (c)

Lamellae
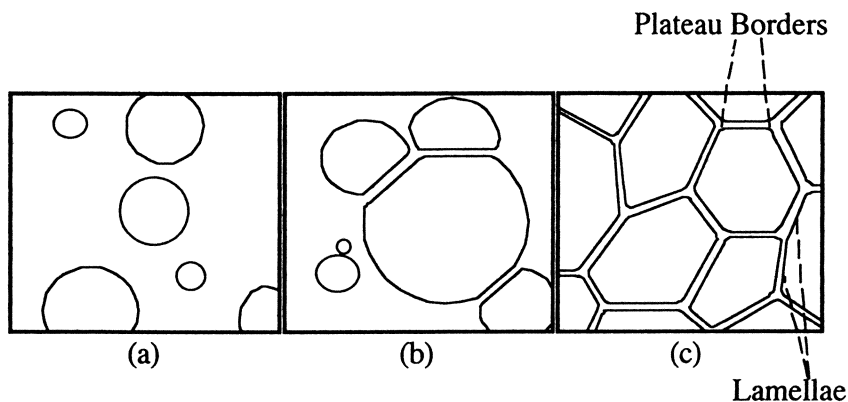
Figure 1. Transition from the klugelschaum form (a) through the transition stage (b) to the polyederschaum form (c). (Reproduced with permission from reference 26. Copyright 1994 Chapman and Hall.)

DIAMETER MEASURED AS	SAMPLE A (mm)	SAMPLE B (mm)
ARITHMETIC MEAN DIAMETER $d_1 = \Sigma n_i d_i / \Sigma n_i$	122	121
MEAN LENGTH DIAMETER $d_2 = \Sigma n_i d_i^2 / \Sigma n_i d_i$	231	187
MEAN VOLUME-SURFACE DIAMETER $d_3 = \Sigma n_i d_i^3 / \Sigma n_i d_i^2$	350	225

Figure 2. Different expressions for calculating diameter values. (Reproduced with permission from reference 26. Copyright 1994 Chapman and Hall.)

concerned with relationships, such as cell size and volume weight, or the wall thickness and volume weight with the homogeneity of cellular matrix. Although cellular structures have been studied for over three hundred years, the serious evaluation of polymeric foams began with the studies of Gent and Thomas on foamed rubber *(9, 10)*. They proposed a model intended to help understand the observed mechanical properties of the cellular foam. Over the years this model and associated mathematical expressions has been modified in attempts to better correlate theory with experimental observations *(11-15)*. During all this time it was not generally accepted that the cell geometry had any great influence on the foam behavior. Although Rusch suggested that the equations should incorporate a geometrical factor, interest was slight mostly because there was no reliable way in which to document the cell geometry *(16)*. Then an almost completely different line of foam investigation or study was simultaneously progressing in which experimentalists were measuring the physical properties of foams and correlating them simply with cell size. Although these studies gave results that now seem almost too obvious, they did provide support to the fact that cell morphology can play an important role in foam performance *(17-19)*. Today it is generally accepted that equations that are to predict the behavior of foams must accommodate a wide variety of parameters that are associated with every aspect of cell morphology. These can include in addition to cell sizes, shapes and orientations, such variables as resin diffusibility, the specific nature of the gas as well as the partial pressure of the gas *(20)*.

Measurements on Cell Morphology

When one stops to consider just what morphology associated with the cell can be quantitatively determined, it is obvious that cell size is the first characteristic that comes to mind. However other features can also be informative. Thus window thickness, uniformity, anisotropy, and defects as well as strut material amount, anisotropy or uniformity, can all be significant morphological features to measure *(21-23)*. The experimental design for any of these morphology measurements will be completely distinct from cell size measurements, primarily due to experimental difficulty in acquiring multiple measurements.

Cell size has always been and will continue to be the easiest measure to implement. However, as mentioned previously, there has seldom been good agreement among the various methods that have been employed. This is primarily due to the different models from which the measurements are derived. Additionally another reason is the choice of "diameters" that can be measured These can include a Martin's diameter, a Ferret diameter, a nominal diameter, a horizontal intercept, or a long axis *(24)*. Another variation leading to a discrepancy in diameter value agreement can be found in the specific expression by which a diameter is calculated. The arithmetic mean for very abnormal size distributions can be a misleading description of the population *(25)*. Figure 2 illustrates diameter values that relate to two samples with different types of cell size distributions *(26)*.

Methods for Measuring Cell Size. Following is a brief description of the more often used methods for the determination of cell size in polymeric foams.

1. Standard Test from the American Society for Testing and Materials
(D-3576) *(27)* . This method gives a diameter derived from an average chord length. The derivation assumes that the cell shape is spherical and that there is no extreme variation in the cell size distribution. Experimentally the method involves superimposing the image of the foam on a linear scale and measuring the number of cells that intersect a specific length. The diameter is expressed as d = t /0.616. The

constant factor arises as a result of translating the two dimensional linear measure to the three dimensions of a sphere.

2. Diameters Calculated by an Edge-Length-Area Measurement *(28,29)*. This method assumes that the foam cell is best approximated by a pentagonal dodecahedron and can be associated with a circumscribed sphere through the vertices of the polyhedron. Measurement can be maximum chord lengths, edge lengths, or surface areas, and by the appropriate geometrical relationships of polygons and polyhedrons, a cell diameter can be calculated. Although the method can include a means to compensate for the presence of other cellular shapes, this method remains an approximation.

3. Method of Intercepts *(20)*. The method yields values that are identified as cross sectional areas of cells. It is a time consuming operation for the preparation of the samples that are to be measured. However the net result of the excessive time investment is to decrease the number of measurements that need to be made for an acceptable confidence level. But more important, the method assures an unbiased measurement with regard to anisotropy, uniformity and randomness of the cells. (This lack of bias is also an inherent feature associated with the modern stereological methods of measurement.) In this method the measurements are collected from photographs by counting the intersections of cell walls with superimposed gridlines while the grid is rotated in thirty degree intervals from 0 to 150 degrees. The foam sections being measured are seven in number, cut from a rod shaped rectangular sample, originating first from the xy, xz, and yz planes. Then four additional sections are cut in sets of two, from planes that are plus and minus 45° to the axis of the rectangular solid and normal to each other.

4. Prism Method *(30)*. This method uses a most unique approach for obtaining a clear image of the cell geometry. The foam surface is imaged against a prism face in a manner that eliminates the out of focus cellular images.

In spite of the lack or agreement among the methods, each method for determining cell size does offer a valid approach to monitoring foamed systems. Each method is capable of achieving an internal precision and each one does measure cell size giving a value that is some function of the true cell size. The question is whether or not this functional dependence is a constant one for the distribution of cell shapes and sizes representing the cell population.

Computer Interfaced Methods. Although all of the previously mentioned methods function by manual operation, when computer interfaced, these methods expand to include other cell features in addition to size, such as perimeter values, maximum and minimum chord lengths, shape factor, orientation, and cell areas. There are many commercially available software programs and there are also customized programs as well for optical systems that have a specific measurement objective. The basic scheme of image analysis is shown in Figure 3. Usually before an image analysis is undertaken, the image of the sample undergoes some image processing. This can involve, repairing the image field by adding missing detail, adjusting the image field for poor or unequal illumination, and thresholding, the process by which the foreground is separated from the background *(31-33)*. The thresholding (segmentation) process is the most critical one in the measurement process. Lack of uniformity and reproducibility in this operation can result in enormous variation, as much as 70%, in the final quantitative results of measurement.

Despite any of the problems with image processing, computer interfacing can provide a very informative perspective on foamed systems. There are three recently significant literature reports that illustrate the quantitative application of image analysis

to polymeric foams. In a paper by Swartz and Bomberg, the differences in the cell morphology of sprayed urethane foams were evaluated for foams prepared with different blowing agents *(34)*. These researchers reported the average cell size and then used a thinning technique in the image processing step to establish values for strut thickness. Chaffanjon and Verheist studied cell structure through the application of two statistical parameters, the mean cell area and a population relative standard deviation *(35)*. The latter parameter describes the broadness of the cell area distribution. These two parameters were subsequently employed as a classification system for the flexible foam samples. Another report by Lewis and coworkers tabulated cell size and cell size distributions from rigid polyurethane boardstock foams prepared with a variety of blowing agents and with specific surfactants. (36) Each of these reports emphasize the usefulness of such measurements when they are employed within a specific study or process.

However, it is when comparisons are attempted between laboratories that measurement difficulties associated with the image analysis methods come to light. An example of this situation is a Round Robin study involving four laboratories (37). A polystyrene foam was prepared by the laboratories associated with the National Research Council of Canada and distributed as thin sectioned material and as small solid rectangular samples. Some of the results are shown in Figure 4. Laboratories I and III employed the same software program, while Laboratory IV used the prism method of cell size measurement. The major reason for this lack of agreement is considered to be the inherent difficulty establishing reproducible images.

Statistical validity can prove to be a major concern even within a specific laboratory that maintains a constant routine method of measurement. The following figures illustrate this situation. Figure 5 shows the variation found among individuals measuring the same image fields, while Figure 6 shows the variation found among the different software programs when measuring the same foam sample. There are three sources of indeterminate errors in the foam cell measurements, two of which are usually Gaussian in nature, one dealing with the measurement method and the other with the sampling procedure. The third contribution is the inherent variability of the foam sample itself and more than often is not of a normal distribution. Options for treating data such as this include non-parametric methods and cell size frequency plots *(38, 39)*. Insight into the nature of the process or mechanism that produces the abnormal distribution can be obtained from these alternative approaches.

Stereological Methods. Among the computer interfaced methods, stereology offers the most promising route for characterizing the foam cell. Stereology has been a well established method in the fields of metallurgy, mineralogy and biology for some time as a true statistical representation of multiphase systems *(40,41)*. Stereology adds the interpretation of the two dimensional image, thus going one step beyond just the documentation of this image. In the stereological approach, the two dimensional images are subjected to a statistical geometric analysis and the parameters that result are representative of a three dimensional statistical description of the foam. Figure 7 lists some of the stereological parameters that can be generated relevant to morphological features of the cell *(42)*. Figure 8 illustrates a typical computer output from a stereological measurement made on a polyurethane foam sample.

Except for density, no one individual characteristic is likely to demonstrate a correlation with the bulk foam behavior. Even in simple foam systems such as aqueous surfactant systems, the complex interaction of the physical, mathematical and thermodynamic properties suggest the need for a composite morphological parameter to most completely describe a foam. Figure 9 illustrates that for aqueous foams there is little significance to the cell morphological values until a parameter ϕ, which incorporates the volume density, surface area and mean curvature of the cells is
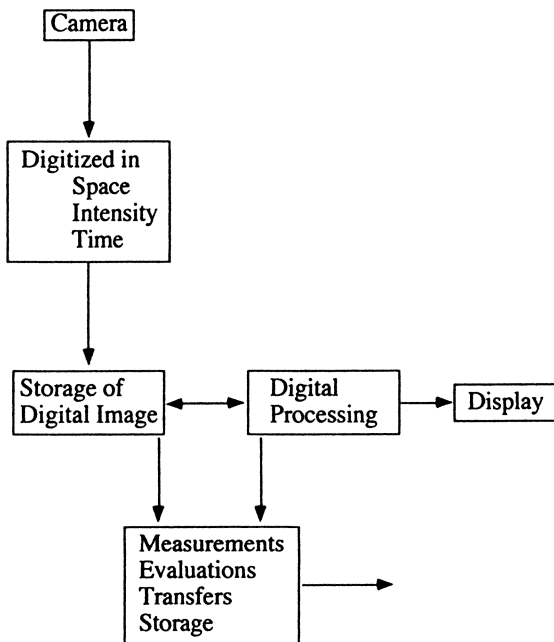
Figure 3. The digital image process illustrating the steps involved in image processing. (Reproduced with permission from reference 26. Copyright Chapman and Hall 1994.)

SAMPLE	LABORATORY			
	I	II	III	IV
	Diameters (μm)			
C	139	112	142	
D	146	89	121	180
E	173	94	169	220
F	260	253	267	490
G	233	159	240	320
H	254	201	219	310

Figure 4. Selected diameter values for polystyrene foam samples from a Round Robin study.

INDIVIDUAL	MEAN CELL AREA (mm^2)	STANDARD DEVIATION ± (mm^2)
1	0.0289	0.0306
2	0 0384	0.0720
3	0.0230	0.0242
4	0 0248	0.0431

Figure 5. Variation resulting from different individuals measuring cell area from the same sample of a urethane foam.

PROGRAM	AREA	RELATIVE STANDARD DEVIATION
OPTIMAS	0.0173 mm^2	± (0.014)
IMAGE PRO PLUS	0.0129 mm^2	± (0.295)
GLOBAL LAB	0.0174 mm^2	± (0.244)
STEREOLOGY	0.0179 mm^2	± (0.012)

Figure 6. Variation resulting from different software programs measuring cell area for a urethane foam sample. (Adapted from reference 26).

P_T	TOTAL NUMBER OF TEST POINTS
P_H	SUM OF THE HIT POINTS
P_I	SUM OF THE INTERSECTION POINTS IN THE TEST AREA
VD	VOLUME DENSITY, VOLUME OF THE TEST FEATURES PER UNIT TEST VOLUME
SD	SURFACE DENSITY, SURFACE AREA OF FEATURES PER UNIT TEST VOLUME
SS	SPECIFIC SURFACE, SURFACE AREA OF THE FEATURES PER UNIT TEST VOLUME OF THE FEATURES
MSA	SURFACE AREA OF THE FEATURES PER TEST VOLUME RELATED TO TOTAL VOLUME OF FEATURES IN THE TEST VOLUME
MD	MEAN DIAMETER OF THE FEATURES
MIL	MEAN INTERCEPT LENGTH OF THE FEATURES
MFD	MEAN FREE DISTANCE BETWEEN THE FEATURES
MC	MEAN CURVATURE OF THE SURFACES

Figure 7. A selection of stereological parameters applicable to foam cell characterization. (Adapted from reference 42).

PARAMETERS	ACCUMULATION OF 7 FIELDS	STANDARD DEVIATION
VOLUME DENSITY	.175E+00	.101E-01
SURFACE DENSITY	.426E-01	.333E-02
SP ECI F IC SURFACE	.243E+00	.100E-01
MEAN INTERCEPT LENGTH	.1 65E 02	.663E+00
MEAN FREE DISTANCE	.779E+02	.726E+01
MEAN DIAMETER	.248E+02	.994E+00
NUMBER OF FEATURES (STATISTICAL)	2895	
ELONGATION RATIO	.104E+01	.202E-01
DEGREE OF ORIENTATION	.270E-01	.122E-01
MEAN AREA	.578E+03	.459E+02
MEAN VOLUME	.798E+04	.936E+03
MEAN PERIMETER	.845E+02	.349E+01
MEAN CURVATURE	.225E-01	.927E-03
EQUIVALENT SPHERE	.247E+02	.999E+00
GRAIN SIZE NUMBER	.132E+02	.117E+00
NUMERICAL DENSITY	.1 23E-04	.185E-05
MAGNIFICATION	.500E+01	

Figure 8. Typical computer print out from a stereological measurement on a polyurethane foam.

defined.   The first two parameters of this composite description relate the geometrical and statistical distance of the dispersed phase while the third parameter relates to the stability of the cells. Numerical   values for this composite parameter suggests that different   foam systems may   have a great deal in common with each other (42). However,   such a universal foam   description is not applicable to polymeric foams except in their early stages of growth. It is during this time interval that they resemble aqueous foams, but as growth continues, there are additional factors that influence cell morphology and stabilization.

Stereological methods have become potentially more significant with increased application of the modern stereological methods (43).   The older stereological methods are model based and have unrealistic requirements for the type of sample to which the methods are most applicable. The sample was required to be isotropic, random and uniform. Since these requirements are seldom met in the real world, the sampling procedure needed to be modified. (as noted in reference 20)   Now modern stereological methods, which are design based, have compensated for these rigid requirements. These methods employ probes which are essentially a collection of points, lines or planes, specifically designed to eliminate any bias imposed by a sample when it is anisotropic, non-random or non-uniform. These methods make no assumption about the domain size or shape. They have been extensively employed by microscopists in the biological sciences.   However, there is still no easy solution to attaining an adequate optical image on which to make measurements. But research in electronic microscopy continues to develop techniques to give images suitable for making valid measurements (44-46).

Design of an Experiment

Why Measure?   The design of an experiment begins with answering questions such as   "why measure?' and "what will be the significance of any correlation between cell morphology and foam performance ?" If the purpose is one of quality control then   measurements of any type represent a documentation   of some characteristic   that can be   routinely monitored by the control laboratory testing routine. Correlation may eventually emerge when data that has been collected over a long time is studied. But if the reason for measuring is related to problem solving, then not only does one need to carefully decide what morphological feature of the cell is to be measured, but also what will any correlation signify if one is established. For instance, it is not sufficient to discover a correlation of size or surface area to some physical property, one must consider what to do with this information. This requires an understanding how the chemical and physical composition of the foam as well as the specific processing conditions directly affect the cellular morphology. If optimum performance for the foam is the major objective, then cell measurements are superfluous, since variations with the formulation and processing conditions will eventually produces the best possible foam. However, such a philosophy reduces the possibility of developing a functional model to represent the foam performance and essentially to be able to predict long term performance.

Statistics. An important step in the experiment design is an inspection of the foam, usually with a stereomicroscope, to determine the presence of defects or lack of homogeneity. This will prevent improper sampling with subsequent erroneous conclusions. Samples that have discernible differences in their morphologies are obvious candidates for measurement and study and the rationale behind such measurement is seldom in question nor is the statistical validity of the measurements. However, it may sometimes be required to establish the existence of sample differences. This illustrated in Figure 10 in which replicate samples from two phenolic foams, prepared with different blowing agents, have been evaluated for the

PARAMETER	SAMPLE PREPARATION			
	1	2	3	4
Volume Density	0.362	0.480	0.567	0.659
Mean Area, μm^2	15.3	23.9	35.0	45.1
Mean Curvature, $1/\mu m$	0.161	0.129	0.103	0.098
Mean Surface Area, μm^2	91.8	143	211	237
Mean Intercept Length, μm	1.44	2.39	3.52	4.90
Mean Free Distance, μm	2.87	3.58	4.36	2.52
General Foam Parameter, Φ	6.8	6.4	6.4	6.8

Figure 9. A selection of stereological parameter values for a series of aqueous foams. (Reproduced with permission from reference 42. Copyright 1986 American Chemical Society.)
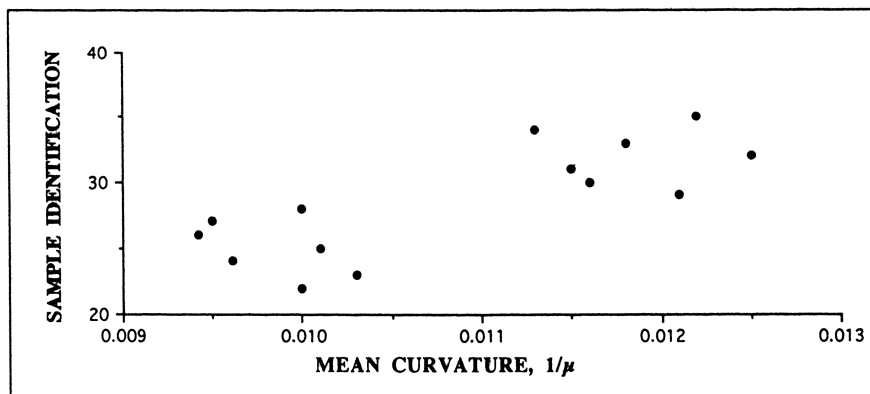
Figure 10. A plot of mean curvature values from replicate measurements made on two phenolic foams.

cellular mean curvature of the cells. Although the two samples had very little macroscopic difference observable, the clustering of the stereological parameter values implies that the two samples might also differ in some bulk physical property which in this case was found to be compression strength.

Finally it is necessary to select the appropriate number of measurements to make. This is related to the reason for the measurements. Quality control, problem solving or basic foam research, each have a different experimental design and each will have a different statistical validation for the data analysis. Inherent sample variability will also influence the number of measurements that one needs to make. Thus a 0.10 relative uncertainty from the measurement of only 100 cells from a uniform sample is contrasted to a nonuniform sample requiring over 300 cells to be measured for that same relative uncertainty.

Sample Preparation. The process of obtaining a proper image can prove to be the most difficult part of any cellular measurement. The usual procedure is to cut a thin section, one just thick enough to maintain the cellular integrity. There are any number of approaches to sectioning foams ranging from freezing to embedding, but the most appropriate procedure must be experimentally determined for each type of foam. No one procedure is applicable for all foam materials. Since the cut samples have a finite thickness, the out of focus information can seriously degrade the principal image. Figure 11a and 11b show two foams, polyurethane and polystyrene. The polystyrene image will be much more difficult to measure, requiring some processing operations before beginning any measurement.

Any technique that yields a good image can be employed for image analysis. In fact, any optical microscopy method that provides the proper contrast is applicable. Fluorescence optics is a useful approach to use for polymers that are naturally fluorescing. Foams with low surface reflectivity, natural or otherwise, can be successfully imaged with reflected (incident) radiation. Foam cell images can be scanned into the computer having originated from photographs, the SEM or TEM. Another approach has been the use of laser scanning confocal optical microscopy. The principles of this method and its application to the study of foam cell morphology has been reported by Macosko and coworkers (*47*). Phase contrast and interference optics are used in a non routine manner to study other cell morphologies.

Interpreting the Results. When the major objective is to investigate correlation, one should select a morphological feature that is likely to be a functional entity in the physical behavior of the foam. For instance Figure 12 illustrates the relationship of some stereological parameters to rigid and flexible polyurethane foam peformance. Surface density (SD) is a significant cellular feature in the performance of the flexible foam but has less importance in the behavior of rigid foams. This data also shows the correlation between the stereological parameters mean free distance (MFD), mean intercept length (MIL) and the 25% and 65% IFD. The values suggest that by the time the foam sample is at the 65% level, the foam is responding as if it were no longer a foamed material but simply the polymer matrix.

Figure 13 illustrates that two of the ways by which surface area is described differ in the manner by which they relate to the tensile behavior of the foam. The difference is found in the manner with which the surface area is expressed, in one case, a simple ratio while in another as normalized for the number of volume domains. If the cell size is not a variable for this collection then the cell size distributions become a significant variable.

Summary

There is still the obvious question, "Is there a relationship between cell morphology and the bulk foam properties?" The answer is " yes" and it is to be found by
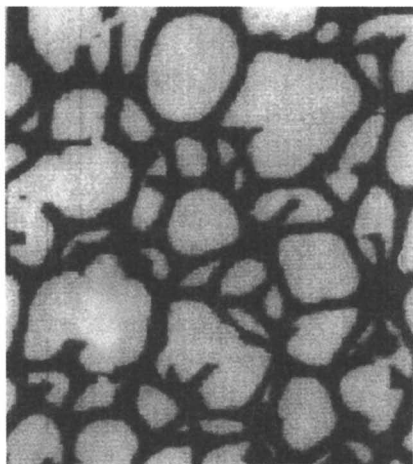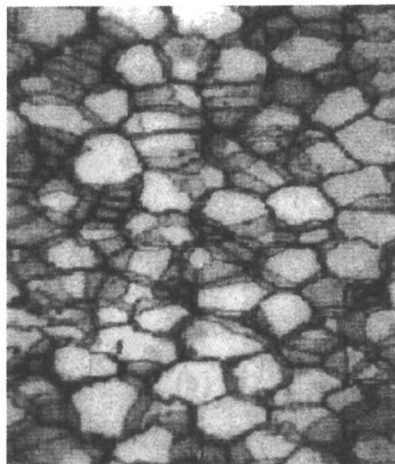
Figure 11. Computer images representing (a) a polyurethane foam and (b) a polystyrene foam.

PARAMETERS	FOAM TYPE	PHYSICAL PROPERTY			
		IFD-25%	IFD-65%	TENSILE	ELONGATION
MEAN INTERCEPT LENGTH	FLEXIBLE	0.769	0.357	-0.948	-0.98
MIL	RIGID	-0.979	-0.979	-0.995	
MEAN FREE DISTANCE	FLEXIBLE	0.942	0.828	-0.859	-0.826
MFD	RIGID	0.367	0.42	0.363	
VOLUME DENSITY	FLEXIBLE	-0.47	-0.753	-0.118	-0.089
VD	RIGID	-0.811	-0.845	-0.816	
SURFACE DENSITY	FLEXIBLE	0.941	-0.699	0.981	0.98
SD	RIGID	0.214	0.161	0.233	

Figure 12. Correlation values for selected stereological parameters with some physical properties of flexible and rigid polyurethane foams.(Adapted from reference 42).
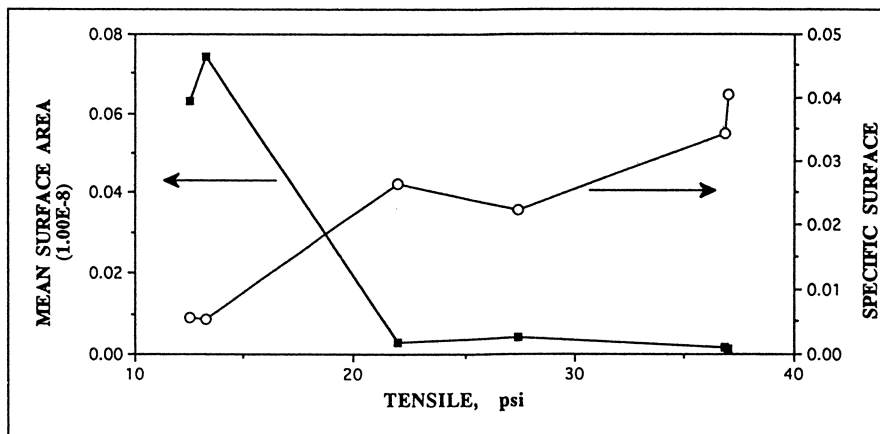
Figure 13. A plot showing the relationship of specific surface and mean surface area with tensile strength for a polyurethane foam.

performing appropriate experiments with a full appreciation of the possible difficulties entailed. These include attaining appropriate statistical validity and successfully associating a population of cells to a specific physical property. In the event that correlation is discovered, one must then be prepared to examine the significance of this relationship. Of what value is this information? Will it lead to producing a better foam? Will it explain some abnormal performance or behavior of the foam? Will it allow a modification in the foam formulation or processing conditions? This type of questioning is almost limitless when one considers the number of physical properties of a foam and the extensive cellular parameters in addition to cell size. But this serves to emphasize that foam performance, cellular structure and molecular makeup are all interrelated. Although it is feasible to assume that cell morphology features are associated with almost all foam properties in some way or another, it is not sensible to believe that they all exert an independent and measurable influence on the foam behavior. It is instructional to consider why one might not observe a correlation between cellular morphology and foam physical properties. For equivalent foam densities, a failure to establish any correlation may have resulted from an inappropriate selection of the parameters. For instance: a composite cellular parameter may be more appropriate than a single cellular parameter; or the physical property has no dependence on the cellular parameter. Even more often, a lack of correlation can be explained by a non-representative sampling of the foam which serves to emphasize the inherent variability frequently found in a bulk foam sample. The most difficult challenge is not in seeking these correlations but rather in effectively utilizing the information that results.

Acknowledgments

Both Zeiss and Dow Chemical, USA have contributed greatly to these studies. Acknowledgment is also made to those individuals who participated in the Round Robin testing. I am indebted to many other individuals, but especially to Boris and Valentina Khaykin and Richard Nathhorst.

References

1. Gibson, L. J.; Ashby, M. F. *Cellular Solids, Structure and Properties*, Pergamon Press, New York, 1988; pp. 11-40.
2. Bikerman, J. J. *Foams*, Springer-Verlag, New York, N.Y., 1973; pp.1-31.
3. Benning, C. *Plastic Foams,* Wiley Interscience, New York, 1969; Vol II, pp. 1-9.
4. Adamson, A. *Physical Chemistry of Surfaces*, 3rd Edition, John Wiley, New York, 1976; pp. 1-6.
5. Kelvin, L. *Phil. Mag.* **1887**, *24*, 505-514.
6. Rhodes, M. B. *J. Thermal Insulation* **1991**; *15* , 101-109.
7. Monsalve, A; Schechter, R.S. *J. Colloid Interface Science* **1984**; *97* , 327-335.
8. Shutov, F. A. *Advances in Polymer Science* **1983**; *51*, 155-217
9. Gent, A. N.; Thomas, A. G. *J. Appl. Polym. Sci.* **1959**; *1*, 107-113.
10. Gent, A. N.; Thomas, A. G. *Rubber Chem. Technol* **1963**; *36*, 597-610.
11. Chan, R.; Nakamura, M. *J. Cellular Plastics* **1969**; *5*, 112-118.
12. Menges, G.; Knipschild, F. *Polymer Engineering and Sci.* **1975**; *15*, 623.
13. Lederman, J. M. *J. Appl. Polym. Sci.* **1971**; *15*, 693-703.
14. Patel, M. R.; Finnie, I. *J. of Materials* **1970**; *5*, 909-922.
15. Barma,P.; Rhodes, M. B.; Salovey, R. *J. Appl. Phys.* **1978**; *49*, 4985-4991.
16. Rusch, K. C. *Appl. Poly. Sci.* **1969**; *13*, 2297-2311.
17. Blair, E. A. *Resinography of Cellular Plastics*, American Society for Testing and Materials, STP 414, Philadelphia, 1967; pp. 84-95.
18. Benning, C. *Plastic Foams,* Wiley Interscience, 1969, Vol II, pp.11-41.
19. Harding, R. H. *J Cellular Plastics* **1965**; *1*, 385-394.
20. Sparks, L. L.; Arvidson, J. M. *Proceedings of the SPI-28th Technical/Marketing Conference*, Society of Plastics Industry, Inc., New York, 1984; pp. 273-279.
21. McDonald, C. E. "Correlation of Physical Chemical Processes During Foam Growth and Stabilization", MS Thesis, Department of Chemistry, University of Massachusetts, Amherst, MA, 1982.
22. Akabori, K.; Fujimoto, H. *International Progress in Urethanes* **1980**; *2*, 41-60.
23. DuCauze de Nazelle, G. "Fundamental Understanding of the Thermal Conductivity Aging in Polyurethane Foams", Presented at the International Workshop on Long-Term Thermal Performance of Cellular Plastics, Niagra-on-the-Lake, Ontario, 1991.
24. Humphries, D. W. *Adv. Optical and Electron Microscopy* **1969**; *3* , 1-31.
25. Green, H. *J. Franklin Institute* **1927**; *12*, 713-729.
26. Rhodes, M. B. *Physics of Foams*; N.Hilyard; A. Cunningham Eds.; Chapman and Hall, London, 1994; Chapter 3, pp 56-77.
27. Annual Book of ASTM Standards, Standard Test method for Cell Size of Rigid Cellular Plastics, D-3576, Vol 08.03.
28. Pugh, A. *Polyhedra*, University of California Press, Los Angles,1976; pp 89-99.
29. *Handbook of Tables for Mathematics*, 4th Edition, Selby, S. M., Ed.; The Chemical Rubber Co., Cleveland, Ohio, 1970; pp. 8-20.
30. Wineland, S. H.; Bartz, A. M. *J. Cellular Plastics* **1986**; *22*, 122-138.
31. Walter, R. J.; Berns, M. W. *Video Microscopy,* S. Inoue Ed.; Plenum Press, New York, 1986; pp. 327-386.
32. Adams, J. R; Driscoll, E. C.; Reader C. *Digital Image Processing Techniques* , M. P. Ekstrom Ed.; Academic Press, New York, 1984; pp. 289-360.
33. Russ, J. C. *Computer Assisted Microscopy*, Plenum Press, New York, 1990; pp.1-11, pp.175-218.
34. Schwartz, N. V.; Bomberg, M. T. *J. Thermal Insulation* **1991**; *15*, 153-171.
35. Chaffanjon, P.; Verhelst, G. *Proceedings of the Polyurethane World Congress*, Society of Plastics Industry Inc., New York, 1991; pp.545-552.

36. Lewis, K. M.; Kijak, J; Reuter, K. B.; Szabat, J. B. *J. Cellular Plastics* **1996;** *32,* 235-259.

37. Rhodes, M. B.; Swanker, S. "Comparing Image Analysis Methods for Characterizing the Cellular Structure in Foams", Presented at the 3rd International Workshop on Long-Term Thermal Performance of Cellular Plastics, Toronto, Ontario, 1993.

38. Miller, J. C.; Miller, J. N. *Statistics for Analytical Chemistry,* Ellis Horwood Ltd., Chichester, England, 1988; pp.137-161.

39. Conover, W.J. *Practical Nonparametric Statistics,* Wiley and Sons, 1971; pp. 61-94.

40. Underwood, E. E. *Quantitative Stereology,* 19 Addison-Wesley, Reading, MA, 1970; pp.1-18.

41. Aherne, W.A.; Dunnill, M. S. *Morphometry,* Edward Arnold, London, 1982; pp.60-74, pp.75-85.

42. Rhodes, M. B.; Khaykin, B. *Langmuir* **1986;** *2,* 643-649.

43. Gundersen, H. J. G., et al, *Acta Pathologica Microbiologica et Immunologica Scandinavica* **1988;** *96,* 857-881.

44.Wang, G. E.; Liou, Wen-shan; Lin, Tein-Hsiang; Cheng, Ping-chin, *Multidimensional Microscopy,* Cheng P. C.; Lin T. H.; Wu W. L.; Wu J. L., Eds.; Springer-Verlag, New York, 1994; Chapter 11, pp. 191-208.

45. Inoue, T. *Electronic Light Microscopy,* David Shotton, Ed.; J.Wiley, New York, 1993; Chapter 4, pp. 95-104.

46. Russ, John C., *The Imaging Processing Handbook,* 2nd Edition, CRC Press, Boca Taton, FL, 1995.

47. Hamza, H.; Zhang, X; Macosko, C.; Stevens, R.; Listerman, M. "Imaging Open Cell Foam via Confocal Microscopy", paper presented at the symposium on *Recent Advances in Polymeric Foam Science and Technology,* American Chemical Society national meeting, Orlando, FL, August 1996, pp 803-804. (Also see Chapter 11 of this volume.)

Chapter 13

A Fundamental Study of Thermoplastic Foam Extrusion with Physical Blowing Agents

Shau-Tarng Lee

Sealed Air Corporation, 301 Mayhill Street, Saddle Brook, NJ 07663

A simple experimental set-up is presented to investigate thermoplastic foaming with a physical blowing agent. It allows to obtain gas/melt equilibrium constant, gas plasticizing effects, foam properties, and permeation. These are fundamental, and yet very critical for complex continuous foam extrusion. In this study, low density polyethylene and various simple organic blowing agents were used. It is an effective tool in blowing agent screening.

Thermoplastic foam has been widely used due to its favorable cushioning, insulation, and surface protection properties. As resin and foaming technology continued to improve in the past decade, highly expanded foam out of continuous process promotes production and, thereof, consumption of foamed products. Low density polyethylene possesses unique long chain branching structure, low melting nature, and strong resistance to chemicals; as a result, sizable efforts have been drawn to develop low density PE foam. In addition, screw mixing and extruder design to best fit polymer rheology improved significantly in the past few years to encourage foam extrusion technology development to render very low density foam possible by applying physical blowing agents. A general foam extrusion diagram with key foaming mechanisms is presented in Figure 1. Accordingly, foam quality is a function of various processing parameters and formulas, and combinations of them. It is not uncommon that a slight variation may cause a related reaction to make a compound impact on the product performances. A deep understanding of foam extrusion is therefore very necessary to further improve foam extrusion technology, and in light of environmentally safe blowing agent, to speed up search of sound blowing agents without wasting valuable research efforts.

Low density foam production in the extrusion process virtually extended traditional extrusion, melting and reshaping, to a higher ground; mixing (saturation), dispersion, and stabilization (*1*). Dissolution of blowing agent in the

195

B.A.

Resin → | Melting |▶| Mixing |▶| Cooling |◀| Shaping |▶| Foaming |▶| Aging |

Solubility   Stabilization   Dispersion   Nucleation   Solidification
                                            Growth   Permeation
                                            Coalescence
                                            Rupture
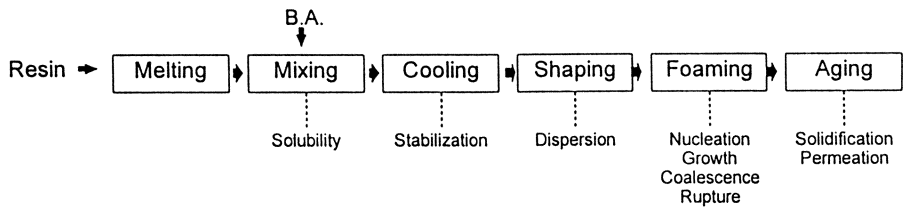
Figure 1.   Foam Extrusion Units and Their Mechanisms

Table I: State of Foam Extrusion Process

	1	2	3	4
Material	Resin, Blowing Agent	Gas/Melt	Gas/Polymer	Air/Polymer
Mechanism	Feeding	Mixing, Cooling	Expansion	Permeation
State	Low Pressure Low Temperature	High Pressure High Temperature	Low Pressure High Temperature	Low Pressure Low Temperature

polymeric melt tends to plasticize melt matrix to develop an overall viscosity and elasticity reduction to facilitate processing (2,3). But the associated system pressure causes stability concerns especially for volatile blowing agent, and thereof foaming, which is primarily consisted of nucleation and growth, and, in certain high degree expansion cases, coalescence and rupture. In nucleation, vapor pressure, P_s, directly contributes to degree of superheat defined as:

$$SH = P_s - P \qquad (1)$$

in which P denotes surrounding pressure which is one atmosphere for foam extrusion. In most cases, superheat versus interfacial tension determines nucleation rate (4). But inertial force and viscous force become important factors in dynamic foam extrusion to increase complexity to this already complex foam/melt nucleation, however, good qualatative agreement between nucleation and shear force was reported (5). As for growth, expansion rate is primarily determined by volatility and solubility, which have strong influence on both mechanical (expansion) driving force and chemical (diffusion) driving force (6). Since most foaming parameters are heat sensitive, it is sensible to identify primary factors for heat contribution. As reported (2), blowing agent type and loading have a substantial impact upon plasticizing melt, which dictates heat evolvement in processing. To separate formula effects from processing on foaming becomes a reasonable first step in approaching this complex foam extrusion. Moreover, a simple design is necessary to allow independent control of each key parameter to prevent heavy mutual dependency from happening, i.e. increased single screw RPM to cause automatic decrease of residence time. A batch design is highly preferred to enhance understanding of foaming principles on extrusion to avoid being side tracked when analysing results of big scale and complex extrusion trial.

From thermodynamic viewpoint, as outlined in Table I, foam extrusion is a process to convert polymeric material and blowing agent from low temperature and pressure, to high temperature and pressure (processing) to high temperature and low pressure (foaming) and back to low temperature and pressure. Solubility and volatility are directly related to temperature and pressure, aside from temperature effects upon transport properties. Henry's law constant, K_w, is defined as the ratio of system pressure over dissolution.

$$K_w = P_s / W \qquad (2)$$

It is a common chemical engineering practice in determining foam expansion limit by setting aside kinetic factors in the first place. In search of a new blowing agent, K_w becomes a very necessary parameter for foaming. Although it is independent of aging characteristics, for LDPE foaming, a comparative approach on K_w referencing to well established CFC/LDPE system appears to be useful both in qualifying this set-up and in search of blowing agent replacement.

RESIN PELLETS

ADDITIVES

RETRACTABLE
CHAMBER

HEATING OIL

ROTOR
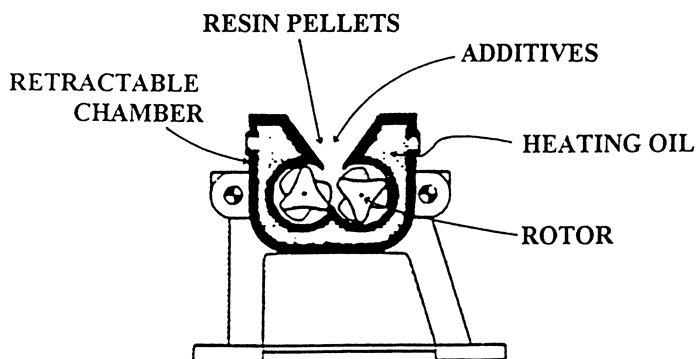
Figure 2.   Brabender Mixer Set-up

N₂   GAS SUPPLY

PRESSURE GAUGE

PRESSURE VESSEL

MELT/GAS

RUPTURE DISC + HOLDER

CAPILLARY DIE
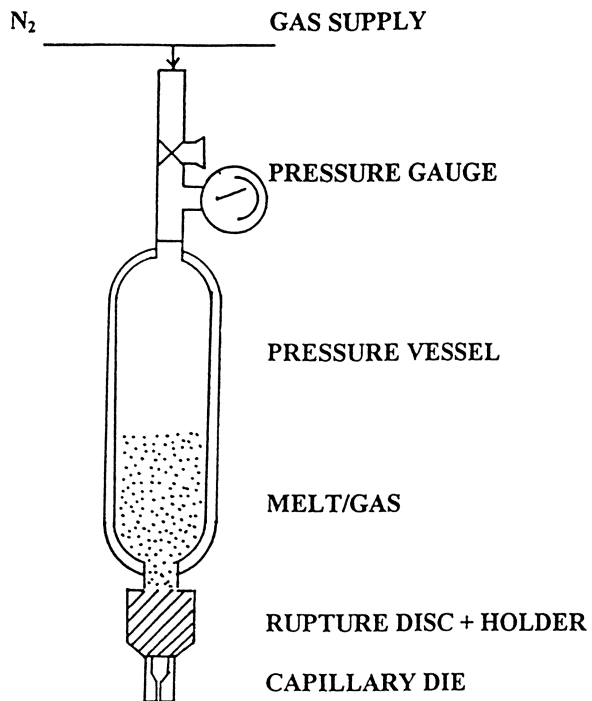
Figure 3.   Pressure Vessel Foaming Experiment Set-up

A static lab set-up was used to study the diffusion coefficient of various organic solvents in molten LDPE by recording vapor pressure variation as experiments went on (*7*). This principle was also carried on glass transition temperature reduction by equilibrating with a blowing agent in a pressure vessel (*8*). A simple pressure vessel was presented to study blowing agent in molten polymer and its foaming in the sixties (*9*). More improvements have been established since then. A logical extension is to include simple flow phenomena by exerting pressure to control pressure gradient across a narrow flow channel, during which shear can be calculated for shear heat effects on foam nucleation. Another important foaming operation is aging to cover high temperature molten state to room temperature solid state. Permeation becomes the key factor. When exiting from die, a natural exchange between saturated foam and surrounding air occurs. In general, most gas permeates faster than air to cause dimensional stability concern for LDPE foam (*10*). It appears that the time-related mechanisms, such as: dissolution, diffusion, foaming and permeation are difficult to separate in actual extrusion experiments. A simple set-up is virtually important to understand foaming principles for future developments.

Experiments

Conventional high pressure low density polyethylene (LDPE) with 0.918 g/cm^3 density was blended with nucleating agent (magnesium silicate) and, in some cases, other additives in a batch Brabender mixer as shown in Figure 2 to accomplish adequate mixing and dispersion. A 500 ml pressure vessel was equipped with a capillary die, L/D=12 , D=0.16mm; in between a rupture disc (yield @ 800 psi) and disc holder were used to maintain vapor pressure during gas/melt saturation. A gas supply unit was connected to allow blowing agent charge and enough pressure to break rupture disc. The set-up schematic is shown in Figure 3. This design generally includes most features of extrusion; namely melting, mixing, shaping and foaming.

The mixture out of Brabender mixer was then hot pressed to thin plaques to be sliced and dispensed in the pressure vessel. 0.21 mole blowing agent per 70 gram LDPE blend was charged and the whole vessel assembly was left in a vented oven thermostatted at 177 $^\circ$C over night for equilibrium. Initial pressure and equilibrium pressure were recorded for dissolution calculation (Henry's law constant) via mass balance. In order to allow the melt contents to exit from the capillary die, 800 psi was needed to break the rupture disc. After that, head pressure can be set even below 800 psi to control shear rate in the die. As the gas/melt exit the die, immediate expansion occurred. Samples were collected for immediate and subsequent density measurements for permeation analysis. After foaming was completed, the pressure vessel was adequately soaked in a hot xylene bath to clean away residual LDPE for the next experiment.

Table II: Selected Properties of Physical Blowing Agents

	CFC-12	CFC-114	HCFC-22	HCFC-142b
FORMULA	CCl_2F_2	$CClF_2CClF_2$	$CHClF_2$	CH_3CClF_2
MW. G/MOL	120.9	171	86.5	100.5
BOILING POINT @ 1 ATM F	-21.6	38.8	-41.4	14.4
SURFACE TENSION DYNES/CM @ 77 F	9.0	13.0	8.0	11.8

Table III: Experimental Results at 176.7 C

	*WEIGHT g.	P. psi	Kw, atm	DENSITY, PCF	CELL
CFC-12	26	360	200	4	COARSE UNIFORM
HCFC-22	19.35	400	600	7.5	FINE
ACETONE	12.5	200	117	12.5**	COURSE
HCFC-142b	21.6	300	190	4.5	MEDIUM
HFC-152a***	14.5	380	504	7.8	FINE

*   0.22 mole
**   collapsed
***   187.8 C

Results and Discussion

Key foaming properties of various physical blowing agents are listed in Table II. They were tried on an equal molar basis with LDPE for dissolution, foaming and aging analysis. Selected experimental results are tabulated in Table III in which Henry's law constant results on CFC-12 and HCFC-22 are in good agreement with the literature's (*11*). Since solubility and volatility have primary effects on expansion limit and processing status, generally, a low Henry's law constant is desirable. HCFC-22, HCFC-142b and HFC-152a appear favorable in making a low density foam in the extrusion process.

Variation of oven temperature caused variation of solubility and volatility; increased vapor pressure at higher temperature makes higher Henry's law constant. Figure 4 shows Henry's law constant follows an Arrhenius relation with temperature in the processing temperature ranges. Also included are other polymer/solvent systems (*11,12*). All show liner distribution in the log-linear scale between Henry's law constant and inverse absolute temperature. Vapor pressure is a linear function of temperature; and solubility also follows a linear mode at increased pressure as long as it is far below saturation, which is true for foam extrusion. Recall Equation 2 of K_w, these two factors seem to cancel out to leave the attention to melt sustaining ability on blowing agent at elevated temperature. This linear mode in log-linear scale suggests that thermal dependency of melt holding ability on gas molecules is similar to diffusion and viscosity dependency on temperature variation. Nonetheless, this information is very useful in determining processing temperature window and designing a foam die during which non-isothermal condition prevails to render simulation surmountable difficulties in figuring out system vapor pressure to optimize die pressure gradient to prevent premature foaming from happening..

After rupture disc was broken, a pure pressure flow through capillary die was established by the gradient between head pressure and surrounding atmospheric pressure. As shown in Figure 5, a pure pressure flow appears to be established. In fact, flow rate allows us to calculate melt viscosity to figure out viscosity reduction resulted from plasticization of blowing agent dissolution. According to Figure 6, a straight line in the viscosity vs shear rate plot suggests a power law fluid nature which is agreeable with reference (*2*) except its magnitude. It is primarily attributed to a low die temperature setting, $100°C$. Also noted is that this set-up allows viscosity calculation at a low shear rate, i.e. 5 sec^{-1}.

As a result of gas concentration gradient, mutual diffusion begins as soon as rod foam forms. Most blowing agents possess a much higher permeability over air to develop a cell pressure under one atmosphere, as a result, foam product dimension, for instance thickness, decreases. Sometimes, as aging progresses, enough air will make up one atmosphere pressure. But original thickness is not likely restored, probably because of a initial cell pressure slightly above one atmosphere. However, dimensional stability is shown in the aging trends of Figure 7. Butane foam rod takes about two weeks to stabilize. Effective and timely replacement by air poses a major production concern, especially when blowing
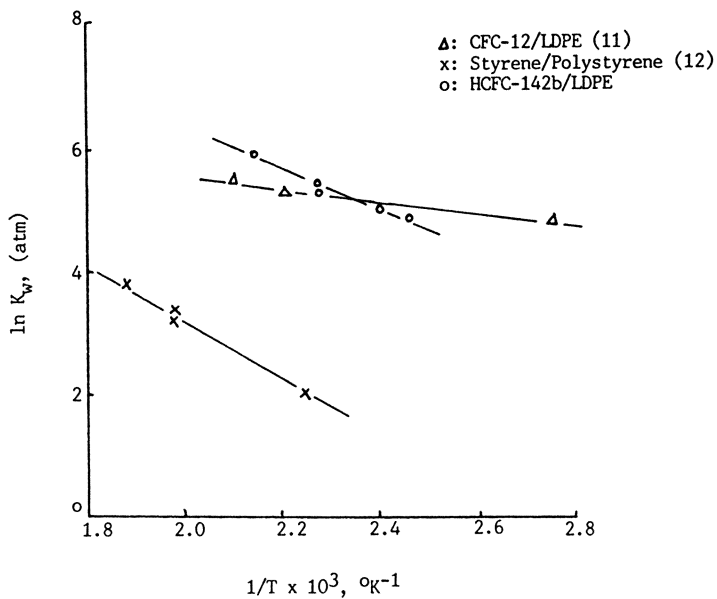
Figure 4.   Variation of Henry's Law Constant vs Inverse Absolute
             Temperature
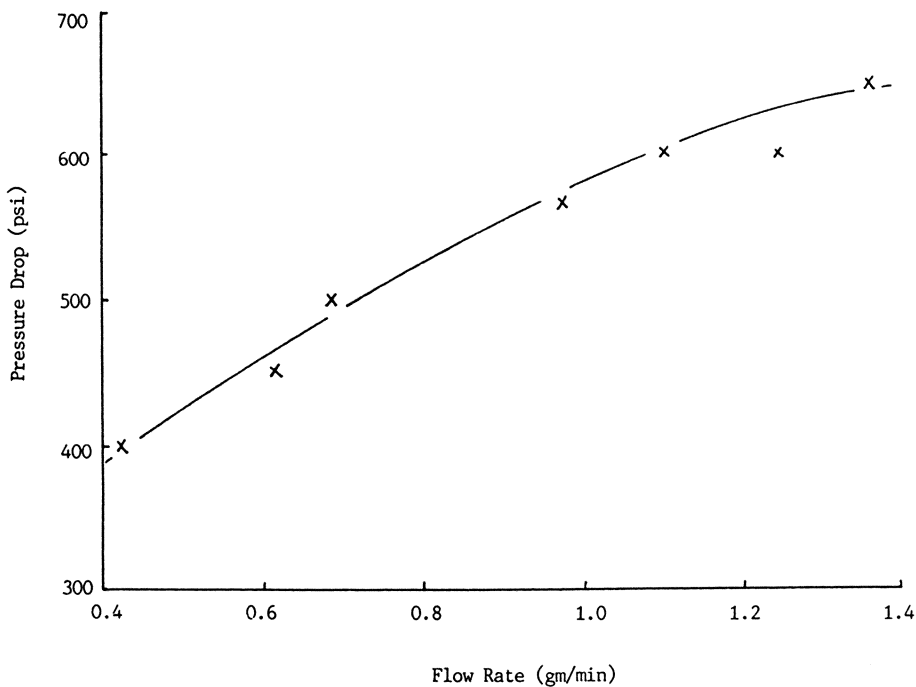
Figure 5.   Effects of Pressure Drop vs Flow Rate
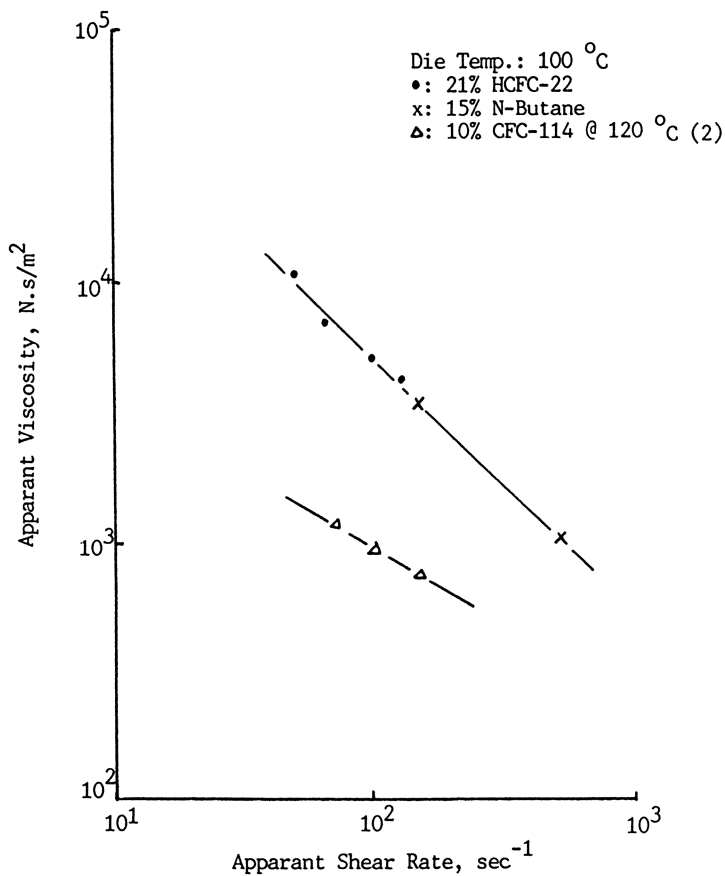
Figure 6.   Apparent Shear Viscosity vs Apparent Shear Rate
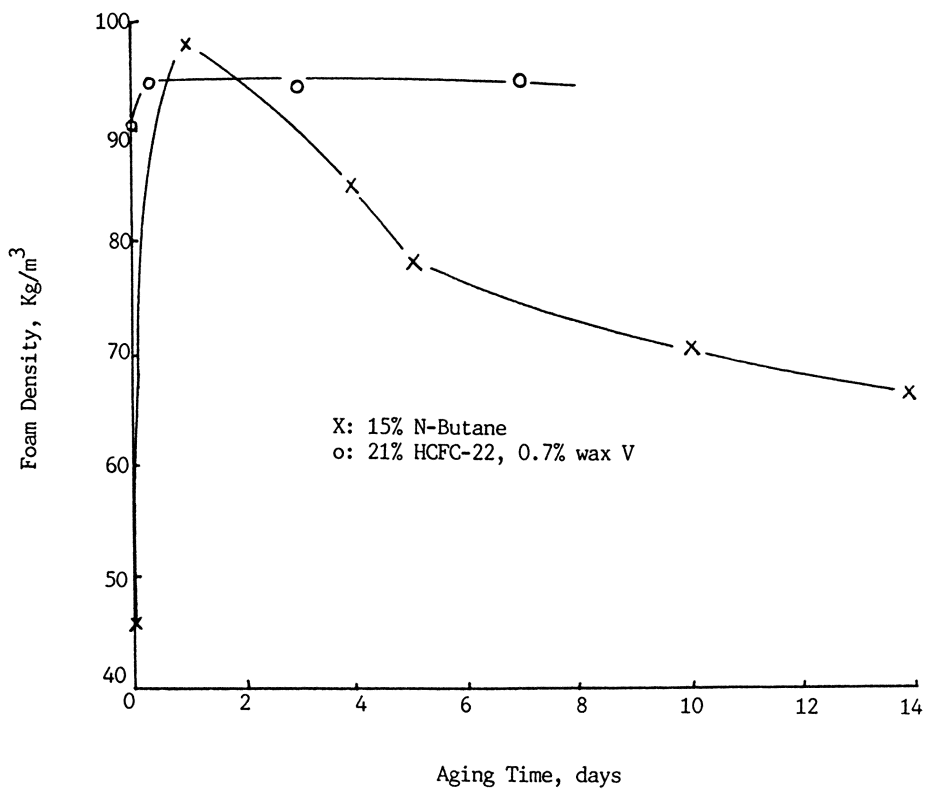
Figure 7.   Foam Aging Performances

agent arises health, safety, and environmental concerns. Additives are necessary to regulate blowing agent permeation. According to this figure, polyvinyloctadecyl (wax V) appears to slow down HCFC-22 diffusion. Also noted is that, even though a same molar basis was kept, initial density variation is large enough to suggest that factors other than molecular weight have strong impact on foaming. That means foam growth is not a pure thermodynamic phenomena. Kinetics and rheology are necessary elements to make the foaming dynamics picture more complete.

Conclusion

A simple experimental set-up is proposed to investigate foaming mechanisms; it can be used to search for new blowing agent and additives for permeation control. Key factors, such as: Henry's law constant, gas-induced viscosity decrease, foaming capacity, and permeation characteristics can be obtained from this lab set-up without major extrusion investment. It appears to be an effective screening tool to select new blowing agents and to investigate flow and aging control additives for low density foam extrusion. In the past, it was successful in discovering HCFC-22, -142b and HFC-152a in LDPE foam extrusion. In the future, when new blowing agents become available, this unit can be used as a preliminary foaming screener.

Acknowledgments

References

1. Park, C. P., *Polymeric Foam;* ed. by D. Klempner and K. C. Frisch, Hanser, New York, 1991; Chapter 9, pp 224.
2. Han, C. D.; Ma, C. Y., *J. App. Poly. Sci.*, **1983**, *28*, 831
3. Lee, S. T.; Ramesh, N. S., *Adv. in Poly. Technology,* **1995,** *15*, 297
4. Blander, M.; Katz, J. L., *AIChE J.,* **1975,** *21*, 833
5. Lee, S. T., *Poly. Eng. Sci.*, **1993,** *33*, 418
6. Lee, S. T., Master's thesis, Chem. Engin. Dept. of Stevens Inst. of Technology, **1982**
7. Durrill, P. L.; Griskey, R. G., *AIChE J*, **1966,** *12*, 1147
8. Dey, S. K.; Jacob, C.; Biesenberger, J. A., *SPE Annu. Conf.*, **1994,** 52nd ANTEC, 2197
9. Reubens, L. C.; Griffin, J. D.; Urehik, D., U.S. Patent 3,067,147, 1962
10. Watanabe, S.; Matsuki, Y., U.S. Patent 4,214,054, 1980
11. Gorski, R. A.; Ramsey, R. B.; Dishart, K. T., Proc. SPI 29th Ann. Tech. Mark. Conf., 1983
12. Mehta, P. S., *Polymer Devolatilization*, ed. R. J. Albalak, Marcel Dekker Inc, New York City, 1996; Chapter 8, pp202.

Chapter 14

Bubble Growth Dynamics in Olefinic Foams

N. S. Ramesh and Nelson Malwitz

**Corporate Chemical Research, Sealed Air Corporation,
10 Old Sherman Turnpike, Danbury, CT 06810**

An extruded foam sheet expands and cools simultaneously when exposed to ambient temperature. The existing viscoeleastic cell model was modified to include the effect of concentration on diffusivity during foam formation. The concentration and temperature effects on diffusion, viscosity and bubble growth results are discussed.. Literature reports show that the diffusion coefficient is a strong function of temperature and blowing agent concentration for low-density polyethylene and n-butane system. An attempt has been made in this paper to contrast the influence of concentration of blowing agent on foaming characteristics.

Thermoplastic foam has diverse applications which are realized through various foaming technologies. Insulation, surface protection, sports, recreation, and cushioning are some of the major applications of olefinic and styrenic foam products. Extrusion has been conventionally used for producing low-density foam sheet with physical blowing agents in the last decades. Foam nucleation, foam growth, and foam coalescence are the three major mechanisms in the foaming process. The dynamic nature in extrusion certainly introduces extra variables to this already complicated foaming process.

Foam growth has been investigated extensively in the literature. Most studies have focused on the isothermal condition, in which the principal thermodynamic properties are kept constant. The transient cooling of the foam sheet, combined with the effect of concentration of blowing agent upon the diffusion controlled foam growth process were not previously investigated. The objective of this paper to modify our previous model (1) to include the concentration effects. The non-Newtonian nature of the polymer/blowing agent mixture was modeled using the convected Maxwell model. Experiments were conducted to understand the rheology of the polymer/blowing agent mixture and its role on foam processing.

Review of Previous Work

Numerical and Experimental studies of Bubble Growth in Microcellular Foaming Process (1991). Ramesh et al developed a new experimental technique for studying the dynamics of bubble growth in thermoplastics using Scanning Electron Microscopy during the microcellular foaming process *(6)*. The influence of temperature, saturation pressure, molecular weight, and the nature of physical blowing agent were investigated. The experimental results show that the above process variables control the growth of foams during processing. The published Newtonian model for the growth of a single bubble in an infinite amount of polymer was modified to account for the non-Newtonian effects by modeling the polymer as a power law fluid. The experimental data were compared with the appropriate viscoelastic cell model which considers the growth of closely spaced spherical bubbles during the foaming process. The simulation results indicate that the predictions of the cell model are in qualitative agreement with the trends of the experimental data and the quantitative agreement is reasonable. The cell model also gives an equilibrium radius which agrees with the experimental data. Other viscous models do not predict the equilibrium radius of the bubble and underpredict the experimental data. Polystyrene-Nitrogen and Polystyrene-carbon dioxide systems were used for experimental foam growth studies.

Study of Thermoplastic Foam Sheet Formation (1996) Our recent work *(7)* discusses theory and experiments on nonisothermal foam growth during foam sheet formation in an extrusion process. The extruded foam sheet expands and cools simultaneously when exposed to ambient temperature. A viscoelastic cell model in the literature was modified to include heat transfer and gas loss effects during foam sheet formation. Experiments were conducted using a twin-screw extruder to study the effect of ambient temperature an initial sheet thickness on foam characteristics. The foam was made using low-density polyethylene with CFC-12 as the blowing agent. The experimental results are compared with theoretical predictions to check the validity of the model. The results reveal that heat transfer effects become important when sheet thickness decreases to the millimeter range. Agreement between theory and experiment is good when an appropriate boundary condition, to account for the gas loss, is included in the model.

Foam Growth Modeling and Experiments

As foam sheet exits from a die, we assume the one dimensional heat transfer. Heat conduction becomes the dominant heat transfer mechanism. The heat loss effects on foam growth are found to be less important when the thickness of the foam sheet exceeds 10 *mm* in thickness. The average temperature of the thin foam as it is exposed to ambient conditions can be expressed as:

$$T_{avg} = T_s - \frac{8}{\pi^2}(T_s - T_0)\exp\left(\frac{\alpha\pi^2}{1^2}\right) \qquad (1)$$

The foam sheet formation is pictured in Figure 1. The schematic diagram of the cell model is shown in Figure 2. The standard bubble growth modeling equations according to the cell model are listed here. The detailed analysis of the cell model are presented elsewhere*(1-4)*.
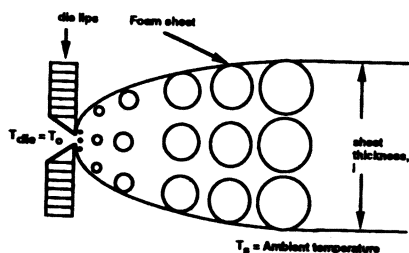
Figure 1: Schematic diagram of the foam sheet formation
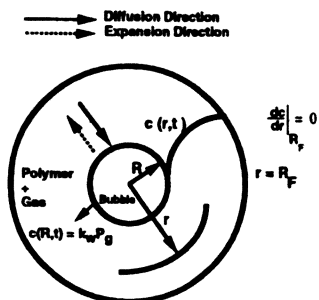
Figure 2: Schematic diagram of the bubble growth model

Foam Growth Equations:

Continuity Equation:

$$V_r = \frac{R^2 \dot{R}}{r^2}$$

(2)

Momentum Equation:

$$P_g - P_\infty - \frac{2\sigma}{R} + \int_R^{R_f} (\tau_{rr} - \tau_{\theta\theta}) \frac{dr}{r} = 0$$

(3)

Rheological Equations

$$\tau + \frac{\eta_o^*}{G} \tau_{(1)} = -\eta_o^* \dot{\gamma}$$

(4)

$$\eta_o^* = \exp\left[\frac{E_v}{R_g}\left(\frac{1}{T} - \frac{1}{T_o}\right)\right] * f(c)$$

(5)

Conservation of Mass:

$$\frac{d}{dt}\left(\rho_g R^3\right) = 3\rho D R^2 \left[\frac{\partial c}{\partial r}\right]_{r=R}$$

(6)

Concentration Equation:

$$\frac{\partial c}{\partial t} + V_r \frac{\partial c}{\partial r} = \frac{1}{r^2} \frac{\partial}{\partial r}\left(Dr^2 \frac{\partial c}{\partial r}\right) \tag{7}$$

Boundary Conditions:

The initial Boundary conditions are:

$$c(r,o) = c_0 = k_w P_{g_0} \tag{8}$$

$$c(R,t) = k_w P_g \tag{9}$$

$$\left[\frac{\partial c}{\partial r}\right]_{R_f} = 0 \tag{10}$$

$$R(t = 0) = R_0 \tag{11}$$

The boundary condition, Equation 10, represents a closed cell system where there is no gas loss or escape to its surroundings.

But in practice, we often encounter gas loss from the bubbles which are adjacent to the top and bottom surfaces of the foam sheet especially when they are thin. When the foam sheet is thin, it can be imagined that, some of the gas molecules closer to the surface, instead of diffusing into the cell, diffuse to surface and evaporate into atmosphere. As a result, the final surface cell size is smaller that that of the core cell. When density is lower, or the sheet is thinner, more gas escape is anticipated. In other words, high concentration of blowing agents, and/or high surface-to-volume ratio foam sheets, accelerate gas loss from sheet surface and thus lowering foam efficiency. This phenomenon is compounded when the atmospheric temperature gets lower which increases the foam growth time. The surface evaporation or gas loss condition can be mathematically expressed as:

Surface bubbles in the foam sheet: $D\dfrac{\partial c}{\partial r} = k_m(c_s - c_\infty)$ $\tag{12}$

Core bubbles in the foam sheet: $\dfrac{\partial c}{\partial r} = 0$ $\tag{13}$

where $\quad k_m = 2\sqrt{\dfrac{D}{\pi\, t}}$ $\tag{14}$

"k_m" is defined as the mass transfer coefficient derived from penetration theory *(8)* and "t" is the foam growth time.

The above system of equations were solved numerically by an iterative finite-difference scheme. Rheological properties for LDPE with n-butane were obtained using Haake capillary rheometer. An experimental set up is shown in Figure 3. Dissolution of blowing agent tends to plasticize the molten polymer and decreases the polymer viscosity. Rheological results for LDPE/n-butane system are shown in Figure 4, from which viscosity reduction factor, f(c), for appropriate blowing agent concentration was determined for the
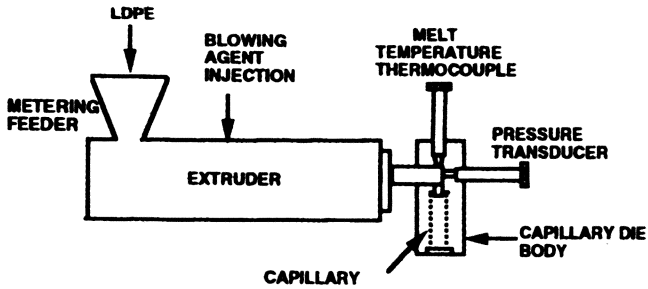
Figure 3: Schematic Diagram of Haake Rheocord 90 Extrusion Capillary Rheometer
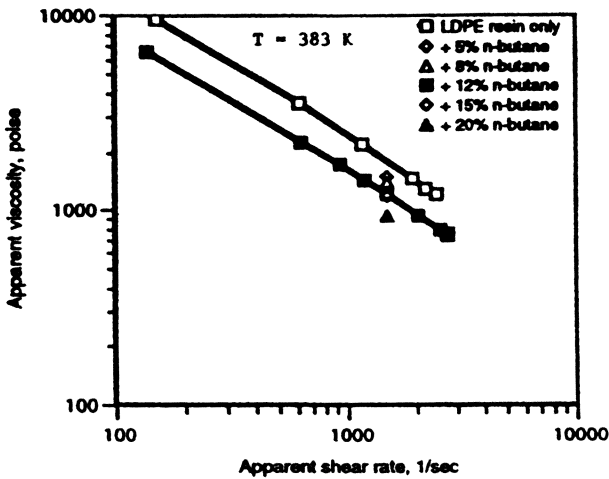
Figure 4: Influence of butane on LDPE viscosity

LDPE/n-Butane System
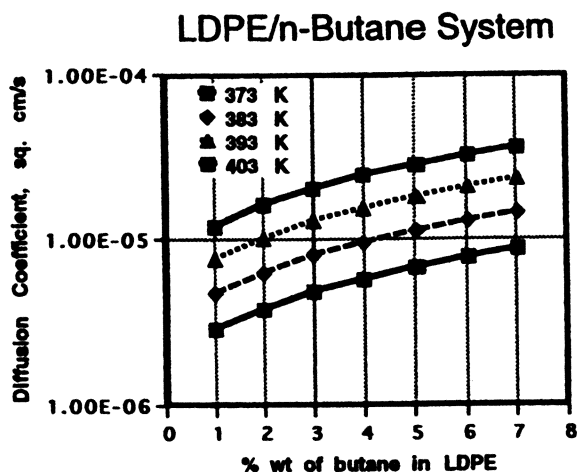
Figure 5: *Effect of concentration and temperature on diffusion coefficient*

bubble growth simulation. The concentration and temperature effects on diffusion of n-butane in LDPE is shown in Figure 5. These results are obtained by fitting data presented in Connahan's Ph.D. thesis work *(5)*. The diffusion coefficient of n-butane in LDPE as a function of temperature and concentration can be expressed as,

$$D (c, T) = [1 + 0.5334 \, c] \, 10^{-7} * \exp [21.93 - 7090/T] \, cm^2 /s \qquad (15)$$

The other simulation parameters used for all cases in this study are listed in Table I. A comprehensive analysis of the simulation work and results are not presented here due to space restriction. Therefore, one comparative case is discussed in this paper.

Table I: Simulation Parameters for Bubble Growth Calculations

Process Variables	Values
1. Surface Tension of low-density polyethylene (LDPE)	30 dyne/cm
2. Molecular Weight of butane (blowing agent)	58 gm/mole
3. Initial blowing agent concentration	6.4% by weight
4. Foaming Temperature, T_o	383 K
5. Ambient Temperature, T_s	293 K
6. Henry's law constant, k_w	2235 atm
7. Density of LDPE	0.92 g/cc
8. Modulus of LDPE	10000 dynes/cm^2

Results and discussion

Figure 6 illustrates the dynamics of bubble growth with bubble expansion time. The prediction of the final bubble size seems to agree well with the experimental data when the concentration dependent diffusion coefficient was used in the model. When concentration effects are neglected the bubbles appear to take longer time (25% more time) to grow due to lower values of diffusion coefficient. Furthermore, the induction time seems to be significantly longer when concentration effects are neglected. This conclusion is crucial to the present work, and therefore a careful analysis including concentrations effects into the model is essential to understand foam growth characteristics in industrial processes.
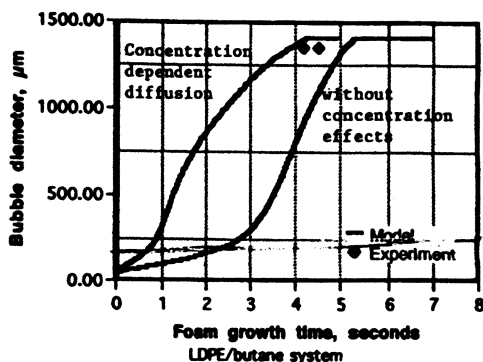
Figure 6: Dynamics of bubble growth in low-density polyethylene at 100°C

Rapid expansion of nucleated bubbles within 4 seconds makes it difficult to collect the bubble growth data. Hence, the average value of the final bubble diameter is only reported here. This area of research requires further investigation. Figure 7 shows that the foam density decreases with increase in growth time. Once again, the predictions of the model seems to be in good agreement with the experimental observation only when concentration effects are considered. This advancement to include concentration effects into the model is just one more step to improve the existing model closer to understanding of real life foam processes.
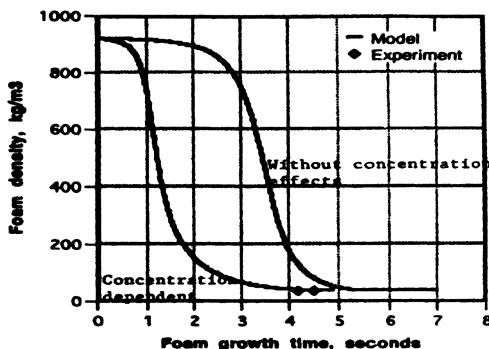
Figure 7: Dynamics of bubble growth for LDPE/butane system

Nomenclature

c	=	Gas concentration
c_s	=	Surface gas concentration
c_∞	=	Surrounding gas concentration
D	=	Diffusion coefficient
E_v	=	Activation energy for viscosity equation
$F(c)$	=	Viscosity reduction factor
G	=	Elastic modulus
k_w	=	Henry's law constant
l	=	Foam sheet thickness
P_g	=	Gas pressure at time t
P_{go}	=	Initial gas pressure inside the bubble
P_∞	=	Surrounding pressure
R_g	=	Gas constant
R	=	Gas-polymer interfacial radius
r	=	Radial coordinate
R_f	=	Cell outer radius
R_o	=	Initial bubble radius
T	=	Foaming temperature, °K
T_o	=	Initial Sheet temperature, °K
T_s	=	Surrounding room temperature, °K
t	=	Foam growth time
V_r	=	Radial component of Velocity
α	=	thermal diffusivity
η_0^*	=	Zero shear viscosity according to equation
$\tau_{rr}, \tau_{\theta\theta}$	=	Stress in radial and circumferential directions
$\tau_{(1)}$	=	Convected time derive of stress tensor
γ	=	Rate of strain tensor
ρ	=	Density of polymer
ρ_g	=	Density of blowing agent
σ	=	Surface tension of the polymer, N/m

References

1. Ramesh, N.S.: Malwitz, N.; *SPE ANTEC*; 1995; pp 2171-2177.
2. Lee, S.T.; Ramesh, N.S. *SPE ANTEC*, 1995; pp 2217-2224.
3. Denson, C.D.; Amon, M.; *Polymer Engineering Science;* 1984; **24**; pp 1026.
4. Arefmanesh, A.; Advani, S.G.; *Rheo. Acta.*; 1991; **20**; pp 274.
5. Coonahan, V.D.; *Ph.D. Thesis, Dept. of Chem. Engg.;* 1971; Univ. of Maryland.
6. Ramesh, N.S.; Rasmussen, D.; Campbell, G.A.; *Poly. Eng. Sci.*; 1991 **31**; pp 1657-64.
7. Lee, S.T.; Ramesh, N.S., Campbell, G.A.; *Poly Eng. Sci.;* 1996; **36**; pp 2477-82.
8. Welty, J.R.; Wicks, C.E.; Wilson, R.E.; *Fundamentals of Heat and Mass Transfer*, 1969; John Wiley and Sons, NY; Chapter 27, pp 556-557.

Chapter 15

Physical Modeling of Intumescent Fire Retardant Polymers

Kathryn M. Butler

Building and Fire Research Laboratory, National Institute of Standards and Technology, Mail Stop B258, Gaithersburg, MD 20899

Intumescent chemical systems are designed to swell into a thick, robust foam upon exposure to heat, protecting the underlying material from fire by providing a physical barrier to heat and mass transfer. The mechanisms determining the fire-resistant properties of these materials are not well understood. Various approaches to modeling intumescent behavior are reviewed. A three-dimensional model that incorporates physical and chemical phenomena at the scale of a single bubble is described.

The fire resistant capabilities of intumescent materials, which respond to heat by swelling into an insulating char of thickness between 5 and 100 times that of the original material, are well known and widely applied. These materials provide thermal protection to the underlying surface through the absorption of heat by endothermal chemical reactions and through the insulating properties of the final char. Flame spread is inhibited through mechanisms common to other charring materials. The closed foam structure inhibits the transport of volatiles to the environment and the transport of oxygen to unburned regions beneath the char (1), and the retention of mass in the char limits further involvement of the underlying materials in the fire.

The first commercial patent for a foaming fire retardant system was issued to Tramm in 1938 (2). A variety of coating formulations, in the forms of paints and mastics, have been developed and put into commercial use starting in the 1950's (3). The increasing use of organic polymers, which are highly flammable in their natural state, has encouraged the development of intumescent additive systems (4-10). Current research on this topic has been boosted by concerns regarding traditional halogen-based fire retardants, which tend to generate obscuring, toxic, and corrosive smoke during a fire (11). Intumescent coatings have been reviewed by Vandersall (12) and Kay et al. (13), and additive systems have been reviewed by Camino et al. (14,15).

Applications of intumescent fire retardants cover a wide range. Intumescent paints are used for protection in hazardous situations on aircraft carriers and off-shore

oil platforms (*16*). They may be applied to bring landmark buildings up to current fire protection codes (*17*). In the construction industry, intumescent coatings for structural steel provide structural integrity during a fire and are less messy to install than alternative fire protection systems that must be sprayed into place (*18,19*). The expanded foam provides a physical barrier to smoke and fire when intumescent material is used in the form of strips applied to edges of doors. Penetration seals consisting of intumescent mastics, putties, and collars restore protection for fire walls breached by holes for cables and pipes (*20,21*).

Mechanistic studies have provided a general understanding of the chemical and physical processes that must occur for intumescence to take place. When subjected to a high heat flux, the rising temperature within an intumescent material puts into motion the following sequence of events. First, an inorganic acid, typically stored in the form of a salt, is released. The acid dehydrates a carbon-rich polyhydric compound, in preparation for the eventual formation of a solid char. This reaction may be catalyzed by an organic amine or amide. The intumescent mixture melts. At a temperature corresponding to the proper viscosity an endothermal chemical reaction generates gases. The gases diffuse into small bubbles with diameter typically on the order of 10-60 microns, resulting in the formation of a foam. The material then solidifies through cross-linking into a thick multicellular char.

Careful design is required to ensure that the above events occur in the proper order and with the proper timing. Intumescent chemical formulations are often complicated, requiring a carefully matched set of components (*12,15*) and attention to the effects of other chemicals in the mixture, which may be synergistic or antagonistic to the desired fire retardant properties (*22-24*). The timing of chemical events is critical to the protective qualities of the final char. Of particular importance is the decomposition of the blowing agent with respect to the melt viscosity. If gasification takes place when the melt viscosity is too high, bubble growth will be strongly opposed, and the gas will tend to diffuse through the mixture without generating bubbles. If the molten polymer is too fluid, i.e. the melt viscosity is too low, the bubbles will be large, resulting in a fragile and ineffective char. A uniform, fine, close-celled foam structure is highly desirable as an endpoint for these materials due to the need for long-lasting physical integrity and the improved insulating properties of such structures.

The empirical approach that has characterized the development of intumescent coatings and additives has resulted in the successful design of a number of chemical formulations. Further development efforts would be considerably aided, however, by an improved understanding of the fundamental physical and chemical mechanisms responsible for intumescent behavior and its fire protection capabilities. The chemical reactions responsible for the various steps in the gasification and charring processes have been studied in detail for some common intumescent mixtures (*25,26*). The foaming process and its effects on heat transfer are complex, and few models have been developed to investigate the physical aspects of intumescence.

Heat Transfer Modeling

Since thermal protection is the main purpose of intumescent materials, several models have been developed to study the effects of intumescence on heat transfer to the underlying surface. These have been primarily one-dimensional in nature, and concentrate on the effects of swelling on the thermal properties of a coating.

One-dimensional Models. The one-dimensional models that have been developed to investigate intumescent behavior apply the equations of energy and mass conservation to some variation of the geometry illustrated in Figure 1. In this schematic the thickness of virgin material and char layers and the location of the pyrolysis zone are functions of time, and each layer is assigned its own values of thermodynamic parameters.

The earliest model of this kind was developed by Cagliostro et al. (27) to investigate the sensitivity of backwall temperature to swelling behavior and material properties. The model replaces thermal conductivity k in a standard ablation model with an "effective" thermal conductivity k/E, where $E(y,t)$ is an expansion factor relating the original position y of a point in the intumescent layer to its position during and after swelling. Assuming an empirical form for E, lower backwall temperatures are attained for rapid expansion, greater coating thickness, thicker expansion, and endothermal heat of reaction. For model parameters obtained from experiment, prediction of behavior is found to be accurate within 20%. A similar approach has been taken by Zverev et al. (28).

Anderson and Wauters (16) use the pyrolysis zone between virgin material and char to represent the active region of intumescent behavior. This model assumes an expansion factor similar to that proposed by Cagliostro et al., but also takes into account the velocity at each point. The velocity is zero within the virgin material, constant within the char, and a function of the expansion factor and mass loss rate within the pyrolysis zone. Heating of the substrate and radiative losses at the surface are also included. Given empirical curves of mass loss and thermodynamic parameters as functions of temperature, comparisons of the predicted substrate temperature with experiment suggest that a better understanding of the expansion factor is necessary.

In accordance with experimental evidence that the region in which intumescence takes place is thin relative to the coating thickness, a frontal model was developed by Buckmaster et al. (29). In this model the pyrolysis zone is reduced to a thin front, across which material properties, velocity, and temperature gradient are discontinuous. The temperature at the front is assumed fixed at a specified critical value. The problem reduces to a Stefan problem that is readily solved numerically. Results of this model show that, in qualitative agreement with experiment, the temperature of the substrate tends to level off as the front traverses through the intumescent coating, followed by a rapid temperature increase. This trend in temperature is attributed to the convection associated with the expansion, which counters the conductive flux of heat. The temperature plateau is lengthened by endothermicity of the chemical reactions. The frontal model is compared with experimental results in a paper by Anderson et al. (30).

Effects of the insulating properties of the intumescent char were studied using a simple thermal resistance model by Anderson, et al. (31). Thermal conductivities of samples were estimated from temperature vs. time data and compared to values computed assuming a porous material that can be represented by layers of solid and trapped gas. The authors conclude that the likely cause of low thermal conductivity for an intumescent char is gases that are trapped within the char.

All of these one-dimensional models rely on empirical information about the amount and rate of expansion. Their scope is limited to heat transfer, and they are not capable of supplying insights into the swelling process itself.

Penetration Seal Model. In order to investigate the heat transfer for the specialized geometry of an intumescent penetration seal, a simple numerical three-dimensional model was developed by Pehrson and Barnett (*32*). The penetration through a floor above a furnace is modeled as an annular space bounded by the cylindrical concrete wall of the hole and by a cylindrical pipe. The pipe is not necessarily centered in the hole; in fact, the most severe exposure is expected to occur for the pipe in contact with the side of the hole. The intumescent caulk of even initial thickness forms an upper wall for the annular space. The caulk is divided into a regular array of rectangular control volumes, each of which multiply into a specified number of new char elements when a sufficient amount of heat is absorbed. Finite difference calculations solve the heat transfer problem, which includes radiation, convection, and conduction through both pipe and concrete materials. Temperature as a function of time is predicted at locations within the caulk and along the concrete and pipe walls. These plots show rough qualitative agreement with thermocouple measurements taken in full-scale tests of floor assemblies. Limitations of the model due to the control volume approach, the simple representation of intumescent expansion, and the difficulty of obtaining accurate thermal property data for the intumesced char are acknowledged.

Physical Modeling

Although the heat transfer models discussed above have given insights into some of the mechanisms by which intumescent materials provide fire protection, none attempt to understand the basic mechanisms that cause swelling. Attempts to optimize fire resistant properties would greatly benefit from improved understanding of the fundamental phenomena of intumescent foam development and its sensitivity to material properties, chemistry, and fire conditions. Models that focus on the mechanisms of swelling and bubble formation are found in the literature on foam fabrication, gasification of heated thermoplastics, and softening coal pyrolysis.

Foam models. Because of its commercial importance, considerable effort has gone into understanding the evolution of thermoplastic structural foams. Bubbles are typically introduced during injection molding by dissolving a gas into the polymer melt at high pressures. When the solution enters the mold, a sudden decrease in pressure results in a supersaturated state, and bubbles nucleate and grow. The morphology that develops during fabrication determines the uniformity and physical properties of the final product. Many models have been developed to characterize bubble nucleation and growth in the manufacturing environment.

Early models of bubble growth in a supersaturated solution address the problem of a single bubble growing in a fluid of infinite extent (*33-35*). Given an initial cavity that exceeds a critical size (*34*), the bubble growth process is driven by diffusion opposed by elastic and surface tension forces at small radii and by viscous forces. Inertial terms may be neglected in foam calculations. Street et al. (*36*) includes variations in gas concentration and temperature with radial distance from the bubble, and includes mass, momentum, and energy conservation.

Amon and Denson introduced the concept of a cell model (*37*), in which the bubble grows in a sphere containing a specified amount of fluid, which forms a concentric shell around the bubble. Figure 2 provides a schematic of this model. This
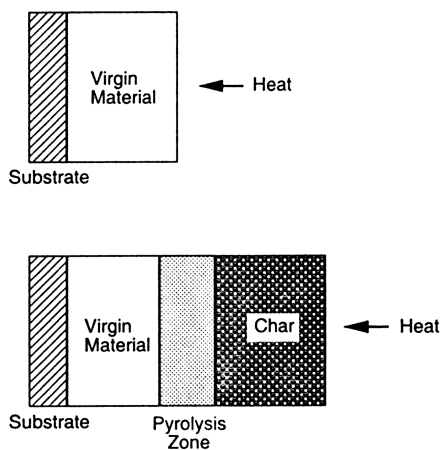
Figure 1. Typical one-dimensional model for an intumescent coating: Initial configuration (top) and configuration during swelling process (bottom).
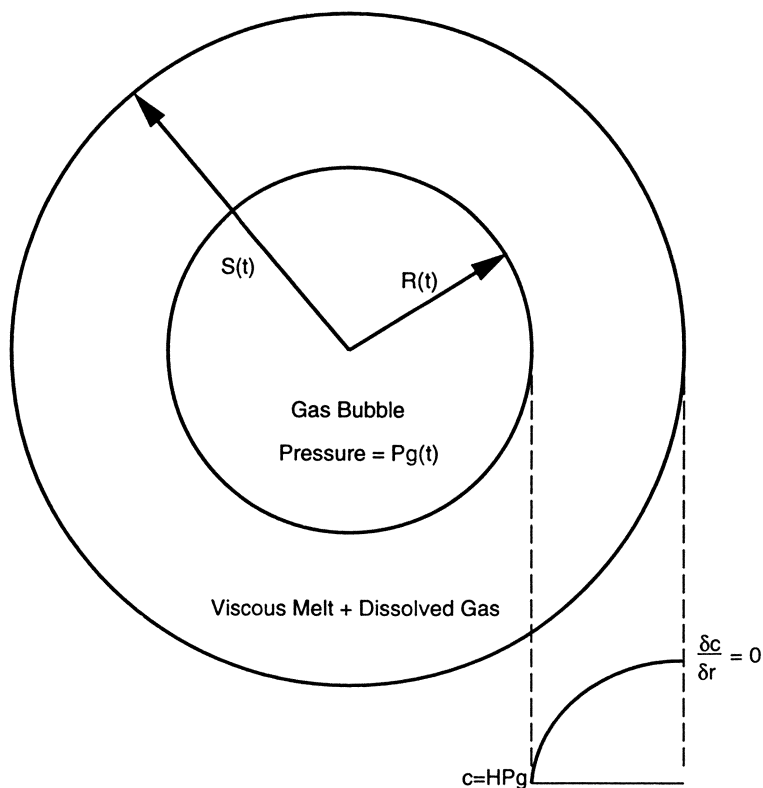
Figure 2. Schematic of cell model for foam analyses.

approach enables the consideration of bubbles separated from their neighbors by a thin film and adds the important factor of depletion of the dissolved gas. Use of the cell model as a building block for the study of macroscopic foam behavior is demonstrated in a later paper (*38*). In this investigation, the melt temperature, bulk foam pressure, and fraction of solidified foam are inputs, and the bulk foam density and bubble size distribution are calculated.

The cell model is used by Arefmanesh et al. (*39*) to study the size distribution and density variations during foam fabrication by taking into account the flow velocity of the melt. As the developing foam fills a narrow elongated mold, the bubbles are assumed to be transported with the same velocity as the melt. Larger bubbles are predicted close to the melt front than near the inlet gate, in agreement with experiment. Heat transfer from the sides of the mold has been added to this model (*40*) through the dependence of viscosity and other material properties on temperature.

Many foam models take into account the viscoelastic properties of the polymeric melt. Non-Newtonian effects have been determined to be most important in the early stages of bubble growth (*36, 40, 41*).

An intumescent foam differs from the structural foams treated by the above models in that the concentration of gas in the melt surrounding a bubble derives from chemical reactions rather than from the expansion of dissolved gases. The gasification chemistry is highly dependent on temperature, whose large spatial variations must also be taken into account.

A Model of Thermoplastic Gasification. When subjected to an incident heat flux, non-charring thermoplastic materials form a molten layer. Temperatures above the boiling point of the monomer may be attained at locations within the material. In addition to vaporization occurring at the surface, therefore, gasification occuring in-depth frequently results in bubbles that transport volatiles to the surface. There, (unlike during intumescence) the bubbles burst and release gases to the environment. The resulting increase in steady-state surface regression rate was studied by Wichman (*42*) using a theoretical model that describes the evolution of bubble number distribution. The model includes bubble nucleation, translation driven by the temperature gradient, and growth. Results of this model demonstrate the insulating properties of the bubbles by showing that their presence increases the temperature gradient in the melt. The regression rate is shown to be determined by a balance among the surface heating rate, the rate of heat absorption in the interior of the melt, and the rate at which the monomer forms bubbles.

Models of Softening Coal Pyrolysis. The transport of volatiles from the interior of coal particles by bubbles is of significant importance in the pyrolysis process. Coal melts and often swells when heated, and several models have been developed to better understand the effects of bubbles on coal pyrolysis behavior, such as weight loss and changes in mechanical properties.

Attar (*43*) concentrates on bubble nucleation, modifying classical bubble nucleation theory to account for the accumulation of gases due to a chemical reaction. The nucleation rate is found to be controlled by the viscosity of the coal melt, and the critical gas concentration for homogeneous nucleation to take place is determined.

A model developed by Oh et al. (*44*) explores the effects of pressure, particle diameter and temperature, and heating rate on tar yields, weight losses, swelling ratio, and plasticity. This model assumes isothermal spherical coal particles, in accordance

with observed sizes on the order of 70 μm in diameter and a heating rate of 1000 °C/s. Equations are derived to track the number of bubbles of a given size, allowing for bubble growth due to diffusion, chemical reactions within the bubble, changes in pressure, and coalescence, and to maintain the mass balance for gas and decomposable polymers (metaplast) in the molten coal. The mass balance includes depletion of the metaplast. Buoyancy is neglected due to the high melt viscosity, and the gas is released when the bubble boundary intersects the particle surface. Physical properties of the melt, gases, and metaplast are entered into the model using empirical correlations. Initiation of the bubbles is assumed to take place at pore sites in the original solid coal. Unlike Attar's work, these calculations indicate that bubble nucleation is not a rate-limiting process. The model predicts that the bubble size distribution is relatively uniform throughout the particle. Depletion of the metaplast results in resolidification of the melt. Predictions of weight loss, swelling, yields of tar, gases, and metaplast, and sensitivity to various parameters are in good qualitative agreement with experiment.

These models of softening coal pyrolysis include the chemistry of gasification and solidification, phenomena that are also important in intumescence. However, their direct applicability is limited by the differences in geometry, size, and heat transfer between the small, isothermal coal spheres and the extended intumescent layers containing high thermal gradients.

Three-dimensional Model of Intumescence

Clearly, intumescent materials present considerable difficulties to modellers. As demonstrated by the one-dimensional heat transfer models, swelling is central to their fire protective capabilities, and a fundamental understanding of the mechanisms that cause expansion is important. Unlike foams and softening coals, temperature gradients and heat transfer play a central role in intumescent behavior. In particular, the effect of the growing bubbles on the temperature field cannot be neglected. The sizes of nearby bubbles may be quite different due to the large temperature gradients within the intumescent melt.

In an attempt to address these factors, a three-dimensional model that incorporates bubble and melt hydrodynamics, heat transfer, and chemical reactions is currently under development (45). In this model, the intumescent system is represented as a highly viscous incompressible fluid containing a large number of expanding bubbles. The bubbles obey equations of mass, momentum, and energy on an individual basis according to the values of local parameters, and their collective behavior is responsible for the swelling and fire retardant properties of the material.

Initially, the sample is in the shape of a rectangular solid containing a large number (up to 10,000) of infinitesimally small bubble nucleation sites randomly distributed throughout the volume. A specified heat flux is applied to the upper surface of the sample and the energy equation is solved to determine the temperature field in the sample. When the temperature at a given nucleation site exceeds the degradation temperature of the blowing agent, gas is produced, and the bubble begins to grow. Both viscosity and surface tension are functions of temperature, and the strong temperature gradient plus gravity cause migration of the expanding bubble. The presence of the bubble, with thermal conductivity an order of magnitude lower than than of the surrounding melt, distorts the temperature field, as do the endothermal chemical reactions that generate the gas.

The number of bubbles that will be included in this model is far too high to consider solving the equations of mass, momentum, and energy exactly, meeting all boundary conditions. The approach taken is to consider the behavior of a single bubble in a fluid containing a temperature gradient, as pictured in Figure 3. A simple description of the physics and chemistry, either as an analytical solution or a lookup table, is sought for the individual bubble. It is then presumed that the total field in the melt can be reasonably approximated as a summation of the individual fields. This is strictly valid only for bubbles far apart compared to their radius, although insight into intumescent behavior is expected even at larger bubble sizes.   When the bubbles are sufficiently large, and/or solidification has taken place, the bubbles no longer move independently and the material behaves like a foam.

The basic components of the three-dimensional model are bubble growth, hydrodynamics, and heat transfer. The current status and direction for each of these submodels are discussed below. A more complete description of the mathematics will be published in the near future (Butler, K. M., Baum, H. R., and Kashiwagi, T. *Fire Safety Science, Proceedings of the Fifth International Symposium*, in press.).

Bubble Growth Submodel. The growth rate of bubbles in the intumescent material depends on the chemistry of the decomposition of the blowing agent and on the physical properties of the gas and surrounding melt. As in foam fabrication, bubble growth is primarily due to diffusion of gas, although the gas is generated from chemical decomposition rather than supersaturation.   In the model, the number and locations of nucleation sites are provided as inputs. When the temperature at the position of one of these sites reaches the value at which decomposition begins, as determined by the three-dimensional heat transfer calculations, growth is initiated. Currently, the intumescent model uses a simple analytic expression for the bubble growth rate $\dot{R}$ in a supersaturated fluid from early work by Epstein and Plesset (*33*):

$$\dot{R} = DS \left(\frac{P_0}{P_c} - 1 \right) \left[\frac{1}{R} + \frac{1}{(\pi D t)^{1/2}} \right] ,$$

where R is radius, t time, D the diffusion coefficient, S the gas solubility, P_0 the initial supersaturation pressure, and P_c the minimum critical pressure for bubble inflation. Growth is triggered instantaneously instead of being driven by chemical kinetics. This is a place holder for a more sophisticated submodel currently under development and based on the cell model for foams. The critical factors to be included in this submodel include viscous resistance to bubble expansion, reaction chemistry, depletion of the blowing agent, and solidification.

Hydrodynamics Submodel. Each expanding bubble experiences forces due to gravity, to gradients of viscosity and surface tension over its surface due to the local temperature gradient (*46*), and to the motions of other bubbles. The problem can be simplified by setting the velocity in the melt surrounding the bubble equal to the sum of a radial expansion field plus a velocity field due to translation. The Reynolds number, $Re = \rho U (2R)/\mu$, with translation velocity U, melt viscosity μ, and melt density ρ, is very small for these bubbles. A small Reynolds number is consistent with an assumption that the bubble remains spherical. With the additional assumption
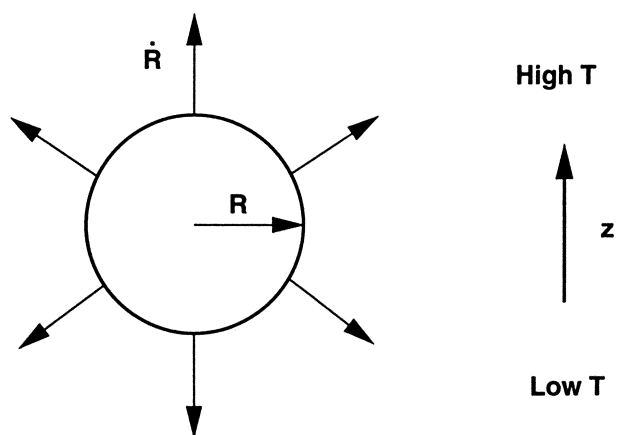
Figure 3.   Geometry for a single bubble in a fluid containing a temperature gradient in the z-direction.
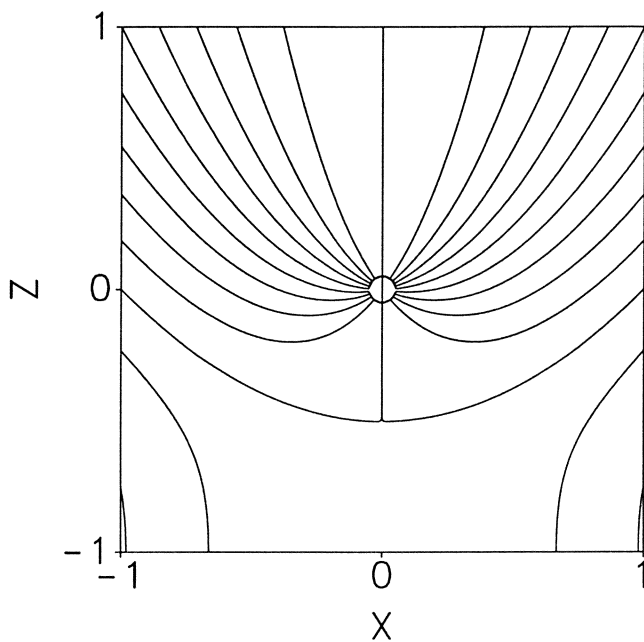
Figure 4. Velocity field for an expanding bubble translating in the z direction.

that the expansion velocity is much greater than the translation, the flow field around a solitary bubble can be described analytically by a simple Stokes equation driven by a force due to the viscosity gradient. The polymeric melt is not expected to be free of surface-active contaminants, so internal circulation is assumed to be absent, and the force due to surface tension gradients is neglected. The translation velocity of the bubble through the melt is determined by calculating the terminal velocity resulting from a balance of forces on the bubble, and is given by

$$U = -\frac{2}{3}R\dot{R}\frac{\partial \ln\mu}{\partial T}G - \frac{2}{9}\frac{\Delta\rho \, gR^2}{\mu} \quad ,$$

where $G=dT/dz$ is the local temperature gradient at the bubble, $\Delta\rho$ is the difference between melt and bubble density, and g is acceleration due to gravity. Here gravity is taken to act in the z-direction. For thermal gradients at an angle to gravity, the translation velocity is given by a vector sum. The total velocity field, shown in Figure 4, is similar to the field determined by Sadhal and Ayyaswamy (47) for a slowly moving evaporating drop.

   To handle the intumescent problem, the motion of a large number of bubbles must be determined. A simple summation of individual flow fields provides a reasonable approximation for the total flow field if the spacing between bubbles is large compared with their size. This assumption is most accurate, of course, at small times, although the tendency of expansion velocity fields to cancel each other improves the validity of this assumption at later times. The addition of image bubbles beneath the lower surface of the sample maintains a no-flux boundary condition.

   The outer surface of the intumescent sample is forced upward by the sum of forces from the bubbles expanding within the melt. As a first approximation for the surface properties of the intumescent material, the bubbles are assumed to be retained by the sample. The upper surface therefore stretches to prevent bubbles from bursting and releasing gases to the exterior. The polymeric melt changes shape only in response to bubble growth and movement, and is assumed to be sufficiently viscous that gravity and other forces have negligible effect on the melt itself.

   The variation of viscosity with temperature is currently estimated by the WLF equation for polymer melts (48),

$$\ln\mu = 13 - \frac{17.44\,(T-T_g)}{51.6 + (T-T_g)} \quad ,$$

where T_g is the glass temperature of the polymer melt. This relationship can be readily modified within the model to include other important factors such as molecular weight.

Heat Transfer Submodel. Upon exposure to the heat flux from a fire, the temperature within the intumescent sample rises, triggering gasification reactions at locations progressively farther from the outer surface. By adding a simple one-dimensional model of heat transfer through a slab to bubble growth and hydrodynamics submodels, the progress of nucleation and the bubble size distribution
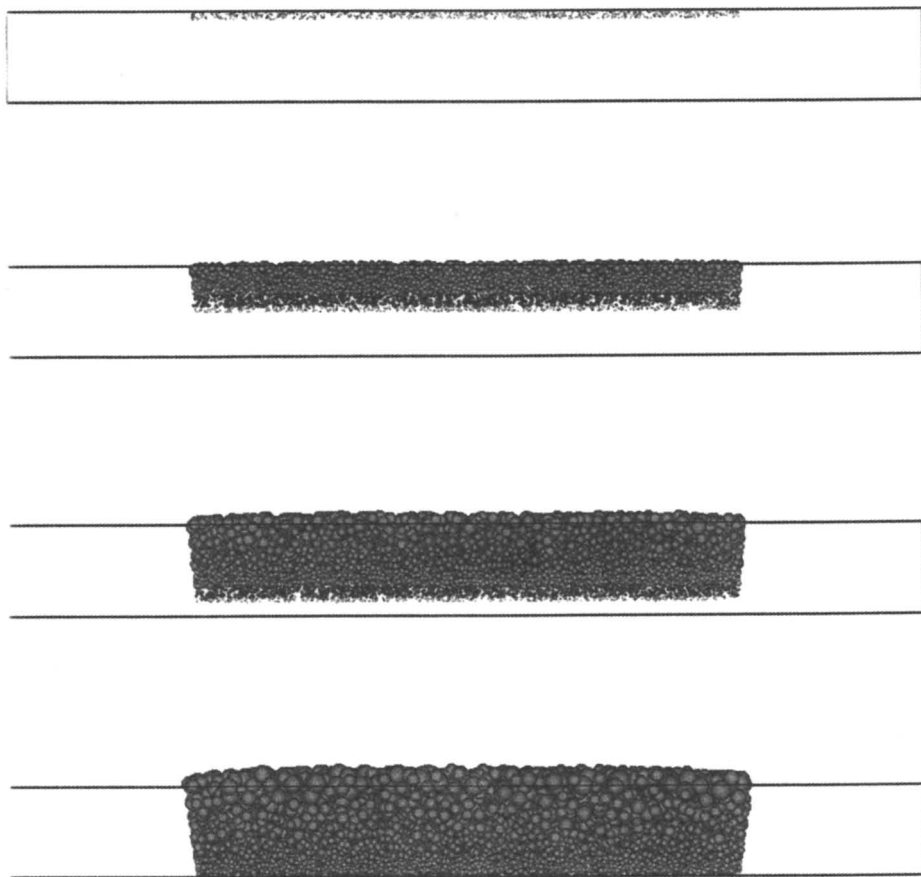
Figure 5. Development of 10,000 bubbles with time as a heat flux is applied to the upper surface of a volume whose initial dimensions in centimeters are 10 × 10 × 1. The bubbles are randomly distributed in the central 6 × 6 × 1 region. As the internal temperature increases, nucleation occurs progressively deeper in the melt.
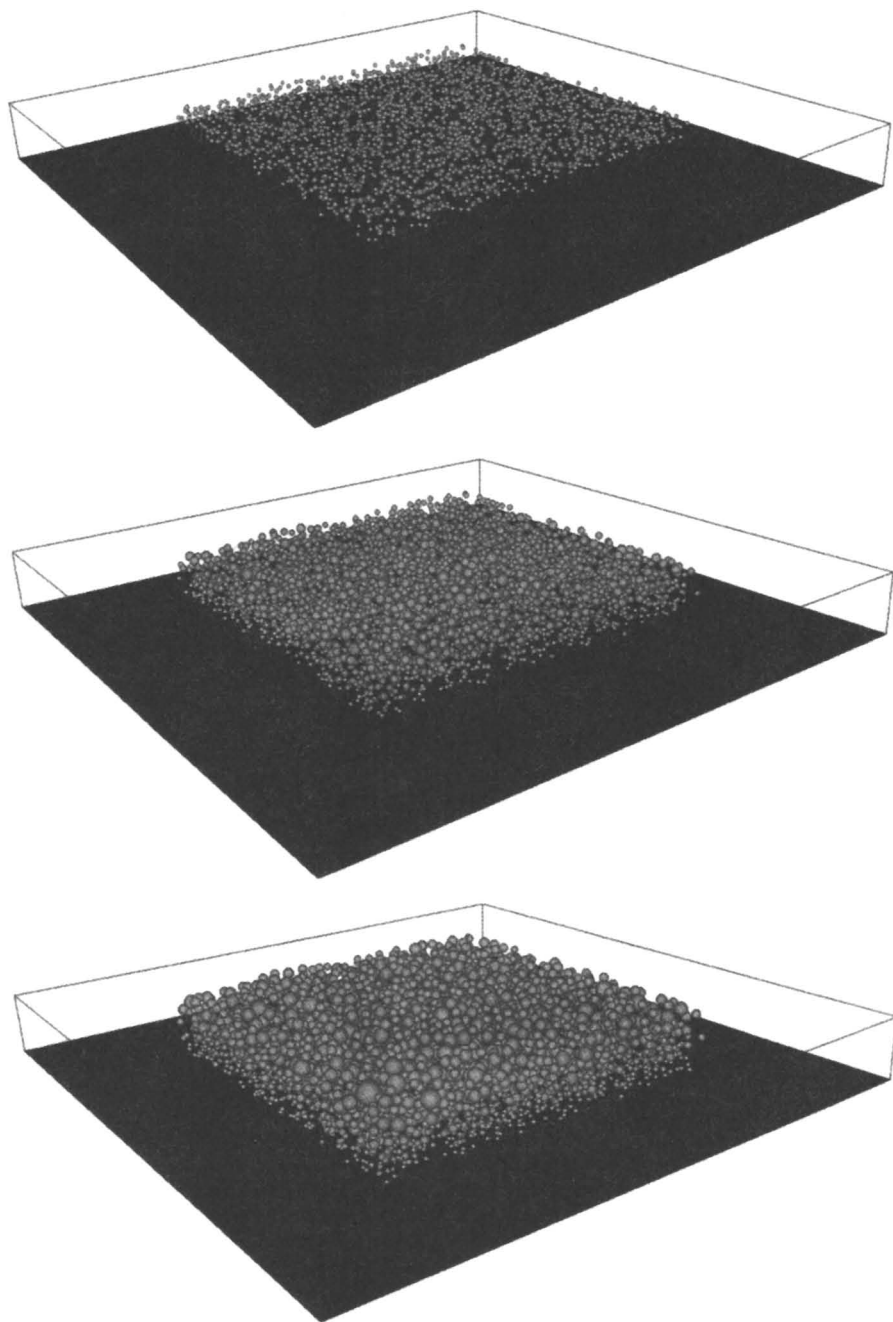
Figure 6. Perspective views of bubble development corresponding to the final three times illustrated in Figure 5.
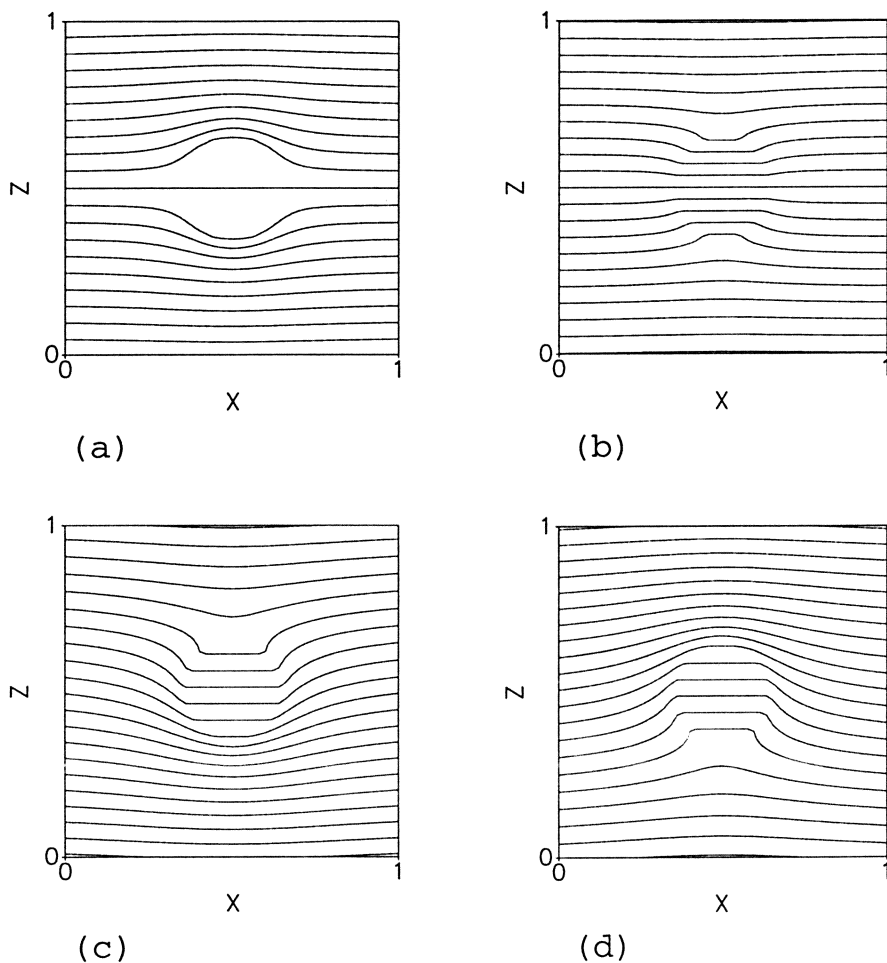
Figure 7. Temperature contours for single bubble in a fluid of infinite extent. The background temperature increases in the positive z-direction. The bubble is a) a thermal conductor, b) a thermal insulator, c) a heat source, and d) a heat sink.

may be observed. Figures 5 and 6 illustrate the behavior of the model over time for a computer run in which the central region is randomly seeded with 10,000 bubble nucleation sites.

In order to capture the thermal mechanisms responsible for the fire resistance of intumescent materials, the effects of the bubbles on heat transfer must be included. One-dimensional models have identified two important mechanisms: the endothermal chemical reactions that absorb heat during gasification, and the insulating properties of the final char.

Efforts to determine the transport of heat through a suspension of particles, such as composites, have focused on the determination of an effective thermal conductivity (49-50). Although the particles may be randomly distributed, statistical homogeneity is assumed. This does not describe the intumescent problem, in which an intumescent "front" is observed to move through the material. Bubble nucleation and growth are strongly dependent on local temperature, which is in turn dependent on the locations and sizes of bubbles closer to the heat source.

To investigate this problem, therefore, we again consider the single expanding spherical bubble in a uniform background temperature gradient as shown in Figure 3. In the intumescent melt, we can safely assume that the timescale for thermal diffusion is much shorter than the timescales for bubble expansion and translation. The solution to the transient energy equation is therefore well approximated by the solution of the Laplace equation with boundary conditions that account for a background temperature gradient and for continuity of temperature and heat flux at the surface of the sphere. If the endothermal chemical reaction is introduced as a heat sink at the bubble surface, then the temperature field in the surrounding fluid is identical to that from the sum of a dipole singularity plus a source:

$$T = Gz + Gz \frac{R^3}{r^3} \left(\frac{1-\alpha}{2+\alpha} \right) + \frac{\dot{q}'' R^2}{kr} \quad ,$$

where G is the local temperature gradient, r the radial distance from the center of the sphere, k the thermal conductivity of the melt, $\alpha = k_s/k$ the ratio of the thermal conductivity of the sphere to that of the melt, and s the heat source. This analytical solution may be summed over multiple bubbles (45).

Figure 7 shows the temperature contours in the neighborhood of a sphere centered in each plot. The temperature increases in the positive z-direction. The results of thermal conductivity differences between the sphere and the surrounding fluid are illustrated in Figures 7a and b. In (a), the sphere is highly conductive, with thermal conductivity of the sphere ten times that of its surroundings. The temperature of this sphere is nearly uniform. In (b), the sphere represents a bubble, with thermal conductivity an order of magnitude less that the surrounding fluid. Figures 7c and d shows the effect of a heat source and a sink, respectively, on the surface of the sphere, representing exothermal and endothermal chemical reactions. Note that for the case of a bubble with endothermicity, combining Figures 7b and d, the temperature in the region directly beneath the bubble is decreased as expected.

As in the case of the velocity field, a reasonable approximation to the total temperature field is obtained by summation of the individual fields if the separation of multiple bubbles is larger than their radii.

Discussion

The physical and chemical behavior of intumescent fire retardant materials in the presence of a fire is highly complex. Although some questions about their heat transfer properties may be answered by relatively simple one-dimensional models, a better understanding of the complex mechanisms behind intumescence requires a modeling approach that considers fundamental physical and chemical processes. Many scientific fields can contribute to this problem. In addition to the literature on intumescent heat transfer, foams, bubbling thermoplastic materials, and softening coal pyrolysis discussed in this chapter, modeling of intumescent behavior can also benefit from research in such areas as bulk properties of suspensions and porous media, N-body simulations, and char behavior.

This modeling effort seeks an improved understanding of the mechanisms leading to intumescence and of the sensitivity of intumescent characteristics to various physical and chemical parameters.   Pursuit of these insights in cooperation with developers of intumescent systems is expected to contribute to the further development of this important category of fire-resistant materials.

Acknowledgments

References

1. Bertelli, G.; Camino, G.; Marchetti, E.; Costa, L.; Casorati, E.; Locatelli, R. *Polym. Deg. & Stab.* **1989**, *25*, 277-292.
2. Tramm, H.; et al., U.S. Patent 2,106,938; Feb. 1938; assigned to Ruhrchemie Aktiengesellschaft.
3.   Chang, W.-H.; Scriven, R. L.; Ross, R. B. In *Flame-Retardant Polymeric Materials*; Lewin, M.; Atlas, S. M.; Pearce, E. M., Eds.; Plenum Press, New York, NY, 1975; pp. 399-454.
4. Bertelli, G.; Locatelli, R.; Marchetti, E.; Camino, G.; Costa, L. In *Proc. of the Int'l. Symp. on Flame Retardants*; Beijing, China, 1-5 Nov. 1989; Yuxiang, O.; Minxiu, Z., Eds.; Intl. Acad. Publ.; pp. 191-198.
5. Bertelli, G.; Camino, G.; Goberti, P.; Marchetti, E.; Luda Di Cortemiglia, M. P.; Costa, L. In *Fire Safety Science - Proceedings of the Third International Symposium*; Edinburgh, Scotland, 8-12 July 1991; Cox, G.; Langford, B., Eds.; Elsevier Appl. Sci.: New York, NY, 1991; pp. 537-546.
6. Camino, G.; Luda, M. P.; Costa, L. In *Recent Advances in Flame Retardancy of Polymeric Materials*; Lewin, M., Ed.; Business Communications Co., Inc.: Norwalk, CT, 1993, Vol. 4; pp. 12-22.
7. Agunloye, F. F.; Stephenson, J. E.; Williams, C. M. In *Flame Retardants '94; 6th International Conference*; London, England, 26-27 Jan. 1994; Interscience Communications Ltd.: London, England, 1994; pp. 109-116.
8. Marchal, A.; Delobel, R.; Le Bras, M.; Leroy, J.-M.; Price, D. *Polym. Deg. & Stab.* **1994**, *44*, 263-272.
9. Camino, G.; Luda, M. P.; Costa, L. In *Fire and Polymers II; Materials and Tests*

for Hazard Prevention; Nelson, G. L., Ed.; ACS Symposium Series 599; American Chemical Society: Washington, DC, 1995; pp. 76-90.

10. Lewin, M.; Endo, M. In *Fire and Polymers II; Materials and Tests for Hazard Prevention*; Nelson, G. L., Ed.; ACS Symposium Series 599; American Chemical Society: Washington, DC, 1995; pp. 91-116.

11. Pagliari, A.; Cicchetti, O.; Bevilacqua, A. In *Flame Retardants '92; 5th International Conference*; London, England, 22-23 Jan. 1992; Elsevier Applied Science: New York, NY, 1992; pp. 41-52.

12. Vandersall, H. L. *J. Fire & Flamm.* **1971**, *2*, 97-140.

13. Kay, M.; Price, A. F.; Lavery, I. *J. Fire Ret. Chem.* **1979**, *6*, 69-91.

14. Camino, G.; Costa, L. *Polym. Deg. & Stab.* **1988**, *20*, 271-294.

15. Camino, G.; Costa, L.; Martinasso, G. *Polym. Deg. & Stab.* **1989**, *23*, 359-376.

16. Anderson, C. E.; Wauters, D. K. *Int'l Engrg. Sci.* **1984**, *22*, 881-889.

17. Harp, D. W. *Techn. & Conserv.* **1981**, *6*, 30-31.

18. Allman, F. *Bldg. Control* **1987**, *24*, 32-33.

19. Sakumoto, Y.; Yamaguchi, T.; Okada, T.; Yoshida, M.; Tasaka, S.; Saito, H. *J. Struct. Eng.* **1994**, *120*, 1103-1121.

20. Becker, W. *Fire and Mat.* **1991**, *15*, 169-173.

21. Hulin, K. *Fire Surveyor* **1993**, *22*, 12-15.

22. Scharf, D.; Nalepa, R.; Heflin, R.; Wusu, T. *Fire Safety J.* **1992**, *19*, 103-117.

23. Levchik, S. V.; Levchik, G. F.; Camino, G.; Costa, L. *J. Fire Sci.* **1995**, *13*, 43-58.

24. Bourbigot, S.; Le Bras, M.; Bréant, R.; Trémillon, J.-M.; Delobel, R.; *Fire & Mat.* **1996**, *20*, 145-154.

25. Camino, G.; Costa, L.; Trossarelli, L. *Polym. Deg. & Stab.* **1984**, *6*, 243-252.

26. Camino, G.; Martinasso, G.; Costa, L.; Gobetto, R. *Polym. Deg. & Stab.* **1990**, *28*, 17-38.

27. Cagliostro, D. E.; Riccitiello, S. R.; Clark, K. J.; Shimizu, A. B. *J. Fire & Flam.* **1975**, *6*, 205-221.

28. Zverev, V. G.; Isakov, G. N.; Nesmelov, V. V.; Nazarenko, V. A. *Intl. J. Polym. Mat.* **1993**, *20*, 91-99.

29. Buckmaster, J.; Anderson, C.; Nachman, A. *Intl. J. Engng. Sci.* **1986**, *24*, 263-276.

30. Anderson, C. E., Dziuk, J., Mallow, W. A. and Buckmaster, J., *J. Fire Sci.* **1985**, *3*, 161-194.

31. Anderson, C. E.; Ketchum, D. E.; Mountain, W. P. *J. Fire Sci.* **1988**, *6*, 390-410.

32. Pehrson, R.; Barnett, J. R. *J. Fire Prot. Engr.* **1996**, *8*, 13-30.

33. Epstein, P. S. and Plesset, M. S., *J. Chem. Phys.* **1950**, *18*, 1505-1509.

34. Gent, A. N.; Tompkins, D. A. *J. Appl. Phys.* **1969**, *40*, 2520-2525.

35. Prosperetti, A.; Plesset, M. S. *J. Fluid Mech.* **1978**, *85*, 349-368.

36. Street, J. R.; Fricke, A.L.; Reiss, L. P. *Ind. Eng. Chem. Fundam.* **1971**, *10*, 54-64.

37. Amon, M.; Denson, C. D. *Polym. Eng. & Sci.* **1984**, *24*, 1026-1034.

38. Amon, M.; Denson, C. D. *Polym. Eng. & Sci.* **1986**, *26*, 255-267.

39. Arefmanesh, A.; Advani, S. G.; Michaelides, E. E. *Polym. Engr. & Sci.* **1990**, *30*, 1330-1337.

40. Arefmanesh, A.; Advani, S. G. *Polym. Engr. & Sci.* **1995**, *35*, 252-260.

41. Ramesh, N. S.; Rasmussen, D. H.; Campbell, G. A. *Polym. Engr. & Sci.* **1991**, *31*, 1657-1664.

42. Wichman, I. S. *Comb. & Flame* **1986**, *63*, 217-229.

43. Attar, A. *AIChE J.* **1978**, *24*, 106-115.

44. Oh, M. S.; Peters, W. A.; Howard, J. B. *AIChE J.* **1989**, *35*, 775-792.

45. Butler, K. M.; Baum, H. R.; Kashiwagi, T. *Proceedings of the International Conference on Fire Research and Engineering*; Orlando, FL, 10-15 Sept. 1995; pp. 261-266.

46. Young, N. O.; Goldstein, J. S.; Block, M. J. *J. Fluid Mech.* **1959**, *6*, 350-356.

47. Sadhal, S. S.; Ayyaswamy, P. S. *J. Fluid Mech.* **1983**, *133*, 65-81.

48. Williams, M. L.; Landel, R. F.; Ferry, J. D. *J. Amer. Chem. Soc.* **1955**, *77*, 3701.

49. Jeffrey, D. J. *Proc. R. Soc. Lond. A* **1973**, *335*, 355-367.

50. Batchelor, G. K. *Ann. Rev. Fluid Mech.* **1974**, *6*, 227-255.

51. Lee, Y.-M.; Haji-Sheikh, A.; Fletcher, L. S.; Peterson, G. P. *J. Heat Trans.* **1994**, *116*, 17-27.

Author Index

Ashida, K., 81
Bartholin, M., 37
Behravesh, Amir H., 115
Butler, Kathryn M., 214
Davis, H. T., 130
Della Martina, A., 8
Dutruch, L., 37
Elwell, Michael J., 143
Goto, J., 81
Grünbauer, Henri J. M., 143
Hamza, Rida, 165
Hedrick, J. L., 8
Hilborn, J. G., 8
Khemani, Kishan C., 1,54
Kiefer, J., 8
Kumar, Vipin, 101
Lee, Shau-Tarng, 195
Listemann, Mark, 165
Macosko, Christopher W., 130,165

Malwitz, Nelson, 206
Miller, R. D., 8
Mison, P., 37
Park, Chul B., 115
Ramesh, N. S., 206
Rhodes, M. B., 178
Ryan, Anthony J., 143
Saiki, K., 81
Sasaki, K., 81
Senneron, M., 37
Sillion, B., 37
Srinivasan, S., 8
Steckle, Warren P., Jr., 26
Stevens, Robert, 165
van Lieshout, Henry C., 143
Venter, Ronald D., 115
Weller, John E., 101
Zhang, Xiaodong D., 130,165

Affiliation Index

Air Products and Chemicals, Inc., 165
Centre National de la Recherche
    Scientifique, 37
Dow Benelux N.V., 143
Eastman Chemical Company, 1,54
Honeywell Technology Center, 165
IBM Almaden Research Center, 8
Institut Français du Pétrole, 37
Los Alamos National Laboratory, 26
National Institute of Standards and
    Technology, 214

Nippon Polyurethane Industries
    Company, Limited, 81
Sealed Air Corporation, 195,206
Swiss Federal Institute of Technology, 8
University of Detroit Mercy, 81
University of Manchester Institute of
    Science and Technology, 143
University of Massachusetts, 178
University of Minnesota, 130,165
University of Toronto, 115
University of Washington, 101

231

Subject Index